

**MODIFICATION OF THERMOPLASTIC ELASTOMER BASED  
ON POLYPROPYLENE/POLYBUTADIENE BLEND USING  
NANOCLAY AND CARBON NANOFIBRE**

*Thesis submitted to  
Cochin University of Science and Technology  
in partial fulfilment of the requirements  
for the award of the degree of  
Doctor of Philosophy*

**Sreedevi P. G.**



**Department of Polymer Science and Rubber Technology  
Cochin University of Science and Technology  
Kochi- 682 022, Kerala, India**

**July 2017**

**Modification of Thermoplastic Elastomer Based on  
Polypropylene/Polybutadiene Blend Using Nanoclay and Carbon  
Nanofibre**

*Ph. D Thesis*

*Author*

**Sreedevi P. G.**

Research Scholar

Department of Polymer Science and Rubber Technology

Cochin University of Science and Technology

Cochin- 682 022, Kerala, India

E-mail: sreedevipramod@gmail.com

*Supervising guide*

**Dr. Rani Joseph**

Professor (Emeritus)

Department of Polymer Science and Rubber Technology

Cochin University of Science and Technology

Cochin- 682 022, Kerala, India

E-mail: rani@cusat.ac.in

Department of Polymer Science and Rubber Technology

Cochin University of Science and Technology

Cochin- 682 022, Kerala, India

July 2017



**Department of Polymer Science and Rubber Technology**  
**Cochin University of Science and Technology**  
Cochin- 682 022, Kerala, India

---

**Dr. Rani Joseph**  
Professor

Email: rani@cusat.ac.in

/07/2017

## **Certificate**

This is to certify that the thesis entitled “**Modification of Thermoplastic Elastomer Based on Polypropylene/Polybutadiene Blend Using Nanoclay and Carbon Nanofibre**” is an authentic record of research work carried out by **Sreedevi P. G.** under my supervision and guidance in the Department of Polymer Science and Rubber Technology, Cochin University of Science and Technology, Cochin-22. No part of the work reported in this thesis has been presented for any other degree from any other institution. All the relevant corrections and modifications suggested by the audience during the pre-synopsis seminar and recommended by the Doctoral committee have been incorporated in the thesis.

***Dr. Rani Joseph***  
(Supervising Guide)



## *Declaration*

I hereby declare that the thesis entitled “**Modification of Thermoplastic Elastomer Based on Polypropylene/Polybutadiene Blend Using Nanoclay and Carbon Nanofibre**” is the bonafide work carried out by me under the supervision of **Dr. Rani Joseph** Professor (Emeritus), Department of Polymer Science and Rubber Technology, Cochin University of Science and Technology, Cochin-22 and has never been included in any other thesis submitted previously for the award of any degree.

Cochin – 22  
/07/2017

*Sreedevi P. G.*



*Dedicated to my  
beloved mother, mother-in-law  
and husband.....*





---

## Acknowledgements

*I thank God almighty for all the blessings he had showered on me to accomplish my research.*

*I owe a deep sense of gratitude to my supervising guide, Prof. Dr. Rani Joseph for the timely guidance and suggestions which helped me to accomplish this research. I felt defeated many times, but teacher...you lifted me up during all those difficult times.*

*I express my sincere thanks to Dr. K. E. George for giving me valuable recommendations regarding the thesis. I put on record my deepest gratitude to Dr. Philip Kurian whose timely involvement helped me in doing this research. I express my sincere gratitude to Dr. Sunil K Narayanan Kutty who supported me with constructive suggestions that enabled me to improve my research. I am extremely grateful to Dr. Eby Thomas Thachil and Dr. Thomas Kurien for their guidance and support.*

*I am grateful to the Head of the department Dr. Honey John and other faculty members Dr. Shailaja, Dr. Prasanth and Dr. Jyothish kumar for their support..*

*I am extremely grateful to Dr. Jayalata for the valuable suggestions given to me whenever I approached her. I am thankful to Dr. Jinu for giving me valuable corrections and suggestions.*

*I express my gratitude to all the teaching and nonteaching staff of Department of Polymer Science & Rubber Technology for their support during my research.*

*I will be failing in my duty, if I am not mentioning the name of my loving friend "Shadhiya" who helped me all through my research. No words can express my gratitude to her and I would have never crossed the stream of difficulties without her support.*

*I express my sincere gratitude to Denny mol teacher who supported, guided and cared me throughout my research and in the submission of the thesis. Thank You, Julie and Neena for the strength and support given to me for submitting journal papers and completing my thesis. Your presence have always made me feel strong and confident. It*

is a great pleasure to express my heartfelt thanks to Dr. Sunitha for her support and suggestions that helped me in completing my thesis.

I take this opportunity to thank Dr. Aiswarya who introduced to me almost all the instruments. She was always there to clear my doubts. I am grateful to Dr. Ajalesh who helped me a lot in the beginning of my research. I express my gratitude to Dr. Renju for the suggestions given to me. I am extremely thankful to Dr. Asha for the guidance and support offered to me. I would like to thank Preetha teacher for the love and care she had shown to me during my research work.

I am extremely thankful to Dhanya Bhavya, Neethu and Anju for helping me whenever I was in need. I sincerely acknowledge Remya, Bagesh, Jisha, Soumya, Midhun and Nishad for their valuable help during my research. I am extremely thankful to Neena Satheesh for being a constant support to solve my problems.

I express my heartfelt thanks to Venu sir and Gean sir, two strong supports for all the research scholars in the department, for the help and support given to me in these years. I sincerely thank Dr. Bipin, who know the pulse of each instrument in this department. His presence always made me feel relaxed while working with the instruments. My sincere thanks to Rohit who supported me a lot with his technological skills throughout my research work.

I am thankful to Bindu teacher for the help and guidance given to me during my research. I am extremely grateful to Dr. Nimmy, Dr. Anna, Dr. Zeena, Dr. Vidya, Dr. Saisy, Dr. Newly, Dr. Nisha, Dr. Pramila, Dr. Shobha Dr. Sona, Dr. Reshmi, Dr. Abhilash, Dr. Sreejesh, Dr. Teena, Jolly sir and Jebin teacher for the support they have given to me. I am thankful to Vishnu for the help given to me in completing the research.

I am grateful to Shinu, Asha Paul, Rehna, Dilip, Archana, Nisha, Sumitha, Aswathy, Sneha, Lizz, Ashwin and Kingsley for the help rendered to me.

I thank Dr. Anjana and Shiji for helping me to do rheological analysis at GEC, Thrissur, I am extremely grateful to Dr. Sinto and Dileep for helping me in doing the tensile tests at Rubber Park. I take this opportunity to thank Dr. Shibu who helped me

*with the XRD and TEM analysis of the samples. I am extremely thankful to Melbin with whom I used to have fruitful interactions regarding SEM analysis. I would like to thank Anu who have taken the effort to do the TEM analysis of the samples at M G University, Kottayam.*

*I gratefully acknowledge the support given to me by all the principals of schools I have worked with. I thank Prasantha Kumari teacher, Murali sir and Savithri teacher who encouraged me to complete my research work. I take this opportunity to thank Maya teacher, (former RDD, Ernakulam) for providing me the opportunity do research without affecting my professional career. I thank Dhanalakshmi teacher, Saudamini teacher, Sajana teacher, Sindu teacher and Usha teacher for their support and motivation. I am extremely grateful to Jyothi teacher and Soumya teacher who shared my responsibilities at school. I take this opportunity to thank Dr. Reneesh Konnole who introduced me to the concept of theoretical modeling and helped me in completing my research. I am grateful to all my colleagues especially Tancy, Melba and Shobha teacher for supporting me. I thank Dr. Sreeshha who always motivated me during my research.*

*I thank Mr. Binoop, for sincerely helping me to submit the thesis with in time.*

*I express my deepest sense of gratitude to my beloved family members for their encouragement and support. I strongly believe that my amma's prayers had helped me to complete my research. I thank my father who always taught me to be determined in every aspect of life. I thank my brother and sister-in-law for the support given to me. My sincere thanks to Ammukutty for helping me in completing the thesis.*

*I thank God for being blessed with such a wonderful husband and mother-in-law. ....The sacrifices made and the pain that you have experienced all these years made my dream come true. I thank my loving kids Nanda and Namish for their support and sorry for making you feel that laptop is my first child.*

*I express my sincere gratitude to all those who motivated, supported and guided me in the course of my research. ...*

**Sreedevi P. G.**



## ||| Preface |||

Thermoplastic Elastomers (TPEs) are the manifestation of the polymeric architecture where the processability of the thermoplastics is blended with elastomeric nature of rubber. Among the TPE blends, thermoplastic olefins (TPOs) can be prepared by blending thermoplastics and rubber. A plastic rich TPO usually comprises of thermoplastic as the matrix and elastomer as the dispersed phase. The dispersed elastomer phase aids to improve the impact strength of thermoplastic polymer. Polypropylene is one of the most widely used thermoplastics and is usually toughened with elastomers to increase its engineering applications. Polybutadiene is rarely toughened with polypropylene even though it has high elasticity, good abrasion resistance and low heat build-up. In this study, thermoplastic elastomer based on polypropylene/polybutadiene (PP/BR) blends are proposed to be developed by melt mixing technique.

The reduction in stiffness and strength of the thermoplastic matrix associated with the introduction of elastomer is often compensated by the addition of inorganic fillers to the polymer blend. The enhancement in stiffness by the addition of inorganic fillers often requires high loading of the nanofiller leading to poor processability. In this perspective, the introduction of nanofillers in the blend offers great potential for extensive applications. Proper distribution of nanofillers in the polymer matrix may result in the achievement of desired end use properties at low loading levels.

Among the nanofillers incorporated in the polymer matrices, organically modified nanoclays, carbon nanofibres and carbon nanotubes are promising to revolutionize several fields in material science. The importance of nanofillers is that its nanoscale dispersion within the polymer matrices leads to remarkable enhancement in properties at lower loading. A systematic study on the effect of nanofillers as reinforcing agents in polypropylene/polybutadiene (PP/BR) blend is carried out in this study. The improvement in the properties of the PP/BR blend has been attempted by use of non polar modifiers such as styrene-(ethylene-co-butylene)-styrene (SEBS)

and styrene butadiene styrene (SBS) as compatibilizers. The influence of nanoclay and carbon nanofibre (CNF) on SEBS compatibilized polypropylene/polybutadiene blend are investigated.

The thesis consist of six chapters:

A brief introduction is given in **chapter 1**. Review on thermoplastic elastomer nanocomposites based on polymer blends with special reference to fundamentals of blends, nanocomposites and compatibilization of the blends are briefly conferred. Scope and objectives of the present work are also presented in this chapter.

The particulars of the materials used and the experimental techniques for the preparation of nanocomposites are given in **chapter 2**. A concise report about the different techniques used for investigating the mechanical, thermal, rheological and morphological properties of the blend and the composites are also discussed in this chapter.

The preparation and optimization of a thermoplastic elastomer based on polypropylene/polybutadiene (PP/BR) blends by melt blending technique is given in **chapter 3**. The effect of polybutadiene content on the mechanical, morphological, thermal and rheological properties of polypropylene matrix was evaluated. Theoretical analysis of the tensile strength data using the Nielsen's first power law model, Nielsen's two-third power law model and Nicolais-Narkis model were made. PP/BR blends are characterized using SEM, DMA, DRA, DSC and TGA.

**Chapter 4** is divided into two sections

**Part A:** This part deals with the fabrication and characterization of PP/BR/nanoclay composites. XRD and TEM are used to study the morphology of PP/BR/nanoclay composites. The experimental data on tensile modulus is compared with Halpin-Tsai model, modified Halpin-Tsai model, Voigt rule of mixtures and Reuss inverse rule of mixtures. The characterization of the PP/BR/nanoclay composites using SEM, DMA, DRA, DSC and TGA is also presented in this part.

**Part B:** This part deals with the effect of carbon nanofibre (CNF) on the structural, mechanical, thermal and rheological properties of PP/BR blend. XRD and TEM studies are used to characterize the morphology of PP/BR/CNF composites. A modified Halpin-Tsai equation that accounts for the effect of orientation and agglomeration of CNF is used to evaluate the Young's modulus of the nanocomposite. The characterization of CNF based composites is done using SEM, DMA, DRA, DSC and TGA is made.

**Chapter 5** is divided in to two parts:

**Part A:** This part discusses the effect of SEBS and SBS as compatibilizers on polypropylene/polybutadiene blend. The characterization of the PP/BR/SEBS and PP/BR/SBS blends using FTIR, SEM, TGA, DRA and DSC is also made.

**Part B:** This part describes the effect of nanoclay and CNF on the properties of SEBS compatibilized PP/BR blend. TEM analysis is used to investigate the localization of the nanofillers in the matrix. The prepared nanocomposites are characterized using SEM, DSC, DRA and TGA.

The summary and conclusions of the study are presented in **chapter 6**.





## Contents

### Chapter 1

<b>INTRODUCTION .....</b>	<b>01- 62</b>
1.1 Thermoplastic elastomers .....	01
1.2 Classification of thermoplastic elastomers .....	03
1.3 Thermoplastic polyolefin blends .....	04
1.3.1 Miscibility of polymer blends .....	05
1.4 Methods of compatibilization .....	07
1.4.1 Physical compatibilization .....	07
1.4.1.1 Compatibilization by block copolymers .....	08
1.4.1.2 Compatibilization by graft copolymers .....	11
1.4.1.3 Compatibilization by random copolymers .....	12
1.4.2 Reactive compatibilization .....	13
1.5 Polypropylene/rubber blends .....	15
1.6 Toughening mechanism in rubber toughened polypropylene .....	19
1.6.1 Matrix shear yielding and particle cavitation .....	20
1.7 Thermoplastic elastomers from polypropylene/polybutadiene (PP/BR) blends .....	24
1.7.1 Polypropylene (PP) .....	24
1.7.2 Polybutadiene (BR) .....	26
1.7.3 PP/BR blends .....	27
1.8 Polymer nanocomposites .....	28
1.8.1 Nanofillers .....	28
1.9 Preparation of the nanocomposites .....	29
1.9.1 Melt blending .....	30
1.9.2 Intercalation of Polymer or Prepolymer from Solution .....	31
1.9.3 <i>In situ</i> polymerization .....	31
1.10 Carbon nanofibre as filler for polymer matrices .....	32
1.10.1 PP/CNF composites .....	35
1.10.2 PP/elastomer/CNF composites .....	38
1.11 Nanoclay as filler for polymer matrices .....	39
1.11.1 PP/organoclay composites .....	45
1.11.2 PP/elastomer/organoclay composites .....	46
1.12 Applications of polymer nanocomposites .....	49
1.13 Scope and objectives .....	50
References .....	51

### Chapter 2

<b>MATERIALS AND EXPERIMENTAL TECHNIQUES .....</b>	<b>63-78</b>
2.1 Materials .....	63
2.1.1 Polymers .....	63

2.1.1.1	Polypropylene (PP).....	63
2.1.1.2	Polybutadiene rubber (BR).....	64
2.1.2	Compatibilizers .....	64
2.1.3	Fillers.....	65
2.1.3.1	Nanoclay (NC) .....	65
2.1.3.2	Carbon nanofibre (CNF).....	65
2.2	Methodology .....	66
2.2.1	Preparation of the blends.....	66
2.2.2	Preparation of the PP/BR nanocomposites.....	66
2.2.3	Preparation of test specimen .....	66
2.3	Characterization techniques .....	67
2.3.1	X-ray Diffraction (XRD).....	67
2.3.2	Scanning electron microscopy (SEM).....	68
2.3.3	High resolution transmission electron microscopy (HRTEM) .....	69
2.3.4	Mechanical properties .....	69
2.3.5	Fourier transform infrared spectroscopy (FTIR).....	71
2.3.6	Dynamic rheological analysis (DRA) .....	71
2.3.7	Dynamic mechanical analysis (DMA) .....	73
2.3.8	Differential scanning calorimetry (DSC) .....	74
2.3.9	Thermogravimetric analysis (TGA) .....	76
	References .....	77

### **Chapter 3**

#### **THERMOPLASTIC ELASTOMERS BASED ON POLYPROPYLENE /POLYBUTADIENE BLENDS ..... 79-112**

3.1	Introduction .....	80
3.2	Methodology .....	82
3.2.1	Materials .....	82
3.2.2	Preparation of the blends .....	82
3.3	Results and Discussion .....	83
3.3.1	Mechanical properties .....	83
3.3.1.1	Tensile properties .....	83
3.3.1.2	Impact strength .....	86
3.3.2	Theoretical modeling of tensile strength .....	87
3.3.3	Scanning electron microscopy (SEM).....	89
3.3.4	Dynamic rheological analysis (DRA) .....	93
3.3.5	Dynamic mechanical analysis (DMA) .....	98
3.3.6	DSC analysis of the PP/BR blends .....	99
3.3.7	Differential scanning calorimetry (DSC) .....	102
3.3.8	Reprocessibility of blends .....	104
3.4	Conclusions.....	106
	References .....	107

## **Chapter 4**

### **POLYPROPYLENE/POLYBUTADIENE BLEND: EFFECT OF NANOFILLERS..... 113-185**

#### **Part A**

##### **POLYPROPYLENE/POLYBUTADIENE/NANOCLAY COMPOSITES**

4A.1 Introduction .....	114
4A.2 Methodology .....	117
4A.2.1 Materials.....	117
4A.2.2 Preparation of the PP/BR/nanoclay composites.....	117
4A.2.3 Theoretical modeling of Young's modulus.....	118
4A.3 Results and Discussion .....	120
4A.3.1 X-ray Diffraction (XRD) .....	120
4A.3.2 Transmission electron microscopy (TEM).....	121
4A.3.3 Scanning electron microscopy (SEM).....	123
4A.3.4 Mechanical properties .....	125
4A.3.4.1 Tensile properties.....	125
4A.3.4.2 Impact strength.....	127
4A.3.4.3 Theoretical modeling of Young's modulus .....	128
4A.3.5 Dynamic rheological analysis (DRA) .....	130
4A.3.6 Dynamic mechanical analysis (DMA).....	135
4A.3.7 Differential scanning calorimetry (DSC) .....	137
4A.3.8 Thermogravimetric analysis .....	139
4A.4 Conclusions .....	141
References .....	142

#### **Part B**

##### **POLYPROPYLENE/POLYBUTADIENE/CARBON NANOFIBRE COMPOSITES**

4B.1 Introduction.....	148
4B.2 Methodology .....	151
4B.2.1 Materials.....	151
4B.2.2 Preparation and characterization of PP/BR/CNF composites ..	152
4B.2.3 Theoretical Modelling of Young's modulus .....	152
4B.3 Results and Discussion .....	154
4B.3.1 X-ray Diffraction .....	154
4B.3.2 Transmission electron microscopy (TEM).....	155
4B.3.3 Scanning electron microscopy (SEM).....	158
4B.3.4 Mechanical properties .....	162
4B.3.4.1 Tensile properties.....	162
4B.3.4.2 Impact strength .....	163
4B.3.4.3 Theoretical Modeling of Young's modulus .....	165

4B.3.5 Dynamic rheological analysis (DRA) .....	167
4B.3.6 Dynamic mechanical analysis (DMA) .....	172
4B.3.7 Differential scanning calorimetry (DSC) .....	173
4B.3.8 Thermogravimetric analysis (TGA) .....	176
4B.4 Conclusions .....	178
References .....	179

## **Chapter 5**

### **POLYPROPYLENE/POLYBUTADIENE BLEND: EFFECT OF COMPATIBILIZERS AND NANOFILLERS ..... 187-247**

#### **Part A**

##### **POLYPROPYLENE/POLYBUTADIENE BLEND: EFFECT OF COMPATIBILIZERS**

5A.1 Introduction .....	188
5A.2 Methodology .....	190
5A.2.1 Materials .....	190
5A.2.2 Preparation of the PP/BR/SEBS and PP/BR/SBS blends .....	190
5A.3 Results and Discussion .....	191
5A.3.1 Mechanical properties .....	191
5A.3.1.1 Tensile properties .....	191
5A.3.1.2 Impact strength .....	194
5A.3.2 Scanning electron microscopy (SEM) .....	195
5A.3.3 Fourier transform infrared spectroscopy (FTIR) .....	199
5A.3.4 Dynamic rheological analysis (DRA) .....	200
5A.3.5 Differential scanning calorimetry (DSC) .....	202
5A.3.6 Thermogravimetric analysis (TGA) .....	205
5A.4 Conclusions .....	207
References .....	207

#### **Part B**

##### **EFFECT OF NANOFILLERS ON PP/BR BLEND COMPATIBILIZED WITH SEBS**

5B.1 Introduction .....	212
5B.2 Methodology .....	217
5B.2.1 Materials .....	217
5B.2.2 Preparation of PP/BR/SEBS nanocomposites .....	217
5B.3 Results and Discussion .....	218
5B.3.1 Mechanical properties .....	218
5B.3.1.1 Tensile properties .....	218
5B.3.1.2 Impact strength .....	221
5B.3.2 Transmission electron microscopy (TEM) .....	222

5B.3.2.1 PP/BR/SEBS/nanoclay composites.....	222
5B.3.2.2 PP/BR/SEBS/CNF composites .....	225
5B.3.3 Scanning electron microscopy (SEM).....	229
5B.3.4 Dynamic rheological analysis (DRA) .....	234
5B.3.5 Differential scanning calorimetry (DSC) .....	237
5B.3.6 Thermogravimetric analysis (TGA) .....	239
5B.4 Conclusions.....	241
References .....	242

## ***Chapter 6***

<b>SUMMARY AND CONCLUSIONS.....</b>	<b>249-255</b>
-------------------------------------	----------------

<b>List of Publications.....</b>	<b>257-258</b>
----------------------------------	----------------

<b>Curriculum Vitae .....</b>	<b>259</b>
-------------------------------	------------



## ||| List of Abbreviations and Symbols |||

ASTM	American Society for Testing and Materials
BR	Polybutadiene rubber
CNF	Carbon nanofibre
CNT	Carbon nanotube
DMA	Dynamic mechanical analysis
DRA	Dynamic rheological analysis
DSC	Differential scanning calorimetry
DTA	Differential thermal analysis
EPDM	Ethylene propylene diene monomer
EPR	Ethylene propylene rubber
FTIR	Fourier transform infrared spectroscopy
GPa	Giga Pascal
MPa	Mega Pascal
MA	Maleic anhydride
MMT	Montmorillonite
MRF	Modulus Reduction Factor
NC	Nanoclay
NBR	Nitrile rubber
NR	Natural Rubber
PP	Polypropylene
PP-g-MA	Maleic anhydride grafted PP
PS	Polystyrene
SBR	Styrene-butadiene rubber
SBS	Styrene-butadiene-styrene block copolymer
SEM	Scanning electron microscopy
SEBS	Styrene-ethylene-butylene-styrene block copolymer
SEBS-g-MA	Maleic anhydride grafted SEBS
TEM	Transmission electron microscopy
TGA	Thermogravimetric analysis

TPE	Thermoplastic elastomer
TPO	Thermoplastic olefin
TPU	Thermoplastic polyurethane
TPV	Thermoplastic vulcanizate
VGCNF	Vapour grown carbon nanofibre
XRD	X-ray diffraction
$A_f$	Aspect ratio of the filler
$E'$	Storage modulus
$E''$	Loss modulus
$E_c$	Modulus of composite
$E_f$	Young's modulus of filler
$E_m$	Young's modulus of matrix
$G'$	Shear storage modulus
$G''$	Shear loss modulus
$\Delta G_{\text{mix}}$	Gibb's free energy of mixing
$\Delta H_f$	Enthalpy of fusion
$\Delta H_c$	Enthalpy of crystallization
$\Delta H_{\text{mix}}$	Enthalpy of mixing
$K_b$	Adhesion parameter
$\Delta S_{\text{mix}}$	Entropy of mixing
$\tan \delta$	Loss tangent
$T_c$	Peak crystallisation temperature
$T_{c,\text{endset}}$	Crystallisation temperature (endset)
$T_{c,\text{onset}}$	Crystallisation temperature (onset)
$T_g$	Glass transition temperature
$T_m$	Peak melting temperature
$T_{m,\text{onset}}$	Melting temperature (onset)
$T_{m,\text{endset}}$	Melting temperature (endset)
$W_f$	Weight fraction of the filler
$V_f$	Volume fraction of CNF
$\phi_f$	Volume fraction of nanoclay



$\alpha$	Orientation factor
$\rho_f$	Density of the filler
$l_f$	Length of the carbon nanofibre
$d_f$	Diameter of carbon nanofibre
$\zeta$	Shape parameter
$\eta^*$	Complex viscosity
$\omega$	Angular frequency
$\lambda$	Wavelength of X ray
$\gamma$	Strain amplitude
wt %	Weight percentage
Å	Angstrom
$\theta$	Angle corresponding to the peak
$\mu\text{m}$	Micrometer
nm	Nanometer
$\sigma_b$	Tensile strength of the blend
$\sigma_m$	Tensile strength of the matrix
$\Phi_d$	Volume of the dispersed phase
°C	Degree celcius

.....

<i>C o n t e n t s</i>	<i>1.1 Thermoplastic elastomers</i>
	<i>1.2 Classification of thermoplastic elastomers</i>
	<i>1.3 Thermoplastic polyolefin blends</i>
	<i>1.4 Methods of compatibilization</i>
	<i>1.5 Polypropylene/rubber blends</i>
	<i>1.6 Toughening Mechanism in rubber toughened polypropylene</i>
	<i>1.7 Thermoplastic elastomers from polypropylene/polybutadiene (PP/BR) blends</i>
	<i>1.8 Polymer/Nanocomposites</i>
	<i>1.9 Preparation of nanocomposites</i>
	<i>1.10 Carbon nanofibre as filler for polymer matrices</i>
	<i>1.11 Nanoclay as filler for polymer matrices</i>
	<i>1.12 Application of polymer nanocomposites</i>
	<i>1.13 Scope and objectives</i>

## **1.1 Thermoplastic elastomers**

The development of thermoplastic elastomers (TPEs) provided a novel perspective to the field of polymer technology and had emerged as an important class with one foot in rubber industry and the other one in plastic industry as in Figure 1.1<sup>1</sup>. The advent of TPEs led to the manifestation of polymeric architecture where the processability of thermoplastics is blended with the elasticity of the elastomers<sup>2,3</sup>. TPEs consists of a soft component and a hard component, where the hard phase provides the strength and the

soft phase provides elasticity. The technological versatility of TPEs lies in their ability to be processed like thermoplastics and the elasticity similar to that of conventional thermoset rubbers<sup>4</sup>.

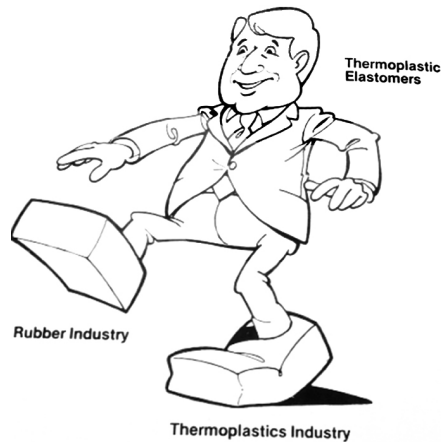


**Figure 1.1. Thermoplastic elastomers**

(Adapted from Elastomer technology handbook)

The processing methods are typically more efficient, significantly less costly and requires fewer steps. TPEs require little or no compounding since they are fully formulated and are ready for fabrication. The low density of TPEs than conventional rubber compounds often makes it volume lower. Shorter molding cycles and simpler processing techniques leads to low energy consumption. The TPE scrap can be reused in the same fashion as with thermoplastics in contrast to thermoset elastomers which are not recyclable. The processing techniques such as blow molding, heat welding and thermoforming that are not suitable for thermoset rubbers can be used for processing TPEs<sup>1</sup>. They have good resistance to impact, compressive and flexural loads and have high value of fracture resistance. They are flexible and break at large elongation. They can be reinforced with inorganic fillers.

The property of melting at elevated temperatures limits the service temperatures of TPEs well below their melting point. Most commercial TPEs are harder and number of materials softer than 50 Durometer A is still rather limited. TPEs require drying prior to processing and this step is not necessary for thermoset rubber<sup>2</sup>.

## 1.2 Classification of thermoplastic elastomers

TPEs can be classified into block copolymers and blends as shown in the Figure 1.2<sup>5</sup>. The block copolymers include styrenic block copolymers (SBCs), polyamide/elastomer block copolymers (COPAs), polyether ester/elastomer block copolymers (COPEs) and polyurethane/elastomer block copolymers (TPUs). Thermoplastic elastomer (TPE) blends are blends of thermoplastics and rubbers classified as Thermoplastic olefins (TPOs) and Thermoplastic vulcanizates (TPVs). Among these, TPOs are blends of thermoplastics and uncrosslinked rubber phase, while TPVs include crosslinked rubber phase.

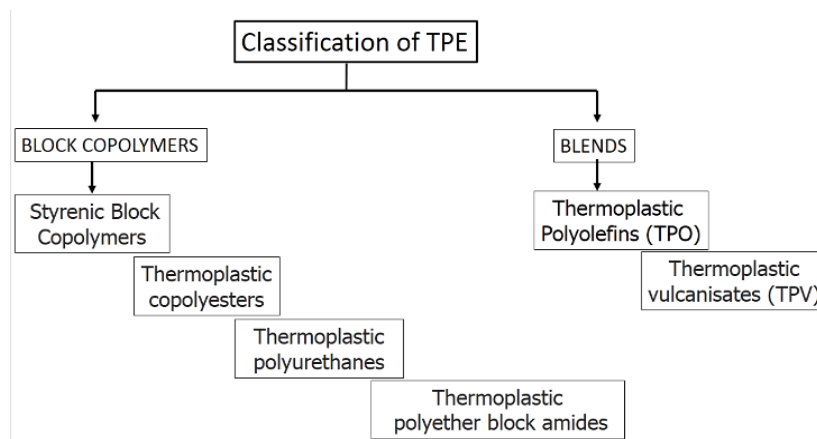


**Figure 1.2. Classification of thermoplastic elastomers (TPE)**

### 1.3 Thermoplastic polyolefin blends

The development of polymer blends have revolutionized the field of polymer technology and are best considered as they can provide tailor made properties by economically viable processing methods. The term polymer blend may be defined as a combination of two or more structurally different polymers or copolymers giving rise to materials with a range of properties, independent of its constituents. Polymer blends can be either homogeneous or heterogeneous. In homogeneous blends, the final properties usually are the arithmetical average of both blend components. In heterogeneous blends, the properties of all the blend components are present. In some cases properties of homogeneous or heterogeneous blend can be better than those of the individual components.

Blending of an elastomer with thermoplastics provides a convenient method for developing TPEs of diverse nature. Plastic/rubber blends can be prepared by melt mixing of plastics and rubbers in an internal mixer. By the proper selection of rubbers and plastics and by controlling their ratios, the required properties can be easily achieved. Commonly used plastics include polypropylene (PP), polyethylene (PE), polystyrene (PS), nylon etc. and rubbers are Ethylene propylene diene monomer (EPDM), natural rubber (NR), styene butadiene rubber (SBR), butyl rubber, nitrile rubber (NBR) etc.

The most commonly used TPOs are melt blended PP/EPDM blend. Based on the ratio of PP and elastomer contents, TPOs with plastic rich ( $\leq 30\%$  elastomer) and rubber-rich ( $\geq 70\%$  elastomer) domains have been fabricated<sup>6</sup>. When the elastomer is the minor component, it will constitute the dispersed phase and will act as a toughening agent for the matrix as shown in Figure 1.3. When the elastomer is the major component it will form the matrix and the overall blend will be an elastomer. If the elastomeric

phase is dominant, then the materials are referred to as thermoplastic polyolefin elastomers<sup>6</sup>. In TPOs, the rubber phase morphology is not fixed. The rubber phase can undergo coalescence or rupture during high shear processes and this allows TPOs to flow freely resulting in good processing characteristics<sup>8</sup>.

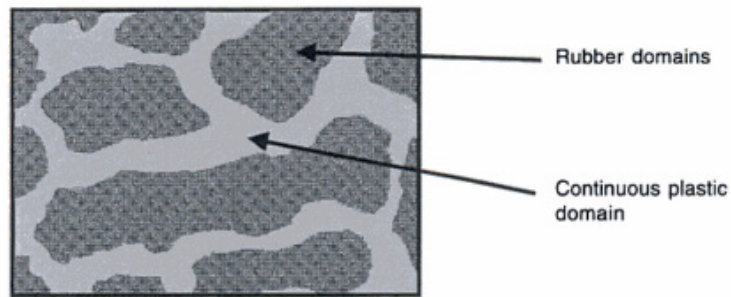


Figure 1.3. TPO rubber/plastic blend morphology

### 1.3.1 Miscibility of polymer blends

Three different types of blends can be distinguished on the basis of miscibility.

- (i) Completely miscible blends, for which  $\Delta H < 0$  due to specific interactions and homogeneities observed at least on a nanometer scale. This type of blend exhibits only one glass transition temperature ( $T_g$ ) which occurs in between the  $T_g$  values of both components in the blend. For a miscible blend, the property of interest 'P' of the polymer is given by equation 1.1.

$$P = P_1\phi_1 + P_2\phi_2 + I\phi_1\phi_2 \dots\dots\dots(1.1)$$

If I is positive, the polymer blending will produce a synergistic effect in the blend. If I is negative, the polymer blend system is antisynergistic.

- (ii) In partially miscible blends a one blend component is dispersed in the other. This type of blend exhibit fine phase morphology and good interfacial adhesion. Both blend phases are homogeneous and have independent  $T_g$ . But both  $T_{g,s}$  are shifted from the values for the pure blend components towards the  $T_g$  of the other blend component.
- (iii) Immiscible blends have a coarse phase morphology with sharp and poor adhesion between both blend phases. Both phases exhibit the  $T_g$  of the pure blend components and these blends are useless without being compatibilized.

For an immiscible polyblend, property of interest ‘P’ of the polymer is given by equation 1.2.

$$\frac{P}{P_1} = \frac{1 + AB\phi_2}{1 - B\phi_2} \dots\dots\dots(1.2)$$

where  $\phi_2$  is the concentration of the dispersed phase. The value of A varies between 0 and  $\infty$  depending upon the shape and orientation of the dispersed phase as well as on the nature of the interface and B depends on the properties  $P_1$ ,  $P_2$  and A.  $\psi$  is the reduced concentration term that is a function of maximum packing fraction; for  $A \rightarrow 0$ , the dispersed phase is soft and  $A \rightarrow \infty$ , the dispersed phase is hard<sup>9</sup>.

From a thermodynamic point of view, the phase stability of polymer systems is defined by equation 1.3.

$$\Delta G^M = \Delta H^M - T\Delta S^M \dots\dots\dots(1.3)$$

Where  $\Delta G^M$  is the Gibbs free energy of mixing,  $\Delta H^M$  is the enthalpy of mixing and  $\Delta S^M$  entropy of mixing, respectively, T is the absolute

temperature<sup>10</sup>.  $\Delta S^M$  for mixing of high molecular weight polymers is very low and the thermodynamic factor contributing to the miscibility of polymers is  $\Delta H^M$ <sup>11</sup>. For a miscible blend,  $\Delta H^M$  has a negative value and there exist some specific interactions like dipole-dipole interactions, ion-dipole interactions, hydrogen bonding, acid-base reactions, charge transfer etc. between the polymers<sup>12</sup>.

#### **1.4 Methods of compatibilization**

Most of the polymer blends are immiscible and often require to be compatibilized. Compatibilization is a method of modification of the interfacial properties of an immiscible polymer blend to reduce the interfacial tension. Compatibilization result in the stabilization of the preferred morphology with enhanced adhesion between the phases<sup>13</sup>. Compatibilization is accomplished either by physical compatibilization or by reactive processing. Different approaches lead to blends with different sets of morphology and properties. Control of the phase morphology during blend processing is a crucial step for the production of novel materials with improved properties compared to the blend constituents. The shape, size and spatial distribution of the phases result from a complex interplay between viscosity of the phases, interfacial properties, processing conditions and blend composition<sup>14</sup>.

##### **1.4.1 Physical compatibilization**

The most popular method of physical compatibilization (non reactive compatibilization) is the addition of block, graft or random copolymers as compatibilizers. It is not necessary for the copolymer to have identical chain segments as those of the main polymers but enough to have segments with specific interactions between the main polymeric components.



### 1.4.1.1 Compatibilization by block copolymers

Addition of a block copolymer reduces the interfacial tension and alters the molecular structure at the interface mainly by preventing coalescence of the dispersed phases<sup>15</sup>. The enhancement of adhesion between the two phases can be accomplished by the copolymer that migrate to the interface. The copolymers exhibit a tendency to form micelles that often leads to the reduced efficiency of the compatibilizer, viscosity increase in the blend and poor mechanical performance. Hence they should be designed in such a way as to maximize miscibility of the blend components and to minimize copolymer concentration in the blend<sup>16</sup>. Figure 1.4 represents a schematic picture of the conformation of diblock and triblock compatibilizer molecules at the interface of a heterogeneous blend of polymers A and B. If each block of a compatibilizer penetrates the parent phase (A and B, respectively) deeply enough to be entangled with the constitutive chains, good interfacial adhesion is accomplished. This will enhance stress transfer between the phases.

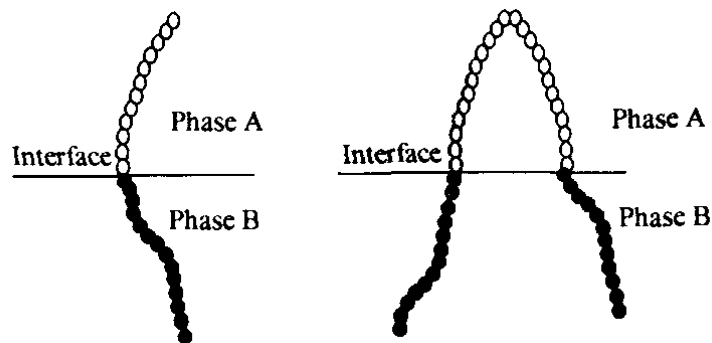


**Figure 1.4. Schematic picture of the conformation of diblock and triblock compatibilizer molecules at the interface of a blend of polymers A and B**

Several investigations have been reported on the compatibilization of block copolymers in polymer blends. Cigana *et al.*<sup>17</sup> investigated the compatibilizing efficiency of poly(styrene-hydrogenated butadiene) tri,di block copolymer on PS/EPR (ethylene propylene rubber) blend. They established that symmetrical diblock copolymers prefer to be at the interface while asymmetrical diblock copolymers are less efficient as they tend to form micelles. Sundararaj *et al.*<sup>18</sup> reported that the addition of compatibilizers to polymer blends resulted in the suppression of the coalescence rate. The interface of compatibilized blend consists of a layer of copolymer that stabilize the dispersed phase against coalescence and can be schematically represented as in Figure 1.5. The interface does not necessarily need to be saturated with diblock copolymer. Only copolymer amount needed to provide enough steric interactions to prevent droplets from coalescing is required.

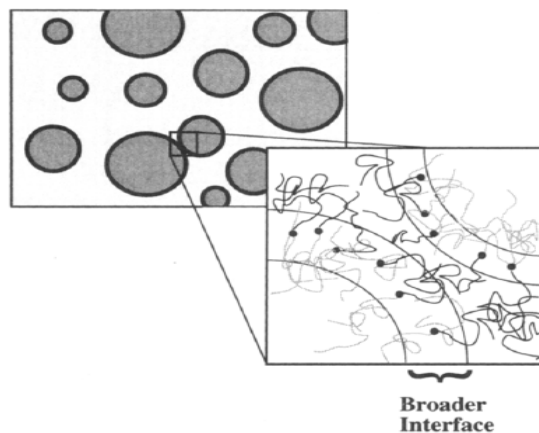


**Figure 1.5. Schematic representation of suppression of coalescence by the layer of diblock at the interface as the copolymer molecules form shells around the drops.**

(Adapted from *Macromolecules*, 28(8), 2647-2657)

The influence of addition of SBS and SEBS triblock copolymers on the morphology of PP/PS immiscible blend was carried out by Macaubas and Demarquette<sup>19</sup>. The morphology of PP/PS/SEBS blend displayed a morphology consisting of droplets of PS encapsulated by SEBS. In PP/PS/SBS blends, morphological studies revealed that SBS tend to segregate as a third phase. The two different morphologies are as represented in Figure 1.6

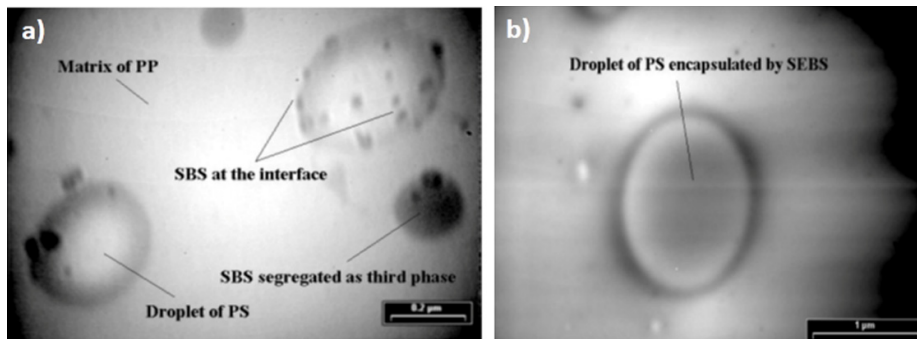


**Figure 1.6. Transmission electron photographs of compatibilized (a) PP/PS/SBS (90/10/0.25) blend. (b) PP/PS/SEBS (90/10/0.25)blend.**  
(Adapted from Polymer, 42(6), 2543-2554)

Investigations by Rek *et al.*<sup>20</sup> on the morphology of atactic polystyrene/high density polyethylene (aPS/HDPE) blends compatibilized by SEBS revealed the existence of SEBS interface layer between the PS and HDPE phase. They reported lower interfacial tension and better adhesion between the phases. The fracture and yielding behaviors of PS/EPR compatibilized by two triblock copolymers of SEBS of different molecular weights, have been investigated by Haanh *et al.*<sup>21</sup>. The study on brittle-ductile transition in fracture of the blend showed that brittle-ductile

transition temperature decreased with the addition of SEBS and is much pronounced for the lower molecular weight compatibilizer.

#### 1.4.1.2 Compatibilization by Graft copolymers

The addition of a graft copolymer is an alternative to compatibilization by a block copolymer. Many studies on the compatibilization of polymeric using graft copolymer as the compatibilizing agent are reported in literature<sup>22-26</sup>. The compatibilizing action of the graft polymer is by locating at the interface preventing coalescence and is schematically represented in Figure 1.7.

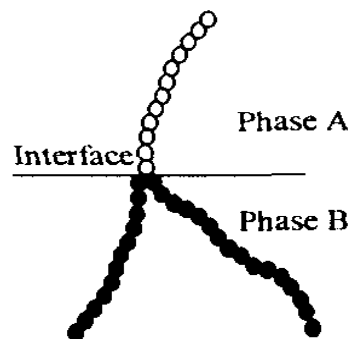


**Figure 1.7. Schematic picture of the conformation of graft copolymer at the interface of a blend of polymers A and B**

Ezzati *et al.*<sup>22</sup> have established that the compatibility between EPDM and PP can be improved by the addition of maleated EPDM (EPDM-g-MAH) and maleated PP (PP-g-MAH) as compatibilizers on PP/EPDM blend. The compatibilizer forms a brush-like structure between matrix and disperse chains leading to better dispersion and stabilization of the blend

morphology. This phenomenon is shown schematically in Figure 1.8 for compatibilized PP/EPDM blend.

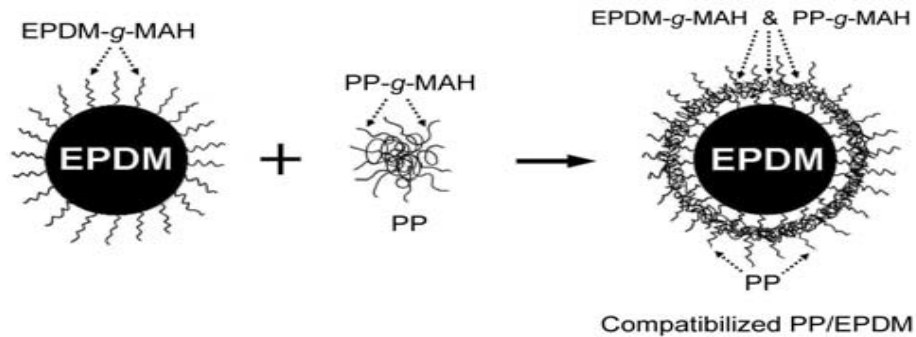


**Figure 1.8. Schematic representation of brush-like for compatibilized PP/EPDM**  
(Adapted from Iran. Polym. J, 17(9), 670-679)

George *et al.*<sup>23</sup> used Phenolic-modified polypropylene (Ph-PP) and maleic-anhydride-modified polypropylene (PP-g-MAH) as compatibilizers in PP/NBR blends and established that mechanical, morphological and viscoelastic properties improved on compatibilization. They proposed that upon compatibilization of an immiscible blend, the compatibilizer will locate at the interface between the dispersed phase and the matrix and prevent coalescence of dispersed NBR domains. They observed that the size of the NBR domains decreased and viscosity increased as the concentration of compatibilizer increased. A levelling-off at higher concentration for both domain size and viscosity was reported and this was attributed to interfacial saturation, above which the compatibilizers form micelles in the continuous PP phase. It is often preferable to obtain a graft copolymer *in situ* by means of a proper chemical reaction than adding it separately and this method offers the widest application of graft copolymers as compatibilizers.

#### 1.4.1.3 Compatibilization by random copolymers

Lyatskaya *et al.*<sup>24</sup> recently examined the efficiency of interfacial tension reduction of compatibilizers such as random, alternating, and diblock copolymers and they established that long random copolymers are more effective than short diblocks of different molecular weight. Investigations by Winey *et al.*<sup>25</sup> demonstrated that relatively small difference in monomer sequence distribution is adequate to change the isothermal ternary phase behavior in blends of poly(styrene-co-methyl methacrylate), poly-(methyl methacrylate), and polystyrene. The two copolymers investigated were having comparable compositions (48-50 mol % methyl methacrylate monomer units) but different sequence distributions, namely alternating and random. Studies on blends of polystyrene (PS)/poly(methyl methacrylate) (PMMA) using a random copolymer of styrene and methyl methacrylate (SMMA) as compatibilizer was carried out by Lee *et al.*<sup>26</sup>. They reported that SMMA moves to the interfaces between PS and PMMA domains during melt mixing and the size of the dispersed phase is reduced significantly. When SMMA is used in excess, it forms a third phase. However, the characteristic size of the dispersed phase increased gradually with annealing time for all the blend systems studied and hence they proposed further investigation for the establishment of efficiency of encapsulating layer of SMMA against static coalescence.

#### 1.4.2 Reactive compatibilization

Reactive compatibilization could lead to the *in situ* formation of compatibilizer through crosslinking, grafting, or some other reactions. Reactive compatibilizers used can be grafted polymers, block copolymers, having reactive functional groups that form *in situ* copolymers by the reaction of reactive groups of the polymer in the blend. A reactive compatibilizer, cannot act as a real compatibilizer before reaction, because it tends to dissolve preferably in one phase during melt blending. This method can be applied to

systems in which at least one component contains functional groups that can interact with the reactive compatibilizer. Alternately, functionalization of one or both blend components, avoiding the addition of a third component can also be considered. In reactive compatibilization, the micelle formation in the phase is minimum since the compatibilizer can localize in the phase and suppress the coalescences. The enhanced interfacial adhesion leads to the development of a stable and fine morphology.

Blend components containing reactive functional groups such  $-NH_2$  of polyamides, the  $-COOH$  and  $-OH$  groups of polyesters more suitable for *in situ* compatibilization<sup>27</sup>. Maleic anhydride grafted polypropylene (PP-g-MAH) has been used as a compatibilizer in various immiscible polymer pairs. Haddout *et al.*<sup>28</sup> established that the viscosity of Polyarylamide/Polypropylene (PA/PP) blends increased upon compatibilization using PP-g-MA. They established that the increase in viscosity can be attributed to the reduction in average size of the dispersed phase and the better adhesion between the two phases in presence of a compatibilizer. Acrylic acid grafted polypropylene (PP-g-AA) have also been used as a compatibilizer in PP/PA blends. Reactive ternary blends of i-PP/PP-MAH/SBS-MAH with varying diamine /anhydride molar ratios were studied by Wilhelm *et al.*<sup>29</sup> and they established optimum improvement in the mechanical properties when the diamine/anhydride molar ratio in the ternary reactive blends was 0.5/1. The effects of compatibilization on the ternary reactive blends (PP/PP-g-AA/SEBS-g-MA/p-phenylene-diamine (PPD)) was studied by Bassani *et al.*<sup>30</sup> showed up to a 30-fold increase in impact strength than neat PP. They proposed that reaction of the bifunctional compound (PPD) with the acid acrylic and maleic anhydride groups rendered both morphological and mechanical stability to these blends and is demonstrated as shown in the Figure 1.9.

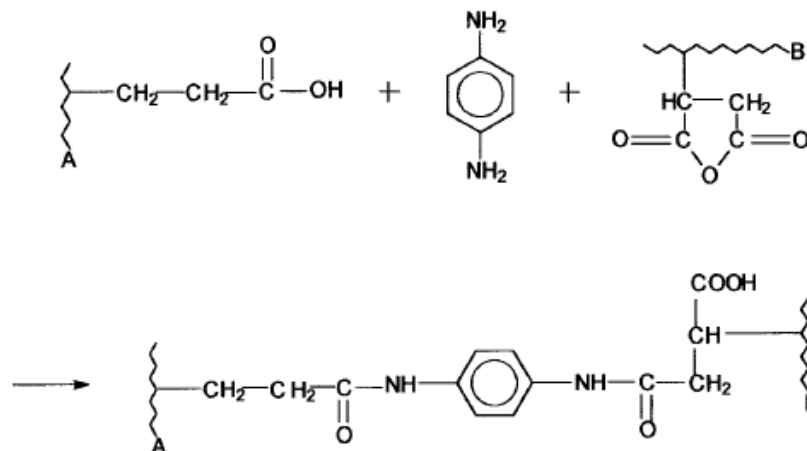


**Figure 1.9.** The proposed reaction between the bifunctional compound (PPD) with the acid acrylic and maleic anhydride group (where (A) represents the chain of PP and (B) the chain of SEBS)  
(Adapted from Journal of applied polymer science, 86(14), 3466-3479)

## 1.5 Polypropylene/rubber blends

Among the different types of TPEs, thermoplastic olefins (TPOs) prepared from physical blends of thermoplastic and rubber are widely accepted. They can be easily prepared by melt blending technique and are an important class in automotive industry due to its low cost, low density and excellent weatherability. In TPOs, where thermoplastic polymer forms the matrix and uncrosslinked elastomer forms the dispersed phase, the toughness of the matrix is usually improved by the dispersed rubber particles.

Polypropylene (PP) is the most versatile thermoplastic polymer with wide variety of applications among the available polyolefin polymer matrices. But the brittle nature and low impact strength limits its application. So in order to improve the impact strength of polypropylene, it is usually



toughened by blending with elastomers. Ethylene propylene copolymer (EPR), ethylene propylene diene monomer (EPDM), styrene butadiene styrene (SBS), styrene ethylene butadiene styrene (SEBS) and Natural rubber (NR) and Polybutadiene (BR) are the most commonly used elastomers to toughen the polypropylene matrix<sup>31-35</sup>.

To improve the impact strength of PP and extend its scope of applications, extensive studies on toughening of PP with elastomers have been reported. The most common and commercially utilized blends of polyolefins involves polypropylene and ethylene propylene diene monomer (EPDM)<sup>36</sup>. EPDM has been added to polypropylene to improve the impact strength of PP for over a decade and is very well document in literature<sup>37-46</sup>. The dynamic mechanical and impact properties of PP/EPDM blends studied by Karger *et al.*<sup>37</sup> established that the impact strength of PP got increased when the melt viscosity of the incorporated EPDM was close to that of PP. The mechanical fracture and ductile-brittle transition (DBT) behavior of PP/EPDM blends were investigated by Lu *et al.*<sup>38</sup>. The studies revealed that the tensile yield stress and Young's modulus decreased with the increase of the EPDM content. They reported that the toughening mechanism of the PP/EPDM blends involve extensive plastic deformation and localized shear yielding of the PP matrix, both initiated by the rubber particles. Studies carried out by Da Silva *et al.*<sup>39</sup> on PP/EPDM blends demonstrated that as the EPDM content was increased, the impact strength of EPDM/PP blends increased while the tensile strength and Young's modulus decreased. They reported that the elongation at break increased but showed a slight decrease at 50/50 composition.

PP/EPDM blends are immiscible blends and are usually compatibilized using maleic anhydride-g-ethylene-propylene-diene monomer (MAH-g-

EPDM), maleated PP (PP-g-MAH), SEBS, SEBS-g-MA. The comparison of the mechanical properties between PP/EPDM and PP/MEPDM(MAH-g-EPDM) was made by Zhao *et al.*<sup>40</sup>. The results revealed that PP/MEPDM showed higher Izod impact strength but lower Young's modulus than PP/EPDM blend. The blend PP/MEPDM shows a much finer dispersion of elastomer particles than PP/EPDM due to part crosslinking nature of MEPDM, which may prevent the elastomer particles from recombining. The finer elastomer particles promoted plastic deformation of the matrix during fracture, thereby leading to higher impact strength for PP/MEPDM than PP/EPDM blend. The morphologies of the impact fracture surfaces for the two blends are quite different as shown in Figure 1.10.

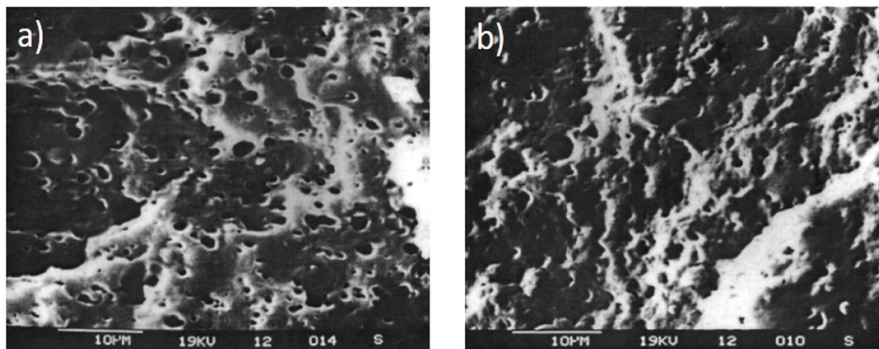


**Figure 1.10. SEM photographs of the impact fracture surfaces: (a) PP/EPDM; (b) PP/MEPDM.**

(Adapted from Journal of applied polymer science, 86(10), 2486-2491)

Investigations were carried out by Purnima *et al.*<sup>41</sup> on PP/EPDM binary blends and PP/EPDM-g-MAH binary blends at constant degree of grafting and at varying blending ratios. The results revealed that MAH grafting of EPDM enhanced the interfacial adhesion leading to improved mechanical properties of the PP/EPDM-g-MAH blends than the PP/EPDM blends. DSC studies revealed that the presence of EPDM chain restricted the

chain mobility of PP thereby reducing the nucleation rate. The effect was more pronounced for PP/EPDM-g-MAH due to improved interfacial adhesion leading to decreased crystallinity.

The effects of compatibilizers on the dynamic rheological behaviour with and without dynamic vulcanization in PP/EPDM blend containing 20% EPDM was studied by Ezzati P *et al.*<sup>22</sup>. Maleated EPDM (EPDM-g-MAH) and maleated PP (PP-g-MAH) were used as compatibilizers. It was established that the fine dispersion of EPDM droplet can be obtained with combination of dynamic vulcanization and compatibilization. The processability and flow properties of thermoplastic elastomers based on blends of PP/EPDM blends carried out by Miguel *et al.*<sup>42</sup> established that a general processing behavior similar to that of PP can be adopted for blends with low content of EPDM.

Investigations on thermoplastic elastomers based on polypropylene/natural rubber (PP/NR) and polypropylene/recycle rubber blends (PP/RR) made by Ismail *et al.*<sup>43</sup> revealed that PP/RR blends need greater energy to cause failure than PP/NR blends. Blends of PP and TPEs such as SBS and SEBS block copolymers were studied by Abreu *et al.*<sup>44</sup> to understand the effectiveness and influence of the concentration of the TPE type as an impact modifier for PP. The studies established that SEBS is a more effective toughening agent for PP than SBS. Evaluation of mechanical properties of PP/SEBS blends were carried out by Balkan *et al.*<sup>45</sup>. The morphological analysis revealed that SEBS elastomer particles were well-dispersed throughout PP matrix in irregular forms displaying a two-phase system formation. Studies on impact behavior of PP/SEBS blends were carried out by Gupta *et al.*<sup>46</sup>. They demonstrated that with 15% SEBS incorporation, the increase in the impact strength of PP was about tenfold

at -30 °C, twofold at -190 °C and no appreciable improvement at ambient temperature. The observed large difference of toughening was attributed to the different mechanisms of toughening.

## 1.6 Toughening mechanism in rubber toughened polypropylene

The toughening mechanism in rubber toughened thermoplastic has been widely investigated by many researchers<sup>47-50</sup>. For PP/rubber blends the relevant toughening mechanism depend on the distribution of rubber particles, interfacial adhesion between the matrix and the rubber phase and the testing conditions<sup>51</sup>. Investigations on PP/rubber blends made by Wu<sup>52</sup> clearly established that the improvement in toughness of a matrix is mainly by the dissipation of energy by the rubber particles which in turn is related to the phase morphology of the blend. Generally plastic/rubbers blends exhibits phase separation with rubber particles forming spherical domains in the thermoplastic matrix. Hence size and volume fraction of rubber particles play a major role in deciding the toughening mechanism. Jang *et al.*<sup>53</sup> showed that particles with smaller sizes were found to be more effective than particles with larger size for toughening PP. Larger particle size also have been reported to favor rubber particle cavitation, one of the factors responsible for shear yielding. When a semi crystalline thermoplastics like PP is modified with rubber, processing and testing conditions strongly influence the toughening mechanisms. For PP/rubber blends, high test rates and low temperature favors crazing while low test rates and high temperature favors shear yielding. It has been established that brittle polymer systems like PS and PMMA undergo crazing in the matrix and ductile polymers like PP experience shear yielding<sup>54</sup>.

The improvement in toughness of a matrix can be explained by the influence of rubber particles on the deformation mechanisms in the blends or by the change of blend microstructures on rubber addition. There are various toughening mechanisms postulated by different researchers and it appears that the major theories interpreting the toughening mechanisms of these blends are shear-yielding theory, multiple-crazing theory, and formation of dilatational bands following rubber cavitation or debonding from the matrix.

### 1.6.1 Matrix shear yielding and particle cavitation

Several aspects on the mechanism of toughening in rubber toughened polyolefins had been reviewed by Panda *et al.*<sup>51</sup> and the important toughening mechanism was identified to be localized shear yielding of the matrix due to stress concentration at the rubber particles initiated by rubber cavitation or debonding. Lu *et al.*<sup>38</sup> showed that toughening mechanism of PP/EPDM blends is mainly due to extensive plastic deformation and localized shear yielding of the PP matrix, both initiated by rubber particles. It has been proposed that when a rubber-toughened plastic is subjected to external loading, cavitation may start at early stage of deformation. If the interfacial adhesion is strong, cavitation may take place inside rubber particles and if the adhesion between rubber particles and matrix is relatively poor, interfacial debonding can occur<sup>55</sup>.

Muratoglu *et al.*<sup>56</sup> proposed the toughening mechanism to be cavitation of the rubber particles followed by large plastic deformation and thereby improved toughness. When the rubber particles cavitate, the resulting holes enlarge and stress whitening will increase. The shear yielding matrix leads to refractive index change, which contributes to stress whitening. Yee and Pearson<sup>57</sup> concluded that cavitation is a crucial

condition for subsequent plastic yielding. Guild and Bonfield<sup>58</sup> suggested that cavitation and matrix shear yielding are two independent processes. Huang and Kinloch<sup>59</sup> also proposed the same mechanism. Investigations made by Chen and Mai<sup>60</sup> on the different toughening mechanisms of rubber modified blends has led to the conclusion that rubber cavitation and matrix shear yielding are two co-existing mechanisms.

Poncot *et al.*<sup>61</sup> proposed that the plastically deformed and damaged sample is a composite system described by two distinct phases such as matrix and cavities as shown in Figure 1.11. They considered three main cavity morphologies in uniaxially stretched polymers which can be illustrated in Figure 1.12. They suggested the growth of cavities in the stretching direction with a slight closure of the width of cigar-like shapes, attributed to a highly fibrillar microstructure.

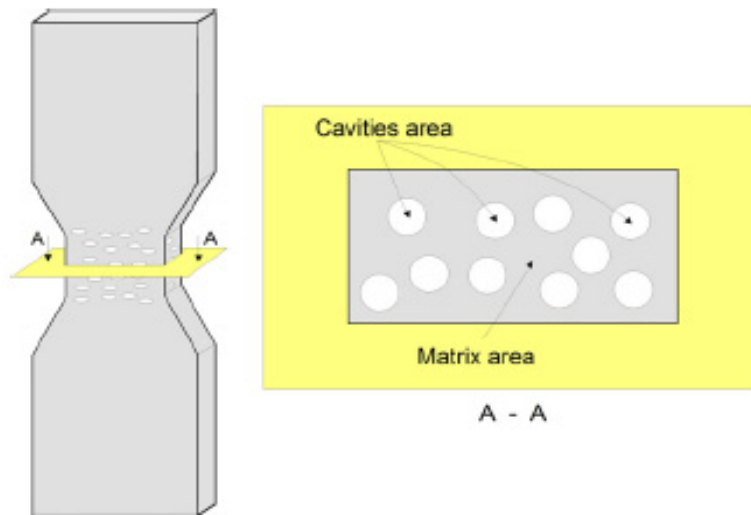


**Figure 1.11. Damaged samples considered as a two-phase system**  
(Adapted from International Journal of Plasticity, 40, 126-139)

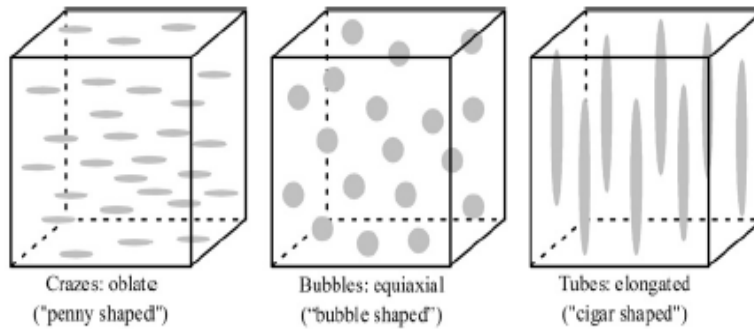


**Figure 1.12. Three main cavities morphologies observed in uniaxial stretching.**  
(Adapted from International Journal of Plasticity, 40, 126-139)

Bartczak and Grala<sup>62</sup> investigated the toughening of semicrystalline and amorphous polylactide with atactic Poly(Hydroxy Butyrate)( PHB) and internal cavitation of  $\alpha$ -PHB particles accompanied by plastic deformation of matrix ligaments between  $\alpha$ -PHB inclusions has been established. They proposed that in the case of strong deformation of matrix ligaments the cavities get an elongated sausage-like shape and elongated cavities, indicating plastic deformation of the matrix as shown in Figure 1.13.

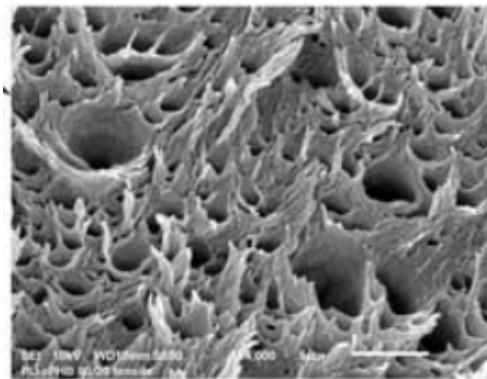


**Figure 1.13. SEM photographs of the fracture plane of tensile specimens indicating a ductile fracture**  
(Adapted from Polymer-Plastics Technology and Engineering, 56(1), 29-43)

Zebarjad *et al.*<sup>63</sup> investigated the role of rubber particles on deformation mechanisms in PP/EPR blends and concluded that the deformation mechanism in the blend can be massive dilatational shear banding due to repeated cavitation of rubber particles. For the PP blends studied in this article, the observed craze like structures in the SEM photographs appear to be highly localized dilatational shear bands and are as shown in the Figure 1.14.

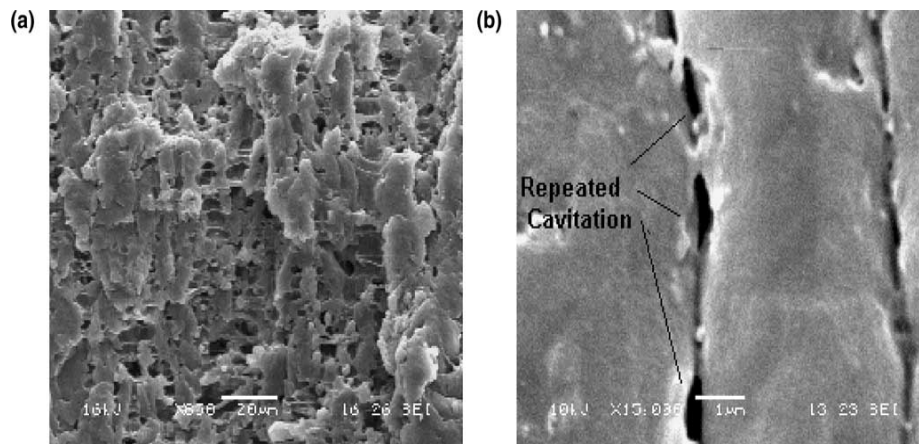


**Figure 1.14. SEM photographs of the surfaces of a tensile specimens of PP/EPR fractured blend along the draw direction showing (a) elongated voids and (b) repeated cavitation**

(Adapted from Journal of applied polymer science, 90(14), 3767-3779)

It can be summarized that during the deformation of rubber-modified PP, the sample starts to cavitate inside the rubber particles around the yield point under the application of strain. The matrix undergoes large deformations resulting in fine fibrillation of the matrix and the cavities elongate in the direction of the applied stress as the deformation progresses<sup>55,64</sup>. These observations can be summarized as shown in the Figure 1.15.



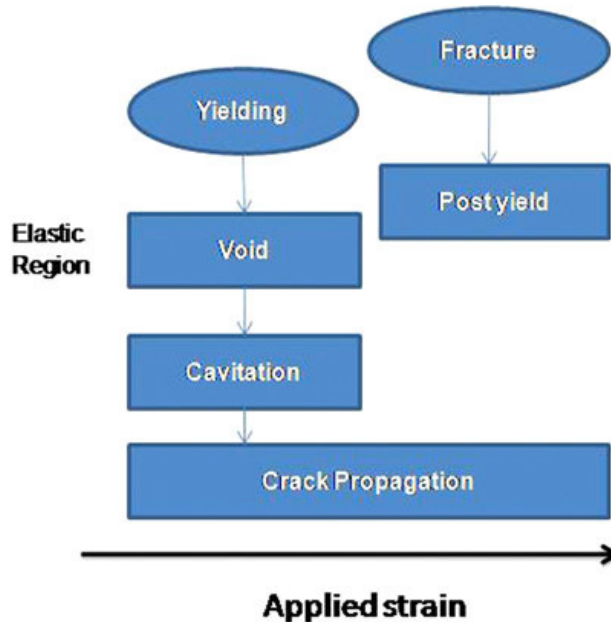


**Figure 1.15. Schematic diagram showing deformation mechanism in rubber-modified PP**

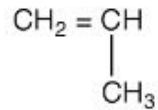
(Adapted from Polymer-Plastics Technology and Engineering, 54(5), 462-473)

## 1.7 Thermoplastic elastomers from polypropylene/polybutadiene (PP/BR) blends

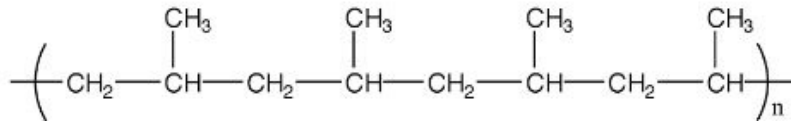
### 1.7.1 Polypropylene (PP)

The moderate cost and favorable properties of polypropylene contributes to its numerous applications. Polypropylene is a versatile thermoplastic compatible with common processing techniques and is one of the lightest of all thermoplastics with better heat resistance and resistance to most organic solvents<sup>65,66</sup> Polypropylene is produced by polymerization of propylene ( $\text{CH}_2=\text{CH}-\text{CH}_3$ ). Depending on the polymerization process, PP can be isotactic (iPP), in which all methyl groups are at the same side of the backbone of the polymer chain, syndiotactic (sPP), in which the methyl groups are present on alternate sides with respect to the backbone of the

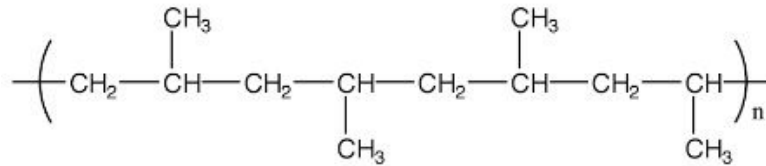
polymer chain, or atactic (aPP), in which the methyl groups are present in a random configuration as shown in Figure 1.15. Only iPP has the requisite properties for a thermoplastic material.



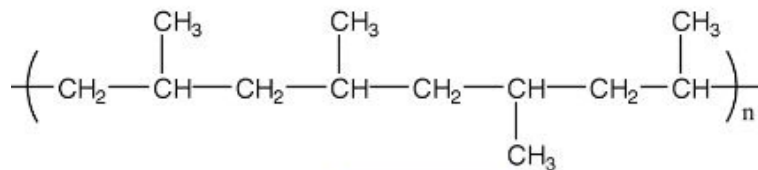
Polypropylene monomer



Isotactic polypropylene



Syndiotactic polypropylene



atactic polypropylene

**Figure 1.16. Tacticity of polypropylene**

### 1.7.2 Polybutadiene (BR)

Polybutadiene is a synthetic rubber formed from the polymerization of the monomer 1,3-butadiene in solution using a coordination catalyst based on transition element like cobalt, nickel, neodymium or titanium. There are 4 stereoregular forms of polybutadiene rubber. They are cis-1,4-polybutadiene, trans-1,4-polybutadiene, isotactic 1,2-polybutadiene and syndiotactic 1,2-polybutadiene. Cis-1,4-polybutadiene is preferred for rubber use than trans-1,4-polybutadiene as it has high melting point that inhibit elastic nature. Isotactic 1,2-polybutadiene and syndiotactic 1,2-polybutadiene are not rubbery materials. Commercial materials are not 100% stereoregular and often result in a combination of polymers. They are classified as highcis-1,4-polybutadiene (96 %), medium cis (92%) and low cis (40%). The structural units are represented in Figure 1.17

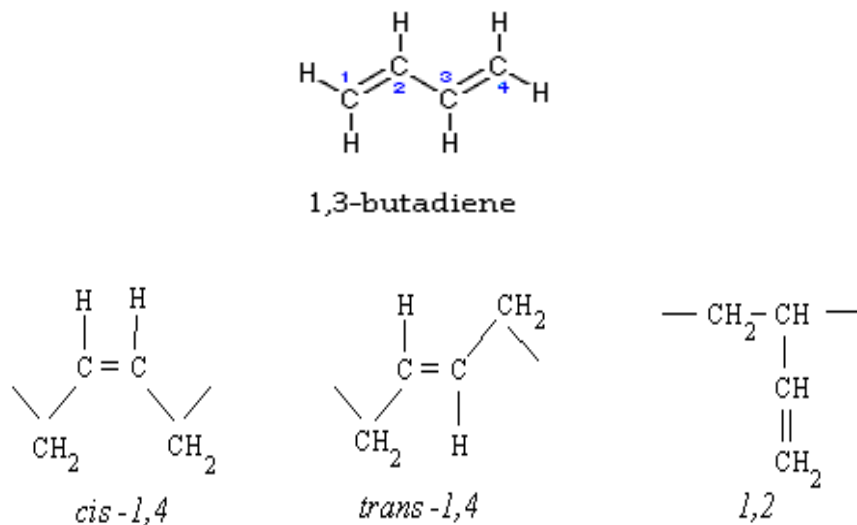


Figure 1.17. Structural units of polybutadiene

Polybutadiene is largely used in various parts of automobile tires and the manufacture of tires consumes about 70 % of the world production of polybutadiene. It has high resilience, resistance to wear and a low rolling resistance. The reasonable resistance of BR to ozone and its good oxidation and chemical stability makes it a suitable substitute for NR in many applications. BR resist break down by mechanical shear and is capable of accepting large amount of oil and black<sup>68</sup>.

### 1.7.3 PP/BR blends

Very few investigations based on PP/BR blends are available to our knowledge and the results are reported in this study. Crystallization, tensile, and impact behavior of PP/BR blend prepared by mixing in a two-roll mill followed by compression molding was investigated by Gupta *et al*<sup>69</sup>. A two-phase morphology with good dispersion of spherical or elliptical BR droplets in PP matrix was established. The rates of nucleation and crystallinity were found to higher in the blend than in PP. The changes in the crystallization behavior with varying BR content was attributed to the morphology of dispersed phase. Addition of 5 wt % BR improved the impact strength of PP by a factor of 1.5 and tensile properties decreased with increasing BR content. Theoretical analysis of yield stress data revealed discontinuities in stress transfer due to stress concentration effect.

Crystallization and phase behavior in solution-cast thin films of crystalline syndiotactic 1,2 polybutadiene (s-1,2-PB) and isotactic polypropylene (i-PP) blends have been investigated by Chen *et al*.<sup>70</sup>. Sheng *et al*.<sup>71</sup> investigated pressed films of blends of polypropylene with poly(cis-butadiene) rubber (PcBR) or grafted copolymer of ethyl acrylate (EA) onto PcBR (PcBR-g-EA).

## 1.8 Polymer nanocomposites

Nanotechnology is one of the promising area of academic and industrial research as its nanoscale dispersion in the polymer matrix leads to enhanced mechanical properties accompanied with weight reduction. Polymer nanocomposites are normally defined as particle filled polymer matrices in which one of the phases are at least in 1-100 nanometer range in one dimension.

### 1.8.1 Nanofillers

The particles in the range 1-100nm is usually referred to as nanoparticles and the unique feature is their high surface area to volume ratio. Three types of nanofillers have been distinguished on the basis of their dimensions and are (i) One dimensional nanofillers which include nanotubes, nanofibres and nanowires (ii) Two dimensional nanofillers such as nanoclays and graphene (iii) Three dimensional nanofillers such as spherical and cubical nanoparticles<sup>72,73</sup>. The schematic representation of the three types of nanofillers can be represented as in Figure 1.18.

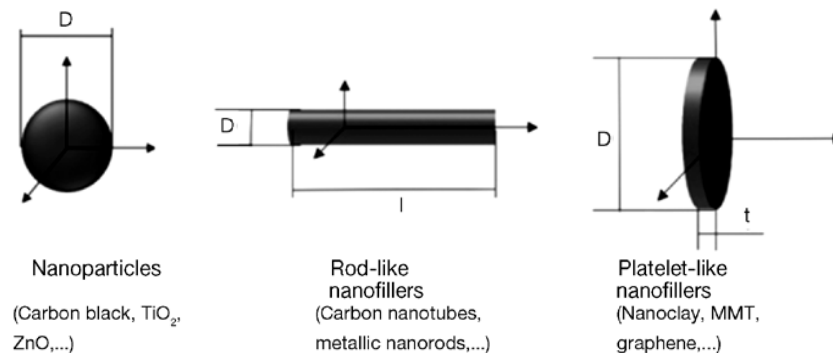


**Figure 1.18. Schematic representation of various types of nanofillers**  
 (Adapted from Cellular Polymers, 30(2), 45)

Particles that are commonly added to the polymer matrices to enhance strength and modulus include silica and alumina particles. Carbonaceous nanofillers such as nanotubes and graphene display excellent properties due to their high mechanical strength and high aspect ratio. Graphene is a two-dimensional single atom thick sheet composed of  $sp^2$  carbon and can be considered as a fundamental building block for all  $sp^2$  hybridized carbon allotropes. It can be wrapped up into 0D fullerenes, rolled into 1D nanotubes or 3D graphite when a number of graphene layers stack up. Research on carbon nanofibres (CNFs) have received less attention than Carbon nanotubes (CNTs) even though CNFs were introduced few years before CNTs. The high Young's modulus and electrical conductivities of CNTs provide better mechanical and electrical properties than CNFs. CNTs have smaller diameter and lower density than CNFs. CNFs are not continuous tubes as the graphene cylinders and they show a  $20^\circ$  angle with respect to fibre axis in a Dixie cup arrangement terminating at the wall of the next outer tube. However, because of their much lower price, CNFs are an excellent alternative for CNTs. Clays are naturally found as platelets and were reported to have Young's modulus ranging between 178 and 265 GPa. These excellent properties of nanofillers make them suitable candidates for reinforcing polymer matrix. Montmorillonite (MMT), is the most widely used clay nanofiller for polymer matrix<sup>73</sup>.

## 1.9 Preparation of the nanocomposites

The ultimate properties of the nanocomposite are dependent on the processing methods. Nanofiller can be dispersed in a polymer matrix using different techniques including in melt blending, solution processing, *in situ* polymerization, spin casting and melt spinning.

### 1.9.1 Melt blending

Melt blending is one of the most economical and environmental friendly methods of preparation of composites. Melt mixing can be carried out using internal mixer, mini-max molder, and chaotic mixer where the polymer and the nanoparticle mixture are heated to form a melt. The mixer imparts shear and elongational stress to the process, helping to break apart the filler agglomerates and dispersing them uniformly in the polymer matrix.

Melt blending technique is considered to be one of the best methods to attain good distribution of CNFs in the polymer matrices, but at the cost of reduction of large aspect ratio. It is reported that melt mixing of Vapour Grown Carbon nanofibre (VGCNF) with high density polyethylene (HDPE) decreased VGCNF aspect ratio from 38 to 23 and with PP, the average length of VGCNF reduced from 20–80  $\mu\text{m}$  to  $10^{74}$ . Hence dispersion of CNFs at low shear by melt blending method without compromising the aspect ratio is still a challenge to the researchers. Researches have shown that functionalization of filler facilitates the dispersion at non-destructive mixing conditions to form CNF/polyolefin nanocomposites<sup>75</sup>.

Polymers /nanoclay composites have been developed by melt blending where exfoliation of clay platelets have attained to a greater extend<sup>76,77</sup>. Stresses generated during melt blending can break up the clay aggregates and the polymer chains are intercalated or exfoliated into the clay galleries. Clays are organically modified and polyolefins without polar groups are modified to enhance their compatibility and to promote exfoliation. Polyolefins modified with maleic anhydride have better properties than unmodified polyolefins.

### 1.9.2 Intercalation of Polymer or Prepolymer from Solution

This method involves the dispersion of nanoparticle in a polymer that is dissolved in a solvent. When the clay particles are dispersed in the solvent, swelling of clay layers take place. When the polymer solution is added to suspended clay, the polymer chains are able to intercalate by displacing the solvent molecules within the clay layers. The intercalation of the polymer chains into the gallery space between the clay layers depends on the polarity of the solvent. The removal of organic solvents by evaporation is not an eco-friendly process. Composites based on modified graphene and polymers have been developed using this method<sup>78</sup>. The development of polymer/clay nanocomposites often uses water soluble polymers, though casting using organic solvent has also been attempted. Grafting of functional group to CNFs is also a favorable method for the dispersion in the polymer matrix. It improves the interaction between the polymer matrix and nanofiller without surrendering the nanofiller aspect ratio. The dispersion of the CNF in mostly epoxy resins to prepare the CNF/thermosetting polymers is mainly by sonication. In order to avoid the temperature increase during the sonication process, external cooling devices are required. The use of solvent makes it an undesirable method for industrial purpose.

### 1.9.3 *In situ* polymerization

The composites that cannot be prepared by solution processing and melt mixing can be prepared by *in situ* polymerization method. Polymerization is initiated by increasing the temperature, adding a chemical that initiates the reaction or by mixing two monomers in the presence of fillers<sup>79,80</sup>. These composites possess improved mechanical properties and lower percolation threshold than the composites developed by melt blending and solution



methods. The major disadvantage of this technique is that the dispersion of fillers into polymer consumes lot of electrical energy thus making it economically nonviable.

### **1.10 Carbon nanofibre as filler for polymer matrices**

Carbon nanofibres are  $sp^2$  based linear filaments with diameter of about 100nm and consisting of regularly stacked conical or planar layers along the filament length. The relatively low cost and the easy incorporation of CNFs into polymers makes CNFs a judicious choice for the production of high performance lightweight materials. A large number of investigations using carbon nanofibres (CNF) have been carried out in several matrices to increase the mechanical, thermal and electrical properties of the composites<sup>81,82</sup>.

Carbon nanofibres (CNF) have been widely used in polymer matrices to improve mechanical, thermal and electrical, and many other properties<sup>83,84</sup>. CNFs can be mainly prepared by two approaches such as catalytic thermal chemical vapor deposition growth method and electrospinning followed by heat treatment. The catalytic thermal chemical vapor deposition grown method of production of CNF involves the pyrolysis of a hydrocarbon or carbon monoxide on a metal catalyst like iron and are known as Vapour Grown Carbon nanofibre (VGCNF). The decomposition of the hydrocarbon result in the growth of nanofibres as shown in Figure 1.19. The thickness of the fibre depends on the size and activity of the catalyst and processing conditions. As the activity of the catalyst decreases and reaction temperature increases thickening of the fibre take place<sup>85</sup>.

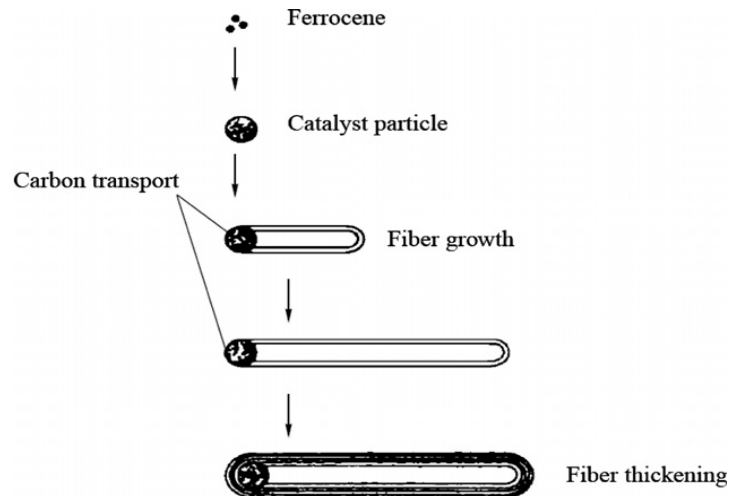


**Figure 1.19. Proposed mechanism for the growth in VGCNF diameter and length**  
(Adapted Composites Part A: Applied Science and Manufacturing, 42(12), 2126-2142)

VGCNF can be of cup-stacked structure or platelet structure as illustrated in the Figure 1.20.(a),(b) (c) and (d)<sup>86</sup>.

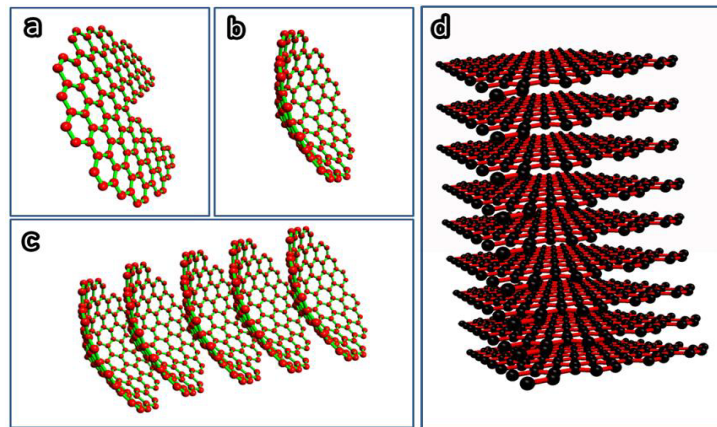


**Figure 1.20. Schematic demonstration of (a–c) formation of cup-stacked CNF structure; and (d) platelet CNF structure**  
(Adapted from Materials, 7(5), 3919-3945)

The most common type of VGCNF is cup-stacked, the structure with more reactive carbon edges that can be functionalized so that dispersion is facilitated and stress transfer from the polymer matrix to the nanofiller is enhanced. VGCNFs have high aspect ratio with diameters in the range of 50–200 nm and length in the range 20–100  $\mu\text{m}$ . They are reported to have Young's moduli in the range 100–1000 GPa and strengths between 2.5 and 3.5 GPa<sup>87</sup>

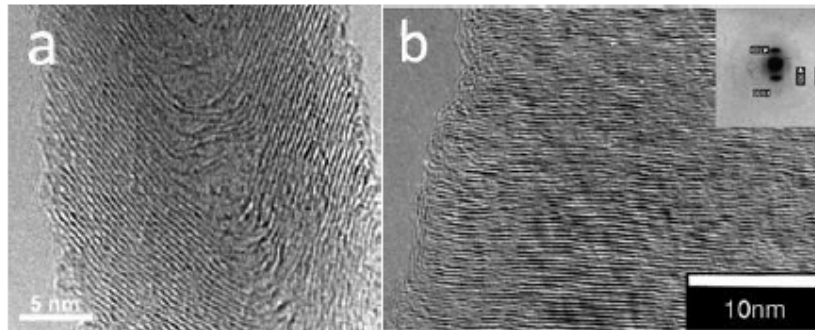


**Figure 1.21. High resolution transmission electron microscope (HRTEM) image of (a) cup-stacked CNF and (b) platelet CNF**  
(Adapted from Materials, 7(5), 3919-3945)

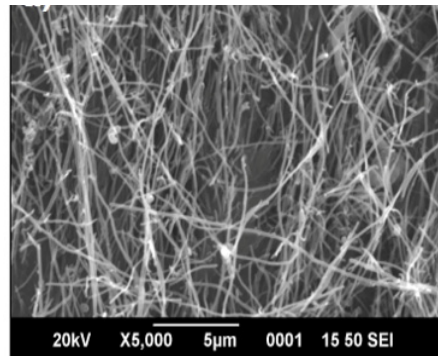


**Figure 1.22. SEM photograph of CNFs**

High resolution transmission electron microscope (HRTEM) image of cup-stacked CNF and platelet CNF is as shown in Figure 1.21. As seen from the SEM photograph in Figure 1.22, CNFs are highly entangled. These interwoven fibres are held together by van der Waals forces and are difficult to distribute uniformly in polymer matrices as they show strong tendency to agglomerate. The enhancement in mechanical properties of VGCNF composites requires good dispersion and distribution of nanofibres in the polymer matrix while sustaining the aspect ratio of nanofibres. Excellent dispersion of filler reduces the stress concentration centers and improves the stress distribution.

### 1.10.1 PP/CNF composites

A large number of PP/CNF composites have been prepared by melt mixing technique and their mechanical, thermal and rheological properties have been studied and reported in literature<sup>88</sup>. Investigations by Tong *et al.*<sup>89</sup> on PP/CNF composites prepared by melt blending reported that CNFs acted as a reinforcing filler to improve the modulus at any loadings but decreased the strength at higher loadings due to poor dispersion. Besides, higher loading is favorable on the crystallization behavior of PP. Ceccia *et al.*<sup>90</sup> investigated the rheological properties of two different PP/CNF systems with different aspect ratio. Linear viscoelasticity studies showed the formation of a network structure for both systems and increase of moduli was more pronounced for the nanocomposite characterized by CNF with larger aspect ratio. TGA investigations on the thermal degradation of PP/VGCNF composites established excellent dispersion of VGCNFs in PP matrix and revealed enhancement of the thermal stability of PP on addition of VGCNFs<sup>91</sup>. Investigations on thermal stability of PP/CNF composite system carried out by Chaterjee *et al.*<sup>92</sup> established that the incorporation

of CNF in PP enhanced the thermal stability of the polymer. Thermal analysis of PP/CNF composites by Lozano *et al.*<sup>93</sup> reported that at a lower concentration of CNF, they act as nucleation sites enhancing the spherulite growth of PP leading to increased crystallinity. When the concentration of VGCFs increased, the fibres started to obstruct the PP chains from obtaining a highly ordered spherulite structure resulting in declined crystallinity. Investigations on the PP/CNF composites prepared via twin-screw extrusion and compression moulding by Paleao *et al.*<sup>94</sup> showed 23% modulus enhancement with addition of CNF. Studies on PP/CNF composites made by Sui *et al.*<sup>95</sup> reported the uniform dispersion of CNF in the PP matrix by means of melt blending with increasing degree of crystallinity of the PP with CNF loading up to 3 wt %. Their studies revealed improved thermal conductivity and electrical conductivity of the nanocomposites with CNF loading.

The electrical conductivity of a polymer nanocomposite depends on the concentration of the conductive filler used. At low filler concentrations, the electrical conductivity of the composite is close to the polymer matrix where the filler particles act like conductive islands in the sea of electrically insulating polymer matrix. Further introduction of fillers, tends the conductive particles to come in contact with each other. At a critical volume concentration (the percolation threshold), most of the filler particles form conductive network. These conductive networks allows electricity to pass easily through a composite, making it electrically conductive<sup>96</sup>. Schematics showing the distribution and dispersion of fillers and the dependence of electrical conductivity on filler volume fraction of the polymer composite is as represented in Figure 1.23 and 1.24, respectively.

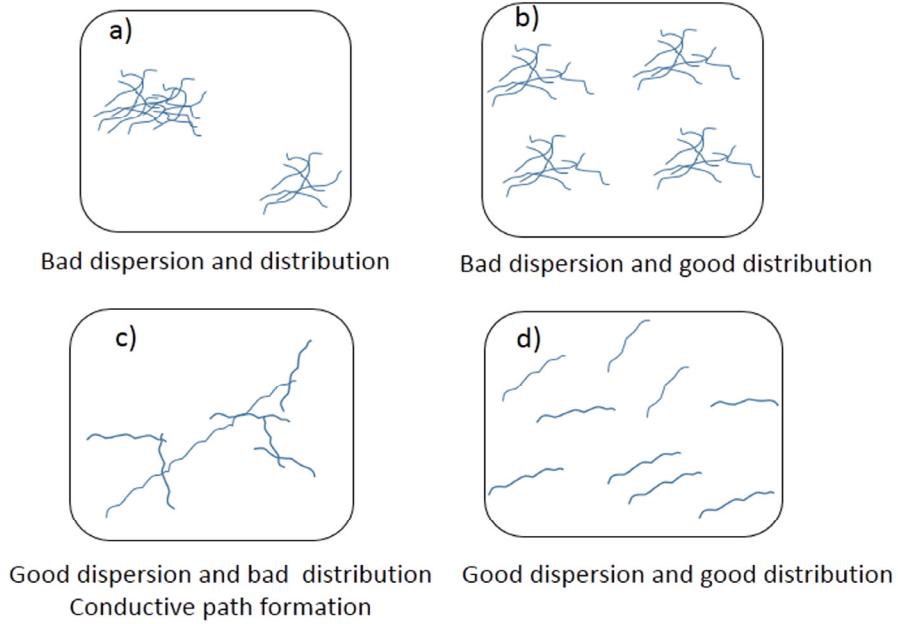


**Figure 1.23.** Schematics representation of distribution and dispersion of fillers

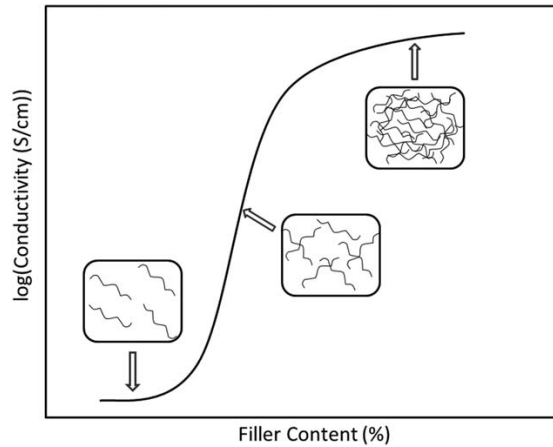


**Figure 1.24.** Dependence of electrical conductivity on filler volume fraction  
(Adapted from Polymer composites, 35(5), 900-914)

### 1.10.2 PP/elastomer/CNF composites

Most of the studies are concentrated on single polymer/CNF nanocomposites only very few reports are available on the properties of CNF reinforced PP/elastomer blends. The introduction of CNF in plastic/rubber blends leads to the development of thermoplastic olefin (TPO) nanocomposites. PP/SEBS-g-MA blends reinforced with low content of CNFs (0.2–2.5 wt%) by Liao *et al.*<sup>97</sup> reported synergistic interaction of CNF with SEBS-g-MA elastomer to toughen PP/SEBS-g-MA. Melt blended binary (PP/PS) and ternary (PP/PS/SEBS) blends and their composites with (CNF) has been studied by P.J. *et al.*<sup>98</sup>. They have reported that PP/PS/SEBS/0.1 wt% CNF hybrid composites exhibited excellent mechanical properties. Evaluation of the mechanical, thermal and crystallization properties of PP/SEBS/CNF composites revealed a dispersion of CNFs in the PP/SEBS interface and in the SEBS phase<sup>99</sup>. The studies also reported that the optimum level of reinforcement was observed at 0.1 wt% of CNF and the thermal stability of composites got marginally improved. The crystallinity of PP got drastically reduced by the addition of CNF. These nanocomposites were reported to exhibit good strength, excellent toughness and modulus suitable for cost effective, light-weight material for high performance applications.

Among the various conductive fillers used for preparing conductive polymers, CNT, CNF and graphene have received greater attention due to their superior functional properties when compared with conventional fillers. The maximum electrical conductivity of PP composites prepared by using various fillers, it can be observed that for PP/CNF and PP/CNT composites, high electrical conductivity could be achieved at low filler loading.

### **1.11 Nanoclay as filler for polymer matrices**

The easy availability, environment friendliness and low cost of nanoclays make them an excellent choice as a nanofiller. Numerous studies have been carried out on various perspectives of nanoclays over the past few decades and most of them are based on (i) synthesis and characterization (ii) development of polymer/nanoclay composites (iii) surface properties and stability and (iv) the use of nanoclays as predecessors for the development of novel materials. The choice for surface modification provides incredible scope for altering the polarity, surface area, interlayer spacing, acidity, and pore size of nanoclay that render them as a resourceful nanofiller in different applications. The ability of clay minerals to delaminate into individual layers, their relevant characteristics that have been extensively exploited in the development of unique nanocomposites. When the layers are delaminated, the structure offers tortuous path for molecular diffusion and reduce the effect of gas and moisture transmission through the film<sup>100</sup>.

Montmorillonite (MMT) has the widest acceptability over other nanoclays for use in polymers due to its natural abundance, well-explored chemistry, high surface area, and surface reactivity. It is a hydrous aluminosilicate clay mineral with a 2:1 expanding layered crystal structure, with aluminum octahedron sandwiched between two layers of silicon tetrahedron as illustrated in Figure 1.25. Each layered sheet is approximately 1 nm thickness, the lateral dimensions of these layers may vary from 30nm to several microns or larger, depending on the particular layered silicate. Each individual MMT layer have a thickness of a few nanometers and lateral dimensions of 200–600 nm. The aspect ratio is about 10–1000 and the aspect ratio of 1000 is possible when a clay platelet is well-dispersed



into the polymeric matrix without breaking. But, during mixing process at high shear and large shear stress condition leads to an aspect ratio of 30–300<sup>77</sup>.

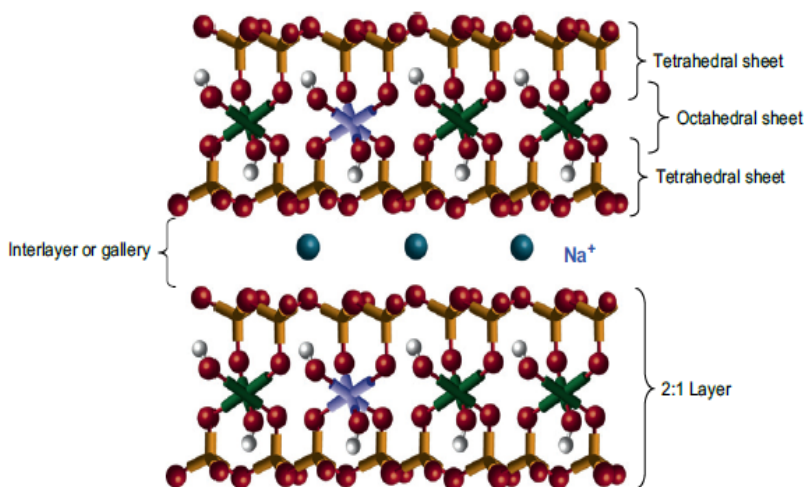
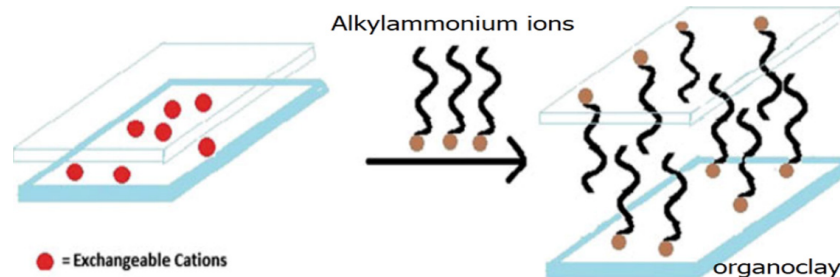


Figure 1.25. Structure of MMT

The pristine clays are hydrophilic and in order to make the clay compatible with hydrophobic polymers, the  $\text{Na}^+$  present in the clay galleries are exchanged with organic cations such as alkylammonium or alkylphosphonium ions. The X-ray d-spacing of dry sodium montmorillonite is 0.96 nm<sup>101</sup>. Modification of layered silicates with alkyl ammonium ions can increase in the d-spacing between the interlayers beyond 2 nm and can be schematically represented as in Figure 1.26<sup>102</sup>. Commercially available clay minerals supplied by Southern clay products (USA) along with surface modifiers are given in table 1.1.



**Figure 1.26. Schematics showing the organophilization of montmorillonite**  
(Adapted from Materials & Design, 46, 391-410)

**Table 1.1. Commercially available clay minerals supplied by Southern clay products<sup>102</sup>**

Nanoclay	Type	Surface-modifier	Modifier concentration (meq/100 g clay)	$d_{001}$ (Å)
Cloisite®Na <sup>+</sup>	MMT	-	-	11.7
Cloisite®10A	MMT	dimethyl, benzyl, hydrogenated tallow, quaternary ammonium	125	19.2
Cloisite®15A	MMT	dimethyl, dehydrogenated tallow, quaternary ammonium	125	31.5
Cloisite®20A	MMT	Dimethyl, dehydrogenated tallow, quaternary ammonium	95	24.2
Cloisite®25A	MMT	dimethyl, dehydrogenated tallow, 2-ethylhexyl quaternary Ammonium	95	18.6
Cloisite®93A	MMT	methyl, dehydrogenated tallow ammonium	95	23.6
Cloisite®30B	MMT	methyl, tallow, bis-2-hydroxyethyl, quaternary ammonium	90	18.5

Organic modification of nanoclay provide surfactants that interact with the polymer matrix and affect the morphology of the nanocomposite. Depending on the strength of the interaction between the layered silicates and the polymer, three morphologies of nanoclay layers in the nanocomposites are obtained. They are (i) immiscible nanocomposites; (ii) intercalated nanocomposites; and (iii) exfoliated nanocomposites. In an exfoliated structure, there will be a high area of interaction between the clay and the polymer, that results in a homogeneous distribution. Even though complete exfoliation of the clay layers is the preferred objective, it is seldom achieved<sup>103,104</sup>. This distribution can be schematically represented as in Figure 1.27.

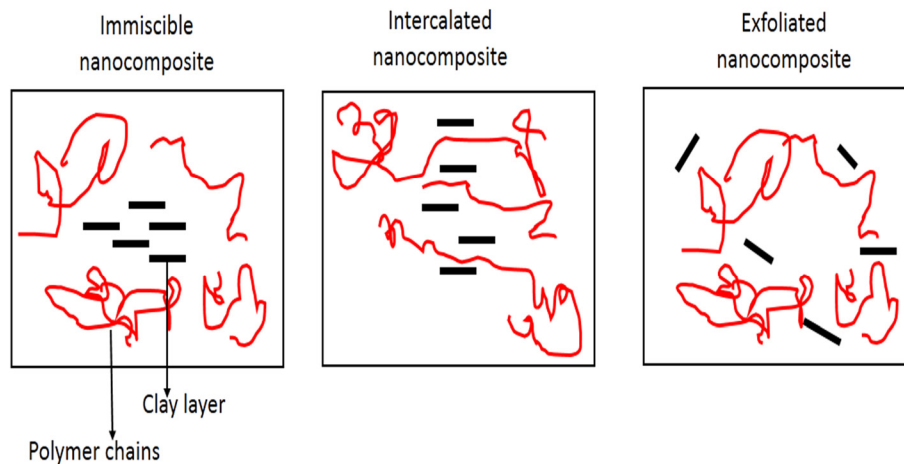


**Figure 1.27. Schematic distribution of nanoclay in polymer composites**

Among the different techniques used to characterize the nanocomposite structure, the two widely used methods are transmission electron microscopy (TEM) and XRD or wide angle XRD (WAXD). The XRD method is based on the measurement of interlayer distances between the silicate layers in the

nanoclay by using Bragg's law. The distribution of nanoclay in polymer/nanoclay composites can be identified from XRD as shown in Figure 1.28.

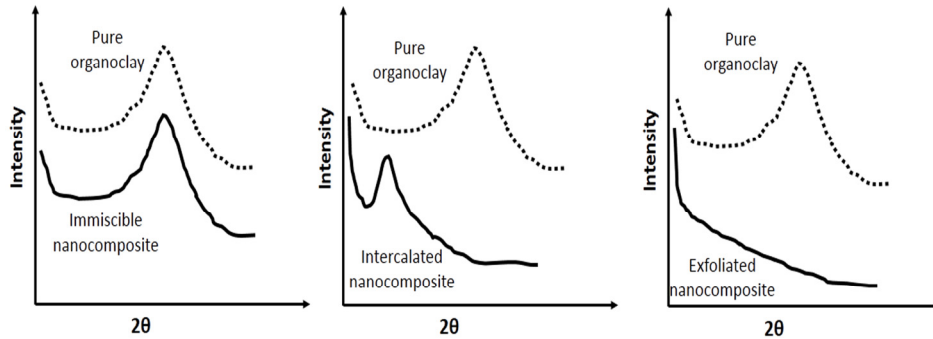


**Figure 1.28. Schematic diagram representing XRD patterns for the immiscible, intercalated and exfoliated structure of nanocomposites**

The wide angle X-ray scan of the immiscible nanocomposite look basically the same as that of the pristine organoclay. There is no shifting of the X-ray d-spacing and the clay layers exist as tactoids or aggregates of tactoids without separation of clay platelets. The presence of a peak with peak shift towards lower  $2\theta$  value indicates that the gallery has been expanded by the intercalation of polymer chains in to the gallery spaces suggesting an intercalated structure. In a completely exfoliated nanocomposite structure, no wide angle X-ray peak is perceived as there is no regular spacing of the platelets and the distances between platelets are greater than what wide angle X-ray scattering can sense<sup>104</sup>.

For a non homogenous distribution of nanoclays, there is little agreement about the spatial distribution of the silicate. Further when some of the layered silicates do not show a well-defined space between the

interlayers which are the basal reflections, systematic analysis using XRD is difficult. However, TEM can provide information about the spatial distribution of the different phases, localization of nanoclays and morphology confirming qualitative understanding of the internal structure. The major obstacle in obtaining good TEM images in microtoming sections that should be thin and uniform enough to reveal the morphology. The silicate layers consist of heavy elements such as Al, Si, and O, and can be observed through TEM as dark lines approximately 1nm thick and no staining is required. TEM analysis is reliable when the structure contains exfoliation and intercalation. The different morphologies observed by TEM analysis is as shown in Figure 1.29.

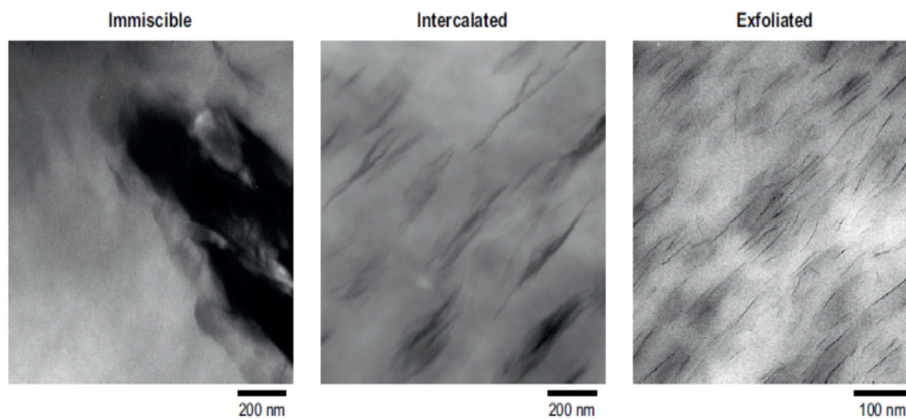


**Figure 1.29. Illustration of different states of dispersion of organoclays in polymers using TEM results**  
(Adapted from Polymer, 49(15), 3187-3204)

Differential scanning calorimetry and scanning electron microscopy can also be used to elucidate the nanocomposite structure and morphology.

### **1.11.1 PP/organoclay composites**

Polymer/nanoclay composites have dominated the current area of research and development with the recognition that modification of polymer matrices with nanoclays could result in significant mechanical property improvement. The first commercial example of PP/clay hybrid composite used in automotive applications is by the Toyota Motor Company in 1991<sup>105</sup>. Reinforcement of polymeric matrices with rigid nanoclays hinder the movement of polymer chains neighboring to the filler. The filler behaves as load bearing material provided the interfacial adhesion between the filler and the polymer chains is adequate. Apart from the improvement in the mechanical properties of polymers, nanoclays also have been reported as potential filler to reduce the permeability of gases, increased flammability and enhanced thermal stability of nanocomposites.

The interaction of polymer matrix with organoclay layers depend on the affinity of polymer chains towards silicate surface. For nylon/clay nanocomposites, increased modulus and impact are due to due to the formation of ionic bonds between the amine groups on nylon and clay layers. Commonly used commodity polymers such as polyolefins do not have any polar groups capable of interacting with the aluminosilicate surface of the clay. Among the different sizes of alkylammonium ions with organoclays and found that the alkylammonium ions with longer alkyl chains have greater potential to enhance the dispersion of the organoclay in the polyolefin matrix<sup>106</sup>. The use of maleic anhydride grafted polyolefin as a compatibilizer to the immiscible clay and the polymer chain has been found useful for developing PP-clay and PE-clay nanocomposites<sup>107,108</sup>. The maleic anhydride (~ 1%) functionalized polymers gave better mechanical properties systems than the uncompatibilized polymer systems. In all cases, the finest exfoliation

is achieved only when the process parameters and the structure of the surfactant are optimized. Rheological studies of melt compounded polypropylene and organically modified montmorillonite clay in the presence or absence of a maleic anhydride grafted polypropylene (PP-MA) oligomer as a compatibilizer was studied by Galgali *et al.*<sup>109</sup>. They reported that the chance of exfoliation is greatly improved by the presence of a compatibilizer.

### 1.11.2 PP/elastomer/organoclay composites

The incorporation of nanoclay in plastic/rubber blends (TPOs) leads to the development thermoplastic polyolefin (TPO) nanocomposites and is mainly aimed at the impact/modulus balance. TPO materials containing conventional fillers like talc or glass fibre are widely used to produce automotive parts. Unfortunately, due to the size (or aspect ratio) of such fillers, large loadings are required to significantly increase the stiffness, which can result in poor processability. The prospect for weight reduction with the introduction of nanoclay thus widens its horizon of applications and have emerged as a promising area in the development of polymeric materials that provide the preferred physical properties required for the specific applications. Studies have established that addition of only 5 wt% montmorillonite (MMT) to a thermoplastic polyolefin (TPO) gives equivalent stiffness enhancement as 20 wt % talc. Paul *et al.*<sup>107</sup> developed nanocomposites by melt compounding PP, an ethylene–octene based elastomer and a master batch material containing equal parts of maleated PP (PP-g-MA, MA content-1.0 wt %) and an organically modified montmorillonite (di-methyl, dihydrogenated tallow- montmorillonite). In the TEM photographs given in Figure 1.30, the elastomer particles appear to be much smaller and comparable to those of clay platelets with the addition of 3 wt % of nanoclay. These apparent changes in the morphology of the elastomer may

be due to the increase in melt viscosity and the role of clay particles in preventing coalescence of elastomer particles during processing. This schematically represented as in Figure 1.31.

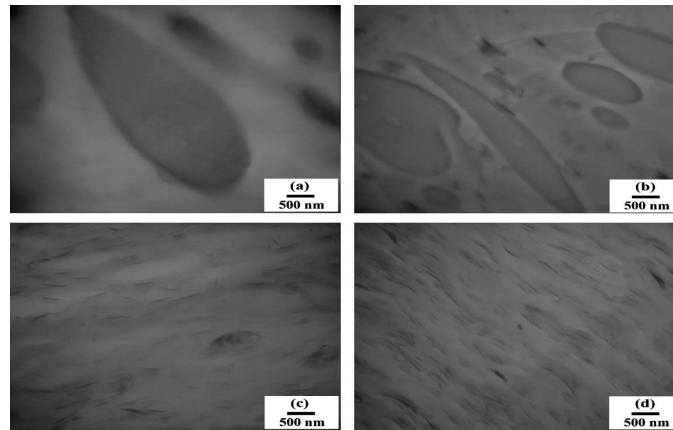


**Figure 1.30.** TEM photographs of PP/elastomer/ nanocomposites with 30 wt% elastomer and varying MMT contents: (a) 0 wt%, (b) 1 wt%, (c) 2.8 wt% and (d) 6.8 wt%. (Adapted from Polymer 46, 11673–11689)

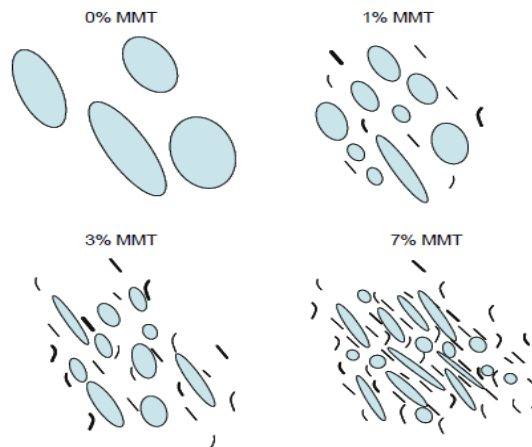


**Figure 1.31.** Schematic illustration of the morphological change in PP/elastomer/- masterbatch with varying MMT content at a fixed elastomer concentration. (Adapted from Polymer 46 , 11673–11689)



For PP/elastomer/masterbatch nanocomposites, a substantial increase in tensile modulus at low MMT concentrations was observed while the rate of increase is less pronounced at higher clay concentrations. Addition of MMT to PP and PP/elastomer composites resulted in a marginal increase in yield strength with addition of MMT. Nanocomposites containing 10 and 20 wt% elastomer displayed decrease in the elongation at break and impact strength with the addition of MMT, while nanocomposites containing 30 and 40 wt% of elastomer showed enhancement in elongation at break and impact strength at higher MMT concentrations due to the fine dispersion of elastomer phase with smaller particle size<sup>107</sup>.

Studies made by Mehta *et al.*<sup>110</sup> on the Thermoplastic olefin (TPO)/clay nanocomposites showed progressive particle breakup and decrease in the particle size of the dispersed ethylene-propylene rubber (EPR) particles as the clay loading increased from 0.6 to 5.6 wt %. They also reported the distribution of the clay platelets at the EPR/matrix interface and in the matrix. Tough organoclay nanocomposites have been developed from melt blended Impact-modified (PP-SEBS-g-MA)/VMT ternary nanocomposites toughened with SEBS-g-MA<sup>111</sup>. Mishra *et al.*<sup>112</sup> reported a substantial increase in the tensile modulus as well as storage modulus of thermoplastic polyolefin (TPO)/organoclay nanocomposite using maleic anhydride functionalized PP as a compatibilizer. The toughness of a polypropylene (PP)/ethylene-octene copolymer (EOC)/maleic anhydride-grafted poly(ethylene-co-octene) (EOC-g-MA)/clay nanocomposite have been investigated by Kazemabad *et al.*<sup>113</sup>. They established an improvement in the toughness of PP/EOC/EOC-g-MA blend than the PP/EOC blend due to the enhanced compatibility and the reduced crystallinity of the blend in the presence of EOC-g-MA. Filippi *et al.*<sup>114</sup> studied the effect of organoclay on the morphology and properties of

nanocomposites based on LDPE/PA-6 Blends and reported that when organoclay and SEBS-g-MA compatibilizer were used together, the mechanical properties could not be improved strongly. They suggested a competitive interaction of SEBS-g-MA compatibilizer with the amine end groups of PA-6 and with the surface of the silicate layer of 20A as a possible reason for not showing strong mechanical property improvements. In the case of PP/SBS/clay system studied by Li *et al.*<sup>115</sup> enhanced toughness was attributed to the rubber particle cavitation facilitated by the presence of clay particle inclusions inside the SBS rubber particles.

Kazemabad *et al.*<sup>109</sup> investigated the effects of the blending sequences on morphology and properties of the ternary nanocomposite of polypropylene (PP)/ethylene–octene copolymer (EOC)/clay with double compatibilizers of maleated PP (PP-g-MA) and maleated EOC (EOC-g-MA). The investigations resulted that a mixture of exfoliated and intercalated structure was obtained in the nanocomposite when clay was first mixed with PP and EOC-g-MA, similar to the nanocomposite prepared by simultaneous addition of all the components. In the case when clay was first mixed with PP and PP-g-MA, intercalated structure was observed. The mechanical properties showed stiffness and tensile strength of all the nanocomposites were similar, But Charpy impact strength of the nanocomposite was higher when the organoclay was dispersed in both phases of EOC and PP.

### 1.12 Applications of polymer nanocomposites

Owing to the high enhancement of mechanical, thermal, and barrier properties, nanocomposites can be used for various applications in aerospace, construction, sports, electronic device, adhesives, defense, automobile industries, food wrapping, tooling, sealants, molding, automobile industries, electronics, casting and construction. In addition, the nanocomposites based

on layered silicate can be used in the coating of anticorrosive applications on aircraft<sup>116</sup>. A combination of thermoplastic, olefin-layered silicate nanocomposites designed for an external automotive body part by General Motors and partners Basell exhibited reduction in weight up to 20% of conventional composites. The major attraction of polymer clay nanocomposites in packaging industry is their permeability to gases like carbon dioxide, oxygen and organic vapours and moisture that are hazardous<sup>73</sup>. Apart from the use of VGCNFs as a reinforcing and conductive filler in the polymer matrices, the application of VGCNFs/polymer composite materials can be extended in electromagnetic interference (EMI) shielding and electrostatic discharge (ESD) protection markets. Propylux CNF RTP is a commercially available electrically conductive PP/CNF composite that possess good chemical resistance, high strength and stiffness and good temperature resistance. The ability of VGCNF to improve the ablation resistance of both phenolic resoles and thermoplastic elastomers makes it useful for ablation resistant rocket motor insulation. VGCNF and silver plated VGCNF-filled adhesives that provide sufficient electrical conductivity and thermal conductivity for many aerospace applications.

### 1.13 Scope and objectives

Polypropylene (PP) is one of the most widely used thermoplastic due to its relatively low cost, density and resistance to oils and solvents. The use of polypropylene as an engineering thermoplastic is limited because of its brittle nature and low impact strength. So polypropylene is usually toughened with elastomers like ethylene propylene copolymer, ethylene propylene diene monomer and natural Rubber. Polybutadiene (BR) is rarely blended with polypropylene even though it has high elasticity, good abrasion resistance, low heat buildup and resistance to breakdown during mastication.

The objective of the work is to prepare thermoplastic elastomers based on polypropylene/polybutadiene (PP/BR) blends by melt mixing.

The specific objectives of the proposed study are:

- (i) Investigation of the effect of nanofillers such as nanoclay and carbon nanofibre as reinforcing agents in polypropylene/ polybutadiene blend.
- (ii) Compatibilization of polypropylene/polybutadiene blend using non polar modifiers such as styrene-(ethylene-butylene)-styrene (SEBS) and poly-(styrene-b-butadiene-b-styrene) (SBS).
- (iii) Study of the effect of nanoclay and carbon nanofibre (CNF) on SEBS compatibilized polypropylene/polybutadiene blend.

## References

- [1] Cheremisinoff, N. P., & Cheremisinoff, P. N. (1993). *Elastomer technology handbook*. CRC press.
- [2] Kear, K. E. (2003). *Developments in thermoplastic elastomers* (Vol. 14). iSmithers Rapra Publishing.
- [3] Drobny, J. G. (2014). *Handbook of thermoplastic elastomers*. Elsevier.
- [4] Holden, G. (2000). *Understanding thermoplastic elastomers*. Hanser.
- [5] Brydson, J. A. (1995). *Thermoplastic elastomers: properties and applications* (Vol. 81). iSmithers Rapra Publishing.
- [6] De, S. K., & Bhowmick, A. K. (1990). *Thermoplastic elastomers from rubber-plastic blends*. Ellis Horwood.
- [7] Dufton, P. W. (2001). *Thermoplastic Elastomers*. iSmithers Rapra Publishing.

- [8] Legge, N. R. (1987). Thermoplastic elastomers. *Rubber Chemistry and Technology*, 60(3), 83-117.
- [9] Rabek, J. F. (1980). *Experimental methods in polymer chemistry: Physical principles and applications*. Wiley.
- [10] Bhowmick, A. K., & Stephens, H. (Eds.). (2000). *Handbook of elastomers*. CRC Press.
- [11] Nesterov, A. E., & Lipatov, Y. S. (1998). *Thermodynamics of polymer blends* (Vol. 1). CRC Press.
- [12] Thomas, S., Grohens, Y., & Jyotishkumar, P. (Eds.). (2014). *Characterization of polymer blends: miscibility, morphology and interfaces*. John Wiley & Sons.
- [13] Utracki, L. A. (2002). Compatibilization of polymer blends. *the Canadian journal of chemical Engineering*, 80(6), 1008-1016.
- [14] Koning, C., Van Duin, M., Pagnouille, C., & Jerome, R. (1998). Strategies for compatibilization of polymer blends. *Progress in Polymer Science*, 23(4), 707-757.
- [15] Vilgis, T. A., & Noolandi, J. (1990). Theory of homopolymer-block copolymer blends. The search for a universal compatibilizer. *Macromolecules*, 23(11), 2941-2947.
- [16] Di Lorenzo, M. L., & Frigione, M. (1997). Compatibilization criteria and procedures for binary blends: A review. *Journal of polymer engineering*, 17(6), 429-460.
- [17] Cigana, P., Favis, B. D., & Jérôme, R. (1996). Diblock copolymers as emulsifying agents in polymer blends: Influence of molecular weight, architecture, and chemical composition. *Journal of polymer science part B: Polymer physics*, 34(9), 1691-1700.
- [18] Sundararaj, U., & Macosko, C. W. (1995). Drop breakup and coalescence in polymer blends: the effects of concentration and compatibilization. *Macromolecules*, 28(8), 2647-2657.
- [19] Macaubas, P. H. P., & Demarquette, N. R. (2001). Morphologies and interfacial tensions of immiscible polypropylene/polystyrene blends modified with triblock copolymers. *Polymer*, 42(6), 2543-2554.

- [20] Rek, V., Vranješ, N., Šlouf, M., Fortelný, I., & Jelčić, Ž. (2008). Morphology and properties of SEBS block copolymer compatibilized PS/HDPE blends. *Journal of Elastomers & Plastics*, 40(3), 237-251.
- [21] Haanh, T., & Vu-Khanh, T. (2001). Fracture and yielding behaviors of polystyrene/ethylene-propylene rubber blends: Effects of interfacial agents. *Polymer Engineering & Science*, 41(12), 2073-2081.
- [22] Ezzati, P., Ghasemi, I., Karrabi, M., & Azizi, H. (2008). Rheological behaviour of PP/EPDM blend: the effect of compatibilization. *Iran Polym J*, 17(9), 670-679.
- [23] George, S., Ramamurthy, K., Anand, J. S., Groeninckx, G., Varughese, K. T., & Thomas, S. (1999). Rheological behaviour of thermoplastic elastomers from polypropylene/acrylonitrile-butadiene rubber blends: effect of blend ratio, reactive compatibilization and dynamic vulcanization. *Polymer*, 40(15), 4325-4344.
- [24] Lyatskaya, Y., Gersappe, D., Gross, N. A., & Balazs, A. C. (1996). Designing compatibilizers to reduce interfacial tension in polymer blends. *The Journal of Physical Chemistry*, 100(5), 1449-1458.
- [25] Winey, K. I., Berba, M. L., & Galvin, M. E. (1996). Ternary phase diagrams of poly (styrene-co-methyl methacrylate), poly (methyl methacrylate), and polystyrene: Monomer sequence distribution effect and encapsulation. *Macromolecules*, 29(8), 2868-2877.
- [26] Lee, M. S., Lodge, T. P., & Macosko, C. W. (1997). Can random copolymers serve as effective polymeric compatibilizers?. *Journal of Polymer Science Part B: Polymer Physics*, 35(17), 2835-2842.
- [27] Lee, P. C., Kuo, W. F., & Chang, F. C. (1994). In situ compatibilization of PBT/ABS blends through reactive copolymers. *Polymer*, 35(26), 5641-5650.
- [28] Haddout, A., Villoutreix, J., & Villoutreix, G. (1995). Polyarylamide/Polypropylene Blends: Relations between Rheology, Morphology and Injection Molding. *International Polymer Processing*, 10(1), 68-73.

- [29] Wilhelm, H. M., & Felisberti, M. I. (2003). Blends of i-PP and SBS. II. Influence of in situ compatibilization on the mechanical properties. *Journal of applied polymer science*, 87(3), 516-522.
- [30] Bassani, A., & Pessan, L. A. (2002). Toughening of polypropylene with styrene/ethylene-butylene/styrene tri-block copolymer: Effects of reactive and nonreactive compatibilization. *Journal of applied polymer science*, 86(14), 3466-3479.
- [31] Tortorella, N., & Beatty, C. L. (2008). Morphology and mechanical properties of impact modified polypropylene blends. *Polymer Engineering & Science*, 48(11), 2098-2110.
- [32] Bagheri, H., Jahani, Y., Nekoomanesh Haghghi, M., Hakim, S., & Fan, Z. Q. (2011). Dynamic shear rheological behavior of PP/EPR in-reactor alloys synthesized by multi-stage sequential polymerization process. *Journal of Applied Polymer Science*, 120(6), 3635-3641.
- [33] Matsuda, Y., Hara, M., Mano, T., Okamoto, K., & Ishikawa, M. (2005). The effect of the volume fraction of dispersed phase on toughness of injection molded polypropylene blended with SEBS, SEPS, and SEP. *Polymer Engineering & Science*, 45(12), 1630-1638.
- [34] Razavi-Nouri, M., Naderi, G., Parvin, A., & Ghoreishy, M. H. R. (2011). Thermal properties and morphology of isotactic polypropylene/acrylonitrile-butadiene rubber blends in the presence and absence of a nanoclay. *Journal of Applied Polymer Science*, 121(3), 1365-1371.
- [35] Bassani, A., Pessan, L. A., & Hage, E. (2001). Toughening of polypropylene with styrene/ethylene-butylene/styrene tri-block copolymer: Effects of mixing condition and elastomer content. *Journal of applied polymer science*, 82(9), 2185-2193.
- [36] Robeson, L. M. (1984). Applications of polymer blends: emphasis on recent advances. *Polymer Engineering & Science*, 24(8), 587-597.
- [37] Karger-Kocsis, J., & Kuleznev, V. N. (1982). Dynamic mechanical and impact properties of polypropylene/EPDM blends. *Polymer*, 23(5), 699-705.

- [38] Lu, M. L., Chiou, K. C., & Chang, F. C. (1996). Fracture behavior of polypropylene/ethylene-diene-terpolymer blends: effect of temperatures, notch radius and rubber content. *Journal of Polymer Research*, 3(2), 73-82.
- [39] Da Silva, A. L. N., & Coutinho, F. M. (1996). Some properties of polymer blends based on EPDM/PP. *Polymer testing*, 15(1), 45-52.
- [40] Zhao, R., & Dai, G. (2002). Mechanical property and morphology comparison between the two blends poly (propylene)/ethylene-propylene-diene monomer elastomer and poly (propylene)/maleic anhydride-g-ethylene-propylene-diene monomer. *Journal of applied polymer science*, 86(10), 2486-2491.
- [41] Purnima, D., Maiti, S. N., & Gupta, A. K. (2006). Interfacial adhesion through maleic anhydride grafting of EPDM in PP/EPDM blend. *Journal of applied polymer science*, 102(6), 5528-5532.
- [42] López Manchado, M. A., Biagiotti, J., & Kenny, J. M. (2001). Rheological behavior and processability of polypropylene blends with rubber ethylene propylene diene terpolymer. *Journal of applied polymer science*, 81(1), 1-10.
- [43] Ismail, H. (2002). Thermoplastic elastomers based on polypropylene/natural rubber and polypropylene/recycle rubber blends. *Polymer Testing*, 21(4), 389-395.
- [44] Abreu, F. O. M. S., Forte, M. M. C., & Liberman, S. A. (2005). SBS and SEBS block copolymers as impact modifiers for polypropylene compounds. *Journal of applied polymer science*, 95(2), 254-263.
- [45] Balkan, O., Demirer, H., & Kayali, E. S. (2011). Effects of deformation rates on mechanical properties of PP/SEBS blends. *Journal of Achievements in Materials and Manufacturing Engineering*, 47(1), 26-33.
- [46] Gupta, A. K., & Purwar, S. N. (1986). Dynamic mechanical and impact properties of PP/SEBS blend. *Journal of applied polymer science*, 31(2), 535-551.
- [47] Karger-Kocsis, J. (Ed.).(2012). *Polypropylene structure, blends and composites: Volume 3 composites*. Springer Science & Business Media.
- [48] Karian, H. (Ed.). (2003). *Handbook of polypropylene and polypropylene composites, revised and expanded*. CRC press.



- [49] Barenblatt, G. I. (2003). Deformation and Fracture Behaviour of Polymers. Edited by W Grellmann and S Seidler. *Applied mechanics reviews*, 56(1), B5-B5.
- [50] Paul, D. R. (2012). *Polymer blends* (Vol. 1). Elsevier.
- [51] Panda, B. P., Mohanty, S., & Nayak, S. K. (2015). Mechanism of toughening in rubber toughened polyolefin—a review. *Polymer-Plastics Technology and Engineering*, 54(5), 462-473.
- [52] Wu, S. (1990). Chain structure, phase morphology, and toughness relationships in polymers and blends. *Polymer Engineering & Science*, 30(13), 753-761.
- [53] Jang, B. Z., Uhlmann, D. R., & Vander Sande, J. B. (1985). The rubber particle size dependence of crazing in polypropylene. *Polymer Engineering & Science*, 25(10), 643-651.
- [54] Keskkula, H. (2000). *Rubber-modified thermoplastics* (Vol.113). iSmithersRapra Publishing.
- [55] Bucknall, C. B. (1977). *Toughened plastics* (p. 188). London: Applied Science Publishers.
- [56] Muratoglu, O. K., Argon, A. S., Cohen, R. E., & Weinberg, M. (1995). Toughening mechanism of rubber-modified polyamides. *Polymer*, 36(5), 921-930.
- [57] Yee, A. F., & Pearson, R. A. (1986). Toughening mechanisms in elastomer-modified epoxies. *Journal of materials science*, 21(7), 2462-2474.
- [58] Guild, F. J., & Bonfield, W. (1993). Predictive modelling of hydroxyapatite-polyethylene composite. *Biomaterials*, 14(13), 985-993.
- [59] Huang, Y., & Kinloch, A. J. (1992). Modelling of the toughening mechanisms in rubber-modified epoxy polymers. *Journal of materials science*, 27(10), 2753-2762.
- [60] Chen, X. H., & Mai, Y. W. (1998). The effects of particle bulk modulus on toughening mechanisms in rubber-modified polymers. *Polymer Engineering & Science*, 38(10), 1763-1769.
- [61] Ponçot, M., Addiego, F., & Dahoun, A. (2013). True intrinsic mechanical behaviour of semi-crystalline and amorphous polymers: influences of volume deformation and cavities shape. *International Journal of Plasticity*, 40, 126-139.

- [62] Bartczak, Z., & Grala, M. (2017). Toughening of semicrystalline and amorphous polylactide with atactic polyhydroxybutyrate. *Polymer-Plastics Technology and Engineering*, 56(1), 29-43.
- [63] Zebarjad, S. M., Bagheri, R., Reihani, S. M., & Lazzeri, A. (2003). Deformation, yield and fracture of elastomer-modified polypropylene. *Journal of applied polymer science*, 90(14), 3767-3779.
- [64] Liang, J. Z., & Li, R. K. Y. (2000). Rubber toughening in polypropylene: a review. *Journal of Applied Polymer Science*, 77(2), 409-417.
- [65] Tripathi, D. (2002). *Practical guide to polypropylene*. iSmithers Rapra Publishing.
- [66] Maier, C., & Calafut, T. (1998). *Polypropylene: the definitive user's guide and data book*. William Andrew.
- [67] Alger, M. (1997). *Polymer Science Dictionary and*, 290, 265.pp639
- [68] Whelan, A. (2012). *Polymer technology dictionary*. Springer Science & Business Media, 51-53
- [69] Gupta, A. K., & Ratnam, B. K. (1991). Crystallization, tensile, and impact behavior of polypropylene/polybutadiene blend. *Journal of applied polymer science*, 42(2), 297-315.
- [70] Chen, Y., Chen, Y., & Yang, D. (2006). Crystallization and phase behavior of crystalline syndiotactic 1, 2-polybutadiene/isotactic polypropylene blends in solution-cast thin films. *Polymer*, 47(5), 1667-1673.
- [71] Sheng, J., Qi, L. Y., Yuan, X. B., Shen, N. X., & Bian, D. C. (1997). Blends of polypropylene with poly (cis-butadiene) rubber. I. Phase structure and morphology of blends. *Journal of applied polymer science*, 64(12), 2265-2272.
- [72] Thostenson, E. T., Li, C., & Chou, T. W. (2005). Nanocomposites in context. *Composites Science and Technology*, 65(3), 491-516.
- [73] Verdejo, R., Bernal, M. M., Romasanta, L. J., Tapiador, F. J., & Lopez-Manchado, M.A. (2011). Reactive nanocomposite foams. *Cellular Polymers*, 30(2), 45.

- [74] Kuriger, R. J., Alam, M. K., Anderson, D. P., & Jacobsen, R. L. (2002). Processing and characterization of aligned vapor grown carbon fiber reinforced polypropylene. *Composites Part A: Applied Science and Manufacturing*, 33(1), 53-62.
- [75] Lee, B. L. (1992). Electrically conductive polymer composites and blends. *Polymer Engineering & Science*, 32(1), 36-42.
- [76] Alexandre, M., & Dubois, P. (2000). Polymer-layered silicate nanocomposites: preparation, properties and uses of a new class of materials. *Materials Science and Engineering: R: Reports*, 28(1), 1-63.
- [77] Hussain, F., Hojjati, M., Okamoto, M., & Gorga, R. E. (2006). Polymer-matrix nanocomposites, processing, manufacturing, and application: an overview. *Journal of composite materials*, 40(17), 1511-1575.
- [78] Romero, R. B., Leite, C. A. P., & do Carmo Gonçalves, M. (2009). The effect of the solvent on the morphology of cellulose acetate/montmorillonite nanocomposites. *Polymer*, 50(1), 161-170.
- [79] Velasco-Santos, C., Martínez-Hernández, A. L., Fisher, F. T., Ruoff, R., & Castaño, V. M. (2003). Improvement of thermal and mechanical properties of carbon nanotube composites through chemical functionalization. *Chemistry of materials*, 15(23), 4470-4475.
- [80] Jin, L., Bower, C., & Zhou, O. (1998). Alignment of carbon nanotubes in a polymer matrix by mechanical stretching. *Applied physics letters*, 73(9), 1197-1199.
- [81] Bhattacharya, M. (2016). Polymer nanocomposites—A comparison between carbon nanotubes, graphene, and clay as nanofillers. *Materials*, 9(4), 262.
- [82] Tibbetts, G. G., & McHugh, J. J. (1999). Mechanical properties of vapor-grown carbon fiber composites with thermoplastic matrices. *Journal of Materials Research*, 14(7), 2871-2880.
- [83] Sandler, J., Werner, P., Shaffer, M. S., Demchuk, V., Altstädt, V., & Windle, A. H. (2002). Carbon-nanofibre-reinforced poly (ether ether ketone) composites. *Composites Part A: Applied Science and Manufacturing*, 33(8), 1033-1039.
- [84] Higgins, B. A., & Brittain, W. J. (2005). Polycarbonate carbon nanofiber composites. *European Polymer Journal*, 41(5), 889-893.

- [85] Al-Saleh, M. H., &Sundararaj, U. (2011). Review of the mechanical properties of carbon nanofiber/polymer composites. *Composites Part A: Applied Science and Manufacturing*, 42(12), 2126-2142.
- [86] Feng, L., Xie, N., & Zhong, J. (2014). Carbon nanofibers and their composites: a review of synthesizing, properties and applications. *Materials*, 7(5), 3919-3945.
- [87] Coleman, J. N., Khan, U., &Gun'ko, Y. K. (2006). Mechanical reinforcement of polymers using carbon nanotubes. *Advanced materials*, 18(6), 689-706.
- [88] Finegan, I. C., Tibbetts, G. G., Glasgow, D. G., Ting, J. M., & Lake, M. L. (2003). Surface treatments for improving the mechanical properties of carbon nanofiber/thermoplastic composites. *Journal of Materials Science*, 38(16), 3485-3490.
- [89] Tong, X., Chen, Y., & Cheng, H. (2005). Influence of carbon nanofiber addition on mechanical properties and crystallization behavior of polypropylene. *Journal of Materials Science and Technology*, 21(5), 686-690.
- [90] Ceccia, S., Ferri, D., Tabuani, D., & Maffettone, P. L. (2008). Rheology of carbon nanofiber-reinforced polypropylene. *Rheologica Acta*, 47(4),425-433.
- [91] Chipara, M., Lozano, K., Hernandez, A., & Chipara, M. (2008). TGA analysis of polypropylene–carbon nanofibers composites. *Polymer Degradation and Stability*, 93(4), 871-876.
- [92] Chatterjee, A., & Deopura, B. L. (2006). Thermal stability of polypropylene/ carbon nanofiber composite. *Journal of applied polymer science*, 100(5), 3574-3578.
- [93] Lozano, K., & Barrera, E. V. (2001). Nanofiber-reinforced thermoplastic composites. I. Thermoanalytical and mechanical analyses. *Journal of Applied Polymer Science*, 79(1), 125-133.
- [94] Paleo, A. J., Van Hattum, F. W. J., Pereira, J., Rocha, J. G., Silva, J., Sencadas, V., & Lanceros-Méndez, S. (2010). The piezoresistive effect in polypropylene—carbon nanofibre composites obtained by shear extrusion. *Smart Materials and Structures*, 19(6), 065013.

- [95] Sui, G., Jana, S., Zhong, W. H., Fuqua, M. A., & Ulven, C. A. (2008). Dielectric properties and conductivity of carbon nanofiber/semi-crystalline polymer composites. *Acta Materialia*, 56(10), 2381-2388.
- [96] Gulrez, S. K., Ali Mohsin, M. E., Shaikh, H., Anis, A., Pulose, A. M., Yadav, M. K.,... & Al-Zahrani, S. M. (2014). A review on electrically conductive polypropylene and polyethylene. *Polymer composites*, 35(5), 900-914.
- [97] Liao, C. Z., & Tjong, S. C. (2011). Effects of carbon nanofibers on the fracture, mechanical, and thermal properties of PP/SEBS-g-MA blends. *Polymer Engineering & Science*, 51(5), 948-958.
- [98] Parameswaranpillai, J., Dubey, V. K., Sisanth, K. S., Jose, S., Zachariah, A. K., Siengchin, S., ... & Hameed, N. (2016). Tailoring of interface of polypropylene/polystyrene/carbon nanofibre composites by polystyrene-block-poly (ethylene-ran-butylene)-block-polystyrene. *Polymer Testing*, 51, 131-141.
- [99] Parameswaranpillai, J., Joseph, G., Shinu, K. P., Salim, N. V., Hameed, N., & Jose, S. (2015). High performance PP/SEBS/CNF composites: Evaluation of mechanical, thermal degradation, and crystallization properties. *Polymer Composites*.
- [100] Gao, F. (2004). Clay/Polymer Composites: the Story, *Materials Today*, 7(11): 50–55.
- [101] Fornes, T. D., & Paul, D. R. (2003). Modeling properties of nylon 6/clay nanocomposites using composite theories. *polymer*, 44(17), 4993-5013.
- [102] Majeed, K., Jawaid, M., Hassan, A., Bakar, A. A., Khalil, H. A., Salema, A. A., & Inuwa, I. (2013). Potential materials for food packaging from nanoclay/natural fibres filled hybrid composites. *Materials & Design*, 46, 391-410.
- [103] Xie, W., Gao, Z., Pan, W. P., Hunter, D., Singh, A., & Vaia, R. (2001). Thermal degradation chemistry of alkyl quaternary ammonium montmorillonite. *Chemistry of Materials*, 13(9), 2979-2990.
- [104] Paul, D. R., & Robeson, L. M. (2008). Polymer nanotechnology: nanocomposites. *Polymer*, 49(15), 3187-3204.

- [105] Okada, A. and Usuki, A. (1995). The Chemistry of Polymer-Clay Hybrids, *Mater. Sci. Eng.*, C3: 109–115.
- [106] Shah, R. K., Hunter, D. L., & Paul, D. R. (2005). Nanocomposites from poly (ethylene-co-methacrylic acid) ionomers: effect of surfactant structure on morphology and properties. *Polymer*, 46(8), 2646-2662.
- [107] Lee, H. S., Fasulo, P. D., Rodgers, W. R., & Paul, D. R. (2005). TPO based nanocomposites. Part 1. Morphology and mechanical properties. *Polymer*, 46(25), 11673-11689.
- [108] Kawasumi, M., Hasegawa, N., Kato, M., Usuki, A., & Okada, A. (1997). Preparation and mechanical properties of polypropylene–clay hybrids. *Macromolecules*, 30(20), 6333-6338.
- [109] Galgali, G., Ramesh, C., & Lele, A. (2001). A rheological study on the kinetics of hybrid formation in polypropylene nanocomposites. *Macromolecules*, 34(4), 852-858.
- [110] Mehta, S., Mirabella, F. M., Rufener, K., & Bafna, A. (2004). Thermoplastic olefin/clay nanocomposites: morphology and mechanical properties. *Journal of Applied Polymer Science*, 92(2), 928-936.
- [111] Tjong, S. C., & Meng, Y. Z. (2003). Impact-modified polypropylene/vermiculite nanocomposites. *Journal of Polymer Science Part B: Polymer Physics*, 41(19), 2332-2341.
- [112] Mishra, J. K., Hwang, K. J., & Ha, C. S. (2005). Preparation, mechanical and rheological properties of a thermoplastic polyolefin (TPO)/organoclay nanocomposite with reference to the effect of maleic anhydride modified polypropylene as a compatibilizer. *Polymer*, 46(6), 1995-2002.
- [113] Bagheri-Kazemabad, S., Khavandi, A., & Chen, B. (2013). Evaluation of toughening mechanisms of polypropylene/ethylene–octene copolymer/maleic anhydride-grafted poly (ethylene-co-octene)/clay nanocomposite. *Polymer International*, 62(4), 566-572.
- [114] Filippi, S., Dintcheva, N. T., Scaffaro, R., La Mantia, F. P., Polacco, G., & Magagnini, P. (2009). Effects of organoclay on morphology and properties of nanocomposites based on LDPE/PA-6 blends without and with SEBS-g-MA compatibilizer. *Polymer Engineering & Science*, 49(6), 1187-1197.

- [115] Li, Y., Wei, G. X., & Sue, H. J. (2002). Morphology and toughening mechanisms in clay-modified styrene-butadiene-styrene rubber-toughened polypropylene. *Journal of materials science*, 37(12), 2447-2459.
- [116] Alateyah, A. I., Dhakal, H. N., & Zhang, Z. Y. (2013). Processing, properties, and applications of polymer nanocomposites based on layer silicates: a review. *Advances in polymer technology*, 32(4).

.....❧.....

**MATERIALS AND EXPERIMENTAL  
TECHNIQUES**

<i>Contents</i>	2.1 <i>Materials</i>
	2.2 <i>Methodology</i>
	2.3 <i>Characterization techniques</i>

*A brief description of the materials and experimental techniques used for the preparation and characterization of the blends and the nanocomposites are given in this chapter.*

**2.1 Materials****2.1.1 Polymers****2.1.1.1 Polypropylene (PP)**

Polypropylene homopolymer (REPOL H110MA) with a melt flow index of 11g/10 min (230 °C/2.16 Kg) was purchased from Reliance Industries limited, Mumbai, India.



**Figure 2.1. Polypropylene**



### 2.1.1.2 Polybutadiene rubber (BR)

The polybutadiene rubber used in this study is Neodymium catalyzed High cis- polybutadiene rubber with a molecular weight 800,000–1,000,000 and density 0.93 g/cm<sup>2</sup> (20 °C) supplied by Nizhnekamskneftekhim Inc.



**Figure 2.2. Polybutadiene rubber**

### 2.1.2 Compatibilizers

Linear triblock copolymers styrene–butadiene– styrene (SBS), Kraton D 1102 CS (styrene 29.5% mass) and styrene–butadiene–styrene with hydrogenated polybutadiene midblock (SEBS), Kraton G 1652 (styrene 30% mass) from Shell Chemicals Company, Houston, USA were used as compatibilizers.



**Figure 2.3. Compatibilizers**

### **2.1.3 Fillers**

#### **2.1.3.1 Nanoclay (NC)**

The nanoclay with trade name Cloisite 93A was obtained from Southern Clay products (USA). It is a ternary ammonium salt modified natural montmorillonite (methyl, dehydrogenated tallow ammonium) designated as nanoclay. The clay had a bulk density of 2.60 g/cc and Young's modulus of 178 GPa<sup>1</sup>.

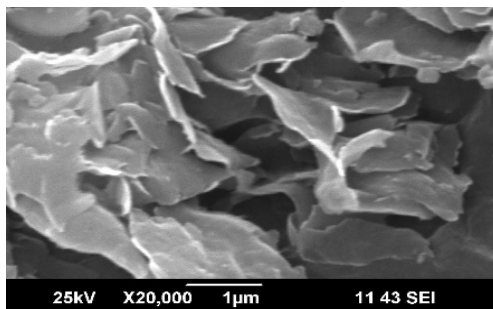


**Figure 2.4. SEM image of nanoclay-Cloisite 93 A**

#### **2.1.3.2 Carbon nanofibre (CNF)**

Vapour grown carbon nanofibre (VGCNF) (Pyrograph–III) was procured from Applied Science, Inc. The diameter of the CNFs diameter was in the range of 70-100 nm and length between 30 to 100 µm.

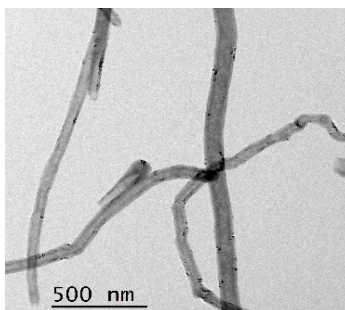


**Figure 2.5. TEM image of vapour grown carbon nanofibre**

## **2.2 Methodology**

### **2.2.1 Preparation of the blends**

Blends of PP and BR were prepared by melt mixing process in a Brabender Plasticorder (PL 3S model) at 170 °C and 60 rpm for 8 minutes. At first PP was allowed to melt, followed by the addition of BR and the blending was continued for another 8 minutes. The molten blends were pressed in a hydraulic press and was sheeted out using a two roll mill. In the case of compatibilized blends, after the addition of BR to molten PP, the mix was blended for 2 minutes followed by the addition of the compatibilizer (SEBS/SBS). The mixing was continued for 5 minutes to obtain a uniform mixture.

### **2.2.2 Preparation of the PP/BR nanocomposites**

PP/BR nanocomposites were prepared by melt mixing process in a Brabender Plasticorder (PL 3S model) at 170 °C and 60 rpm. After softening of PP for 3 minutes, BR was introduced into the mixer and was blended for 2 minutes, followed by the addition of nanofillers (nanoclay/carbon nanofibre). The mixing was continued for further 5 minutes, pressed and sheeted out in the two roll mill. In the case of compatibilized blend nanocomposites, nanofillers were added after the addition of the compatibilizer (SEBS/SBS) and mixed for 5 minutes to obtain a homogenous mixture.

### **2.2.3 Preparation of test specimen**

The hot mix after pressing in a hydraulic press were passed through a two roll mill and cut to small pieces. The dumb bell pieces for tensile tests and rectangular pieces for impact tests were prepared using DSM Micro12cc Injection Molding Machine, at 190 °C. All the specimens were molded at

identical conditions and the properties were taken as the average property of seven samples.



Figure 2.6. Semi micro injection molding machine

## 2.3 Characterization techniques

### 2.3.1 X-ray Diffraction (XRD)

X-ray diffraction data from polymers offer information about crystallite size crystallinity, orientation of the crystallites and phase composition in semicrystalline polymers<sup>2</sup>.

XRD analysis provides information regarding the d-spacing of the nanoclay layers in the nanocomposites by using Bragg's law  $n\lambda=2d\sin\theta$ . The measured  $2\theta$  value is a measure of d-spacing of the nanoclay layers. In the XRD analysis, if the characteristic peak of the nanoclay in the nanocomposites shifts towards lower  $2\theta$  value, it indicates an increase in d-spacing signifying *intercalation*. If the characteristic peak of the nanoclay is absent in the nanocomposites, the XRD pattern indicates complete *exfoliation* and no shift in  $2\theta$  value indicates that the nanoclay and the polymer is *immiscible*; the clay platelets exist as tactoids<sup>3-4</sup>.

XRD analysis was carried out in a Bruker AXS D8 Advance X-Ray Powder Diffractometer (Cu K $\alpha$  radiation). The scannings were made in the 2 $\theta$  range from 2°–25° at the rate of 0.020° corresponding to a wavelength of 1.541 Å operating at 40 kV and 35 mA.

### 2.3.2 Scanning electron microscopy (SEM)

A scanning electron microscope (SEM) produces images of a sample by scanning the surface with a focused beam of electrons. The electrons interact with atoms in the sample, generating various signals including secondary electrons (SE), reflected or back-scattered electrons (BSE), characteristic X-rays and photons and transmitted electrons, that contain information about the sample's surface morphology. The most commonly used mode in SEM includes morphology analysis by means of secondary electrons.

The SEM observations described in this work were carried out on the fractured surface of the tensile and impact specimens using JEOL Model JSM 6390LV scanning electron microscope (SEM). The samples were sputtered with gold prior to electron microscopy to make them conductive<sup>5-6</sup>.

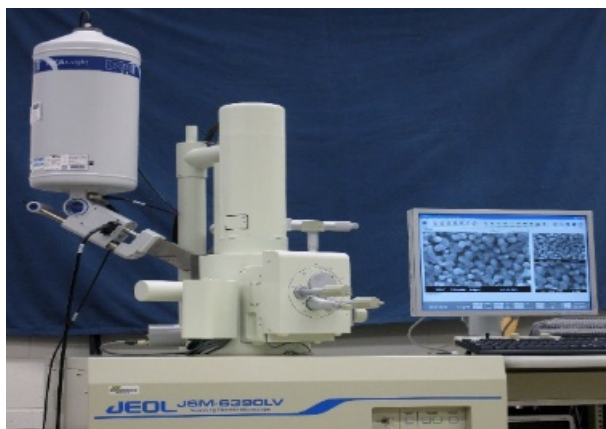


**Figure 2.7. Scanning electron microscope**

### **2.3.3 High resolution transmission electron microscopy (HRTEM)**

TEM analysis helps to characterize the morphology of nanocomposites and the nanoscale dispersion of the fillers in the polymer matrix. TEM analysis of the nanoclay composites provides qualitative information regarding the agglomerated, intercalated and exfoliated distribution of nanoclay in the polymer matrix<sup>7-8</sup>.

Transmission electron microscopy (TEM) was performed on a JEM2100 transmission electron microscope at an acceleration voltage of 200 kV. Ultrathin sectioning of the samples were carried out at -120 °C using an ultra-microtome fixed with a diamond knife. Several images of the samples at various magnifications were taken.



**Figure 2.8. Transmission electron microscope**

### **2.3.4 Mechanical properties**

#### **a) Tensile properties**

Tensile properties were measured using INSTRON Universal testing machine with a load cell of 5 kN capacity according to the ASTM D 638

at a cross head speed of 50 mm/min on dumb bell shaped specimens. Seven specimens were tested and the average value was calculated in each case and reported.

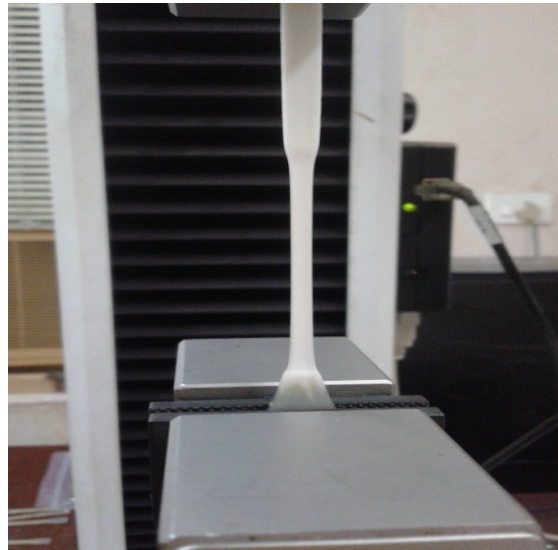


Figure 2.9. INSTRON Universal testing machine

**b) Impact strength**

The notched Izod impact strength of the injection molded samples were determined as per ASTM D256. The test was carried out using RESIL IMPACTOR JUNIOR (CEAST) machine with a pendulum of 4J and striking velocity of 3.4 m/s. Seven specimens were tested and the average value was calculated in each case and reported. The impact energy is measured directly from the machine and impact strength is determined as

Impact strength = Impact energy (J)/thickness (m).



Figure 2.10. Impact tester (RESIL)

### 2.3.5 Fourier transform infrared spectroscopy (FTIR)

FTIR is used to determine functional groups and the structure of a molecule. The FTIR spectra of the samples were recorded in the transmittance mode using a Thermo Nicolet, Avatar 370 FTIR spectrophotometer in the range of  $400\text{--}4000\text{ cm}^{-1}$ . The transmittance % as a function of wave number ( $\text{cm}^{-1}$ ) is presented.

### 2.3.6 Dynamic rheological analysis (DRA)

Melt rheological analysis is a powerful tool that provides information on the melt processability of the polymers. The rheological analysis can be carried out in different types of rheometers depending on the flow types which impose shearing or elongational strains. Among the different types of rheometers, parallel plate rheometer is the most important one to measure the different rheological properties in the linear viscoelastic and nonlinear viscoelastic region. In this method, the sample under investigation is deformed in an oscillatory shearing flow and is placed in between two parallel plates.



In the oscillatory shear experiment based on the strain and the stress response, the storage modulus  $G'$ , the loss modulus  $G''$  and the dynamic viscosity ( $\eta^*$ ) can be determined<sup>9</sup>.

The melt rheological characterization of the samples were carried out in Anton Paar Rheometer model MCR 102 equipped with 25 mm parallel plate geometry and 1 mm gap at 190 °C using the software Rheoplus version 32. The investigations were measured on amplitude sweep and frequency sweep modes. Amplitude sweep tests were performed at an angular frequency of 10 rad/s in the range of 0.01 to 100% log values. Frequency sweep tests were performed at a constant amplitude value of 2.5% and frequency in the range 100 to 0.1 rad/s in a log scale. Rheological parameters (complex viscosity ( $\eta^*$ ), storage ( $G'$ ) and loss ( $G''$ ) modulus) were directly obtained using the Rheoplus software package from the frequency sweep data.



**Figure 2.11. Parallel plate rheometer (MCR 102)**

### 2.3.7 Dynamic mechanical analysis (DMA)

Dynamic Mechanical Analysis is used to analyze the storage modulus ( $E'$ ) and loss modulus ( $E''$ ) of the sample as a function of time, temperature, and frequency. Usually, the measurement of the modulus is made by varying the temperature of the sample at a constant frequency or frequency at a constant temperature. In dynamic mechanical analysis, a sinusoidal stress is applied to a material and the resulting strain is measured. For a perfectly elastic solid the strain and the stress will be in phase and for a purely viscous fluid, there exist a 90 degree phase lag of strain with respect to stress. For viscoelastic materials, when the stress is applied, the strain lags behind and this phase lag is represented by an angle  $\delta$ . The modulus is a complex quantity for viscoelastic materials and is represented as

$$E^* = E' + iE'' \dots\dots\dots(2.1)$$

where  $E'$  represents the storage modulus (stored energy), signifying the elastic portion;

$E''$  represents the loss modulus (dissipated as heat), signifying the viscous portion;

$E''/E' = \tan \delta$  is the loss tangent and the peak of  $\tan \delta$  represents the glass transition Temperature ( $T_g$ )

When a polymer is heated through the glass transition region, storage modulus ( $E'$ ) decreases whereas the loss modulus ( $E''$ ) and  $\tan \delta$  passes through a maximum<sup>12</sup>.

DMA was carried out on a dynamic mechanical analyser (DMA Q-800 TA instruments). Rectangular shaped specimens of dimension  $35 \times 4 \times 3$  mm were used. DMA tests were conducted at a frequency of 1 Hz. A temperature ramp was run from 35 to 123 °C at a heating rate of 3 °C/min. Storage modulus ( $E'$ ), loss modulus ( $E''$ ) and  $\tan \delta$  ( $E''/E'$ ) are evaluated.



**Figure 2.12. Dynamic mechanical analyser**

### **2.3.8 Differential scanning calorimetry (DSC)**

DSC analysis provides valuable information regarding the thermal and crystallization behavior of the polymer blends and nanocomposites. In this technique, heat absorbed or heat released is measured as a function of time or temperature of the sample is compared with that of reference sample. The parameters such as melting point ( $T_m$ ), onset of melting temperature ( $T_{m,onset}$ ), endset of melting temperature ( $T_{m,endset}$ ), Heat of fusion ( $\Delta H_f$ ), and percentage of crystallinity ( $X_c$ ) can be obtained from the heating curves. Parameters such as the crystallization temperature ( $T_c$ ),

onset of the crystallization temperature ( $T_{c,onset}$ ), endset of crystallization temperature ( $T_{c,endset}$ ) and Heat of crystallization ( $\Delta H_c$ ) are obtained from the cooling curves.

In this work DSC analysis of the neat matrix, blend and the nanocomposites were carried out on a DSC Mettler Toledo DSC822e differential scanning calorimeter. The samples were first heated from 30 °C to 200 °C and then cooled to 30 °C at a rate of 10 °C /min in nitrogen atmosphere. The crystallinity of the PP matrix ( $X_c$ ) in the materials was calculated using the following expression

$$X_c = \frac{\Delta H_f}{w_p \Delta H_f^0} \times 100 \dots\dots\dots(2.2)$$

where  $\Delta H_f$  is the heat of fusion of the sample,  $\Delta H_f^0$  is the heat of fusion of 100% pure crystalline PP, which was taken as 209 J/g and  $w_p$  is the weight fraction of PP in the blend and the composites<sup>11-12</sup>.

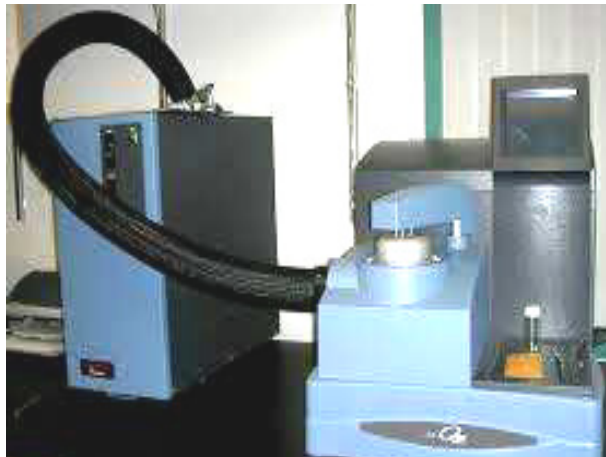


Figure 2.13. Differential scanning calorimeter

### 2.3.9 Thermogravimetric Analysis (TGA)

TGA analysis investigates the thermal degradation behavior of the polymers. The sample is loaded in a small electrically heated oven with a thermocouple to measure the temperature and the changes in weight in as a function of temperature is monitored. The information about thermal stability and extent of degradation of the sample is inferred from the integral (TGA) and derivative (DTG) of the thermogravimetric curves.

Thermal stability of the nanocomposites were analyzed by thermogravimetric analysis (TGA) using TGA Q-50 of TA instruments under N<sub>2</sub> atmosphere. The samples of about 5–7 mg was heated at a rate of 20 °C/min from ambient temperature to 600 °C. The onset of degradation temperature ( $T_{\text{onset}}$ ) and the maximum degradation temperature ( $T_{\text{max}}$ ) were evaluated<sup>13</sup>.

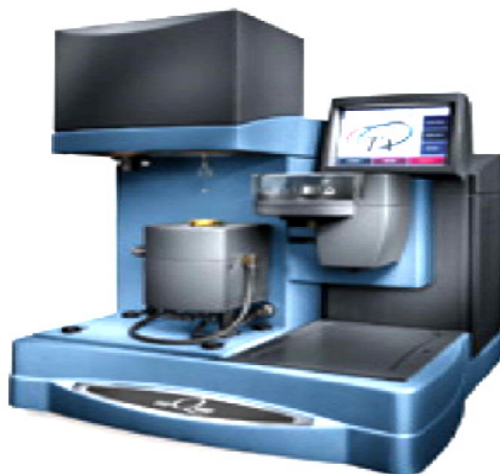


Figure 2.14. Thermogravimetric analyser (TA)

## References

- [1] Huang, J., Geier, S., Schmauder, S., & Weber, U. (2012). Modeling stiffness of nanolayered silicate-modified polyamide 6 via FEM micromechanical modeling and analytical composite models. *Journal of Applied Polymer Science*, 125(6), 4416-4420.
- [2] Sibilina, J. P. (1996). A guide to materials characterization and chemical analysis. John Wiley & Sons.
- [3] Paul, D.R., & Robeson, L. M.(2008). Polymer nanotechnology: nanocomposites. *Polymer*, 49(15), 3187-3204
- [4] Yeniova, C. E., & Yilmazer, U. (2013). Effect of different types of organoclays and compatibilizers on the properties of polystyrene-based *nanocomposites*. *Journal of Applied Polymer Science*, 127(5), 3673-3680.
- [5] Inoue, T. (2003). Morphology of polymer blends. In *Polymer blends handbook* (pp. 547-576). Springer Netherlands.
- [6] Feldman, D. (1990). Atlas of polymer morphology, by AE Woodward, C. Hanser Publishers, Munich, Vienna, New York, 1989, 531 pp.
- [7] Morgan, A. B., & Gilman, J. W. (2003). Characterization of polymer-layered silicate (clay) nanocomposites by transmission electron microscopy and X-ray diffraction: A comparative study. *Journal of Applied Polymer Science*, 87(8), 1329-1338.
- [8] Ray, S. S. (2009). Visualisation of Nanoclay Dispersion in Polymer Matrix by High-Resolution Electron Microscopy Combined with Electron Tomography. *Macromolecular Materials and Engineering*, 294(4), 281-286.
- [9] Hashmi, S. (2014). Comprehensive materials processing. (1).
- [10] Jin, Z., Pramoda, K. P., Xu, G., & Goh, S. H. (2001). Dynamic mechanical behavior of melt-processed multi-walled carbon nanotube/poly (methyl methacrylate) composites. *Chemical Physics Letters*, 337(1), 43-47.
- [11] Razavi-Nouri, M., Naderi, G., Parvin, A., & Ghoreishy, M. H. R. (2011). Thermal properties and morphology of isotactic polypropylene/acrylonitrile-butadiene rubber blends in the presence and absence of a nanoclay. *Journal of Applied Polymer Science*, 121(3), 1365-1371.

- [12] Corcione, C. E., & Frigione, M. (2012). Characterization of nanocomposites by thermal analysis. *Materials*, 5(12), 2960-2980.
- [13] Zhao, C., Qin, H., Gong, F., Feng, M., Zhang, S., & Yang, M. (2005). Mechanical, thermal and flammability properties of polyethylene/clay nanocomposites. *Polymer Degradation and Stability*, 87(1), 183-189.

.....

**THERMOPLASTIC ELASTOMERS BASED ON  
POLYPROPYLENE/POLYBUTADIENE BLENDS**

<b>Contents</b>	3.1 Introduction
	3.2 Methodology
	3.3 Results and Discussion
	3.4 Conclusions

*Thermoplastic elastomers based on the blends of polypropylene (PP) and polybutadiene rubber (BR) were systematically investigated to explore the influence of polybutadiene content on the mechanical, morphological, rheological and thermal properties of polypropylene. The morphology of the blends were analyzed using Scanning electron microscopy (SEM) and it has revealed that shear yielding is the main mechanism of toughening of the PP matrix. Analysis of the stress-strain behavior and mechanical properties like tensile strength, elongation at break, Young's modulus, impact strength etc. revealed that PP/BR blends have resulted in a thermoplastic elastomer with improved properties. Various theoretical models such as Nielsen's first power law model, Nielsen's two-third power law model and Nicolais-Narkis model were used to compare the experimental results of the tensile strength. Dynamic rheological analysis (DRA) of the blends reveal improved complex viscosity, storage modulus and loss modulus signifying the interaction between the blend components. The dynamic mechanical analysis (DMA) and Differential scanning calorimetry (DSC) analysis show reduction in stiffness of the PP phase with the introduction of BR. The thermal properties of the blends characterized using Thermogravimetric analysis (TGA) show improved thermal stability of the blends.*



### 3.1 Introduction

Thermoplastic elastomers (TPEs) combine the elastic property of the elastomer and the processability of the thermoplastics. The importance of TPEs are based on its recycling ability and the ease of processability<sup>1,2</sup>. Among the different types of thermoplastic elastomers, thermoplastic olefins (TPOs) are the blends of thermoplastics and elastomers prepared by melt blending and usually comprises of thermoplastic phase as the matrix and uncured elastomer as the dispersed phase. The low cost, low density and excellent weatherability of TPOs make them an important constituent in automotive applications.

Polypropylene is one of the most widely used thermoplastic due to its relatively low cost and excellent processability. The applications of polypropylene as an engineering thermoplastic is limited because of its brittle nature and low impact strength. So in order to improve the impact strength of polypropylene, it is usually toughened by blending with elastomers<sup>3</sup>. The dispersed rubber particles are found to improve the toughness of the matrix. The principal mechanisms of deformation in rubber-toughened PP are identified to be shear yielding or crazing in the rigid matrix phase, and cavitation or debonding in the soft dispersed phase. Earlier studies revealed that the major toughening mechanism involved in PP/rubber blends is extensive plastic deformation with shear yielding of the semicrystalline PP matrix initiated by the rubber particle cavitation<sup>4,5</sup>. Kim *et al.*<sup>6</sup> suggested that the formation of microvoids combined with extensive plastic deformation of the matrix resulted in the toughening of the matrix.

Commonly used elastomers to toughen the polypropylene matrix are ethylene propylene copolymer (EPR), ethylene propylene diene monomer (EPDM), poly-(styrene-b-ethylene-co-butylene-b-styrene) (SEBS) and poly-(styrene-b-butadiene-b-styrene) (SBS) and natural rubber (NR)<sup>3,7,8</sup>. Numerous investigations on the mechanical morphological, rheological and thermal properties of PP/EPDM blends are well documented in literature<sup>9</sup>. The mechanical fracture and ductile-brittle transition (DBT) behavior, hysteresis phenomenon and the plastic zone size of PP/EPDM blends were investigated by Lu *et al.*<sup>10</sup>. The studies revealed that the mechanical properties, tensile yield stress and Young's modulus, decreased with the increase in EPDM content. The toughening mechanism of the PP/EPDM blends was found to be extensive plastic deformation and localized shear yielding of the PP matrix, both initiated by the rubber particles. Investigations carried out by Purnima *et al.*<sup>11</sup> on PP/EPDM binary blends and PP/EPDM-g-MAH binary blends revealed that maleic anhydride (MAH) grafting of EPDM enhanced the interfacial adhesion leading to improved mechanical properties than the PP/EPDM blends. Manchado *et al.*<sup>12</sup> investigated the processability and flow properties of PP/EPDM blends and established that a general processing behavior similar to that of PP can be adopted for blends with low content of EPDM. In the study of PP/EPDM binary blends by Gong *et al.*<sup>13</sup>. It was established that EPDM could restrict the mobility of PP chains because of the entanglement of EPDM chains leading to the increase in the complex viscosity, storage modulus and loss modulus of the PP/EPDM blends. Polybutadiene rubber (BR) is rarely blended with polypropylene even though it has, good abrasion resistance, high elasticity, resistance to breakdown during mastication and low heat buildup. Very few studies have been reported on the toughening efficiency of BR with PP. Gupta *et al.*<sup>14</sup> studied the crystallization, tensile, and impact behavior isotactic polypropylene and

polybutadiene prepared by mixing in a two-roll mill. The studies revealed that 5 wt % of BR was sufficient to improve the impact strength of PP by a factor of 1.5. A two phase morphology of BR particles dispersed in PP phase with sufficiently spherical BR droplets at low BR content and nonspherical droplets at higher BR content was observed. Chen *et al.*<sup>15</sup> studied the crystallization and phase behavior of solution cast thin films of crystalline syndiotactic 1,2-polybutadiene and isotactic polypropylene (i-PP) blends. Ma *et al.*<sup>16</sup> studied the IR spectra, small-angle X-ray scattering and SEM of the pressed films of the blends of PP with BR.

This part of the thesis focuses on the preparation of thermoplastic elastomers based on polypropylene/ polybutadiene (PP/BR) blends by melt blending and the evaluation of the mechanical, morphological, rheological and thermal properties of the blends. In order to understand the role of rubber particles on the toughening mechanism of PP/BR blends, morphology of the fractured surfaces have been analyzed by means of scanning electron microscope. The rheological and thermal properties of PP/BR blends also have been explored.

## **3.2 Methodology**

### **3.2.1 Materials**

The details of the polymers used for the study are discussed in chapter 2 (section 2.1).

### **3.2.2 Preparation of the blends**

PP/BR blends were prepared by melt mixing in a Brabender Plasticorder at a temperature of 170 °C and rotor speed of 60 rpm for

8 minutes. The hot mix was sheeted on a two roll mill. The compositions of PP/BR blends used in this study are shown in table 3.1

**Table 3.1. Compositions of PP/BR blends**

Sample	P100	P90	P80	P70	P60
PP (wt%)	100	90	80	70	60
BR (wt%)	0	10	20	30	40

The test specimens were injection molded at a barrel temperature of 180 °C and then tested as discussed in chapter 2.

### 3.3 Results and Discussion

#### 3.3.1 Mechanical properties

##### 3.3.1.1 Tensile properties

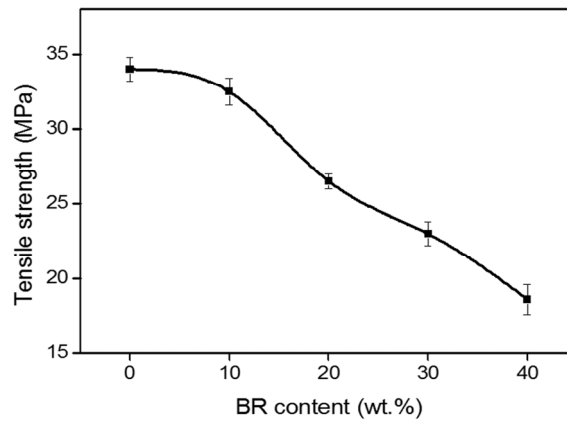


**Figure 3.1. Variation of tensile strength with BR content.**

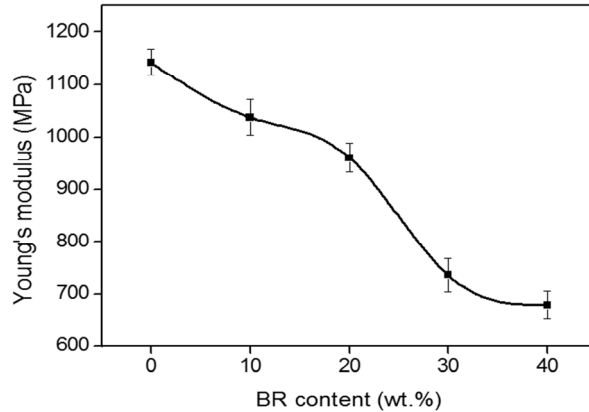


**Figure 3.2. Variation of Young's modulus with BR content**

The variation of tensile strength and Young's modulus of various PP/BR blends are shown in Figures 3.1 and 3.2, respectively. As seen from figures, the tensile strength and Young's modulus of the blends decreased with increasing BR content. The decrease in tensile strength and Young's modulus than pure PP implies the reduction in stiffness associated with low strength amorphous rubbery matrix<sup>17</sup>.

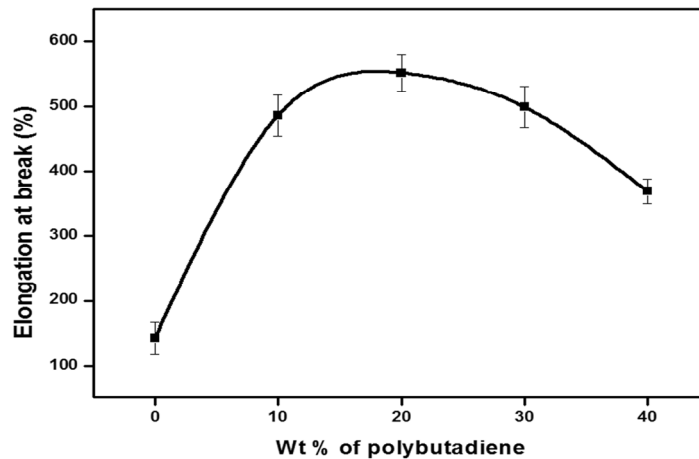


**Figure 3.3. Variation of elongation at break with BR content**

Figure 3.3 shows the variation of elongation at break for the PP/BR blends. It can be seen that the elongation at break increased with the addition of BR, reached a maximum at 20 wt % of BR (P80 sample) and then decreased. A 288 % increase in elongation at break is observed for P80 blend. Further addition of BR decreased the elongation at break. The increase in elongation at break can be attributed to the addition of elastomeric phase. The lowering of the elongation at break at higher BR content may be due to agglomeration of the rubber particles<sup>18,19</sup>.

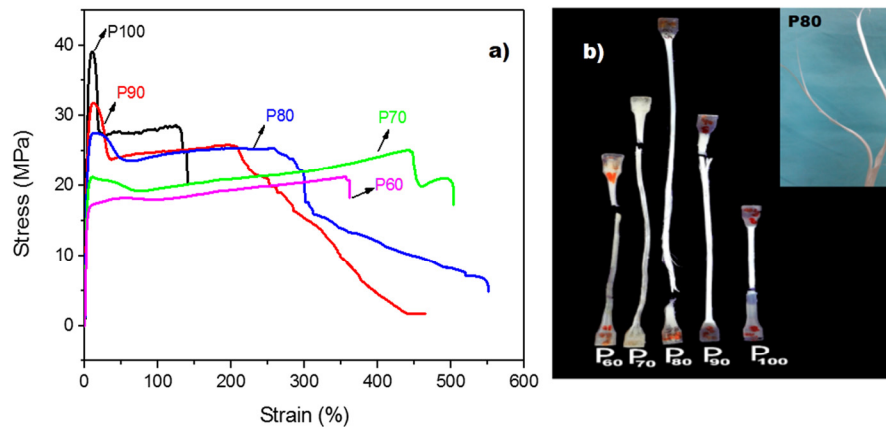


**Figure 3.4. a) Stress-Strain curves of PP/BR blends b) photograph of the tensile fractured surfaces (inset showing the fibrils formed during the tensile failure of P80 sample)**

The stress-strain curves of the P100, P90, P80, P70 and P60 are shown in the Figure 3.4(a). The graphs demonstrated that the nature of the stress strain curves changed considerably with the addition of polybutadiene. Neat PP, exhibited yield maximum, accompanied by the formation of necking, followed by cold drawing. The blends up to 20 % BR showed distinct yield maxima and on further increase in the rubber content, yield maximum disappeared. Blending of PP with BR increased the peak width and

decreased the yield stress over the entire composition studied. The decrease in the yield stress indicates that plastic deformation in the blend begins at a lower stress than pure PP<sup>20</sup>.

Figure 3.4(b) shows the photographs of the tensile fractured surfaces of PP/BR blends. A photograph of highly fibrillated tensile fractured test piece of the P80 sample is shown as inset figure in Figure 3.5(b). From the figure it can be seen that all the blends displayed stress whitening. This can be attributed to the occurrence of microvoids or cavities in the blend during deformation. The formation of microvoids can be either due to debonding of the dispersed particles or due to rubber particle cavitation<sup>21</sup>. Debonding of the rubber particles take place when interfacial adhesion is weak and rubber particle cavitation occurs when the interfacial adhesion is strong.

### 3.3.1.2 Impact strength

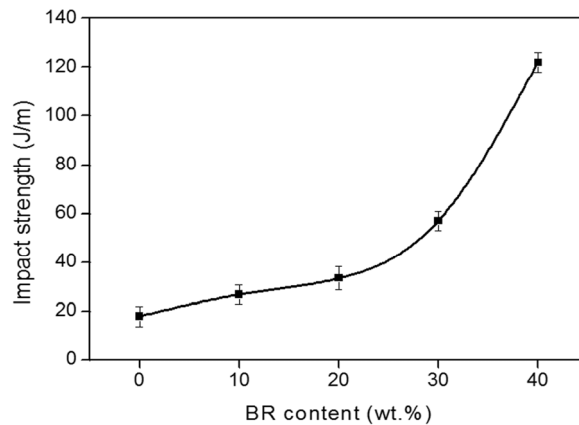


**Figure 3.5. Variation of impact strength with BR content**

Figure 3.5 plots the notched Izod impact strength of PP as a function of BR content. The impact strength of the PP/BR blends is greater than that

of pure PP. An 87% increase in impact strength is observed for the P80 blend. The impact strength of pure PP is very low and the premature failure is due to the brittle fracture. The addition of BR to the PP phase improved the ductility of the matrix leading to increased impact strength for the blends<sup>19</sup>.

### 3.3.2 Theoretical modeling of Tensile strength

Theoretical modeling of the tensile strength data was carried out in order to study the level of interaction between the components in the blend. The predictive models used were:

$$\text{Nielsen's first power law model}^{22,23}: \frac{\sigma_b}{\sigma_m} = (1 - \Phi_d)S \dots\dots\dots(3.1)$$

$$\text{Nielsen's two-third power law model}^{22,23}: \frac{\sigma_b}{\sigma_m} = (1 - \Phi_d^{2/3})S' \dots\dots\dots(3.2)$$

$$\text{Nicolais Narkis model}^{22,23}: \frac{\sigma_b}{\sigma_m} = (1 - K_b \Phi_d^{2/3}) \dots\dots\dots(3.3)$$

Where  $\sigma_b$  and  $\sigma_m$  represents the tensile strength of the blend and the matrix, respectively.  $\Phi_d$  is the volume of the dispersed phase, S and S' are the Nielsen's parameters in the first and two third power law models, respectively, and accounts for the stress concentration effect. According to Nielsen's the value of parameter S and S' are unity for the perfect adhesion or no stress concentration effect. Lower the value of S, the greater the stress concentration effect or poorer is the adhesion.  $K_b$  is the adhesion parameter and the value is 1.21 for spherical inclusions with poor adhesion, values of  $K_b < 1.21$  specify better interphase adhesion<sup>24</sup>. Plots of relative tensile strength ( $\sigma_b/\sigma_m$ ) versus volume fraction of the dispersed phase ( $\Phi_d$ ) of the blends predicted using the three models are presented in Figure 3.6.



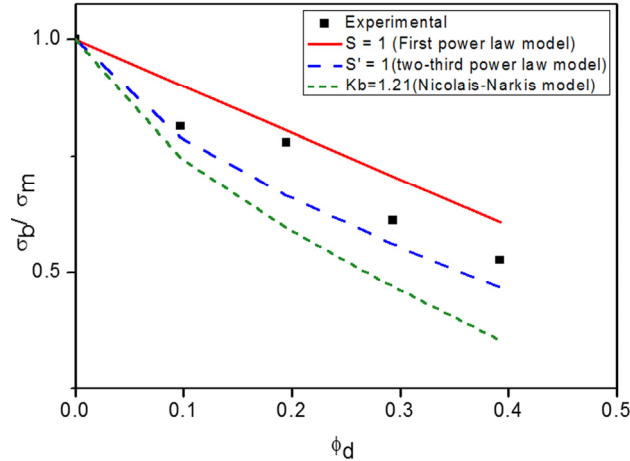


**Figure 3.6.** Plot of relative tensile strength versus volume fraction of dispersed BR phase using different models.

From the Figure 3.6, it is obvious that when PP forms the major phase, the experimental data for all the blend composition are closer to the two-third power law. As two-third power law hold good for spherical inclusions, a morphology with spherical BR elastomer droplets dispersed in the PP matrix can be suggested<sup>23</sup>. In order to investigate the applicability of two-third power law to the PP/BR blends system,  $\log(\sigma_m - \sigma_b / \sigma_m)$  vs  $\log \Phi$  is plotted and the value of the slope is determined (not shown here). The slope of this plot gives the values of the power law exponent according to the equations (3.1) and (3.2), respectively, and is determined to be 0.69. This show that power law exponent is closer to the two-third power law<sup>23,25</sup>.

The values of the relative strength ( $\sigma_b/\sigma_m$ ),  $S$ ,  $S'$  and  $K_b$  are listed in table 3.2. The stress concentration parameter values (close to unity) and  $K_b$  values ( $K_b < 1.21$ ) of the blend systems indicates that stress concentration effect is less in the PP/BR blend<sup>25</sup>.

**Table 3.2. Relative tensile strength and adhesion parameters of PP/BR blends**

Blend	$\sigma_b/\sigma_m$	S	S'	$K_b$
P90	0.813823529	0.901331436	1.029639924	0.888230606
P80	0.779411765	0.967979127	1.17067454	0.660009199
P70	0.611470588	0.865075901	1.090939467	0.884024153
P60	0.526470588	0.866129032	1.129994283	0.886602354

### 3.3.3 Scanning electron microscopy (SEM)

#### a) SEM photographs of the tensile fractured surfaces

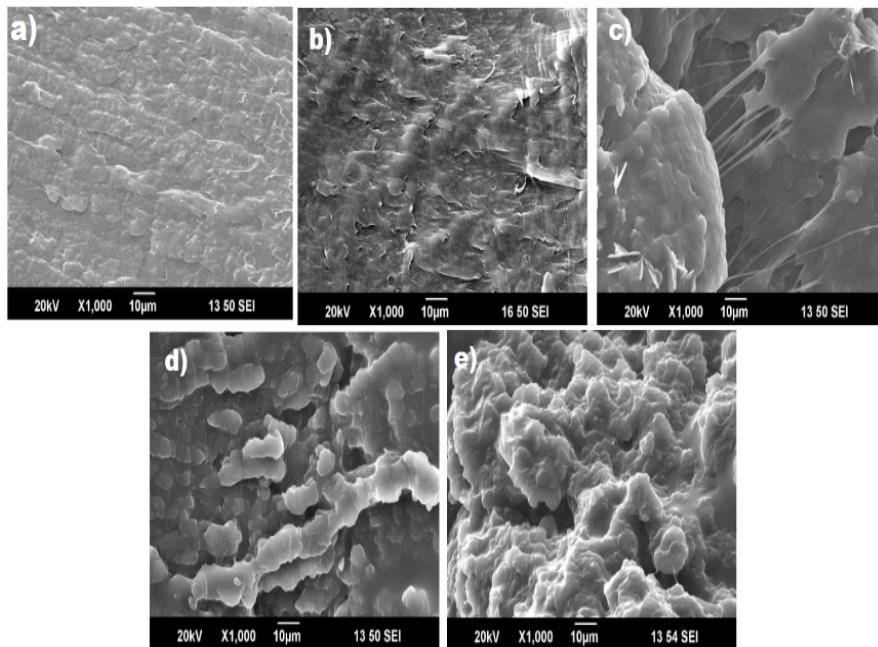


**Figure 3.7. SEM photographs showing Tensile fractured surfaces of PP/BR blends. a) P100 b) P90 c) P80 d) P70 e) P60**

The SEM photographs of the tensile fractured surface of pure PP and the blends are shown in Figure 3.7(a-e). Figure 3.7(a) shows the SEM image

of pure PP which manifests a brittle phase morphology. Figure 3.7(b) shows the fracture surface of P90 sample which exhibited short fibrils indicating plastic deformation. The deformed surface indicates the reduction of brittleness of the matrix by the introduction of rubber. Morphology alteration is observed for higher amounts of rubber in blends as compared to the 90/10 blend. Figure 3.7(c) shows the SEM photograph of the P80 sample which displays fibrils on the fracture surface. This clearly establishes a ductile mode of failure. The morphologies of P70 and P60 blends are shown in Figure 3.7(d) and (e), respectively. These SEM photographs represent typical elastic failure. At low concentration of rubber content the dispersed rubber particles may be smaller in size which is more efficient in improving the plastic deformation of the matrix, where at high concentration, the rubber particles may agglomerate leading to poor stress transfer between the PP matrix and rubber phase.

The high value of elongation at break observed for the P80 blend can be attributed to the ductile mode of failure in the tensile test of the sample as shown in Figure 3.7(c). A fibrillation phenomenon without the distinction between the two phases reflects extensive plastic deformation of the matrix as a result of shear yielding. It seems that the rubber inclusions have undergone cavitation during the deformation. As the elongation proceeds, growth of microvoids have taken place along with the formation of shear bands between the cavitated particles. The craze like structures seen in the photograph of the P80 sample may be due to the shear bands formed as a result of multiple cavitation of rubber particles<sup>4</sup>. Based on the above observations, it can be suggested that under the application of tensile stress, the rubber particles got cavitated around the yield point. On further deformation, extensive plastic stretching of the matrix followed by the elongation of the cavities in the

direction of the applied stress might have taken place<sup>26</sup> Hence it can be concluded that matrix shear yielding produced rubber particle cavitation is the responsible factor for the high elongation at break of P80 blend<sup>3,5,27</sup>. A schematic representation of the tensile fracture mechanism responsible for the high elongation at break for the P80 sample can be given as shown in the Figure 3.8.

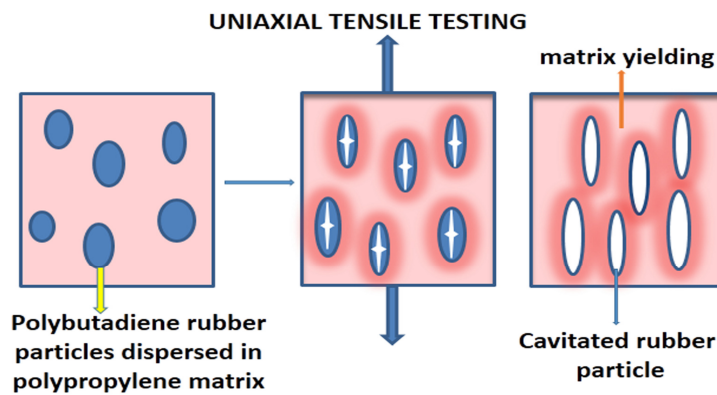


**Figure 3.8. Schematic representation of the tensile fracture mechanism responsible for the high elongation at break for the P80 sample**

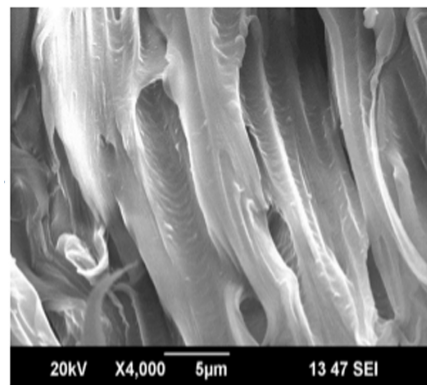


**Figure 3.9. SEM photograph of the microfibrils of the P80 sample**

SEM photograph of the microfibrils of the P80 sample is shown in Figure 3.9. The sausage like shapes seen can be associated with the growth of cavities in the tensile drawing direction of the sample resulting in a highly fibrillated microstructure due to extensive shear yielding of the matrix<sup>28,29</sup>.

**b) SEM photographs of the impact fractured surfaces**

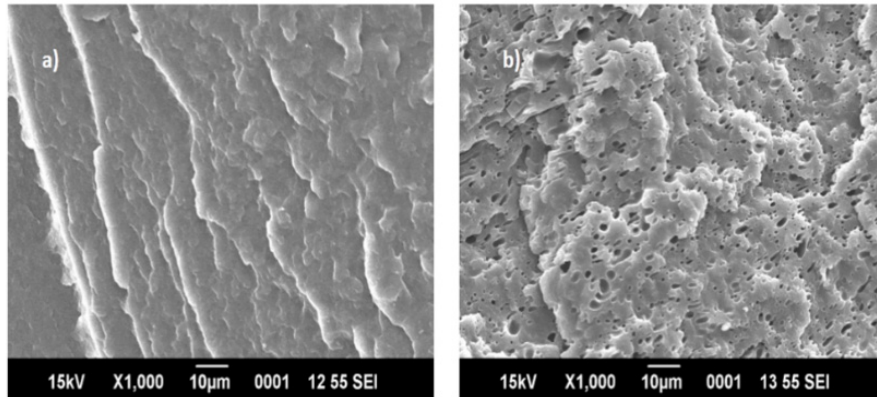


**Figure 3.10. SEM photograph of impact fractured surface of a) P100 b) P80 samples**

The impact fracture morphology of pure PP and P80 blend is displayed in Figure 3.10(a) and (b), respectively. In Figure 3.10(a), the SEM morphology of pure PP clearly indicates a typical brittle fracture and P80 blend shown in Figure 3.10(b) shows the presence of elongated voids indicating rubber particle cavitation and shear yielding of the matrix. The improved impact strength of P80 sample can be attributed to the shear yielding of the PP matrix initiated by rubber particle cavitation<sup>27</sup>.

### 3.3.4 Dynamic rheological analysis (DRA)

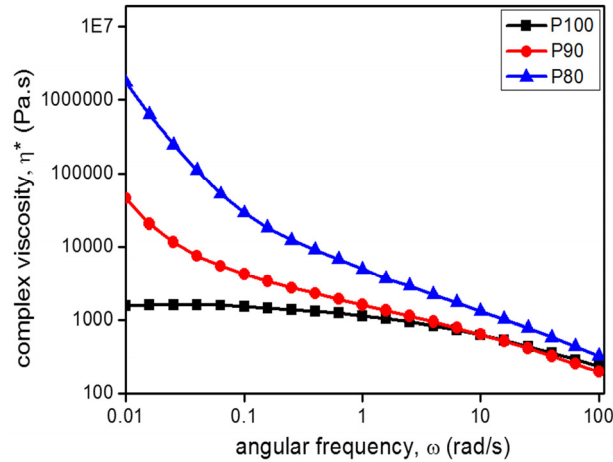


**Figure 3.11. Complex viscosity,  $\eta^*$  as a function of angular frequency of PP/BR blends 190 °C**

The plot of complex viscosity ( $\eta^*$ ) as a function of angular frequency ( $\omega$ ) for P100, P90 and P80 samples is given in Figure 3.11. From the figure it is clear that the complex viscosities of pure PP and the blends (P90 and P80 samples) decreased with increase in frequency. Pure PP exhibited a Newtonian plateau of viscosity at lower frequencies and shear thinning behavior at higher frequencies while the blends revealed marked shear thinning behavior at lower frequencies. The viscosities of the blends are greater than that of pristine PP in the studied frequency range. These observations can be attributed to the restricted mobility of the PP chains by incorporation of BR phase in the PP matrix suggesting interaction between the blend components<sup>30</sup>. Similar results for plastic/rubber blends have been reported by earlier studies<sup>31</sup>.

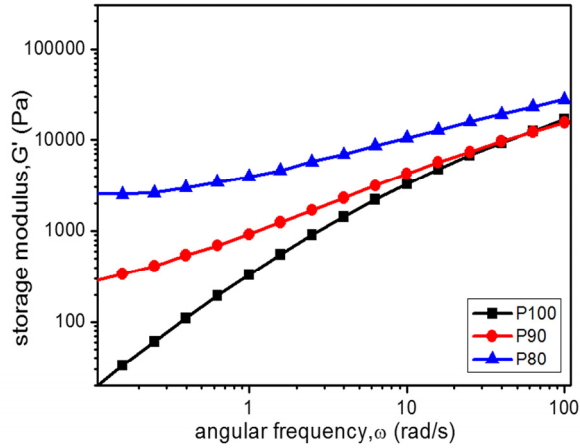


**Figure 3.12. Storage modulus,  $G'$  vs. angular frequency,  $\omega$  of PP/BR blends at 190 °C**

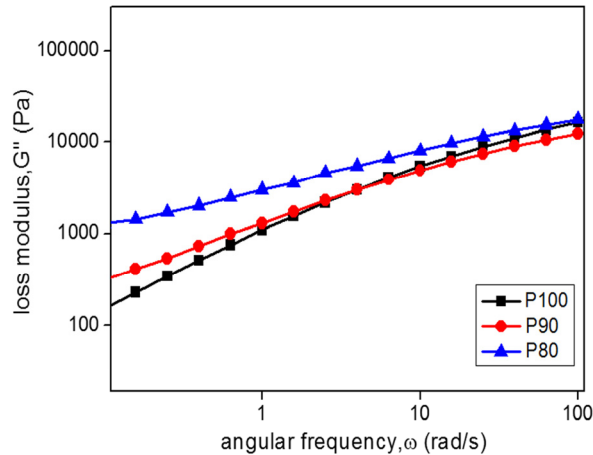


**Figure 3.13. Loss modulus,  $G''$  vs. angular frequency,  $\omega$  of PP/BR blends at 190 °C**

Figures 3.12 and 3.13 represent the storage modulus ( $G'$ ) and loss modulus ( $G''$ ) of P100, P90 and P80 samples, respectively, as a function of angular frequency ( $\omega$ ) at 190 °C. From the Figure 3.12, it is clear that the

storage modulus ( $G'$ ) of pure PP and the blends increased with increase in frequency. At lower frequencies there is enough time for the polymer chains to undergo chain relaxation and hence lower values of  $G'$ . But at higher frequencies, the molecular chains do not get sufficient time for chain relaxation hence  $G'$  values got increased. Storage modulus of the blends are higher than that of pure PP over the studied range of frequency. The storage modulus increased with increase in the rubber content. The interaction between the blend components restricted the mobility of the PP chains there by increasing the storage modulus of the blends. The plot of loss modulus ( $G''$ ) vs. angular frequency ( $\omega$ ) is shown in Figure 3.13. Loss modulus of pure PP and the blends increased with increase in frequency. For the blends, only a very small increase in loss modulus is observed in comparison with storage modulus. From the values of storage modulus ( $G'$ ) and loss modulus ( $G''$ ), it can be seen  $G'$  is greater than  $G''$  in the studied frequency range. This suggests an increasing solid like elastic response for the blends in the entire frequency range. This can be attributed to the interaction between the blend components<sup>32</sup>.

The complex viscosity,  $\eta^*$  as a function of angular frequency,  $\omega$  is given as

$$\eta^* = k\omega^n \dots\dots\dots(3.4)$$

where  $\eta^*$  is a complex viscosity,  $k$  is the exponential factor,  $\omega$  is the oscillation frequency and  $n$  is the shear thinning exponent. The value of  $n$  can be determined from the slope of  $\log \eta^*$  vs.  $\log \omega$ <sup>33</sup>. The relationship between  $G'$  and  $G''$  with angular frequency  $\omega$  is given as

$$G' \propto \omega^{n_1} \quad (n_1=2) \dots\dots\dots(3.5)$$

$$G'' \propto \omega^{n_2} \quad (n_2=1) \dots\dots\dots(3.6)$$



The slopes of the terminal zone  $n_1$  and  $n_2$  can be determined from the slopes of  $\log G'$  and  $\log G''$  vs.  $\log \omega$ <sup>34</sup>. The value of  $n$ ,  $n_1$  and  $n_2$  is as shown in table 3.3. The values of shear thinning exponent varies from  $n = -0.34$  to  $n = -0.59$  indicating high shear thinning behavior of the PP/BR blends. The decrease in the terminal slope  $n_1$  and  $n_2$  supports interaction between the blend components<sup>35</sup>.

**Table 3.3. Slopes of  $\log \eta^*$ ,  $\log G'$  and  $G''$  vs.  $\log \omega$  at 190 °C ( $n$ ,  $n_1$  and  $n_2$ ), respectively, as observed from frequency sweep experiments**

Sample	$n$	$n_1$	$n_2$
P100	-0.34	0.99	0.68
P90	-0.49	0.58	0.52
P80	-0.59	0.37	0.39

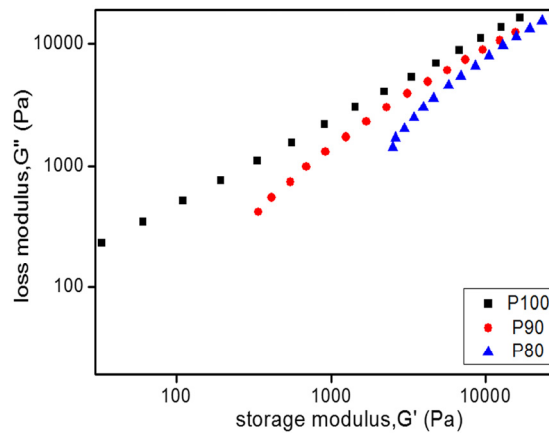


**Figure 3.14. Cole-Cole plots of  $G''$  vs.  $G'$  of PP/BR blends with angular frequency,  $\omega$  as a parameter**

Figure 3.14 shows Cole-Cole plots of  $G''$  vs.  $G'$  for PP/BR blends. At lower frequencies, data is scattered for the samples, but at the higher frequencies all the curves are super imposed. The plot shows a straight line

for P100 but there is variation in the shape of P90 and P80 curves. The change in the shape of the curves signifies the change in melt behavior of the blends. The curves suggest that the samples show different relaxation mechanism in the low frequency region and similar relaxation mechanisms in the high frequency region. Also, the curves for the blends are positioned to the right side of that of P100 ( $G' > G''$ ) showing increased elasticity of the blends<sup>36,37</sup>.

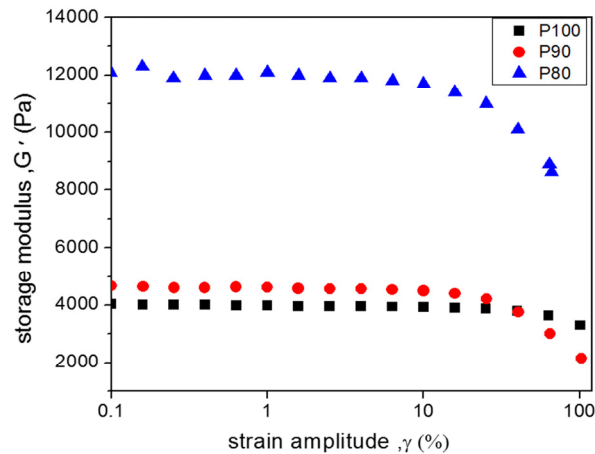
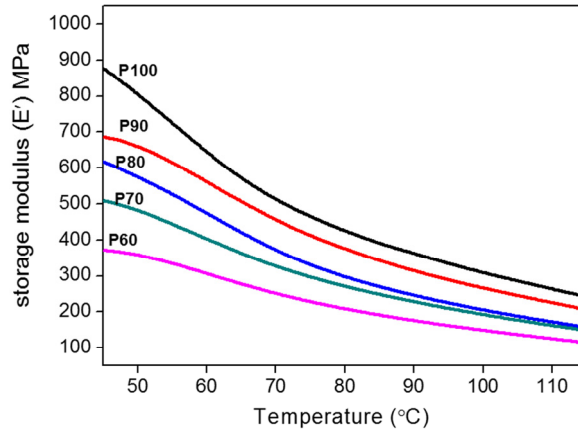


Figure 3.15. Storage modulus vs. strain amplitude of PP/BR blends

Figure 3.15 represents the variation of storage modulus ( $G'$ ) with strain amplitude ( $\gamma$ ) for P100, P90 and P80 blends at 190 °C. It was observed that P100 show linearity with strain up to 100 %, whereas P90 exhibit strain independent behavior up to 25 % strain and P80 up to 16% strain. Thus the linear viscoelastic region of the PP/BR blends got decreased. The lower value of critical strain for the blends than pristine PP demonstrated that the microstructure formed due to the entanglements between amorphous BR rubber and PP chains cannot resist large deformation in the molten state<sup>38,39</sup>.

Similar results for PP/EPDM blends were reported in by Manchado *et al.*<sup>12</sup> on the investigations of the rheological properties of PP/EPDM (75/25) blend in which the elastomer particles were found to be dispersed in the PP matrix. It was established that the incorporation of the rubber increased the complex viscosity and elastic modulus of PP. Cole–Cole plots exhibited a single curve for compositions with low content of rubber in these blends indicating good compatibility. Gong *et al.*<sup>13</sup> reported that at lower frequencies, complex viscosities ( $\eta^*$ ), storage modulus ( $G'$ ) and loss modulus ( $G''$ ) of the PP/EPDM blends were found to be greater than that of pure PP and increased with EPDM content in the blend. These observations established the restriction of mobility of PP chains by the entanglements in EPDM chains.

### 3.3.5 Dynamic mechanical analysis (DMA)



**Figure 3.16. Variation of Storage modulus,  $G'$  with temperature of PP/BR blends**

The storage modulus ( $E'$ ) of pure PP and PP/BR blends is plotted as a function of temperature in Figure 3.16. Storage modulus,  $E'$  indicates the

stiffness of the material and  $E''$  represents the damping behavior. The storage modulus of polypropylene decreased with increase in the BR content the blends and also with increase in temperature for all the samples. Semicrystalline PP possess inherently higher modulus and the addition of amorphous rubber phase results in the decrease of crystallinity of the PP matrix. Hence storage modulus got reduced<sup>40,41</sup>.

**Table 3.4. Storage modulus ( $E'$ ), Loss modulus ( $E''$ ) and  $\tan \delta$  of the PP/BR blend systems**

Sample	$E'$ (MPa)			$E''$ (MPa)			Tan $\delta$		
	50 °C	75 °C	100 °C	50 °C	75 °C	100 °C	50 °C	75 °C	100 °C
<b>P100</b>	804	464	308	67	52	35	0.084	0.113	0.116
<b>P90</b>	659	412	265	59	48	32	0.089	0.118	0.122
<b>P80</b>	574	331	205	50	39	26	0.087	0.120	0.130
<b>P70</b>	481	296	192	47	38	26	0.098	0.129	0.138
<b>P60</b>	357	228	148	36	30	21	0.102	0.134	0.145

Table 3.4 shows the variation of storage modulus ( $E'$ ), loss modulus ( $E''$ ) and  $\tan \delta$  at various temperatures for the PP/BR blend systems. It is seen that the decrease in storage modulus is more prominent with the addition of higher amount of BR. From table 3.4 it can be seen that PP/BR blends show similar values for  $E''$  and  $\tan \delta$  so that no prominent transition is observed with the addition of BR in the studied temperature range.

### 3.3.6 Differential scanning calorimetry (DSC)

DSC was carried out to analyze the effect of BR content on the crystallization behavior of PP. Figure 3.17 shows the DSC heating curves of the PP/BR blends in the temperature range 30 °C to 200 °C. The parameters such as melting point ( $T_m$ ), onset of melting temperature ( $T_{m,onset}$ ), endset of

melting temperature ( $T_{m,endset}$ ), Heat of fusion ( $\Delta H_f$ ), and percentage of crystallinity ( $X_c$ ) obtained from the heating curves is given in table 3.5.

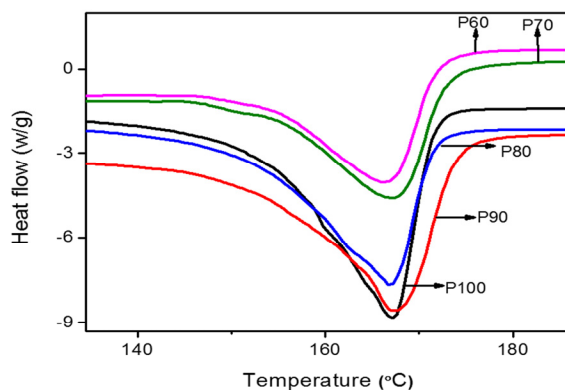


Figure 3.17. DSC heating curves of PP/BR blends

Table 3.5. Melting characteristics of PP/BR blends

Sample	$T_{m,onset}$ (°C)	$T_m$ (°C)	$T_{m,endset}$ (°C)	$\Delta H_f$ J/g	$X_c$ (%)
P100	154	167	171	93.76	45
P90	157	167	174	69.26	37
P80	153	167	171	70.57	42
P70	152	167	172	47.16	32
P60	152	166	172	37.41	29

DSC cooling curves of PP/BR blends are shown in Figure 3.18. Parameters such as the crystallization peak temperature ( $T_c$ ), onset of the crystallization temperature ( $T_{c,onset}$ ), endset of crystallization temperature ( $T_{c,endset}$ ) and Heat of crystallization ( $\Delta H_c$ ) are obtained from the cooling curves are shown in table 3.6.

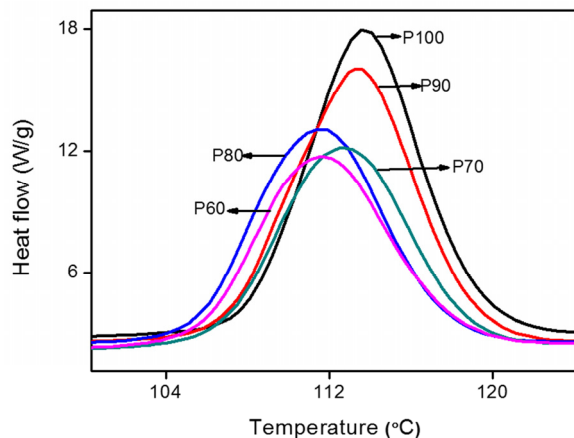


Figure 3.18. DSC cooling curves of PP/BR blends

Table 3.6. Crystallization characteristics of PP/BR blends

Sample	T <sub>c,onset</sub> (°C)	T <sub>c</sub> (°C)	T <sub>c,endset</sub> (°C)	T <sub>m</sub> -T <sub>c</sub> (°C)	ΔH <sub>c</sub> J/g
P100	119	114	108	53	111.68
P90	119	113	107	54	78.82
P80	118	111	106	56	88.23
P70	119	113	107	54	59.20
P60	118	112	106	55	50.44

Only single melting peak and crystallization peak corresponding to that of PP is observed in the DSC scans, since BR is amorphous. From the results it is clear that the addition of polybutadiene rubber did not show significant changes in T<sub>m</sub> and T<sub>c</sub> of the PP phase. The degree of super cooling represented as T<sub>m</sub>-T<sub>c</sub> also remains unaltered. All these results indicated the weak nucleating effect of BR. The value of heat of fusion of 100% crystalline PP is 209J/g and the degree of crystallinity of pure PP is estimated to be about 45% using equation (2.2). As seen from the tables 3.5

and 3.6, percentage crystallinity of PP got decreased in the same manner as enthalpies of fusion and crystallization with the addition of BR content. This can be attributed to the fact that the introduction of the rubbery phase into the semi-crystalline PP matrix restricts the mobility of PP chains, thereby hindering the spherulite growth process resulting in the reduction of crystallinity<sup>42,43</sup>.

Investigations on DSC studies of PP/EPDM blends and PP/EPDM-g-MAH blends made by Purnima *et al.*<sup>11</sup> revealed that the presence of EPDM chain restricts chain mobility of PP in the EPDM in the interfacial region and thereby reducing the nucleation rate. DSC studies revealed that both the blends with and without interfacial modification exhibited unaltered  $T_m$ , whereas a decrease in  $T_{m,onset}$  was revealed. This implies slowing down of the nucleation rate.

### 3.3.7 Thermogravimetric analysis (TGA)

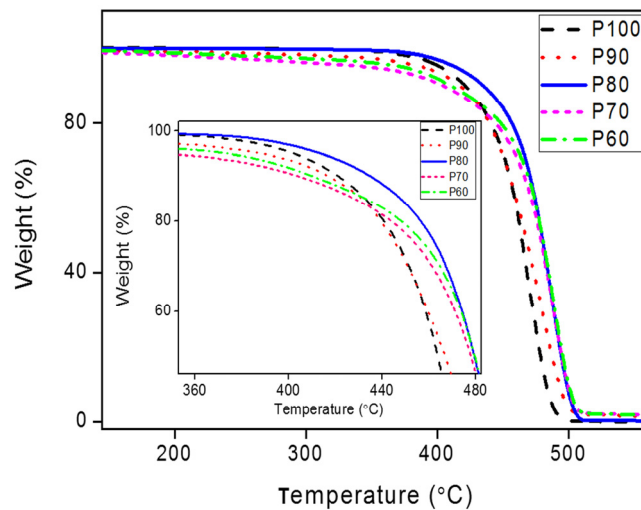


Figure 3.19. TGA curves of PP/BR blends

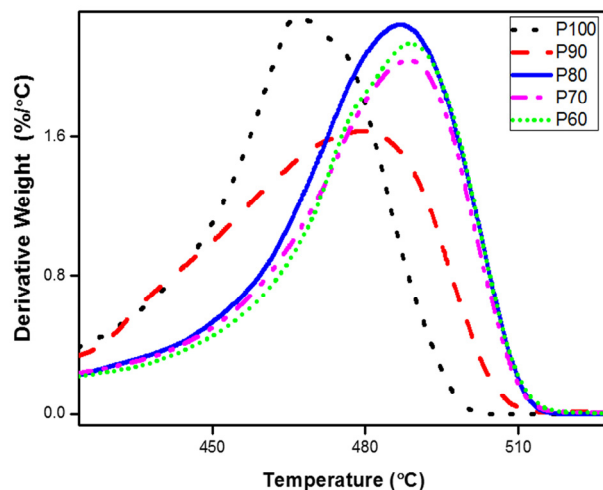


Figure 3.20. DTG curves of PP/BR blends

Figures 3.19 and 3.20 shows the TGA and DTG profiles of the PP/BR blends, respectively. The thermal degradation parameters such as onset degradation temperature  $T_{onset}$ , temperature at 10% weight loss ( $T_{10}$ ) and temperature at 50% weight loss ( $T_{50}$ ), maximum degradation temperature ( $T_{max}$ ) and final decomposition temperature ( $T_f$ ) are listed in table 3.7.

Table 3.7. TGA parameters of PP/BR blends

Sample code	$T_{onset}$	$T_{10}$	$T_{50}$	$T_{max}$	$T_f$
P100	360	421	463	466	500
P90	358	416	466	479	510
P80	365	435	479	486	514
P70	368	404	477	488	513
P60	375	410	479	488	512

From the Figures 3.19 and 3.20, it can be observed that all the samples displayed single step degradation process. From the table 3.7, it is clear that the presence of BR in the blends enhanced the thermal stability of the



blends. The blend with 20 wt % of BR showed the highest decomposition temperature. The TG and DTG curves demonstrated that both the initial and final decomposition temperatures of the blends increased.

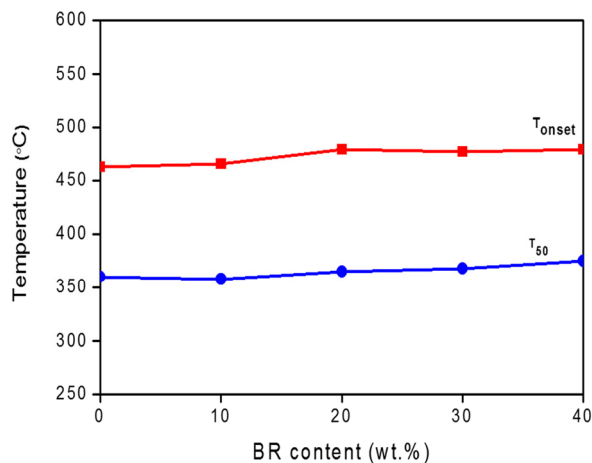


**Figure 3.21. Variation of  $T_{\text{onset}}$  and  $T_{50}$  of PP/BR blends**

The initial decomposition temperature ( $T_{\text{onset}}$ ) and temperature at 50% decomposition ( $T_{50}$ ) are plotted as a function of blend composition in Figure 3.21. Both  $T_{\text{onset}}$  and  $T_{50}$  showed an increase with BR content. The enhancement in thermal stability can be attributed to the retention of the volatile PP degradation products by the rubber phase. The improvement in thermal stability reflects better interaction between PP and BR phases, as the blends need more thermal energy for the decomposition of polymer matrix leading to delay in the decomposition of PP<sup>44,45</sup>.

### 3.3.8 Reprocessability of blends.

Table 3.8 illustrates the effect of recyclability on the mechanical properties of PP/BR blends. R1 and R2 refers to the 1<sup>st</sup> and 2<sup>nd</sup> recycling, respectively. On recycling, elongation at break values got reduced, but well

within the limit for TPEs (greater than 100 % elongation). Chakraborty *et al*<sup>46</sup> reported an increase in the strength of EPDM/PP (74/26) blend in the presence of maleated ethylene propylene diene rubber (MAEPDM) and sulphonated ethylene propylene diene rubber (SEPDM) as phase modifiers after the first and second recycling. They suggested that in the presence of phase modifiers, reprocessing might have broken down the dispersed rubber domain sizes into smaller ones. The improved tensile strength and modulus in the case of recycled PP/BR blends also may be due to the breakdown of rubber domain sizes in to smaller ones under shear during reprocessing. It has been established that particle cavitation makes an important contribution to the toughening mechanism. Several studies have reported that rubber particle size is one of the main factors governing cavitation. Hence the decrease in impact strength may be due to the reduction of the effective rubber particle size<sup>47</sup>. After the first and second recycling, elongation at break and moduli values show that these blends can be termed as TPEs.

**Table 3.8. Effect of recycling on mechanical properties of PP/BR blends**

<b>Samples with Recycling cycles</b>	<b>Tensile strength MPa</b>	<b>Elongation at break %</b>	<b>Young's modulus MPa</b>	<b>Impact strength J/m</b>
<b>P90</b>	32.5	486	1038	26.8
R1	32.2	221	1027	21.7
R2	32.8	227	970	19.3
<b>P80</b>	26.5	552	961	33.5
R1	27.2	323	958	23.2
R2	26.8	327	951	21.1
<b>P70</b>	23	499	736	57
R1	25.8	224	744	25.9
R2	26.2	227	729	27.4
<b>P60</b>	18.6	370	680	122
R1	21.2	221	729	54.7
R2	21.8	218	670	48.7

### 3.4 Conclusions

The tensile strength and Young's modulus of polypropylene (PP) decrease with the addition of soft amorphous polybutadiene rubber (BR) in to the PP matrix. The elongation at break and impact strength of PP improve with the addition of BR. The PP/BR blend with 20 wt % of BR content (P80 sample) exhibit maximum elongation at break. SEM studies show that the dominant mechanism of deformation during tensile fracture of the P80 sample is massive shear yielding caused by repeated cavitation of rubber particles. The experimental tensile strength of PP/BR blends was compared with predictive models such as Nielsen's first power law model, Nielsen's two-third power law model and Nicolais-Narkis model. The experimental values are in good agreement with Nielsen's two-third power law model confirming a matrix droplet morphology with BR domains as spherical inclusions. Dynamic rheological analysis (frequency sweep) of the blends show an increase in complex viscosity ( $\eta^*$ ), storage modulus ( $G'$ ) and loss modulus ( $G''$ ) with increasing BR content. DMA studies show decrease in stiffness of the PP matrix with the introduction of the BR phase. DSC studies prove that the percentage of crystallinity of PP phase decrease with polybutadiene content. The addition of BR to PP matrix do not affect the melting temperature ( $T_m$ ) and crystallization temperature ( $T_c$ ) of PP, which shows the weak nucleating effect of BR on PP matrix. Thermogravimetric studies reveal increased thermal stability of PP with the addition of BR. Melt blending of PP with BR generate a TPE having improved mechanical and thermal properties with good reprocessability.

## References

- [1] Legge, N. R. (1987). *Thermoplastic elastomers, a comprehensive review*. Hanser
- [2] Walker, B. M., & Rader, C. P. (Eds.). (1979). *Handbook of thermoplastic elastomers* (pp. 115-205). New York: Van Nostrand Reinhold.
- [3] Panda, B. P., Mohanty, S., & Nayak, S. K. (2015). Mechanism of toughening in rubber toughened polyolefin—a review. *Polymer-Plastics Technology and Engineering*, 54(5), 462-473
- [4] Zebarjad, S. M., Bagheri, R., Lazzeri, A., & Serajzadeh, S. (2004). Dilatational shear bands in rubber-modified isotactic polypropylene. *Materials & design*, 25(3), 247-250
- [5] Bartczak, Z., Argon, A. S., Cohen, R. E., & Weinberg, M. (1999). Toughness mechanism in semi-crystalline polymer blends: I. High-density polyethylene toughened with rubbers. *Polymer*, 40(9), 2331-2346.
- [6] Kim, G. M., Michler, G. H., Gahleitner, M., & Mülhaupt, R. (1998). Influence of morphology on the toughening mechanisms of polypropylene modified with core-shell particles derived from thermoplastic elastomers. *Polymers for Advanced Technologies*, 9(10-11), 709-715.
- [7] Chiu, H. T., Shiau, Y. G., Chiu, W. M., & Syau, S. S. (1995). Toughening isotactic polypropylene and propylene-ethylene block copolymer with styrene-ethylene butylene-styrene triblock copolymer. *Journal of Polymer Research*, 2(1), 21-29.
- [8] Abreu, F. O. M. S., Forte, M. M. C., & Liberman, S. A. (2005). SBS and SEBS block copolymers as impact modifiers for polypropylene compounds. *Journal of applied polymer science*, 95(2), 254-263
- [9] Karger-Kocsis, J. (1995). Microstructural aspects of fracture in polypropylene and in its filled, chopped fiber and fiber mat reinforced composites. In *Polypropylene Structure, blends and composites* (pp. 142-201). Springer Netherlands.

- [10] Lu, M. L., Chiou, K. C., & Chang, F. C. (1996). Fracture behavior of polypropylene/ethylene-diene-terpolymer blends: effect of temperatures, notch radius and rubber content. *Journal of Polymer Research*, 3(2), 73-82.
- [11] Purnima, D., Maiti, S. N., & Gupta, A. K. (2006). Interfacial adhesion through maleic anhydride grafting of EPDM in PP/EPDM blend. *Journal of applied polymer science*, 102(6), 5528-5532.
- [12] López Manchado, M. A., Biagiotti, J., & Kenny, J. M. (2001). Rheological behavior and processability of polypropylene blends with rubber ethylene propylene diene terpolymer. *Journal of applied polymer science*, 81(1), 1-10.
- [13] Gong, L., Yin, B., Li, L. P., & Yang, M. B. (2012). Morphology and properties of PP/EPDM binary blends and PP/EPDM/nano-CaCO<sub>3</sub> ternary blends. *Journal of Applied Polymer Science*, 123(1), 510-519.
- [14] Gupta, A. K., & Ratnam, B. K. (1991). Crystallization, tensile, and impact behavior of polypropylene/polybutadiene blend. *Journal of applied polymer science*, 42(2), 297-315.
- [15] Chen, Y., Chen, Y., & Yang, D. (2006). Crystallization and phase behavior of crystalline syndiotactic 1, 2-polybutadiene/isotactic polypropylene blends in solution-cast thin films. *Polymer*, 47(5), 1667-1673.
- [16] Ma, G. Q., Yuan, X. B., Sheng, J., & Bian, D. C. (2002). Blends of polypropylene with poly (cis-butadiene) rubber. II. Small-angle X-ray scattering studies of the phase structure of immiscible blends of polypropylene with poly (cis-butadiene) rubber. *Journal of applied polymer science*, 83(10), 2088-2094.
- [17] George, S., Joseph, R., Thomas, S., & Varughese, K. T. (1995). Blends of isotactic polypropylene and nitrile rubber: morphology, mechanical properties and compatibilization. *Polymer*, 36(23), 4405-4416.
- [18] Bassani, A., Pessan, L. A., & Hage, E. (2001). Toughening of polypropylene with styrene/ethylene-butylene/styrene tri-block copolymer: Effects of mixing condition and elastomer content. *Journal of applied polymer science*, 82(9), 2185-2193.

- [19] Ismail, H. (2002). Thermoplastic elastomers based on polypropylene/natural rubber and polypropylene/recycle rubber blends. *Polymer Testing*, 21(4), 389-395.
- [20] Gupta, A. K., & Purwar, S. N. (1984). Tensile yield behavior of PP/SEBS blends. *Journal of applied polymer science*, 29(11), 3513-3531
- [21] Li, Z. M., Xie, B. H., Yang, S., Huang, R., & Yang, M. B. (2004). Morphology-tensile behavior relationship in injection molded poly (ethylene terephthalate)/polyethylene and polycarbonate/polyethylene blends (II) Part II Tensile behavior. *Journal of materials science*, 39(2), 433-443.
- [22] Nielsen, L. E. (1966). Simple theory of stress-strain properties of filled polymers. *Journal of Applied Polymer Science*, 10(1), 97-103.
- [23] Jose, S., Thomas, S., Biju, P. K., & Karger-Kocsis, J. (2013). Mechanical and dynamic mechanical properties of polyolefin blends: effect of blend ratio and copolymer monomer fraction on the compatibilisation efficiency of random copolymers. *Journal of Polymer Research*, 20(12), 303.
- [24] Parameswaranpillai, J., Joseph, G., Jose, S., & Hameed, N. (2015). Phase morphology, thermomechanical, and crystallization behavior of uncompatibilized and PP-g-MAH compatibilized polypropylene/polystyrene blends. *Journal of Applied Polymer Science*, 132(24),42100.
- [25] Soni, R. K., Singh, H., Dutt, K., & Arora, P. (2010). Effect of dynamic cross-linking on mixing torque behavior and tensile yield behavior of isotactic polypropylene (iPP)/ethylene-propylene diene rubber (EPDM)/nitrile rubber (NBR) elastomeric blends. *Journal of polymer research*, 17(3), 411-427.
- [26] Maiti, S. N., & Das, R. (2005). Mechanical properties of impact i-PP/CSM rubber blends. *International Journal of Polymeric Materials*, 54(6), 467-482.
- [27] Liang, J. Z., & Li, R. K. Y. (2000). Rubber toughening in polypropylene: a review. *Journal of Applied Polymer Science*, 77(2), 409-417.
- [28] Bartczak, Z., & Grala, M. (2017). Toughening of semicrystalline and amorphous polylactide with atactic polyhydroxybutyrate. *Polymer-Plastics Technology and Engineering*, 56(1), 29-43.

- [29] Ponçot, M., Addiego, F., & Dahoun, A. (2013). True intrinsic mechanical behaviour of semi-crystalline and amorphous polymers: influences of volume deformation and cavities shape. *International Journal of Plasticity*, 40, 126-139.
- [30] Liu, Y., & Kontopoulou, M. (2006). The structure and physical properties of polypropylene and thermoplastic olefin nanocomposites containing nanosilica. *Polymer*, 47(22), 7731-7739.
- [31] Wagener, R., & Reisinger, T. J. (2003). A rheological method to compare the degree of exfoliation of nanocomposites. *Polymer*, 44(24), 7513-7518
- [32] Thompson, A., Bianchi, O., Amorim, C. L., Lemos, C., Teixeira, S. R., Samios, D., Giacomelli, C., Crespo, J.S., Machado, G. (2011). Uniaxial compression and stretching deformation of an i-PP/EPDM/organoclay nanocomposite. *Polymer*, 52(4), 1037-1044.
- [33] Mishra, J. K., Hwang, K. J., & Ha, C. S. (2005). Preparation, mechanical and rheological properties of a thermoplastic polyolefin (TPO)/organoclay nanocomposite with reference to the effect of maleic anhydride modified polypropylene as a compatibilizer. *Polymer*, 46(6), 1995-2002.
- [34] Nakason, C., Saiwari, S., & Kaesaman, A. (2006). Rheological properties of maleated natural rubber/polypropylene blends with phenolic modified polypropylene and polypropylene-g-maleic anhydride compatibilizers. *Polymer testing*, 25(3), 413-423.
- [35] Zou, D., Li, X., Long, S., & Chen, Q. (2015). Effect of compatibiliser on rheological behaviour of straw fibre/low density polyethylene composites. *Plastics, Rubber and Composites*, 44(6), 238-244.
- [36] Kim, T. H., Lim, S. T., Lee, C. H., Choi, H. J., & Jhon, M. S. (2003). Preparation and rheological characterization of intercalated polystyrene/organophilic montmorillonite nanocomposite. *Journal of Applied Polymer Science*, 87(13), 2106-2112.
- [37] Hui, S., Chaki, T. K., & Chattopadhyay, S. (2010). Dynamic and capillary rheology of LDPE-EVA-based thermoplastic elastomer: Effect of silica nanofiller. *Polymer Composites*, 31(3), 377-391.

- [38] Barick, A. K., & Tripathy, D. K. (2011). Effect of organically modified layered silicate nanoclay on the dynamic viscoelastic properties of thermoplastic polyurethane nanocomposites. *Applied Clay Science*, 52(3), 312-321.
- [39] Rinawa, K., Maiti, S. N., Sonnier, R., & Cuesta, J. M. L. (2015). Dynamic rheological studies and applicability of time-temperature superposition principle for PA12/SEBS-g-MA blends. *Polymer Bulletin*, 12(72), 3305-3324.
- [40] George, K. E., Komalan, C., Kumar, P. A. S., Varughese, K. T., & Thomas, S. (2007). Dynamic mechanical analysis of binary and ternary polymer blends based on nylon copolymer/EPDM rubber and EPM grafted maleic anhydride compatibilizer. *Express Polymer Letters*, 10(1), 641-653.
- [41] Satapathy, S., Nag, A., & Nando, G. B. (2010). Thermoplastic elastomers from waste polyethylene and reclaim rubber blends and their composites with fly ash. *Process Safety and Environmental Protection*, 88(2), 131-141
- [42] Martuscelli, E., Silvestre, C., & Abate, G. (1982). Morphology, crystallization and melting behaviour of films of isotactic polypropylene blended with ethylene-propylene copolymers and polyisobutylene. *Polymer*, 23(2), 229-237.
- [43] Jarntong, M., Nakason, C., Lopattananon, N., & Peng, Z. (2012). Influence of incorporation sequence of silica nanoparticles on morphology, crystallization behavior, mechanical properties, and thermal resistance of melt blended thermoplastic natural rubber. *Polymer Composites*, 33(11), 1911-1920.
- [44] Iqbal, J., Pandey, K. N., Verma, V., Singh, P., & Mishra, R. M. (2015). Physico-mechanical and thermal behaviour of binary blends of EPDM and LLDPE. *European Journal of Advances in Engineering and Technology*, 2(10), 43-48.
- [45] Choudhury, N. R., Chaki, T. K., & Bhowmick, A. K. (1991). Thermal characterization of thermoplastic elastomeric natural rubber-polypropylene blends. *Thermochimica acta*, 176, 149-161.



- [46] Chakraborty, P., Ganguly, A., Mitra, S., & Bhowmick, A. K. (2008). Influence of phase modifiers on morphology and properties of thermoplastic elastomers prepared from ethylene propylene diene rubber and isotactic polypropylene. *Polymer Engineering & Science*, 48(3), 477-489.
- [47] Bucknall, C. B., Karpodinis, A., & Zhang, X. C. (1994). A model for particle cavitation in rubber-toughened plastics. *Journal of Materials Science*, 29(13), 3377-3383.

.....❧.....

**POLYPROPYLENE/POLYBUTADIENE BLEND:  
EFFECT OF NANOFILLERS****Contents***Part A**Polypropylene/Polybutadiene/nanoclay Composites**Part B**Polypropylene/Polybutadiene/carbon nanofibre composites***Part A****POLYPROPYLENE/POLYBUTADIENE/NANOCLAY COMPOSITES**

*The effect of nanoclay (Cloisite 93A) content on thermoplastic elastomer (TPE) based on polypropylene/polybutadiene (PP/BR) blend (80/20) prepared by melt blending process was investigated. The distribution of nanoclay studied using transmission electron microscopy (TEM) show partially exfoliated and intercalated distribution of nanoclay. The mechanical properties like tensile strength, impact strength and Young's modulus of the PP/BR blend show improvement even at low loadings of nanoclay. Halpin-Tsai (H-T) micromechanical model was used to estimate the aspect ratio ( $A_f$ ) of the clay layers and the average value of  $A_f$  was found to be 45. Nanocomposite reveals good filler/polymer interaction in the Dynamic rheological analysis (DRA) carried out in the frequency sweep and Dynamic mechanical analysis (DMA) carried out in the temperature sweep experiments. Differential scanning calorimetry (DSC) studies show that the introduction of nanoclay in the blend hardly affect the degree of crystallization of PP. Thermogravimetric analysis (TGA) reveal enhancement in the thermal stability of the nanocomposites.*

### 4A.1 Introduction

The versatility of thermoplastic elastomers (TPEs) is that they combine the processability of thermoplastics and the elasticity of the elastomer. Thermoplastic elastomers based on plastic/rubber blends are commonly referred to as thermoplastic polyolefins (TPOs)<sup>1</sup>. Polypropylene (PP) is one of the most widely used thermoplastic because of its low density, low cost and easy processability. The use of polypropylene as an engineering thermoplastic is limited because of its brittle nature and low impact strength. Elastomers such as ethylene propylene copolymer (EPR), ethylene propylene diene monomer (EPDM), styrene butadiene styrene (SBS), styrene ethylene butadiene styrene (SEBS), polybutadiene rubber (BR) and natural rubber (NR) are mainly used for improving the toughness of PP<sup>2</sup>. It is generally observed that in TPOs, where the PP content is high, PP forms the continuous phase and the elastomer forms the dispersed phase. The dispersed elastomer aids to improve the impact strength of PP matrix, but provide an adverse effect on the stiffness and strength of the material<sup>3</sup>. This issue is often alleviated by the addition of inorganic fillers in to the polymer matrix, but high loading of inorganic filler is needed which leads to poor processability<sup>4</sup>. In this perspective, the development of TPO nanocomposite offers great potential for applications, as they contribute to balanced stiffness and toughness properties and weight reduction<sup>5</sup>. Polymer nanotechnology is an important multidisciplinary research area with extensive applications, as the nanoscale dispersion of the filler within the polymer matrix is achieved at very low loading levels of the nanofiller and leads to significant improvements in the properties<sup>6</sup>.

Researches on polymer nanocomposites are largely based on characteristic nanomaterials like nanoclay or a layered silicate. The most

generally studied nanoclay is Montmorillonite (MMT), owing to its natural abundance, well-studied chemistry and environmental friendliness. Organically modified layered silicates commonly referred as ‘nanoclays’ proves to be an excellent choice for the development of nanocomposites, because of the high aspect ratio and large surface area that provide better reinforcement in two dimensions<sup>5,7</sup>. Cation exchange of sodium or potassium cations in MMT for alkyl ammonium cations makes the layers hydrophobic and is expected to be compatible with a preferred polymer matrix. In literature<sup>8</sup>, the dispersion of nanoclay in the polymeric matrix is described in terms of morphologies defined as immiscible, intercalated and exfoliated. In an immiscible composite, organoclay exist as tactoids. Whereas in an intercalated structure, the clay layers will expand the gallery spaces due to the diffusion of the polymer chains in between. In an exfoliated structure, the layered structure of the nanoclay will be demolished and will get individually distributed in the polymer matrix. Even though complete exfoliation of nanoclay in the polymer matrix is the desired goal for the improvement of mechanical properties, true and complete exfoliation is rare and most matrices display a combination of both exfoliated and intercalated structure of nanoclay.

Researches have shown that proper distribution of nanoclay in the polymer matrix is required to achieve desired end use properties<sup>9</sup>. Hence, careful choice of the method adopted for the preparation of the nanocomposites is of great significance. The development of TPO nanocomposites by direct melt blending have been reported by many researchers as a potential method to achieve better dispersion of nanoclay in enhancing the properties. Melt blending technique is worth mentioning as it is very simple, easy, do not require any solvent and is ecofriendly<sup>13</sup>. Melt intercalation technique

involves the blending of the nanoclay with the thermoplastic above the melting point of the thermoplastic. During the blending process, the polymer chains can get into the interlayer spaces leading to the formation of either an intercalated or an exfoliated nanocomposite. Many researchers have investigated the relationship between the location of the nanoclay in thermoplastic elastomers and the corresponding mechanical properties<sup>10</sup>. Good level of distribution of nanoclay is significant to obtain best balance between toughness and stiffness properties in the blends. Studies made by Maiti *et al.*<sup>11</sup> showed that the dispersion of nanoclay in the elastomeric phase resulted in enhancement of properties. Studies made by Chandran *et al.*<sup>12</sup> on PP/NR /nanoclay composites prepared by melt blending established the localization of nanoclay in the PP continuous phase and at PP/NR the interface. Since non polar PP does not essentially attain a high level of dispersion of organoclays without any compatibilizer, maleated PP, or PP-g-MA, is used to attain improved dispersion of the silicate platelets in the TPO matrix. Mishra *et al.*<sup>13</sup> reported the successful preparation of intercalated (TPO)/organoclay nanocomposite with enhanced mechanical properties by using maleic anhydride modified polypropylene as a compatibilizer. Hence the development of TPO/nanoclay composites with good processability and improved balanced stiffness to toughness properties grabs much attention.

There has been no systematic study in literature regarding nanoclay as a reinforcing agent for PP/BR blend. In this study, effect of nanoclay (Cloisite 93A) on the mechanical, morphological, rheological and thermal properties of PP/BR (80/20) blend by melt mixing technique without using a compatibilizer is reported. The structure-property relationship, and dispersion of nanoclay were explained using TEM and SEM studies. The interaction of the blend components and nanoclay were established using rheological

characterization. The thermal properties of PP/BR nanocomposites were characterized by means of DSC and TGA analysis.

## **4A.2 Methodology**

### **4A.2.1 Materials**

The details of the polymers used for the study are discussed in chapter 2 (sections 2.1).

### **4A.2.2 Preparation of the PP/BR/nanoclay composites**

The TPE nanocomposites based on 80 wt % Polypropylene, 20 wt % of BR and 0.25, 0.5, 1, 2, 3, 4, 7 wt % of nanoclay were prepared by melt mixing process in a Brabender Plasticorder at 170 °C and 60 rpm for 8 minutes. The hot mix was sheeted out using a two roll mill and is cut into small pieces. The composition of the nanocomposites is as given in table 4A.1.

**Table 4A.1. Composition of PP/BR/nanoclay composites**

<b>PP (wt %)</b>	<b>BR (wt %)</b>	<b>NC (wt %)</b>	<b>Sample Code</b>
100	-	-	P100
80	20	-	P80
80	20	0.25	P80NC0.25
80	20	0.5	P80NC0.5
80	20	1	P80NC1
80	20	2	P80NC2
80	20	3	P80NC3
80	20	4	P80NC4
80	20	7	P80NC7

The test specimens were injection moulded at a barrel temperature of 180 °C and characterizations were carried out as given in chapter 2.

#### 4A.2.2 Theoretical modeling of PP/BR nanoclay composites

In the present investigation, Halpin-Tsai model, Voigt upper bound model and Reuss lower-bound prediction models have been employed to analyze tensile modulus of the nanocomposites. Among the different micromechanical models valid for the analysis of tensile modulus, the most popular model is the Halpin-Tsai model that predict the modulus of the polymer composites as a function of filler content, aspect ratio of the filler, moduli of the matrix and the filler<sup>14</sup>. The reinforcement of polymer matrices by fibres or flake like fillers can be predicted by Halpin- Tsai equation. The Halpin-Tsai equation is given as equation 4A.1.

$$\frac{E_c}{E_m} = \frac{1 + 2A_f \mu \Phi_f}{1 - \mu \Phi_f} \dots\dots\dots(4A.1)$$

where  $E_c$  and  $E_m$  are the elastic moduli of composite and blend matrix, respectively.  $A_f$  refers to the aspect ratio of the filler ( $l/t$ ) which is the ratio of lateral dimension ( $l$ ) of a nonspherical filler to its thickness ( $t$ ). The volume fraction of the filler is  $\Phi_f$  and is related to filler weight fraction  $W_f$  according to the equation 4A.2<sup>15</sup>.

$$\Phi = \frac{W_f / \rho_f}{\frac{W_f}{\rho_f} + (1 - W_f) / \rho_m} \dots\dots\dots(4A.2)$$

where  $\rho_f$  and  $\rho_m$  are the mass densities of the filler and the matrix, respectively. The geometric factor  $\mu$  is given by equation 4A.3.

$$\mu = \frac{\frac{E_f}{E_m} - 1}{\frac{E_f}{E_m} + 2A_f} \dots\dots\dots(4A.3)$$

where  $E_f$  is the elastic modulus of the filler. The modulus ratio of the filler and the matrix ( $E_f/E_m$ ) is also defined as relative modulus ( $E_r$ )<sup>14</sup>.

Contribution to the modulus by a 2-D disc -like clay platelets is less than 1-D fibre-like filler, a modulus reduction factor (MRF) is introduced to modify the Halpin-Tsai model<sup>16,17</sup> and is given as in equation 4A.4.

$$\frac{E_c}{E_m} = \frac{1 + (MRF)2A_f\mu\Phi_f}{1 - \mu\Phi_f} \dots\dots\dots(4A.4)$$

MRF =0.66 has been shown to well predict the tensile moduli of rubber/clay nanocomposites over a wide range of clay volume fractions.

When  $A \rightarrow \infty$ , the Halpin-Tsai model reduces to the rule of mixtures (upper bound), referred to as the Voigt rule of mixtures (ROM) and is given as an equation 4A.5<sup>18</sup>

$$E_c = \Phi E_f + (1 - \Phi_f)E_m \dots\dots\dots(4A.5)$$

Conversely, when  $A \rightarrow 0$ , the Halpin-Tsai model equation reduces to the inverse rule of mixtures (lower bound) referred to as Reuss inverse rule of mixtures (IROM) and is given as an equation 4A.6<sup>18</sup>.

$$\frac{1}{E_c} = \frac{\Phi_F}{E_f} + \frac{(1 - \Phi_f)}{E_m} \dots\dots\dots(4A.6)$$



### 4A.3 Results and Discussion

#### 4A.3.1 X-ray Diffraction (XRD)

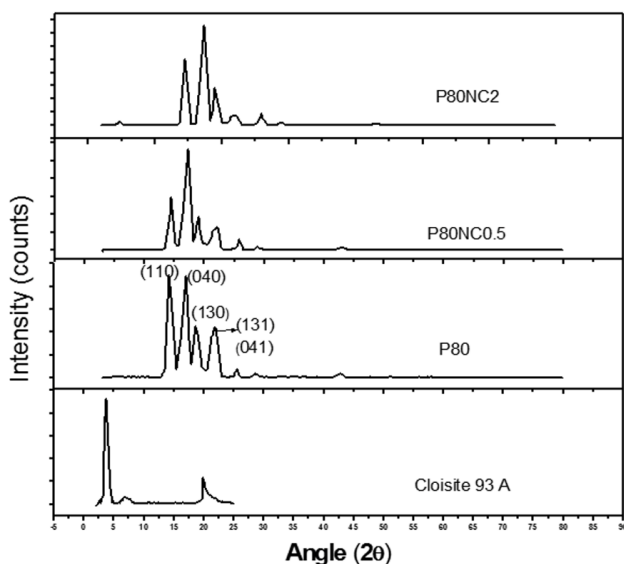


**Figure 4A.1.** XRD patterns of PP/BR/nanoclay composites

Figure 4A.1 shows the XRD patterns of nanoclay (Cloisite 93A), PP/BR blend and PP/BR/nanoclay composites. The XRD pattern of the pristine organoclay displayed a distinct diffracting peak ( $d_{001}$ ) at  $2\theta=3.722^\circ$  corresponding to a  $d$  spacing of 2.372 nm. The diffracting peaks in the blend and the PP/BR nanocomposites is observed at  $2\theta=14.18^\circ$ ,  $16.88^\circ$ ,  $18.58^\circ$ , and  $21.28^\circ$ . The peaks observed in the XRD pattern represent only characteristic type of  $\alpha$ -monoclinic crystal structures of PP phase corresponding to (110), (040), (130), and the overlapped (131,041) planes. The XRD pattern suggests that the introduction of nanoclay have not resulted in the conversion of PP from  $\alpha$  phase to  $\beta$  phase<sup>19</sup>. Also the XRD pattern did not show the characteristic diffracting peak of nanoclay  $2\theta = 3.722^\circ$  in the nanocomposites. The disappearance of diffracting peak ( $d_{001}$ ) of nanoclay in the nanocomposites

indicates delamination or exfoliation of nanoclay layers. Here it can be proposed that during melt mixing, application of shear stress have resulted in the diffusion of polymer chains into the silicate layers leading to exfoliation of the clay layers.

#### 4A.3.2 Transmission electron microscopy (TEM)

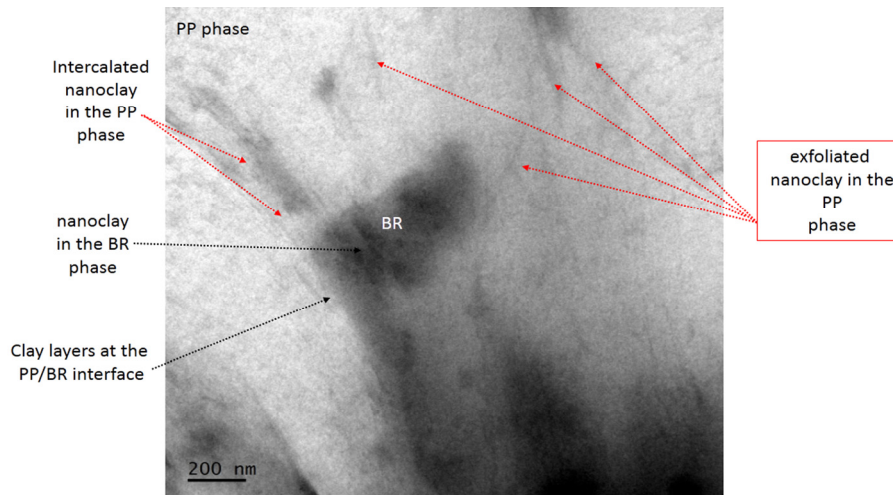


**Figure 4A.2. TEM images of P80NC0.5 nanocomposite at 200 nm**

TEM photograph of the P80NC0.5 sample (sample which showed optimum mechanical properties) is shown in Figure 4A.2. The white and dark regions in the TEM photographs correspond to the PP and BR phase, respectively. Unlike the XRD results, TEM analysis indicated morphology with intercalated clay layers and a small amount of exfoliated clay layers. XRD results suggested exfoliation of nanoclay layers as no peak was detected in  $3\text{--}10^\circ$  range. This can be attributed to the orientation of nanoclay layers in different directions during XRD analysis. The changing orientation of samples in the XRD analysis may lead to the presence or absence of peak in the XRD pattern and has been well detailed in literature<sup>11</sup>.

From the TEM photograph, it can be seen that nanoclay layers are dispersed in the PP matrix, BR phase and at the PP/BR interface. The nanoclay layers in the BR phase appears to be agglomerated while intercalated and exfoliated clay layers are visible in the PP matrix. The migration of clay layers from the thermoplastic matrix to the rubber phase in physical blends can be suggested, even though it depends on the sequence of addition of the components in the melt blending process. Studies on PP/SEBS/CNF composites prepared by one step melt mixing have established the distribution of CNF in the PP/SEBS interface and in the SEBS phase under the application of shear<sup>20</sup>. It can be suggested that during one step melt mixing, with the effects of the shearing force, nanoclay platelets are intercalated simultaneously by polypropylene and polybutadiene rubber chains and organoclay platelets could expand only partially so that the complete exfoliation has not taken place. Hence it can be concluded that the resultant morphology of the nanocomposite is a hybrid morphology of exfoliated and intercalated clay layers in the PP matrix, BR phase and at the PP/BR interphase<sup>21,22</sup>. A schematic representation of the fabrication of the PP/BR/nanoclay composites by melt mixing and the resultant morphology based on the TEM results is represented in Figure 4A.3.

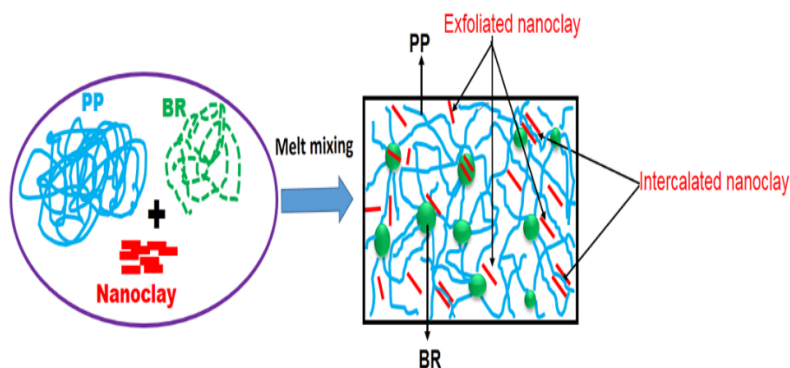
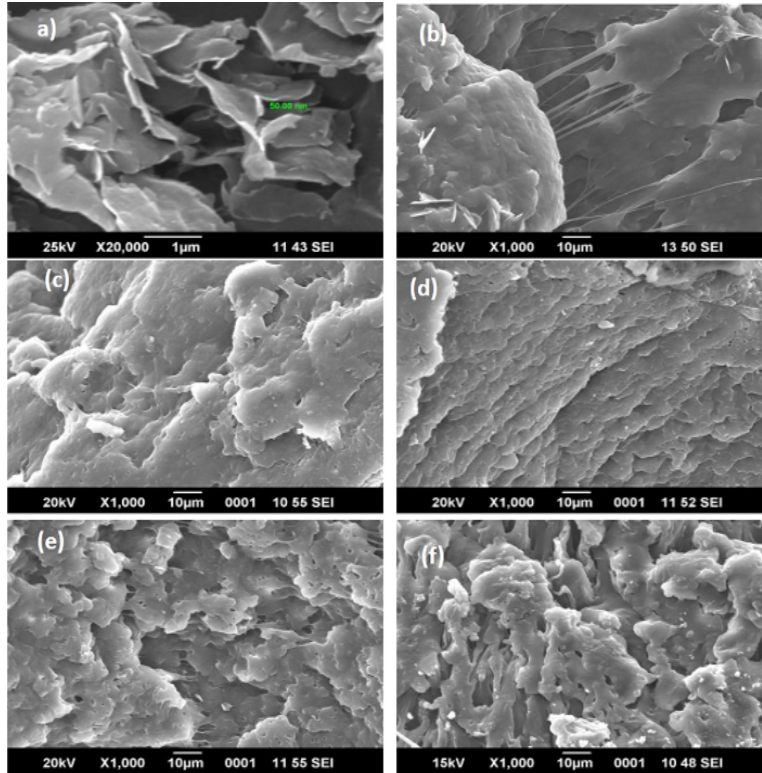


Figure 4A.3. Melt blending scheme of PP/BR/nanoclay composite

### 4A.3.3 Scanning electron microscopy (SEM)

#### a) SEM photographs of tensile fractured surfaces



**Figure 4A.4. SEM photographs showing tensile fracture morphology of PP/BR nanocomposites a) pure nanoclay b) P80 c) P80NC0.5 d) P80NC1 e) P80NC4 f) P80NC7**

The SEM photographs of pristine Cloisite 93 A and tensile fractured morphology of PP/BR blend with various amounts of clay are presented in Figure 4A.4 (a-f). The SEM photographs revealed a layered structure for pure nanoclay as shown in Figure 4A.4(a). SEM photograph of the PP/BR blend (P80) is shown in Figure 4A.4(b). Shear yielding of the matrix in the form of shear bands by repeated rubber particle cavitation is evident in the morphology of P80 blend<sup>23</sup>. Figures 4.4(c-f) shows the morphologies of

PP/BR/nanoclay composites. It can be seen that addition of nanoclay has resulted in a brittle morphology. The interaction of clay layers with PP matrix might have reduced the extent of shear yielding of the matrix leading to a brittle fracture. Hence it can be concluded that introduction of nanoclay has improved the stiffness of the blend. However, as the nanoclay content increases to 7 wt %, agglomeration takes place as shown in Figure 4A.4(f) which leads to lower mechanical properties.

**b) SEM photographs of impact fracture surface**

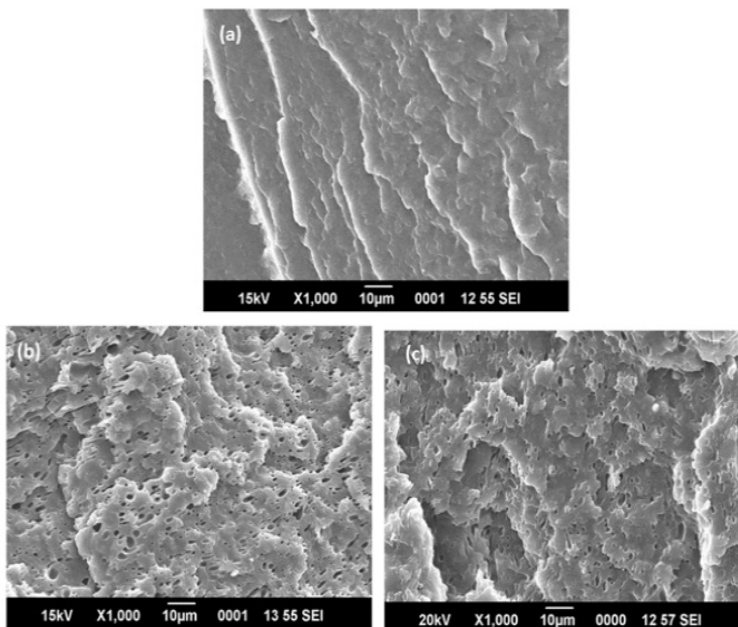


**Figure 4A.5. SEM photographs showing impact fracture morphology of PP/BR nanocomposites a) P100 b) P80 c) P80NC0.5**

The impact fracture morphology of PP/BR blend and its nanocomposites are displayed in Figure 4A.5(a-c). As seen in Figure 4A.5(a) pure PP displayed a brittle failure. In Figure 4A.5(b) for the P80 sample, elongated voids are found which indicates a ductile fracture due to rubber particle cavitation. From

the Figure 4A.5(c), it is clear that with the introduction of nanoclay in the P80 blend, the size of the voids got reduced and suppression of void coalescence by the barrier effect of clay can be proposed. The presence of nanoclay at the PP/BR interphase might have acted as barriers preventing the void coalescence, thereby marginally improving the impact strength<sup>12</sup>. As the nanoclay content is increased, there exists a greater tendency for nanoclay agglomeration, which ultimately leads to considerable reduction in impact strength.

#### **4A.3.4 Mechanical properties**

##### **4A.3.4.1 Tensile properties**

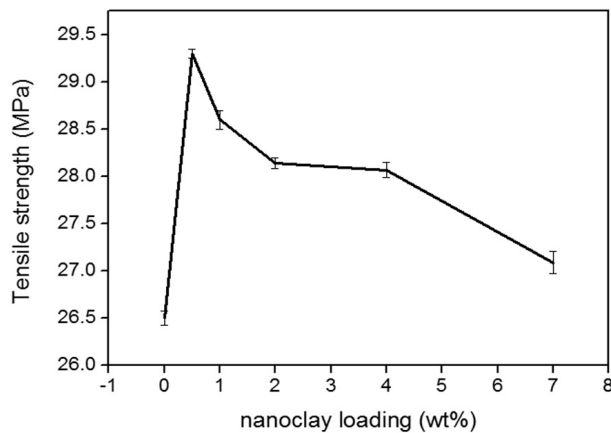


**Figure 4A.6. Variation of tensile strength with nanoclay loading**

From the Figure 4A.6, it can be seen that tensile strength of the PP/BR/nanoclay composites showed a maximum at 0.5 wt % loading of nanoclay and then decreased marginally up to 4 wt %. The increase in tensile strength with the incorporation of 0.5wt % nanoclay can be attributed to the distribution of intercalated/exfoliated clay layers in the PP matrix thereby increasing the stiffness of the matrix. A drastic decrease in tensile strength at 7 wt % nanoclay loading can be due to the agglomeration of clay particles as evident in the SEM photographs.

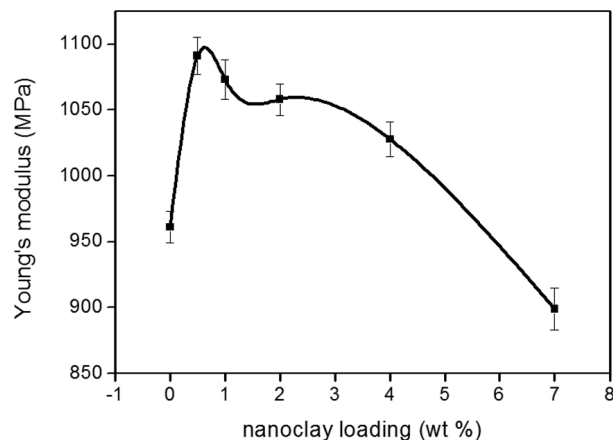


**Figure 4A.7. Variation of Young's modulus with nanoclay loading**

Figure 4A.7 shows the variation of Young's modulus with nanoclay loading. From the figure it is clear that with the addition of 0.5 wt % nanoclay to the P80 blend, enhancement in Young's modulus could be achieved. The increase in stiffness of the blend with 0.5 wt % loading of nanoclay can be attributed due to the dispersion of nanoclay in the PP matrix as envisaged by TEM photograph.

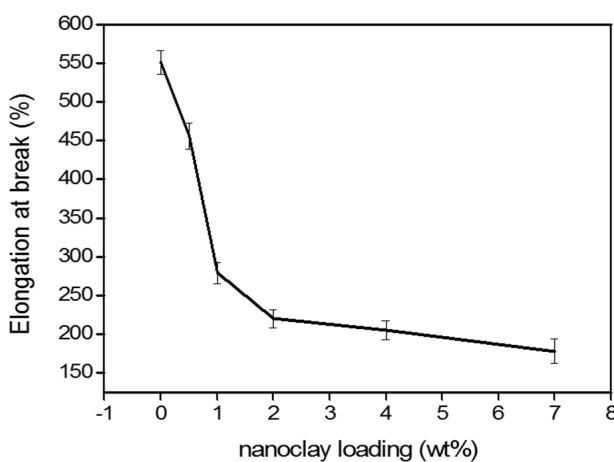


**Figure 4A.8. Variation of elongation at break with nanoclay loading**

The variation of elongation at break of the PP/BR/nanoclay composites with nanoclay content is shown in Figure 4A.8. It can be seen that the elongation at break got reduced with the addition of nanoclay in the blend. This can be associated with the interaction of nanoclay and PP chains, restricting the ability of the matrix to undergo plastic deformation<sup>24</sup>.

#### 4A.3.4.2 Impact strength

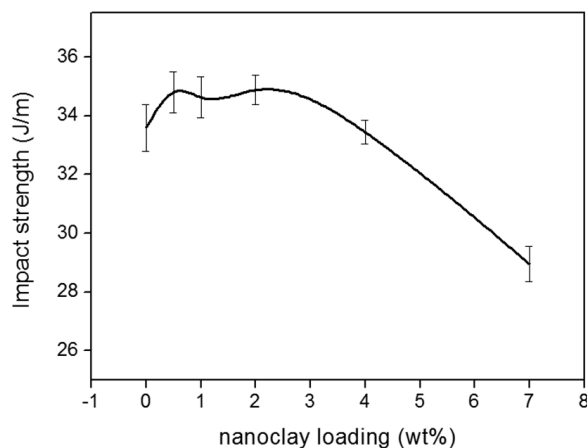


**Figure 4A.9. Variation of impact strength with nanoclay loading**

The variation of impact strength of the PP/BR/nanoclay composites with nanoclay content is shown in Figure 4A.9. From the figure it is evident that there is only marginal increase in the impact strength of the P80 blend with 0.2 wt % loading of nanoclay. The impact strength exhibited an initial increase followed by a constant, but modest, decrease in impact strength with increase in clay loading up to 2 wt % of the nanoclay. Similar results have been reported by Mehta *et al.*<sup>25</sup> in their studies on TPO/organoclay composites. The dispersed clay platelets at the PP/BR interface act as physical barriers, preventing void coalescence, arising from rubber cavitation there by improving the stress transfer in the matrix leading to improved



impact strength. The distribution of nanofillers in the elastomeric phase is expected to improve the impact strength of the blend by a core shell morphology as described in literature<sup>4,26</sup>. From the TEM photographs, in P80NC0.5 nanocomposite, the clay platelets present in the BR phase seems to be agglomerated. Martins *et al.*<sup>27</sup> reported that the impact strength of PP/EVA/organoclay system got decreased because the clay platelets were not well distributed in the EVA phase. Similarly, the presence of agglomerated clay particles in the BR phase might have resulted in the reduction of impact strength in PP/BR/nanoclay composites. At higher clay loadings, the decrease in mechanical properties can be related to the agglomeration of clay particles. Thus very low loading levels of nanoclay (0.5%) have modified the thermoplastic elastomer based on PP/BR blend with slight improvement in tensile strength and Young's modulus with slight improvement in impact strength.

#### **4A.3.4.3 Theoretical modeling of tensile modulus**

##### **a) Estimation of aspect ratio of clay platelets**

Q.T. Nguyen *et al.*<sup>28</sup> had shown that for fully exfoliated clay platelets, aspect ratio can be taken to be approximately 100 and it was established that due to absence of proper orientation and complete exfoliation, the aspect ratio will be lower than the expected value of 100. In this study, TEM images shown in Figure 4A.2 revealed the morphology of the P80NC0.5 nanocomposite to be a hybrid morphology with partial exfoliation and intercalation of nanoclay. Hence here the aspect ratio cannot be assumed to be 100. Although the aspect ratio of clay layers can be determined from the TEM images by measuring the length and thickness of the clay layers, it requires exceptionally high contrast. Hence the aspect ratio of the nanoclay in this study is obtained by fitting the experimental modulus with theoretical

modulus for various aspect ratios<sup>29,30</sup>. The densities of the matrix and nanoclay is taken to be 0.906 g/cc and 2.6 g/cc, respectively. Applying the values of Young's modulus,  $E_m$  (Figure 3.2),  $E_f=178 \text{ GPa}$ <sup>31</sup>,  $\Phi_f$  (equation 4A.2) and  $\mu$  (equation 4A.3) in the Halpin-Tsai expression (equation 4A.1), theoretical modulus for various aspect ratios were calculated. Among the different aspect ratio values, H-T model gives the best fit with  $A_f$  at about 45 as shown in Figure 4A.10.

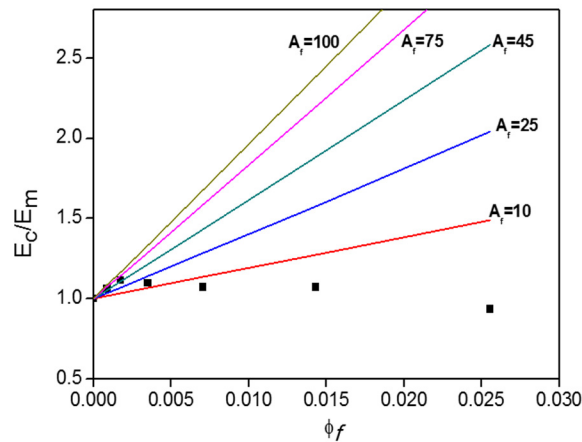


**Figure 4A.10. Comparison of experimental modulus and Halpin-Tsai theory as a function of clay concentration for various exfoliated clay layer aspect ratios**

Figure 4A.11 exhibit the comparison of the experimental modulus and the results obtained from various theoretical models for PP/BR/nanoclay composites. Among the various models, the moduli predicted based on modified Halpin-Tsai equation (with a modulus reduction factor) shows the closest proximity to the experimental values at lower nanoclay loading. At higher clay content, the experimental modulus displayed large difference with modified Halpin-Tsai equation. This may be due to the agglomeration

of clay particles in polymer matrix. At higher loading the experimental modulus is showing agreement with Reuss inverse rule of mixtures.

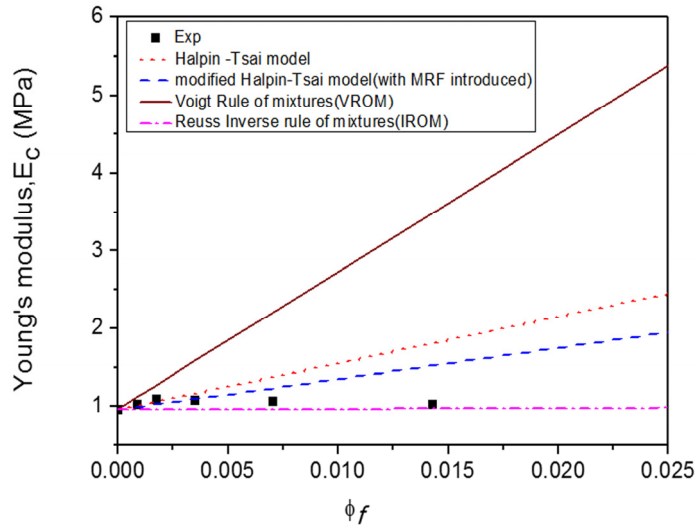


Figure 4A.11. Theoretical modeling of Young's modulus as a function of filler loadings using various models

#### 4A.3.5 Dynamic rheological analysis (DRA)

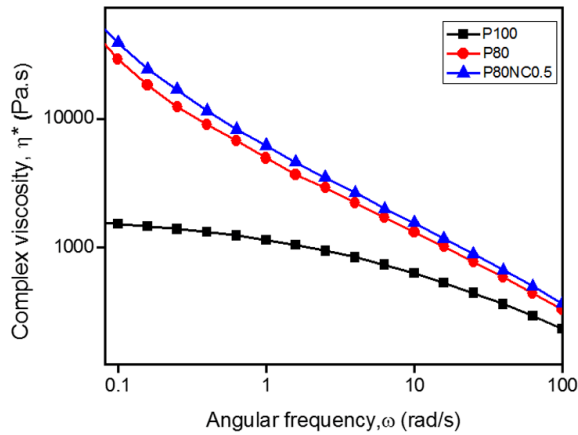
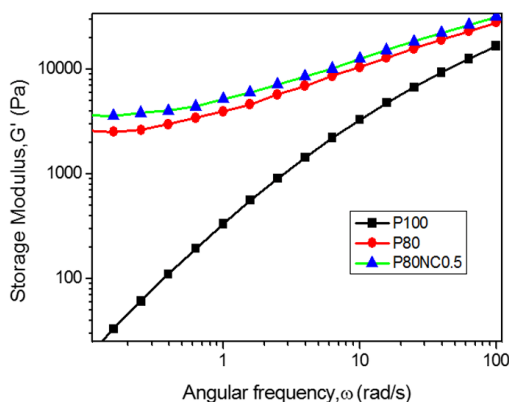


Figure 4A.12. Complex viscosity,  $\eta^*$  as a function of angular frequency of P100, P80 and P80NC0.5 samples at 190 °C

Figure 4A.12 gives the plot of complex viscosity ( $\eta^*$ ) as a function of angular frequency ( $\omega$ ) for P100, P80 and P80NC0.5 samples at 190 °C. From the figure it is clear that pure PP exhibits a Newtonian plateau of viscosity at lower frequencies and shear thinning behavior at higher frequencies. The P80 blend and P80NC0.5 shows increased complex viscosity with marked shear thinning behaviour at low frequency. The significant enhancement in  $\eta^*$  of the P80 blend and the PP/BR/nanoclay composite at lower frequencies is associated with the reduced mobility of the confined polymer chains by the nanoclay layers. The observations are consistent with the previously reported results<sup>32,33</sup>.



**Figure 4A.13. Storage modulus ( $G'$ ) as a function of angular frequency of P100, P80 and P80NC0.5 samples at 190 °C**

Melt rheological moduli such as storage modulus ( $G'$ ) and loss modulus ( $G''$ ) of P100, P80 and P80NC0.5 samples at 190 °C is logarithmically plotted as a function of angular frequency ( $\omega$ ) in Figures 4A.13 and 4A.14, respectively. The addition of nanoclay into the PP/BR blends enhanced the storage ( $G'$ ) and loss modulus ( $G''$ ) of the PP/BR/nanoclay composites in the entire frequency range studied. From the Figure 4A.13, it is clear that enhancement of  $G'$  was more pronounced at lower frequencies, but gradually

approached that of PP at higher frequencies which shows the strong influence of silicate dispersion on the viscoelastic properties of nanocomposites<sup>34</sup>.

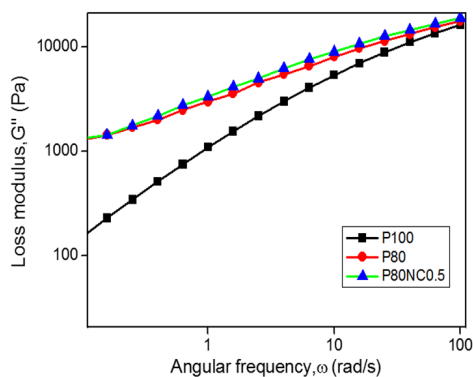


**Figure 4A.14. Loss modulus ( $G''$ ) as a function of angular frequency of P100, P80 and P80NC0.5 samples at 190 °C**

At lower frequencies, the polymer chains get enough time to undergo relaxation due to chain disentanglement and hence smaller value of storage and loss modulus. But at higher frequencies, time for relaxation is very low and the storage and loss modulus values will increase.

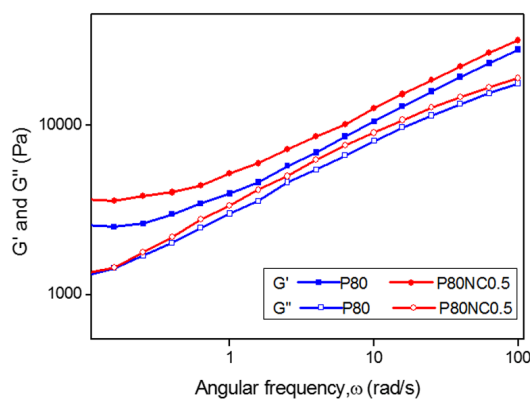


**Figure 4A.15. Storage modulus ( $G'$ ) and Loss modulus ( $G''$ ) vs. angular frequency ( $\omega$ ) of P80 and P80NC0.5 samples at 190 °C**

Figure 4A.15. Shows the storage modulus ( $G'$ ) and loss modulus ( $G''$ ) vs. angular frequency ( $\omega$ ) for P80 and P80NC0.5 samples at 190 °C. In the case of P80 and the P80NC0.5 samples, storage modulus ( $G'$ ) is larger than loss modulus ( $G''$ ) over the entire range of experimental frequency showing high elasticity in the experimental frequency range. These results suggests an increasing solid like elastic response ( $G' > G''$ ) of the blend and the nanocomposite. The introduction of nanoclay platelets in the matrix results in the formation of physical network structures and subsequent reduction in molecular mobility of the PP chains. The increasing trend of storage modulus with frequency shown by nanocomposite are in line with the earlier reported results<sup>35,36</sup>.

The complex viscosity,  $\eta^*$  as a function of angular frequency is given as

$$\eta^* = k\omega^n \dots\dots\dots(4A.7)$$

where  $\eta^*$  is a complex viscosity,  $k$  is the exponential factor,  $\omega$  is the oscillation frequency and  $n$  is the shear thinning exponent. The value of  $n$  can be determined from the slope of the straight line obtained in the  $\log \eta^*$  vs.  $\log \omega$  plot and is shown in table 4A.2. The value of  $n$  is greater for the blend and its nanocomposite than pure PP which reflects a greater pseudoplastic behavior. Investigations by R. Wagener *et al.*<sup>37</sup> established that higher the exponent  $n$ , the more efficient is the reinforcement of the corresponding composite.

The relationship between  $G'$  and  $G''$  with angular frequency  $\omega$  could be described as

$$G' \propto \omega^{n_1} \dots\dots\dots(4A.8)$$

$$G'' \propto \omega^{n_2} \dots\dots\dots(4A.9)$$

The dispersion state of fillers can be evaluated by determining the slope of  $G'$  and  $G''$  vs.  $\omega$ . The slopes of the terminal zone  $n_1$  and  $n_2$  were calculated and are listed in table 4A.2. It is observed that the slopes of  $G'$  and  $G''$  for P80NC0.5 are smaller than the pure PP and P80 blend. The decrease in the terminal slope of the nanocomposite supports interaction between clay platelet and polymer chain in the molten state<sup>38</sup>.

**Table 4A.2. Slopes of  $\log \eta^*$ ,  $\log G'$  and  $G''$  vs.  $\log \omega$  at 190 °C ( $n$ ,  $n_1$  and  $n_2$ ), respectively, as observed from frequency sweep experiments**

Sample	$n$	$n_1$	$n_2$
P100	-0.3449	0.993	0.6825
P80	-0.5813	0.3757	0.3985
P80NC0.5	-0.6054	0.3396	0.4057

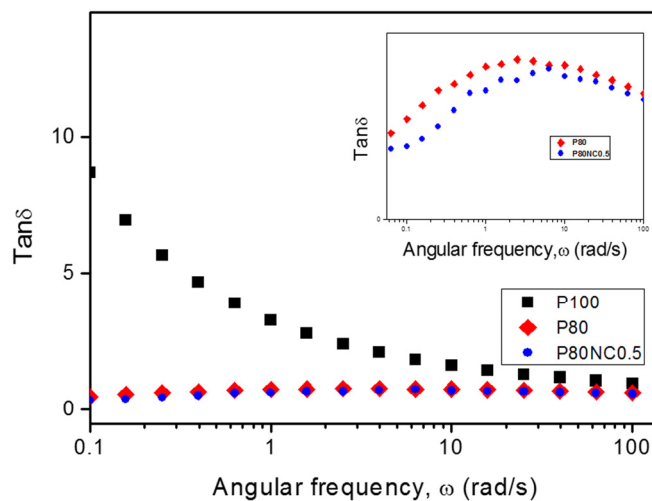


**Figure 4A.16. The  $\tan \delta$  as a function of angular frequency of P100, P80 and P80NC0.5 samples at 190 °C**

The influence of nanoclay on the elastic behavior ( $G'$ ) of polypropylene is further confirmed by plotting  $\tan \delta$  ( $G''/G'$ ) as a function of angular frequency and is shown in Figure 4A.16 (inset showing the behavior of P80 blend and the P80NC0.5 nanocomposite). From the figure, it is revealed that the  $\tan \delta$  values of P80NC0.5 samples are lower than P100 over the whole frequency scan which emphasize an increase in the storage modulus and therefore signifies improved elastic properties. The maximum value of  $\tan \delta$  for the P80NC0.5 sample got shifted to higher frequency compared to that of P80 blend probably due to changes in the microstructure associated to the addition of the nanoclay. The significant decrease in  $\tan \delta$  values for P80 and P80NC0.5 nanocomposite indicates better interaction between the polymer chains and the intercalated/exfoliated nanoclay layers thus hindering the molecular chain mobility<sup>38</sup>. The rheological results revealed improved clay dispersion and are in good agreement with TEM results.

#### 4A.3.6 Dynamic mechanical analysis (DMA)

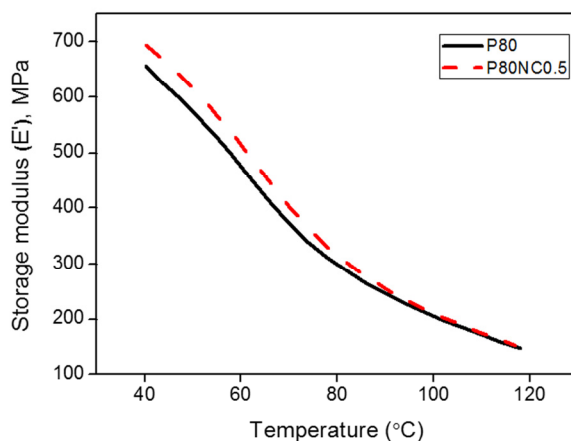


**Figure 4A.17. (a) Variation of storage modulus ( $E'$ ) of PP/BR blend and PP/BR/nanoclay composite with temperature**



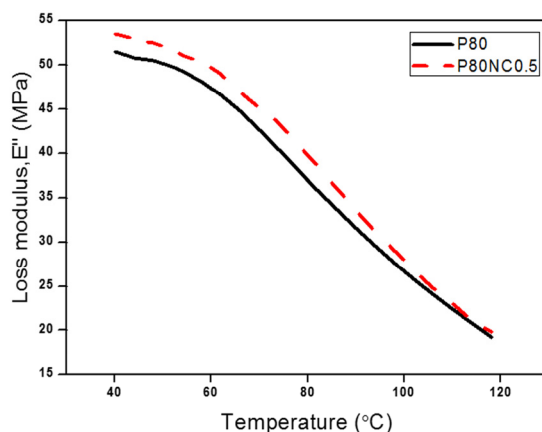


**Figure 4A.17. (b) Variation of loss modulus ( $E''$ ) of PP/BR blend and PP/BR/nanoclay composite with temperature**

The storage modulus ( $E'$ ) and loss modulus ( $E''$ ) of the P80 sample and P80NC0.5 nanocomposite vs. temperature curve is shown in Figure 4A.17 (a) and (b), respectively. From the figure it is seen that the both the storage modulus and loss modulus decreases with increase in temperature. The introduction of nanoclay results in an increase in the storage modulus and loss modulus of the PP/BR matrix over the whole range of temperature studied. This indicated enhanced stiffness and better stress transfer between nanoclay and polymer matrix. The restricted mobility of the polymer chains due to intercalation inside the clay layers, results in the enhancement of storage modulus.

#### 4A.3.7 Differential scanning calorimetry (DSC)

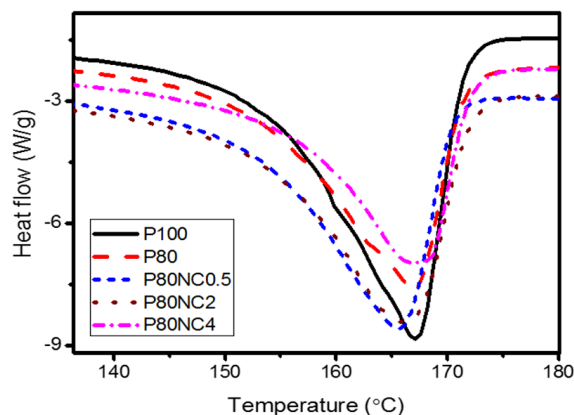
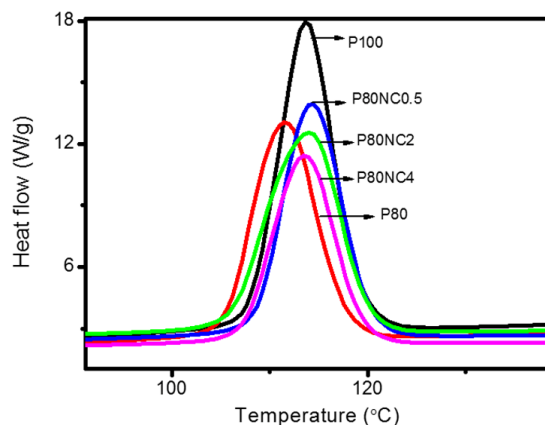


Figure 4A.18. DSC heating curves of PP/BR/nanoclay composites

Table 4A.3. Melting characteristics of PP/BR blends and the nanocomposites

Sample	$T_{m,onset}$ (°C)	$T_m$ (°C)	$T_{m,endset}$ (°C)	$\Delta H_f$ J/g	$X_c$ (%)
P100	154	167	171	93.76	45
P80	153	166	171	70.57	42
P80NC0.5	152	165	170	74.16	44
P80NC2	153	166	172	66.67	40
P80NC4	155	167	172	61.34	36

The melting characteristics of pure PP, P80 blend and the PP/BR/nanoclay composites derived from heating curves are shown in Figure 4A.18 and the onset of melting temperature ( $T_{m,onset}$ ), peak melting temperature ( $T_m$ ), endset of melting temperature ( $T_{m,endset}$ ), enthalpy of fusion ( $\Delta H_f$ ) and percentage of crystallinity ( $X_c$ ) computed are listed in table 4A.3.



**Figure 4A.19. DSC cooling curves of PP/BR/ nanoclay composites**

The crystallization characteristics obtained from cooling curves are given in Figure 4A.19 and the onset of crystallization temperature ( $T_{c,onset}$ ), peak crystallization temperature ( $T_c$ ), endset of crystallization temperature ( $T_{c,endset}$ ) and enthalpy of crystallization ( $\Delta H_c$ ) are listed in table 4A.4.

**Table 4A.4. Crystallization characteristics of PP/BR blend and the nano composites**

Sample	$T_{c,onset}$ (°C)	$T_c$ (°C)	$T_{c,endset}$ (°C)	$\Delta H_c$ J/g
P100	119	114	108	111.68
P80	118	111	106	88.23
P80NC0.5	120	114	109	86.29
P80NC2	120	114	106	70.97
P80NC4	119	113	107	61.34

The data obtained from the DSC thermograms revealed that the melting temperature ( $T_m$ ) and crystallization temperature ( $T_c$ ) of PP remains unaffected. This observation suggests that the presence of the rubber phase and nanoclay content has weak nucleating effect in the PP matrix<sup>39</sup>. The percentage of crystallinity ( $X_c$ ) of PP matrix in the P80 blend also did not show much variation with the introduction of nanoclay. The decrease in  $\Delta H_c$  values results from restraints enacted on the formation of crystalline regions<sup>40</sup>. Based on these observations it can be inferred that the reduction in the mobility of the matrix in the molten state did not interfere with the crystallization process of PP. These results are consistent with the XRD results that revealed  $\alpha$  type crystal form of PP to be predominant, with no evidence of  $\beta$  phase.

#### 4A.3.8 Thermogravimetric analysis

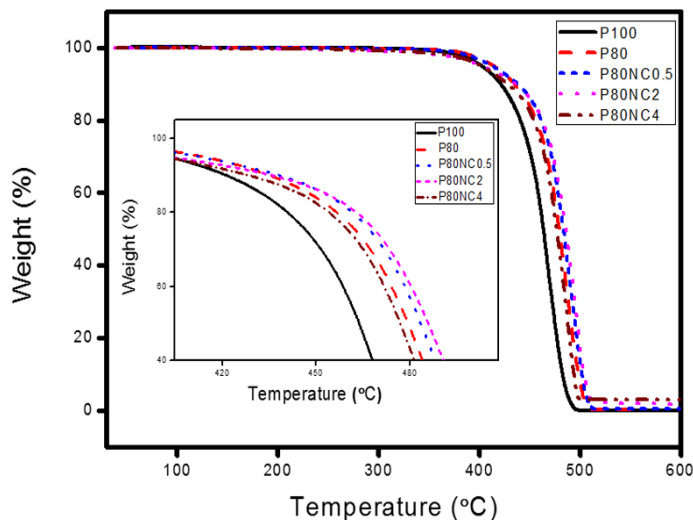


**Figure 4A.20** TGA curves of PP/BR/nanoclay composites

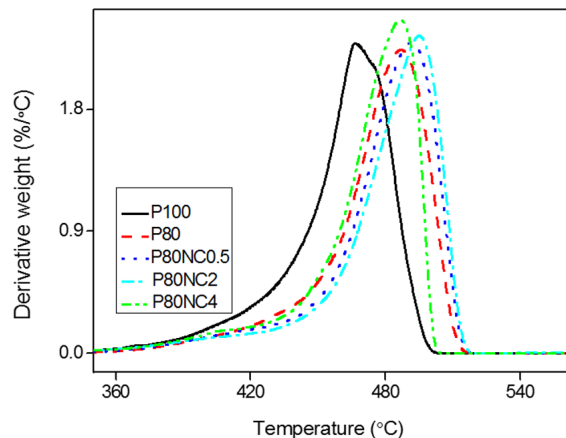


**Figure 4A.21. DTG curves of PP/BR/nanoclay composites**

Figure 4A.20 shows the TGA curves and Figure 4A.21 shows the DTG curves of PP, PP/BR blend and its nanocomposites. The thermal degradation parameters such as onset degradation temperature  $T_{\text{onset}}$ , temperatures at 10% weight loss ( $T_{10}$ ) and 50% weight loss ( $T_{50}$ ), final decomposition temperature ( $T_f$ ) and maximum degradation temperature ( $T_{\text{max}}$ ) is given in table 4A.5.

**Table 4A.5. TGA parameters of PP/BR blend and the nanocomposites**

Sample code	$T_{\text{onset}}$ (°C)	$T_{10}$ (°C)	$T_{50}$ (°C)	$T_{\text{max}}$ (°C)	$T_f$ (°C)
<b>P100</b>	360	421	464	467	500
<b>P80</b>	366	435	479	487	514
<b>P80NC0.5</b>	371	438	484	491	515
<b>P80NC2</b>	373	441	483	492	509
<b>P80NC4</b>	374	402	477	487	502

From the Figure 4A.20, it can be observed that all the samples displayed single step degradation process. From the TGA data, it is envisaged that with the introduction of nanoclay in the matrix, thermal

stability got improved. Lower loading of nanoclay to the polymer matrix have resulted in the well dispersion of clay layers in the matrix as confirmed by the TEM studies. The increased thermal stability of the polymer nanocomposite can be attributed to the barrier effect of the well dispersed clay layers in the blend matrix. The enhanced thermal stability can also be attributed to the creation of a char which hampers the diffusion of the volatile decomposition products, generally observed in exfoliated nanocomposites<sup>41</sup>.

#### **4A.4 Conclusions**

PP/BR/nanoclay composite prepared by melt blending show enhancement in tensile strength, Young's modulus and impact strength of the nanocomposites at 0.5 wt % of nanoclay (P80NC0.5). TEM photograph of PP/BR/nanoclay composite (P80NC0.5) reveals a hybrid morphology of partially exfoliated and intercalated clay layers in the PP matrix. Nanoclay layers are also evident in the BR phase and at the PP/BR interface. The presence of clay layers in the PP matrix reduces the ability of the matrix to undergo plastic deformation resulting in the reduction of elongation at break. The aspect ratio of the clay layer was estimated to be 45 using Halpin-Tsai micromechanical model. Among the various micromechanical models, modified Halpin-Tsai equation with a modulus reduction factor show the closest proximity to the experimental values of Young's modulus at lower nanoclay loading. The rheological properties such as storage modulus, loss modulus and complex viscosity increase on addition of nanoclay. This suggests the restriction on the mobility of PP chains due to interaction with nanoclay layers in the PP matrix. The melting point and the crystallization character of PP matrix are not affected indicating the weak nucleating effect of nanoclay in the PP matrix. Thermal stability improves at lower loading levels of nanoclay due to the barrier effect of delaminated clay layers.

## References

- [1] Holden, G., Kricheldorf, H. R., & Quirk, R. P. (2004). *Thermoplastic elastomers* (Vol. 133). Munich: Hanser.
- [2] Liang, J. Z., & Li, R. K. Y. (2000). Rubber toughening in polypropylene: a review. *Journal of Applied Polymer Science*, 77(2), 409-417.
- [3] Lee, K. Y., & Goettler, L. A. (2004). Structure-property relationships in polymer blend nanocomposites. *Polymer Engineering & Science*, 44(6), 1103-1111.
- [4] Ou, Y. C., Guo, T. T., Fang, X. P., & Yu, Z. Z. (1999). Toughening and reinforcing polypropylene with core-shell structured fillers. *Journal of applied polymer science*, 74(10), 2397-2403.
- [5] Paul, D. R., & Robeson, L. M. (2008). Polymer nanotechnology: nanocomposites. *Polymer*, 49(15), 3187-3204.
- [6] Lee, H. S., Fasulo, P. D., Rodgers, W. R., & Paul, D. R. (2005). TPO based nanocomposites. Part 1. Morphology and mechanical properties. *Polymer*, 46(25), 11673-11689.
- [7] Alexandre, M., & Dubois, P. (2000). Polymer-layered silicate nanocomposites: preparation, properties and uses of a new class of materials. *Materials Science and Engineering: R: Reports*, 28(1), 1-63.
- [8] Alateyah, A. I., Dhakal, H. N., & Zhang, Z. Y. (2013). Processing, properties, and applications of polymer nanocomposites based on layer silicates: a review. *Advances in polymer technology*, 32(4), 21368.
- [9] Panaitescu, D. M., Vuluga, Z., Radovici, C., & Nicolae, C. (2012). Morphological investigation of PP/nanosilica composites containing SEBS. *Polymer Testing*, 31(2), 355-365.
- [10] Kim, D. H., Fasulo, P. D., Rodgers, W. R., & Paul, D. R. (2007). Effect of the ratio of maleated polypropylene to organoclay on the structure and properties of TPO-based nanocomposites. Part I: Morphology and mechanical properties. *Polymer*, 48(20), 5960-5978.

- [11] Maiti, M., Bandyopadhyay, A., & Bhowmick, A. K. (2006). Preparation and characterization of nanocomposites based on thermoplastic elastomers from rubber–plastic blends. *Journal of applied polymer science*, 99(4), 1645-1656.
- [12] Chandran, N., Chandran, S., Maria, H. J., & Thomas, S. (2015). Compatibilizing action and localization of clay in a polypropylene/natural rubber (PP/NR) blend. *RSC Advances*, 5(105), 86265-86273.
- [13] Mishra, J. K., Hwang, K. J., & Ha, C. S. (2005). Preparation, mechanical and rheological properties of a thermoplastic polyolefin (TPO)/organoclay nanocomposite with reference to the effect of maleic anhydride modified polypropylene as a compatibilizer. *Polymer*, 46(6), 1995-2002.
- [14] Fornes, T. D., & Paul, D. R. (2003). Modeling properties of nylon 6/clay nanocomposites using composite theories. *polymer*, 44(17), 4993-5013.
- [15] Maiti, S. N. (2015). Mechanical, morphological, and thermal properties of nanotalc reinforced PA6/SEBS-g-MA composites. *Journal of Applied Polymer Science*, 132(7)..
- [16] Wu, Y. P., Jia, Q. X., Yu, D. S., & Zhang, L. Q. (2004). Modeling Young's modulus of rubber–clay nanocomposites using composite theories. *Polymer Testing*, 23(8), 903-909.
- [17] Zare, Y., & Garmabi, H. (2012). Analysis of tensile modulus of PP/nanoclay/CaCO<sub>3</sub> ternary nanocomposite using composite theories. *Journal of Applied Polymer Science*, 123(4), 2309-2319.
- [18] Facca, A. G., Kortschot, M. T., & Yan, N. (2006). Predicting the elastic modulus of natural fibre reinforced thermoplastics. *Composites Part A: Applied Science and Manufacturing*, 37(10), 1660-1671.
- [19] Wang, W. Z., & Liu, T. (2008). Mechanical properties and morphologies of polypropylene composites synergistically filled by styrene-butadiene rubber and silica nanoparticles. *Journal of applied polymer science*, 109(3), 1654-1660.



- [20] Parameswaranpillai, J., Joseph, G., Shinu, K. P., Salim, N. V., Hameed, N., & Jose, S. (2015). High performance PP/SEBS/CNF composites: Evaluation of mechanical, thermal degradation, and crystallization properties. *Polymer Composites*.
- [21] Babaienejad, M., & Bagheri, R. (2015). Role of nanoclay distribution on morphology and mechanical behavior of rubber-modified polyolefins. *Journal of Applied Polymer Science*, 132(20), 41993.
- [22] Bendjaouahdou, C., & Bensaad, S. (2013). The effects of organoclay on the morphology and balance properties of an immiscible Polypropylene/Natural Rubber blend. *Energy Procedia*, 36, 574-590.
- [23] Panda, B. P., Mohanty, S., & Nayak, S. K. (2015). Mechanism of toughening in rubber toughened polyolefin—a review. *Polymer-Plastics Technology and Engineering*, 54(5), 462-473.
- [24] Aso, O., Eguiazabal, J. I., & Nazabal, J. (2007). The influence of surface modification on the structure and properties of a nanosilica filled thermoplastic elastomer. *Composites science and technology*, 67(13), 2854-2863.
- [25] Mehta, S., Mirabella, F. M., Rufener, K., & Bafna, A. (2004). Thermoplastic olefin/clay nanocomposites: morphology and mechanical properties. *Journal of Applied Polymer Science*, 92(2), 928-936.
- [26] Matonis, V. A., & Small, N. C. (1969). A macroscopic analysis of composites containing layered spherical inclusions. *Polymer Engineering & Science*, 9(2), 90-99.
- [27] Martins, C. G., Larocca, N. M., Paul, D. R., & Pessan, L. A. (2009). Nanocomposites formed from polypropylene/EVA blends. *Polymer*, 50(7), 1743-1754.
- [28] Nguyen, Q. T., & Baird, D. G. (2007). An improved technique for exfoliating and dispersing nanoclay particles into polymer matrices using supercritical carbon dioxide. *Polymer*, 48(23), 6923-6933.
- [29] Durmus, A., Kaşgöz, A., & Macosko, C. W. (2008). Mechanical Properties of Linear Low-density Polyethylene (LLDPE)/clay Nanocomposites: Estimation of Aspect Ratio and Interfacial Strength by Composite Models. *Journal of Macromolecular Science®*, Part B: Physics, 47(3), 608-619.

- [30] Faraz, M. I., Besseling, N. A. M., Korobko, A. V., & Picken, S. J. (2014). Structure–property relationships and modeling of the mechanical properties of a high-temperature resistant thermoset nanocomposite. *Composites Part B: Engineering*, 56, 9-14.
- [31] Huang, J., Geier, S., Schmauder, S., & Weber, U. (2012). Modeling stiffness of nanolayered silicate-modified polyamide 6 via FEM micromechanical modeling and analytical composite models. *Journal of Applied Polymer Science*, 125(6), 4416-4420.
- [32] Gong, L., Yin, B., Li, L. P., & Yang, M. B. (2012). Morphology and properties of PP/EPDM binary blends and PP/EPDM/nano-CaCO<sub>3</sub> ternary blends. *Journal of Applied Polymer Science*, 123(1), 510-519.
- [33] Barick, A. K., & Tripathy, D. K. (2011). Effect of organically modified layered silicate nanoclay on the dynamic viscoelastic properties of thermoplastic polyurethane nanocomposites. *Applied Clay Science*, 52(3), 312-321.
- [34] Zhang, M., & Sundararaj, U. (2006). Thermal, rheological, and mechanical behaviors of LLDPE/PEMA/clay nanocomposites: effect of interaction between polymer, compatibilizer, and nanofiller. *Macromolecular Materials and Engineering*, 291(6), 697-706.
- [35] Borah, J. S., & Chaki, T. K. (2012). Effect of organo-montmorillonite addition on the dynamic and capillary rheology of LLDPE/EMA blends. *Applied Clay Science*, 59, 42-49.
- [36] Thompson, A., Bianchi, O., Amorim, C. L., Lemos, C., Teixeira, S. R., Samios, D., ... & Machado, G. (2011). Uniaxial compression and stretching deformation of an i-PP/EPDM/organoclay nanocomposite. *Polymer*, 52(4), 1037-1044.
- [37] Wagener, R., & Reisinger, T. J. (2003). A rheological method to compare the degree of exfoliation of nanocomposites. *Polymer*, 44(24), 7513-7518.
- [38] Chafidz, A., Kaavessina, M., Al-Zahrani, S., & Ali, I. (2014). Multiwall carbon nanotubes filled polypropylene nanocomposites: Rheological and electrical properties. *Polymer Engineering & Science*, 54(5), 1134-1143.

- [39] Razavi-Nouri, M., Naderi, G., Parvin, A., & Ghoreishy, M. H. R. (2011). Thermal properties and morphology of isotactic polypropylene/acrylonitrile-butadiene rubber blends in the presence and absence of a nanoclay. *Journal of Applied Polymer Science*, 121(3), 1365-1371.
- [40] Hoppner, D., & Wendorff, J. H. (1990). Investigations of the influence on the phase morphology of PP-EPDM-blends on their mechanical properties. *Colloid & Polymer Science*, 268(6), 500-512.
- [41] Corcione, C. E., & Frigione, M. (2012). Characterization of nanocomposites by thermal analysis. *Materials*, 5(12), 2960-2980.

## Part B

### POLYPROPYLENE/POLYBUTADIENE/CARBON NANOFIBRE COMPOSITES

-----

*The effect of concentration of carbon nanofibres (CNFs) on thermoplastic elastomer (TPE) based on polypropylene/polybutadiene (PP/BR) blend (80/20) prepared by melt blending process was investigated. Morphological properties are reported in combination with mechanical, rheological and thermal properties of the nanocomposites. The dispersion of CNFs examined by Transmission electron microscopy (TEM) show uniform dispersion of CNFs in the PP matrix. The mechanical performance is found to be in line with the morphological structure observed in Scanning electron microscopy (SEM). Tensile strength and Young's modulus of the PP/BR blend increase with an increase of filler content up to 3 wt %. Modified Halpin-Tsai equation that accounts for the effect of orientation and agglomeration of CNF was used to evaluate the Young's modulus of the nanocomposite. Dynamic rheological analysis (DRA) in the frequency sweep experiment shows that the introduction of CNF in the polymer matrix improves complex viscosity ( $\eta^*$ ), storage ( $G'$ ) and loss modulus ( $G''$ ) of the nanocomposites than PP/BR blend in the low frequency region. Dynamic mechanical analysis (DMA) in temperature sweep shows better interaction between CNFs and the matrix. The nucleation effect of carbon nanofibres in the crystallization process of the composites was confirmed by Differential scanning calorimetry (DSC) experiments. Thermogravimetric analysis (TGA) results show that CNFs can effectively enhance the thermal stability of the blend.*

-----

### 4B.1 Introduction

Thermoplastic elastomers (TPEs) combine the processability of the thermoplastics and elastic properties of elastomers<sup>1</sup>. Thermoplastic polyolefin (TPO) blends are physical blends of plastics with rubber and finds manifold applications in automotive, electronics and footwear industry. Polypropylene (PP) is one of the most extensively used engineering thermoplastic due to its remarkable properties and processability. The brittle nature and low impact strength of polypropylene limits the scope of applications of PP. In order to improve the impact strength of polypropylene, it is usually toughened with elastomers, but this often leads to the sacrifice of stiffness<sup>2</sup>. Simultaneous incorporation of elastomers and fillers in to the polymer matrix have been made by many researchers to achieve best balance between toughness and stiffness properties. The addition of inorganic fillers like talc in to the polymer matrix are often carried out to improve the stiffness, but requires higher loading of the filler and leads to poor processability<sup>3</sup>. Substitution of fillers with high aspect ratio nanofillers could reduce these issues, provided a proper distribution of the nanofillers in the polymer matrix could be achieved. Thus TPOs reinforced with low loadings of nanofillers have emerged as a class of materials possessing enhanced physical and mechanical properties proposing great potential for varied applications<sup>4</sup>.

The nanofillers used for composite preparation usually involves one dimensional nanofillers like carbon nanofibres (CNFs) and carbon nanotubes (CNTs), two-dimensional nanofillers like clay platelets and graphene and three-dimensional naofillers like silica nanoparticles<sup>5</sup>. There has been cumulative research and development to exploit carbon nanofibre (CNFs) as potential nanoscale reinforcement materials for thermoplastic polymers. The lesser cost of CNFs than carbon nanotubes (CNTs) and their exceptional

electrical, mechanical and thermal characteristics makes it a worthy nanofiller for polymer matrices. The conventional carbon fibres (CFs) have diameters of several micrometers, while CNFs have diameters in the range 50–200 nm and length in the range 20–100  $\mu\text{m}$ .<sup>6</sup> The smaller diameter and high aspect ratio makes CNFs a potential reinforcing filler<sup>7</sup>. CNFs can be prepared by catalytic thermal chemical vapor deposition grown method and are known as Vapour Grown Carbon nanofibre (VGCNF)<sup>8</sup>. VGCNF can be of cup-stacked structure or platelet structure. Several research groups have studied them as promising fillers for thermoplastic polymers<sup>9,10</sup>. The advantageous high aspect ratio can scarcely be explored as CNFs are entangled because of the strong van der Waals force. Melt blending is the most technologically preferred method for preparing the polymer/CNF composites as it evades the usage of solvents. High shear mixing will result in a comparatively good distribution of the CNF in the matrix, but the aspect ratio which overrides the general performances of the CNF/polymer composites will be reduced during the mixing process<sup>11</sup>. Hence, the research of reasonably low shear mixing method without surrendering the dispersion is still a challenge for the preparation of CNF/polymer composites by the melt mixing. Barick *et al.*<sup>12</sup> have reported the melt blending as an effective technique in the preparation of TPU/CNF composites.

CNF has been reported to be a potential reinforcing nanofiller in the improvement of the thermo-mechanical properties of PP by many researchers<sup>13-15</sup>. Investigations based on PP/SEBS-g-MA blends reinforced with CNFs carried out by Cheng *et al.* established CNF to be an effective reinforcing agent. Investigations by Tong *et al.*<sup>16</sup> on PP/CNF composites prepared by melt blending reported that CNFs acted as a reinforcing filler to improve the modulus at any loadings but decreased the strength at higher

loadings due to poor dispersion. Investigations on thermal stability of PP/CNF composite system established that the incorporation of CNF in PP enhanced the thermal stability of the polymer<sup>17</sup>. PP/SEBS/CNF composites prepared by melt-mixing process were reported to show improved strength, toughness and modulus<sup>18</sup>.

The main failure mechanisms for fibre reinforced polymers as reported by earlier studies are fibre pull out, fibre breakage, and fibre matrix debonding/crack bridging<sup>19</sup>. It was established that fibres that are strongly adhered to the matrix and that bridged the crack underwent fibre breakage<sup>20</sup>. It was established that fibre pull out appears to be the best effective toughening mechanism<sup>21</sup>. Schematic representation of the failure modes in fibre reinforced composites are represented in the following Figure 4B.1.

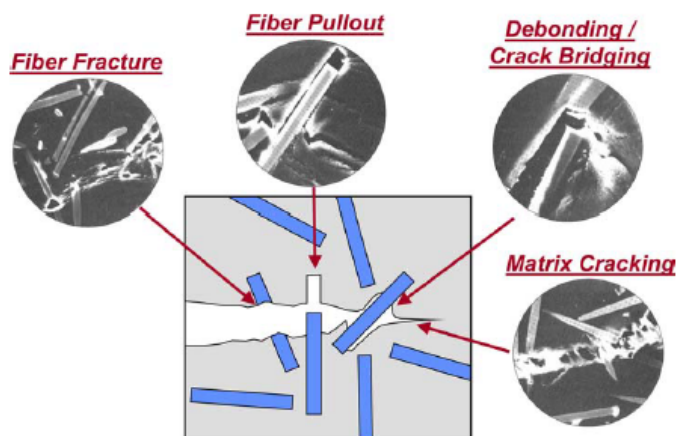


**Figure 4B.1. Mechanisms of energy dissipation identified in the fracture of short as well as continuous fibre-reinforced composites<sup>19</sup>**

This part of the thesis investigate the effects of CNFs on PP/BR (80/20) blend without the use of any compatibilizer or chemical modification on the

surface of the CNF. The PP/BR/CNF composites have been prepared by simple melt blending technique and the effect of CNFs on the morphological, mechanical and thermal properties of uncompatibilized PP/BR blend is studied. On blending with BR, PP suffered a decrease in stiffness and in order to compensate for the loss of stiffness of the PP matrix, care was taken to distribute CNFs in the PP matrix. The experimental results indicated that a uniform distribution of CNFs in PP/BR blend was achieved by melt mixing and the presence of nanofibres in the PP matrix had a cumulative influence on the properties and microstructure of the nanocomposites. Tensile and impact tests were used to evaluate the mechanical properties of nanocomposites and were correlated with morphology examined using SEM. Distribution of CNF in the nanocomposites were analyzed by TEM and XRD technique. The processability of the nanocomposites were established using the dynamic rheological characterization. The thermal properties of PP/BR nanocomposites was analyzed by means of DMA, DSC and TGA studies.

## **4B.2 Methodology**

### **4B.2.1 Materials**

The details of the polymers used for the study are discussed in Chapter 2 (sections 2.1). The characteristics of VGCNF used in the present study is given in table 4B.1.

**Table 4B.1. Characteristics of VGCNF<sup>22</sup>**

<b>Property</b>	<b>Symbol</b>	<b>Unit</b>	<b>Value</b>
<b>Diameter</b>	$d_f$	nm	50-100
<b>Length</b>	$l_f$	$\mu\text{m}$	30-100
<b>Modulus</b>	$E_f$	GPa	400
<b>Density</b>	$\rho_f$	g/cc	1.8



### 4B.2.2 Preparation of PP/BR/CNF composites

PP toughened with 20 wt % of BR and reinforced with 0, 0.2, 0.5, 1.5, 3, and 4 wt % of CNFs were melt blended in a Brabender plasticorder followed by injection molding. The preparation of the nanocomposites involved melt blending process where PP pellets were melted initially followed by the addition of BR, melt mixed for 2 minutes and finally CNF was added. The mixing was continued for further 8 minutes. The designation and composition of the PP/BR/CNF nanocomposites are listed in table 4B.2.

**Table 4B.2. Composition of PP/BR/carbon nanofibre composites**

PP (wt %)	BR (wt%)	CNF (wt %)	Sample Code
100	-	-	P100
80	20	-	P80
80	20	0.2	P80CNF0.2
80	20	0.5	P80CNF0.5
80	20	1.5	P80CNF1.5
80	20	3	P80CNF3
80	20	4	P80CNF4

The test specimens were injection molded at a barrel temperature of 180 °C and then tested as discussed in chapter 2.

### 4B.2.3 Theoretical modeling of Young's modulus

In this study, Halpin-Tsai equation and the modified Halpin-Tsai equation that considers the effect of random orientation and agglomeration of fibres are used to predict the Young's modulus of the PP/BR composites. Theoretical modeling of Young's modulus of the nanocomposites is widely

interpreted using Halpin-Tsai model<sup>23,24</sup>. The Halpin-Tsai model relates the modulus of a unidirectional fibre reinforced composite and may be expressed as in equation 4B.1

$$\frac{E_c}{E_m} = \frac{1 + \xi\eta V_f}{1 - \eta V_f} \dots\dots\dots (4B.1)$$

$$\text{Where } \eta = \frac{\frac{E_f}{E_m} - 1}{\frac{E_f}{E_m} + \xi} \dots\dots\dots (4B.2)$$

where  $E_f$  is the Young's modulus of the carbon nanofibre,  $E_m$  is the Young's modulus of the matrix,  $\xi$  is the shape factor dependent on filler orientation, geometry and loading direction and  $V_f$  is the volume fraction of carbon nanofibre. The values of  $V_f$  and  $\xi$  are given by equations 4B.4 and 4B.5, respectively<sup>25</sup>.

$$V_f = \frac{W_f / \rho_f}{\frac{W_f}{\rho_f} + (1 - W_f) / \rho_m} \dots\dots\dots (4B.3)$$

$$\xi = 2\left(\frac{l}{d}\right) \dots\dots\dots (4B.4)$$

where  $l$  is the length and  $d$  is the diameter of the fibre. Since Halpin-Tsai equation deals with the modulus of unidirectional fibre reinforced composites and in order to account for the random fibre orientation, an orientation factor has been introduced in the Halpin-Tsai equation. Considering the effect of orientation, Cox<sup>26</sup> introduced an orientation factor,  $\alpha$ , thereby modifying the value of  $\eta$  in Halpin-Tsai equation as in equation 4B.5.

$$\eta = \frac{\frac{\alpha E_f}{E_m} - 1}{\frac{\alpha E_f}{E_m} + \xi} \dots\dots\dots (4B.5)$$

when the length of the reinforcement is much smaller than the thickness of the testing specimen,  $\alpha = 1/6$  is used. Further, in order to interpret for the agglomeration of CNF on the modulus of the composite, shape factor  $\xi$  has been modified to an exponential relation<sup>27</sup> and is expressed as:

$$\xi = 2\left(\frac{l}{d}\right)e^{-aV_f-b} \dots\dots\dots (4B.6)$$

The parameters a and b in this equation relates CNF agglomeration<sup>28</sup>.

## 4B.3 Results and Discussion

### 4B.3.1 X-ray Diffraction (XRD)

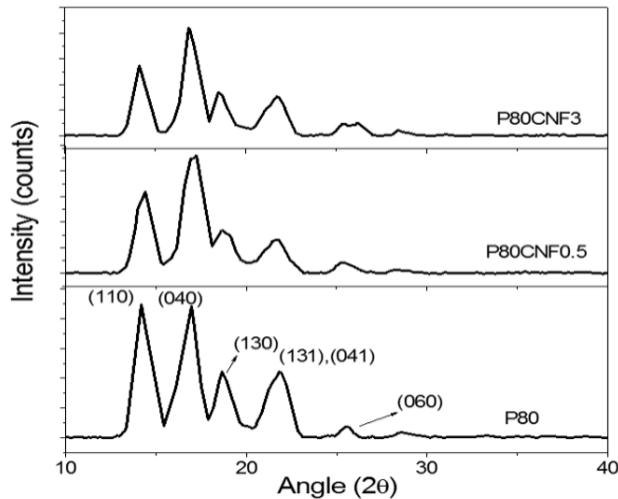
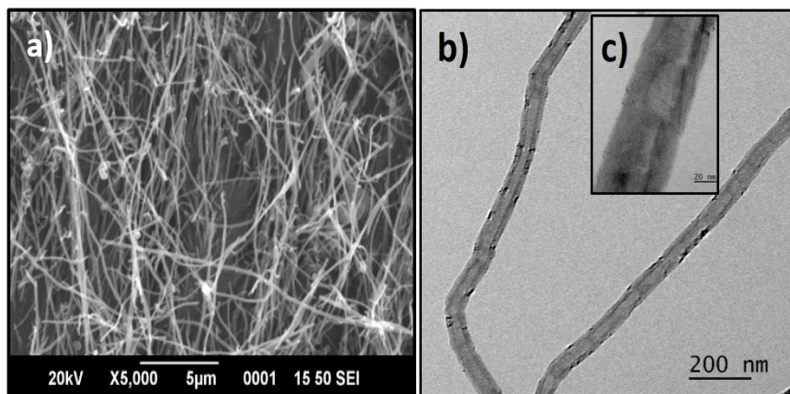


Figure 4B.2. XRD patterns of PP/BR blend nanocomposites

X-ray diffraction is a powerful technique to determine the crystal structures present in polymers. Figure 4B.2 shows the XRD patterns of P80 blend and PP/BR/CNF composites. The diffraction peaks in the XRD pattern is observed at  $2\theta = 14.1^\circ, 16.8^\circ, 18.5^\circ, 21.8^\circ$  and  $25.5^\circ$  for P80 blend and PP/BR/CNF composites. The peaks observed in the XRD pattern represent only characteristic type of  $\alpha$ -monoclinic crystal structures of PP phase and corresponds to (110), (040), (130) overlapped (131,041) and (060) planes. XRD results indicate that all the samples contain  $\alpha$  type crystals and CNF additions do not bring a structural change of PP from the  $\alpha$  phase to  $\beta$  phase.

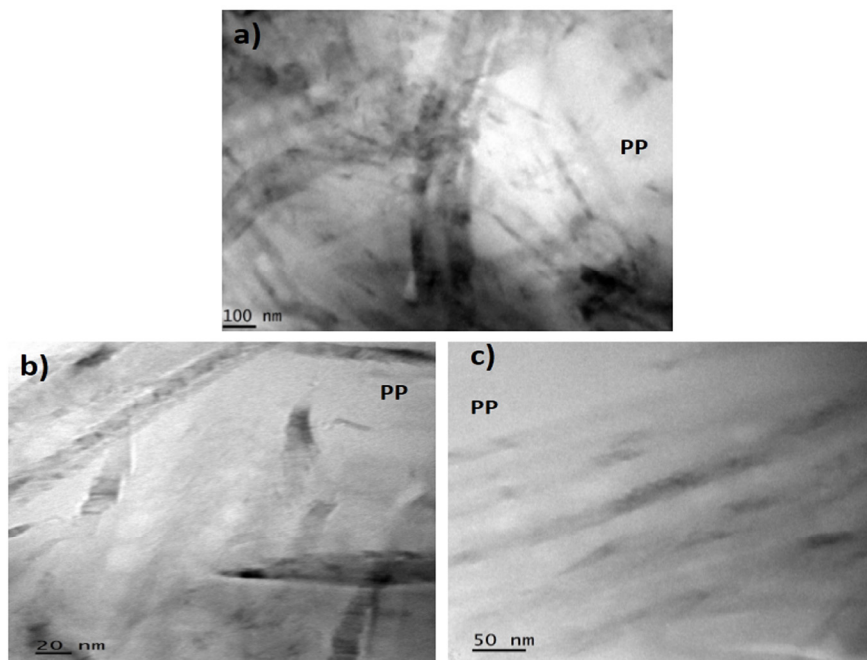
#### 4B.3.2 Transmission electron microscopy (TEM)



**Figure 4B.3. (a) SEM photograph of pristine CNFs (b) TEM photograph of individual pristine CNF (c) inset showing the cup stacked structure of pristine CNF**

The highly entangled interwoven fibres of CNFs as received is represented by the SEM photograph as shown in Figure 4B.3(a). The SEM photograph shows enormous agglomeration of bundles of CNFs because of strong van der Waals forces. The Figure 4B.3(b) shows the TEM

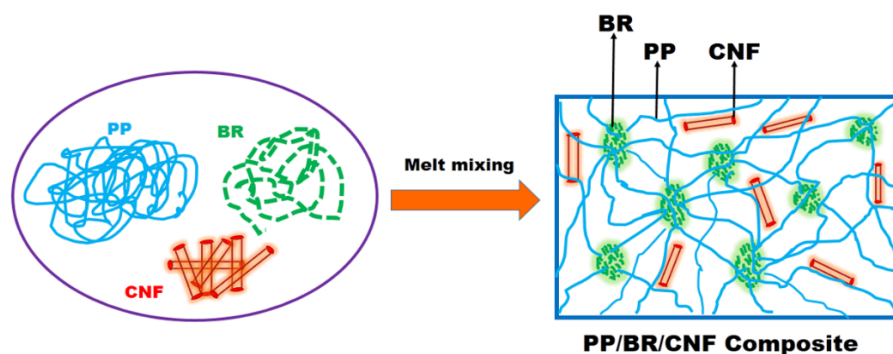
photograph of individual CNF. The inset Figure 4B.3(c) illustrates cup stacked structure of pristine CNF.



**Figure 4B.4(a-c). TEM photograph of PP/BR/CNF composite (P80CNF3) at different magnifications**

TEM photographs of PP/BR/CNF composite (P80CNF3), that showed optimum mechanical properties is shown in Figure 4B.4 (a-c). In order to show the random orientation of CNF in the PP matrix, TEM photographs at different magnifications are chosen. The white regions in the TEM photograph correspond to the PP phase. Even though SEM photographs of pure CNFs revealed interlinked bundles, it can be assumed that on applying shear during the melt blending process, these bundles of CNF become well dispersed as individual fibres preferentially in the low viscous PP matrix of the composite<sup>29</sup>. From the TEM photograph, a

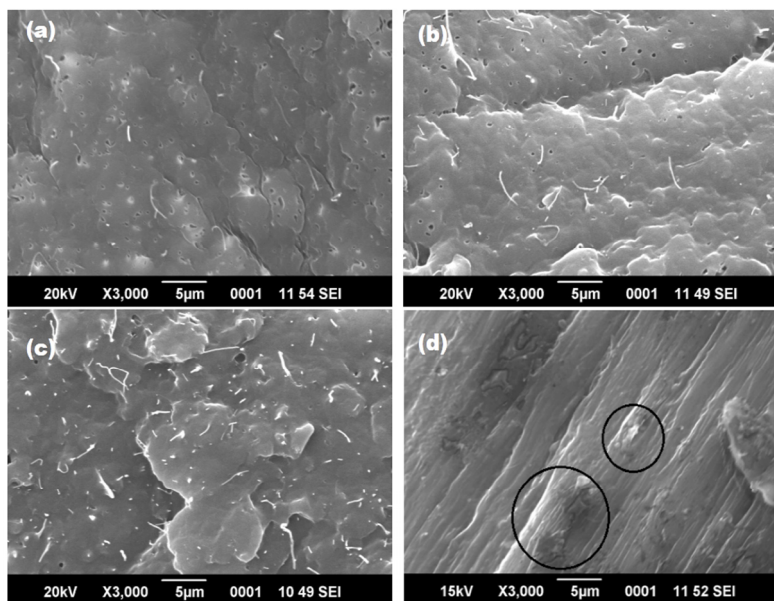
homogenous distribution of randomly oriented CNFs in the PP matrix by melt blending is established. Studies made by P.J *et al.*<sup>18</sup> on PP/SEBS/CNF blends have suggested the probability of migration of CNF from PP phase to the amorphous SEBS phase under shear during melt-mixing. But in the case of PP/BR blend, TEM photographs revealed the presence of CNFs only in the PP phase. The migration of CNFs to the BR phase is not observed in this case and can be attributed to the greater interfacial tension existing between the PP and BR phases. Boronat *et al.*<sup>30</sup> demonstrated a homogenous distribution of CNF in PP matrix by melt blending technique. Hence it can be inferred that in this study, melt blending had proved to be an effective technique for making carbon nanofibre composites with preferential localization of CNFs in the PP matrix<sup>31</sup>. The distribution of CNFs in the PP matrix can compensate for the loss of the stiffness of PP matrix occurred on toughening with BR. A schematic illustration of the fabrication strategy for melt blending of PP, BR and CNF can be given as in Figure 4B.5.



**Figure 4B.5. Fabrication strategy of PP/BR blend nanocomposite by melt blending**

### 4B.3.3 Scanning electron microscopy (SEM)

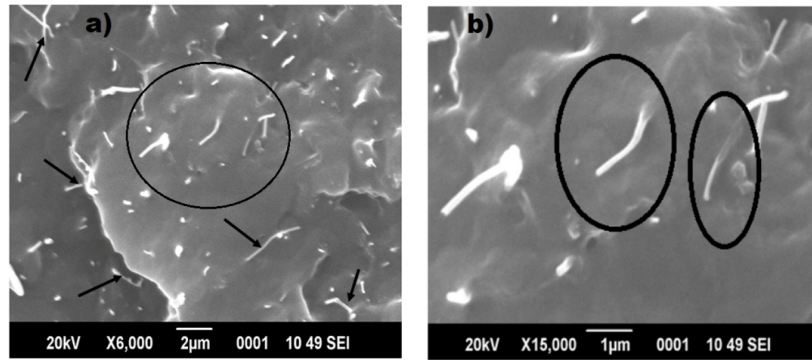
#### a) SEM photographs of tensile fractured surfaces



**Figure 4B.6. SEM photographs showing tensile fracture morphology of a) P80CNF0.5 b) P80CNF1.5 c) P80CNF3 d)P80CNF4**

SEM photograph of the tensile fractured surfaces of the PP/BR/CNF composites is shown in Figure 4B.6(a)-(c). CNFs can be identified as white sprouts like particles in the PP matrix. It can be concluded that the CNFs are relatively well dispersed in the polymer with no apparent agglomeration at lower loading. SEM photographs revealed even distribution of CNFs by the appearance of single fibrils on the surface of PP matrix and CNFs are detected to be fragmented rather than just pulled out of the PP matrix during the breaking of the specimens. Barik *et al.*<sup>12</sup> also suggested a homogenous distribution of CNF in the TPU matrix prepared by melt blending technique. This establishes strong interfacial interaction of CNFs with PP matrix up to 3 wt % loading. At higher loading, low magnification was needed to detect

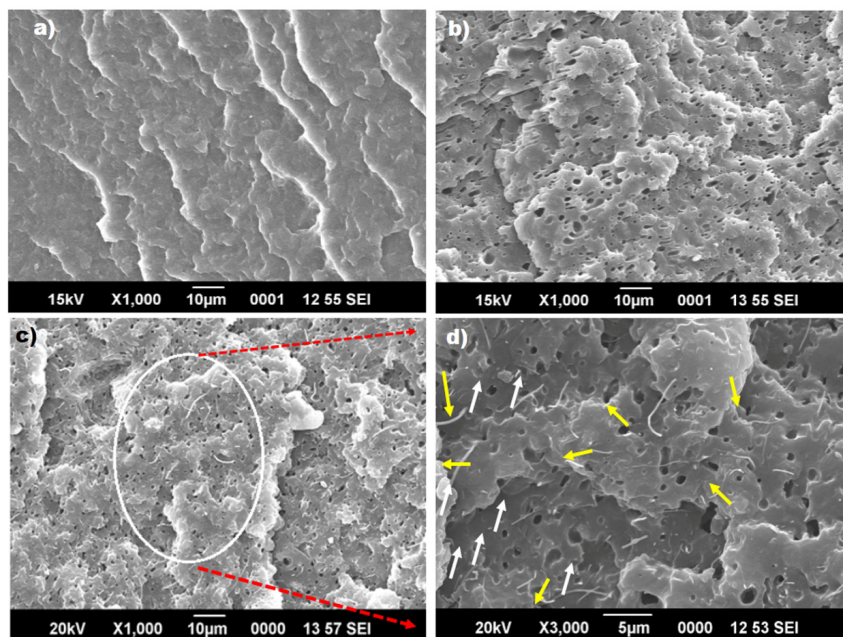
the poor dispersion of nanofibres. The circles in the Figure 4B.6(d) evidently show a large number of unbroken carbon nanofibres, at very high CNF concentrations, indicating a poor polymer nanofibre adhesion. Good distribution of nanofibres at lower loading and agglomeration at higher loading were also reported by Lozano *et al* <sup>32</sup>.



**Figure 4B.7 (a) SEM photographs illustrating randomly oriented CNF (b) SEM photograph under high magnification showing good matrix fibre interaction**

Tensile fractured surface of the P80CNF3 sample at lower and higher magnifications is shown in Figures 4B.7 (a) and (b), respectively. Figure 4B.7(a) demonstrates the random orientation of CNFs in the PP matrix shown by arrows and in small circle. Figure 4B.7(b) showed better dispersion of CNF as discrete fibres and polymer traces could be seen coated on the CNF surface<sup>12</sup>. The fibres were found adhered to the PP matrix and most of the fibres were well coated by the polymer indicating that there exists good interfacial bonding between the CNFs and the PP matrix. This results in the formation of a matrix- fibre interface. The presence of the matrix coating on CNF suggests that failure was initiated by local yielding of the polymer matrix resulting in significant stress concentration at the fibre ends rather than at the matrix-fibre interface leading to fibre breakage<sup>33</sup>.



**b) SEM photographs of impact fractured surfaces**

**Figure 4B.8. SEM photographs showing impact fracture morphology of a) P100 b) P80 c) P80CNF3 d) P80CNF3 under high magnification**

The SEM photograph of the impact fractured surface of pure PP, P80 and P80CNF3 samples are shown in Figures 4B.8(a)-(d). As shown in Figure 4B.8(a), pure PP shows brittle fracture. Figures 4B.8(b) and (c) represent the SEM photograph of the impact fractured surface P80 blend and P80CNF3 samples, respectively. These samples showed a two phase morphology with continuous PP phase and a dispersed BR phase. In Figure 4B.8(b), for the P80 sample, elongated voids indicating a ductile fracture due to shear yielding of the matrix is noticeable. In the Figure 4B.8(c) rubber particle cavitation, with randomly oriented CNFs associated with the PP phase is clear, but extent of shear yielding of the matrix is found to be reduced. This can be attributed to the strong interaction between the PP matrix and CNFs.

From the SEM photographs shown in Figure 4B.8(d), a random distribution of CNFs is visible with no traces of fibre pull out. The nanofibres that have undergone fibre breakage are shown in white arrows. The broken fibre ends are visible as white sprouts. The CNFs that have bridged the matrix are shown in yellow arrows. Fibre breakage is the major mode of impact fracture in P80CNF3 sample. Similarly, Thostenson and Chou<sup>21</sup> also detected nanotube bridging the crack and broken nanotubes in their studies on carbon nanotube reinforced polymer composites. It can be interpreted that strong adhesion between the matrix and the fibre resulted in better stress transfer from the matrix to the fibre ends leading to fibre breakage than fibre pull out. Based on the morphological observations of the impact fractured surfaces of the P80CNF3 sample, schematic diagram demonstrating the orientation of the CNF in the PP matrix and the mode of fracture is depicted in Figure 4B.9.

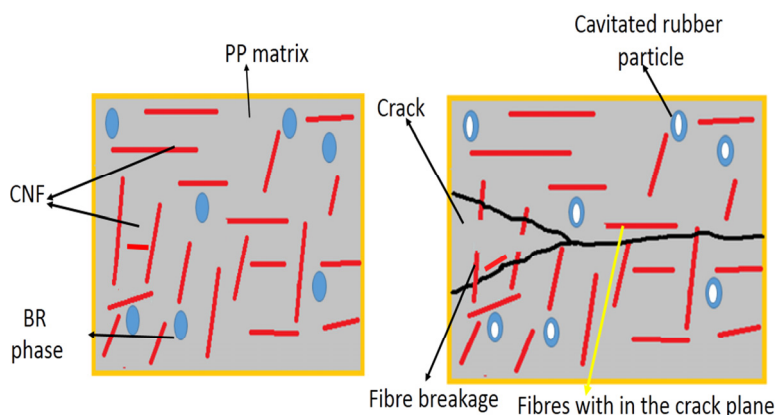


**Figure 4B.9. Schematic illustration of CNF alignment and mode of failure in impact testing of P80CNF3 sample.**

SEM photographs envisage shortening of the CNF with good nanofibre dispersion within the matrix, after composite fabrication which can be attributed to the high shearing action during the melt blending. The shortening of the CNF is speculated to affect the conductive path formation,

the critical parameter for good conductivity<sup>34</sup>. Here melt blending of the polymers and the CNF has resulted in a morphology with good filler dispersion but not forming conductive path formation resulting in low electrical conductivity of the PP/BR/CNF composites.

### 4B.3.4 Mechanical properties

#### 4B.3.4.1 Tensile properties

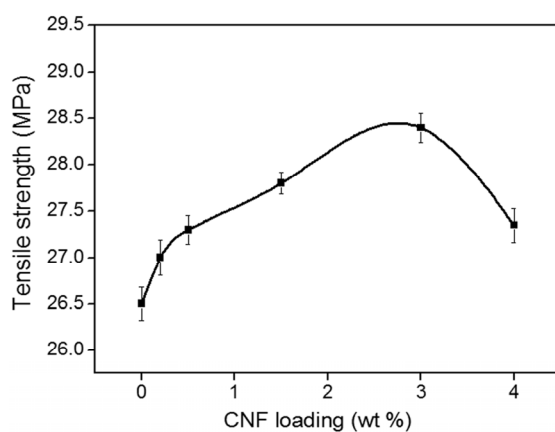


Figure 4B.10. Variation of tensile strength with CNF loading

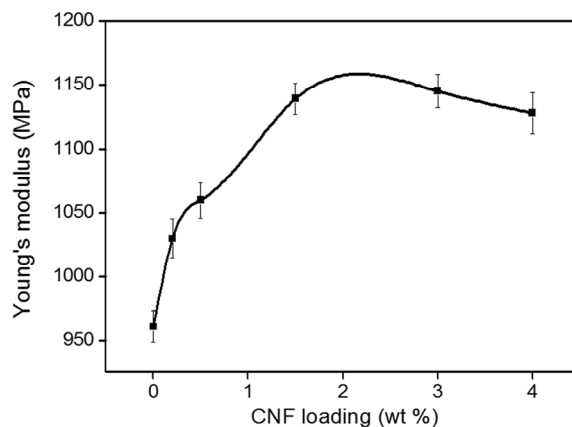
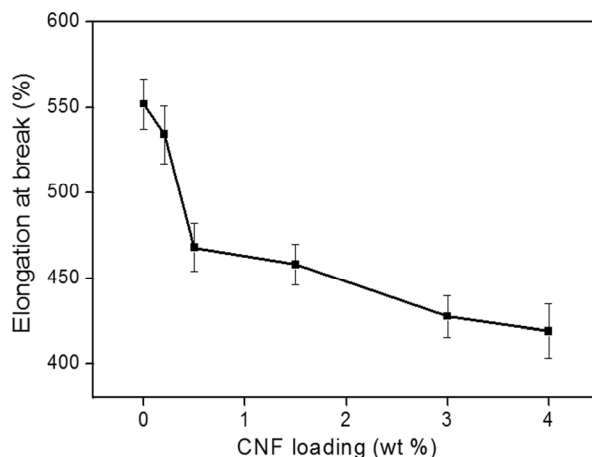


Figure 4B.11. Variation of Young's modulus with CNF loading

The effect of CNF as a reinforcing filler on the tensile strength and Young's modulus of the P80 blend is depicted in Figure 4B.10 and 4B.11, respectively. From the figures, it is clear that tensile strength and Young's modulus increased with increase in CNF content up to 3 wt % and there after showed a reverse trend. With the addition of 3 wt % of CNF, there occurred about 8 % increase in tensile strength and 17 % increase in Young's modulus of the P80 blend. The improvement in tensile strength and Young's modulus of the P80CNF3 sample can be attributed to the good dispersion of CNFs in the PP matrix combined with strong matrix fibre adhesion as shown in the TEM and the SEM photographs. The localization of CNFs in the PP matrix led to improved stiffness of the blend matrix. The strong matrix fibre interaction have resulted in perfect stress transfer from the matrix to fibres<sup>35</sup>. At higher filler content, a reduction in mechanical properties occurred due to agglomeration of CNFs.

#### **4B.3.4.2 Impact strength**



**Figure 4B.12. Variation of elongation at break with CNF loading**

The variation of elongation at break of the P80 blend with CNF content is represented in Figure 4B.12. The addition of CNF content reduced the elongation at break of the P80 sample. This can be attributed to the distribution of CNF in the matrix which would have acted as physical crosslink points restricting the mobility of the PP chains<sup>36,37</sup>. The adhesion of CNF to the PP matrix also contributed to the enhancement of stiffness of the matrix leading to decreased elongation at break.

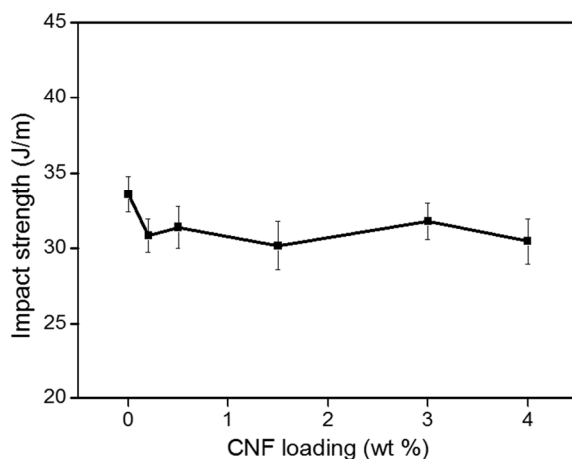


**Figure 4B.13. Variation of impact strength with CNF loading**

Figure 4B.13 shows the variation of elongation at break of P80 blend with CNF loading. Addition of CNFs to the P80 blend decreased the impact strength of the P80 blend. The impact strength of the PP/BR/CNF composites remained constant for a wide range of filler loading. This may be due to the preferential localization of CNFs in the PP matrix as visualized by TEM and SEM photograph. Fibre pullout is established to be an effective toughening mechanism in fibre reinforced polymer matrices. The mode of failure observed in the SEM photographs of the P80CNF3 sample revealed fibre breakage rather than fibre pull out. So an expected increase in the

impact strength of the PP/BR blend is not achieved by the introduction of CNF<sup>38</sup>.

The addition of CNFs to PP/BR blend enhanced the strength and stiffness along with retention of the impact strength of the P80 blend<sup>39,40</sup>.

#### 4B.3.4.3 Theoretical modeling of Young's modulus

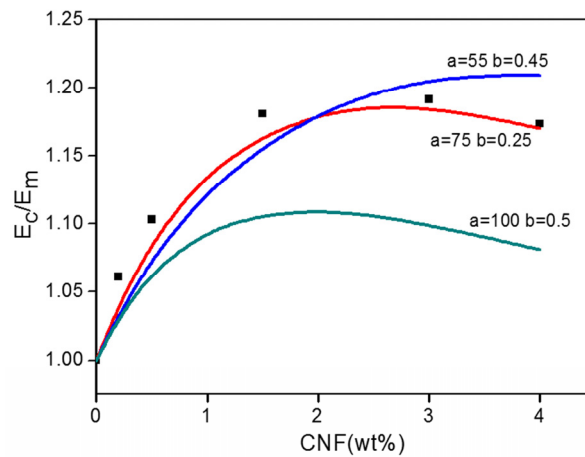
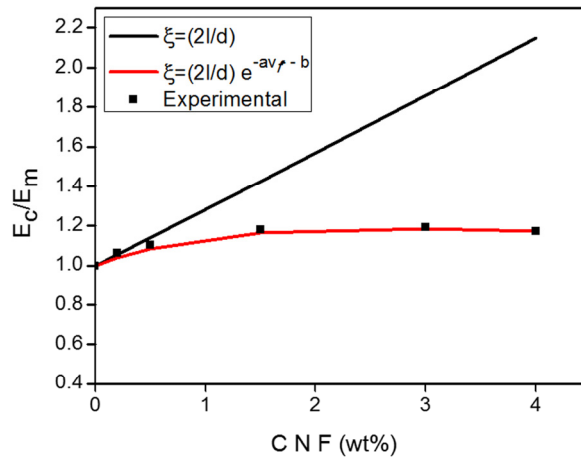


Figure 4B.14. Effect of the constants a and b on the Young's modulus

Halpin-Tsai equation and the modified Halpin-Tsai equation are used to predict the Young's modulus of the PP/BR/CNF composites. The modified Halpin-Tsai equation considers the effect of random orientation and agglomeration of fibres. Experimental Young's modulus predicted by the modified Halpin-Tsai equations with  $\xi = (2l/d) e^{-\alpha v_f^{-b}}$  is shown in Figure 4B.14. In this study, the Young's moduli of the blend matrix and CNF are taken as 0.961 GPa (from Figure 4B.11) and 400 GPa, respectively<sup>22,41</sup>. Based on the diameter and length of the CNFs, the aspect ratio of CNF is set be 150<sup>42</sup>. The orientation factor  $\alpha = 1/6$  will be used, since the length of CNFs used in this study is around 120  $\mu\text{m}$ , which is much smaller than the thickness of the

tensile testing specimens (of 2 mm). The best fit is obtained when  $a=75$  and  $b=0.25$  in the modified Halpin-Tsai equation. Similar results have been reported by Sun *et al.*<sup>27</sup> in the modeling of carbon nanofibre/epoxy nanocomposites.



**Figure 4B.15. Theoretical modeling of Young's modulus of PP/BR/CNF composites as a function of filler loading using Halpin-Tsai and modified Halpin-Tsai equations**

Among the model fits, the predicted moduli based on modified Halpin-Tsai equation (that considers fibre orientation and agglomeration) shows the closest proximity to the experimentally determined Young's modulus as shown in Figure 4B.15. The experimental results are in good agreement with the theoretically predicted results and indicates that the PP/BR/CNF composites are randomly oriented nanocomposites with CNF agglomeration at higher content.

## 4B.3.5 Dynamic rheological analysis (DRA)

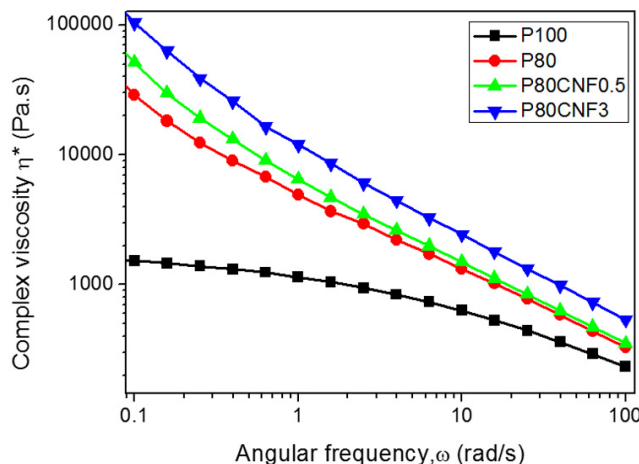


**Figure 4B.16.** Complex viscosity,  $\eta^*$  as a function of angular frequency ( $\omega$ ) of P100, P80, P80CNF0.5 and P80CNF3 samples at 190 °C.

Melt rheological properties are intensely associated with the morphological structure of nanocomposites, distribution of the nanofiller in the matrix and interactions between polymer matrix chains and nanofibres. The plot of complex viscosity,  $\eta^*$  as a function of angular frequency for P100, P80, P80CNF0.5 and P80CNF3 samples at 190 °C is given in Figure 4B.16. As obvious from the plot, the CNFs had a significant effect on the melt rheological performance of the nanocomposites which is pronounced at lower frequencies. The figure clearly shows that that pure PP melt exhibits a Newtonian plateau of viscosity at lower frequencies and shear thinning behavior at higher frequencies. The PP/BR blend (P80 sample) and the PP/BR/CNF nanocomposites showed increased complex viscosity with marked shear thinning behavior even at low frequency values. The shear thinning observed in the nanocomposites can be ascribed to the reduced



movement of the confined polymer chains due to interaction between carbon nanofibres and the polymer chains. The viscosity of the nanocomposites was greater than that of P80 blend and increased with the nanofibre content because of the interaction between the PP matrix and the nanofibre<sup>30,43</sup>. The increase in the viscosity of the nanocomposites is more pronounced at low frequency region than that of the high frequency region. At high frequency range the viscosity value of the nanocomposite is not changed remarkably as compared to the pristine counterpart and the resultant plot appears to converge. This suggests melt blending process a suitable processing method for CNF based nanocomposites<sup>12</sup>.

Figures 4B.17 and 18, respectively, show the logarithmic plots of melt rheological moduli such as storage modulus ( $G'$ ) and loss modulus ( $G''$ ) of P100, P80, P80CNF0.5 and P80CNF3 samples at 190 °C as a function of angular frequency.

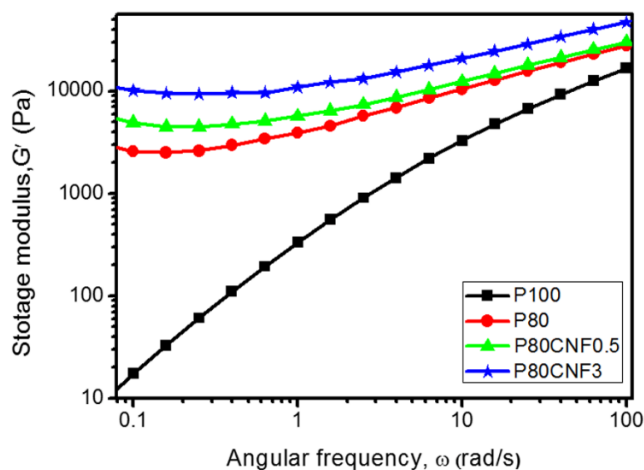


**Figure 4B.17.** Storage modulus vs. angular frequency of P100, P80, P80CNF0.5 and P80CNF3 samples at 190 °C

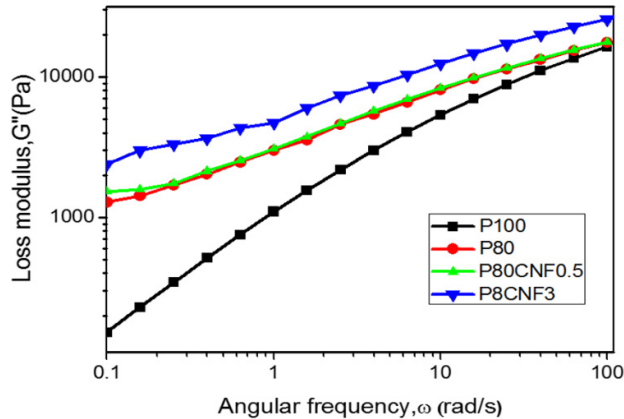


**Figure 4B.18. Loss modulus vs. angular frequency of P100, P80, P80CNF0.5 and P80CNF3 samples at 190 °C**

The storage modulus ( $G'$ ) represents the elastic nature of the polymer showing the ability of the polymer to store energy and loss modulus ( $G''$ ) reveals the viscous behavior of the polymer and specifies the ability of a material to disperse energy. There is considerable increase in storage modulus ( $G'$ ) and marginal increase in loss modulus ( $G''$ ) of the PP/BR/CNF composites in the studied frequency range when compared to the PP/BR (P80) blend. The significant enhancement of  $G'$  at lower frequencies than at higher frequencies as shown in Figure 4B.17 reveals strong influence of nanofibre dispersion. The substantial interaction between the polymer chains and the dispersed carbon nanofibres restrict the mobility of PP chains leading to increased  $G'$  value<sup>30</sup>. In other words, the samples behaved as viscoelastic solid, showing high elasticity in the experimental frequency range.

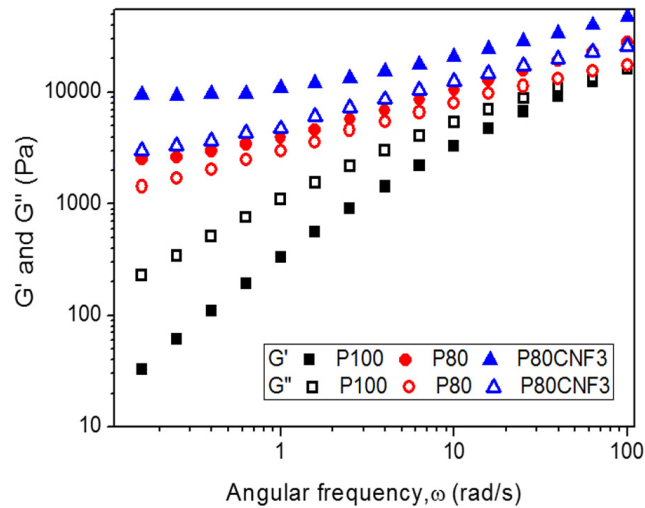


**Figure 4B.19.** Storage modulus ( $G'$ ) and Loss ( $G''$ ) modulus as a function of angular frequency of P100, P80 and P80CNF3 samples at 190 °C

As seen from the Figure 4B.19, it is clear that P100 exhibited higher values of loss modulus ( $G''$ ) than storage modulus ( $G'$ ) in the entire frequency range, replicating the behavior of a characteristic viscous material. In the case of PP/BR blend (P80 sample) and the PP/BR/CNF composite (P80CNF3 sample) storage modulus ( $G'$ ) is higher than loss modulus ( $G''$ ) over the entire range of selected frequency, hence no  $\omega_c$  (crossover frequency) is observed. As  $G'$  is overriding  $G''$  ( $G' > G''$ ) for the nanocomposites in the complete frequency range measured, solid like elastic response can be established due to the restricted molecular mobility of the PP chains. At higher frequencies,  $G'$  and  $G''$  values show the appearance of a plateau, signifying the establishment interconnected nanofibre network within the matrix. This is consistent with the earlier reported results<sup>44,45</sup>.

The complex viscosity,  $\eta^*$  as a function of angular frequency is given as

$$\eta^* = k\omega^n \dots\dots\dots (4B.8)$$

where  $\eta^*$  is the complex viscosity,  $k$  is the exponential factor,  $\omega$  is the oscillation frequency and  $n$  is the shear thinning exponent. The value of  $n$  can be calculated from the slope of the straight line obtained in the  $\log \eta^*$  vs.  $\log \omega$  plot and is shown in table 4.B.3. The value of  $n$  is greater for the blend and its nanocomposite than pure PP which reflects a greater pseudoplastic behavior. Literature reports revealed that higher the exponent  $n$ , the more efficient is the reinforcement of the corresponding composite<sup>43</sup>.

The relationship between  $G'$  and  $G''$  with angular frequency  $\omega$  could be described as

$$G' \propto \omega^{n_1} \quad (n_1=2) \dots\dots\dots (4B.9)$$

$$G'' \propto \omega^{n_2} \quad (n_2=1) \dots\dots\dots (4B.10)$$

The dispersion state of fillers can be evaluated by determining the slope of  $G'$  and  $G''$  vs.  $\omega$ . The slopes of the terminal zone  $n_1$  and  $n_2$  were calculated and are listed in table 4.B.3. It is observed that the slopes of  $G'$  and  $G''$  for the PP/BRCNF composites are smaller than the pure PP and P80 blend. Similar decrease in the values of  $n_1$  have been reported by Naderi *et al.*<sup>46</sup>. Mishra *et al.*<sup>47</sup> reported higher values of  $G'$  and smaller terminal slope ( $n_1$ ) for the nanocomposites over their pristine counterpart and have suggested the formation of three dimensional superstructure for the nanocomposite. The decrease in the terminal slopes ( $n_1$  and  $n_2$ ) of the nanocomposite supports interaction between CNF and polymer chain in the melt state. The rheological results are in agreement with the earlier results that suggested PP/CNF composites to be a better choice from processability point of view<sup>43</sup>.

**Table 4B.3. Slopes of  $\log \eta^*$ ,  $\log G'$  and  $G''$  vs.  $\log \omega$  at 190 °C ( $n$ ,  $n_1$  and  $n_2$ ), respectively, as observed from frequency sweep experiments**

Sample	$n$	$n_1$	$n_2$
P100	-0.3449	0.993	0.6825
P80	-0.5813	0.3757	0.3985
P80CNF0.5	-0.8790	0.3713	0.3962
P80CNF3	-0.9011	0.2456	0.3453

#### 4B.3.6 Dynamic mechanical analysis (DMA)

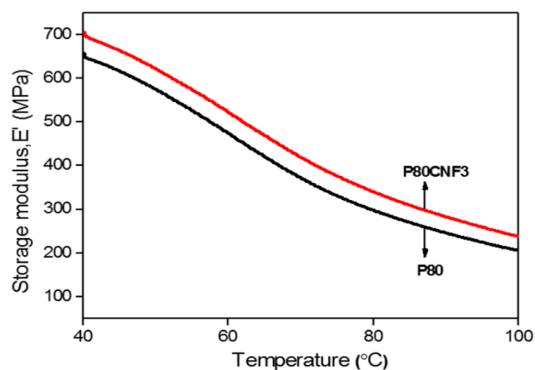


**Figure 4B.20. Variation of storage modulus ( $E'$ ) of PP/BR blend and PP/BR/CNF composite with temperature**

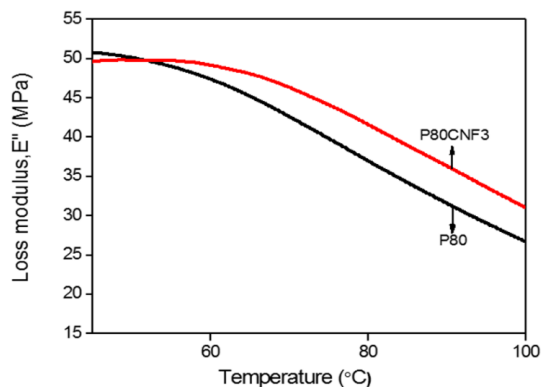


**Figure 4B.21. Variation of loss modulus ( $E''$ ) of PP/BR blend and PP/BR/CNF composite with temperature.**

Figures 4B.20 and 21, respectively, show the results obtained from DMA tests for the PP/BR blend (P80 sample) and the PP/BR/CNF composite (P80CNF3 sample) carried out at frequency, 1 Hz in the temperature range from 40 to 120 °C. The variation of storage ( $E'$ ) modulus with temperature is shown in Figure 4B.20. The storage modulus of the blend and the nanocomposite decreased with increasing temperature. The nanocomposite showed enhanced storage modulus values than the PP/BR blend matrix. The enhancement in storage modulus with CNF loading established an increase in the stiffness of the nanocomposite<sup>48</sup>. The variation of loss modulus with temperature is shown in Figure 4B.21. It is obvious that the nanocomposite possess greater loss moduli compared to the PP/BR blend. This can be attributed to the increased friction between the uniformly dispersed CNFs and the matrix<sup>49</sup>.

#### 4B.3.7 Differential scanning calorimetry (DSC)

**Table 4B.4. Melting characteristics of PP/BR blends and the nanocomposites**

Sample	$T_{m,onset}$ (°C)	$T_m$ (°C)	$T_{m,endset}$ (°C)	$\Delta H_f$ J/g	$X_c$ (%)
P100	154	167	171	93.76	45
P80	153	167	171	70.57	42
P80CNF0.5	154	166	171	73.03	44
P80CNF1.5	154	165	170	76.01	45
P80CNF3	153	166	170	78.62	47
P80CNF4	154	164	168	76.41	46

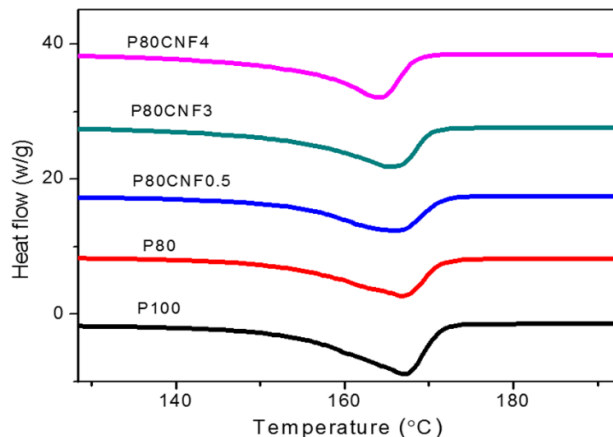


**Figure 4B.22. DSC heating curves of PP/BR nanocomposites**

Melting and crystallization behavior of P100, P80 blend and the nanocomposites were investigated by DSC analysis in the temperature range from 30 to 200 °C and the DSC heating curves are represented in Figure 4B.22. The melting characteristics of PP such as melting onset temperature ( $T_{m,onset}$ ), melting temperature ( $T_m$ ), melting endset temperature ( $T_{m,endset}$ ), enthalpy of fusion ( $\Delta H_f$ ) and percentage of crystallinity ( $X_c$ ) derived from heating curves are listed in table 4B.4. It is obvious that the melting temperature of the nanocomposites remained almost around 165 °C suggesting negligible effect of nanofillers on the melting temperature of pristine PP. This shows that PP crystals exist at  $\alpha$  phase, since  $\beta$  phase PP crystals melt at lower temperature<sup>50</sup>. This approves well with previous XRD studies, where only  $\alpha$  phase crystals were obtained by adding CNFs into PP matrix.

**Table 4B.5. Crystallization characteristics of PP/BR blend and the nanocomposites**

Sample	$T_{c,onset}$ (°C)	$T_c$ (°C)	$T_{c,endset}$ (°C)	$T_{c,onset} - T_c$ (°C)	$T_m - T_c$ (°C)	$\Delta H_c$ J/g
P100	119	114	108	6	54	111.68
P80	118	111	106	5	55	88.23
P80CNF0.5	126	121	115	6	45	89.74
P80CNF1.5	127	123	117	6	43	90.23
P80CNF3	127	123	119	4	42	87.40
P80CNF4	128	124	120	4	40	87.11

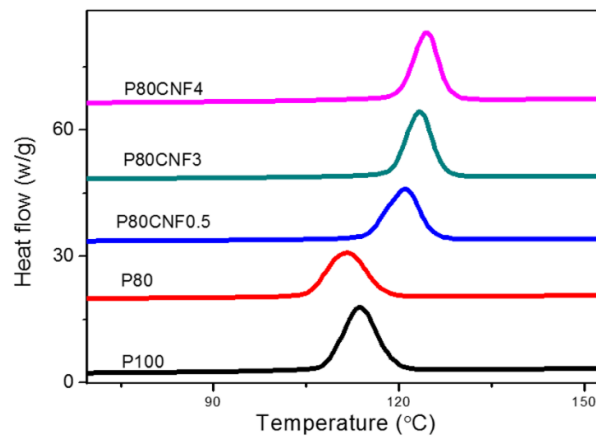


**Figure 4B.23. DSC cooling curves of PP/BR nanocomposites**

DSC cooling curves of PP/BR nanocomposites is presented in Figure 4B.23. The crystallization characteristics of PP such as onset of crystallization temperature ( $T_{c,onset}$ ), peak crystallization temperature ( $T_c$ ), endset of crystallization temperature ( $T_{c,endset}$ ) and enthalpy of crystallization ( $\Delta H_c$ ) obtained from cooling curves are listed in table 4B.5. It is seen that  $T_{c,onset}$ ,  $T_{c,s}$ ,  $T_{c,endset}$  values is largely affected by the presence of CNFs in the



PP/BR matrix. This established the nucleating effect of CNF on the crystallization of PP chains<sup>51-53</sup>. The substantial increase in  $T_c$  values suggest the preferential localization of CNFs in the PP matrix which are acting as heterogeneous nucleating agents<sup>54</sup>. The decrease of  $T_{c,onset} - T_c$  and  $T_m - T_c$  parameters indicates that the overall rate of crystallization of PP is increased when CNF is incorporated into the polymer<sup>55</sup>. The percentage of crystallinity of the nanocomposites also showed enhancement on addition of CNFs. Thus CNF helps the PP macromolecular chains to obtain an ordered alignment of crystal lattices and the degree of crystallinity of specimens got increased accordingly<sup>56</sup>. The increase in stiffness of the matrix resulted in an increase in the degree of crystallinity of PP and accounts for the observed trends in mechanical properties.

#### 4B.3.8 Thermogravimetric analysis (TGA)

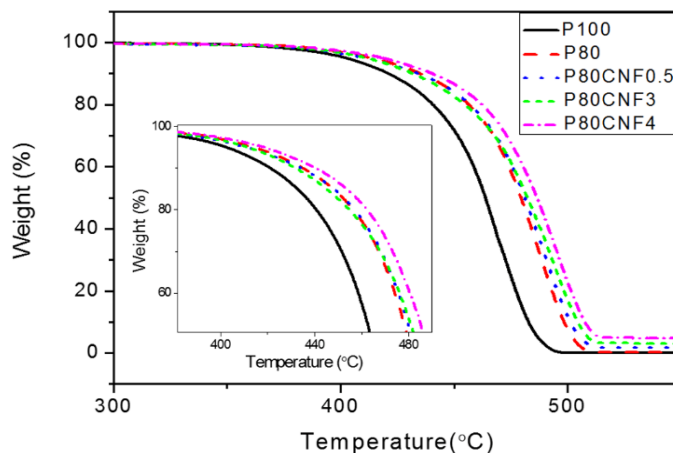
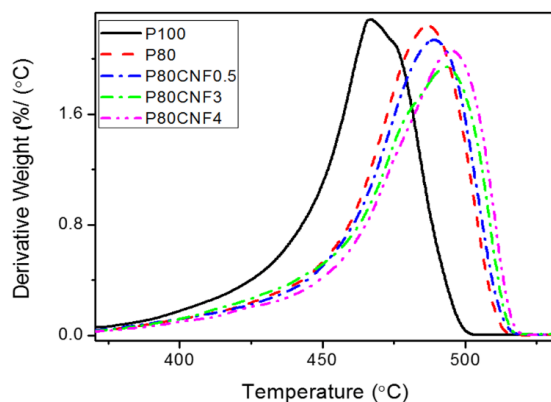


Figure 4B.24. TGA curves of PP/BR/CNF composites



**Figure 4B.25. DTG curves of PP/BR/CNF composites**

Figures 4B.24 and 4B.25 shows the TGA curves and DTG Curves, respectively, of pure PP, PP, PP/BR blend and PP/BR/CNF composites. It can be observed that all the samples displayed single step degradation process. The DTG curve show a single maximum and shifts towards higher temperatures as the concentration of CNF is increased.

**Table 4B.6. TGA parameters of PP/BR blend and the nanocomposites**

Sample code	$T_{\text{onset}}$	$T_{10}$	$T_{50}$	$T_{\text{max}}$	$T_f$
P100	360	421	463	466	500
P80	365	435	479	486	514
P80CNF0.5	372	434	481	489	516
P80CNF1.5	378	436	483	491	517
P80CNF3	379	431	482	493	516
P80CNF4	379	440	486	495	518

The data obtained from the TGA curves such as onset degradation temperature  $T_{\text{onset}}$ , temperatures at 10 wt % and 50 wt % weight loss, maximum degradation temperature ( $T_{\text{max}}$ ) and final decomposition

temperature ( $T_f$ ) are summarized in table 4B.6. From the table it is envisaged that  $T_{max}$  increases with the concentration of CNFs in the blend. The results indicated that the thermal stability of PP/BR matrix improved significantly with the incorporation of CNF. The enhancement in TGA parameters with CNF loading suggests interaction between carbon nanofibre and polymeric matrix. The shift of  $T_{max}$  with CNF loading demonstrates the improvement of the thermal stability of the blend with increasing CNF content and establishes the formation of PP-CNF interface as confirmed by the SEM and TEM studies<sup>57</sup>. The enhancement in thermal stability of nanocomposites can be owed to the homogeneous dispersion of the distributed CNFs in the PP matrix. This enforces a restriction on the mobility of PP macromolecules that hinders the gaseous molecules to take part in the degradation process. Improved thermal stability of PP/CNF composites in both nitrogen and air have been reported by Chaterjee *et al*<sup>17</sup>. They reported that enhancement in degree of crystallinity and restriction of molecular mobility of PP along with the thermal stability of CNFs have resulted in the enhancement of thermal stability of composites. Also, they reported that maximum weight loss occurred after 600 °C.

#### 4B.4 Conclusions

The PP/BR/CNF composites prepared by simple melt intercalation technique without a compatibilizer and surface modification of CNF show improved mechanical, morphological and thermal properties. XRD results reveal that the addition of CNFs do not induce a structural change of PP from  $\alpha$  phase to  $\beta$  phase. HRTEM and SEM photographs show that the CNFs are homogeneously distributed in the form of individual nanofibres in the PP matrix. Tensile tests show that the addition of CNFs significantly improve the tensile strength and modulus of the PP/BR blend with a

maximum at 3 wt %. The predicted values of the Young's modulus using a modified Halpin-Tsai equation that accounts for the effect of the CNF agglomeration matches fairly well with the experimental results. The dynamic rheological studies reveal increased complex viscosity, storage modulus and loss modulus for the nanocomposites signifying the reinforcing effect of CNFs in PP/BR blend. DSC studies reveal that the melting temperature of PP is independent of CNF content. The improvement in percentage of crystallinity ( $X_c$ ) and the crystallization temperature ( $T_c$ ) of the PP matrix shows the nucleating effect of CNFs in the PP matrix. Addition of CNFs improve the thermal stability of PP/BR blend.

## References

- [1] Drobny, J. G. (2014). *Handbook of thermoplastic elastomers*. Elsevier.
- [2] Panda, B. P., Mohanty, S., & Nayak, S. K. (2015). Mechanism of toughening in rubber toughened polyolefin—a review. *Polymer-Plastics Technology and Engineering*, 54(5), 462-473.
- [3] Tjong, S. C., & Bao, S. P. (2005). Impact fracture toughness of polyamide-6/montmorillonite nanocomposites toughened with a maleated styrene/ethylene butylene/styrene elastomer. *Journal of Polymer Science Part B: Polymer Physics*, 43(5), 585-595.
- [4] Paul, D. R., & Robeson, L. M. (2008). Polymer nanotechnology: nanocomposites. *Polymer*, 49(15), 3187-3204.
- [5] Verdejo, R., Bernal, M. M., Romasanta, L. J., Tapiador, F. J., & Lopez-Manchado, M. A. (2011). Reactive nanocomposite foams. *Cellular Polymers*, 30(2), 45.
- [6] Feng, L., Xie, N., & Zhong, J. (2014). Carbon nanofibres and their composites: a review of synthesizing, properties and applications. *Materials*, 7(5), 3919-3945.

- [7] Tibbetts, G. G., Lake, M. L., Strong, K. L., & Rice, B. P. (2006). A Review of the Fabrication and Properties of Vapor-Grown Carbon Nanofiber/Polymer Composites. *Applied sciences Inc.*
- [8] Karger-Kocsis, J., Felhös, D., & Thomann, R. (2008). Tribological behavior of a carbon-nanofibre-modified santoprene thermoplastic elastomer under dry sliding and fretting conditions against steel. *Journal of applied polymer science*, 108(2), 724-730.
- [9] Hine, P., Broome, V., & Ward, I. (2005). The incorporation of carbon nanofibres to enhance the properties of self reinforced, single polymer composites. *Polymer*, 46(24), 10936-10944.
- [10] Lee, S., Kim, M. S., & Ogale, A. A. (2010). Influence of carbon nanofiber structure on properties of linear low density polyethylene composites. *Polymer Engineering & Science*, 50(1), 93-99.
- [11] Gulrez, S. K., Ali Mohsin, M. E., Shaikh, H., Anis, A., Pulose, A. M., Yadav, M. K., Qua, E.H.P. & Al-Zahrani, S. M. (2014). A review on electrically conductive polypropylene and polyethylene. *Polymer composites*, 35(5), 900-914.
- [12] Barick, A. K., & Tripathy, D. K. (2012). Preparation and characterization of carbon nanofibre reinforced thermoplastic polyurethane nanocomposites. *Journal of Applied Polymer Science*, 124(1), 765-780.
- [13] Foster, R. J., Hine, P. J., & Ward, I. M. (2009). Characterisation and modelling of polypropylene/carbon nanofibre nanocomposites. *Polymer*, 50(16), 4018-4027.
- [14] Lozano, K., & Barrera, E. V. (2001). Nanofiber-reinforced thermoplastic composites. I. Thermoanalytical and mechanical analyses. *Journal of Applied Polymer Science*, 79(1), 125-133.
- [15] Liao, C. Z., & Tjong, S. C. (2011). Effects of carbon nanofibres on the fracture, mechanical, and thermal properties of PP/SEBS-g-MA blends. *Polymer Engineering & Science*, 51(5), 948-958.
- [16] Tong, X., Chen, Y., & Cheng, H. (2005). Influence of carbon nanofiber addition on mechanical properties and crystallization behavior of polypropylene. *Journal of Materials Science and Technology*, 21(5), 686-690.

- [17] Chatterjee, A., & Deopura, B. L. (2006). Thermal stability of polypropylene/carbon nanofiber composite. *Journal of applied polymer science*, 100(5), 3574-3578.
- [18] Parameswaranpillai, J., Joseph, G., Shinu, K. P., Salim, N. V., Hameed, N., & Jose, S. (2015). High performance PP/SEBS/CNF composites: Evaluation of mechanical, thermal degradation, and crystallization properties. *Polymer Composites*.
- [19] Thostenson, E. T., & Chou, T. W. (2002). Aligned multi-walled carbon nanotube-reinforced composites: processing and mechanical characterization. *Journal of physics D: Applied physics*, 35(16), L77.
- [20] Ladani, R. B., Wu, S., Kinloch, A. J., Ghorbani, K., Zhang, J., Mouritz, A. P., & Wang, C. H. (2015). Improving the toughness and electrical conductivity of epoxy nanocomposites by using aligned carbon nanofibres. *Composites Science and Technology*, 117, 146-158.
- [21] Thostenson, E. T., Li, C., & Chou, T. W. (2005). Nanocomposites in context. *Composites Science and Technology*, 65(3), 491-516.
- [22] Koo, J. (2016). *Fundamentals, Properties, and Applications of Polymer Nanocomposites*. Cambridge University Press, pp 44
- [23] Halpin, J. C., & Pagano, N. J. (1969). The laminate approximation for randomly oriented fibrous composites. *Journal of Composite Materials*, 3(4), 720-724.
- [24] Afddl, J. C., & Kardos, J. L. (1976). The Halpin-Tsai equations: a review. *Polymer Engineering & Science*, 16(5), 344-352.
- [25] Hsieh, T. H., Kinloch, A. J., Taylor, A. C., & Kinloch, I. A. (2011). The effect of carbon nanotubes on the fracture toughness and fatigue performance of a thermosetting epoxy polymer. *Journal of Materials Science*, 46(23), 7525.
- [26] Cox, H. L. (1952). The elasticity and strength of paper and other fibrous materials. *British journal of applied physics*, 3(3), 72.
- [27] Sun, L. H., Ounaies, Z., Gao, X. L., Whalen, C. A., & Yang, Z. G. (2011). Preparation, characterization, and modeling of carbon nanofiber/epoxy nanocomposites. *Journal of Nanomaterials*, 2011, 12.

- [28] Yeh, M. K., Tai, N. H., & Liu, J. H. (2006). Mechanical behavior of phenolic-based composites reinforced with multi-walled carbon nanotubes. *Carbon*, 44(1), 1-9.
- [29] Zhang, L., Wan, C., & Zhang, Y. (2009). Morphology and electrical properties of polyamide 6/polypropylene/multi-walled carbon nanotubes composites. *Composites Science and Technology*, 69(13), 2212-2217.
- [30] Boronat, T., Garcia-Sanoguera, D., Pascual, J., Peris, F., & Sanchez-Nacher, L. (2012). Comparative study of the rheological behavior of multiwalled carbon nanotubes and nanofiber composites prepared by the dilution of a masterbatch of polypropylene. *Journal of Applied Polymer Science*, 126(3), 1044-1052
- [31] Kumar, S., Doshi, H., Srinivasarao, M., Park, J. O., & Schiraldi, D. A. (2002). Fibres from polypropylene/nano carbon fibre composites. *Polymer*, 43(5), 1701-1703.
- [32] Lozano, K., Bonilla-Rios, J., & Barrera, E. V. (2001). A study on nanofibre-reinforced thermoplastic composites (II): Investigation of the mixing rheology and conduction properties. *Journal of Applied Polymer Science*, 80(8), 1162-1172.
- [33] Weiss, R. A. (1981). Mechanical properties of polypropylene reinforced with short graphite fibres. *Polymer Composites*, 2(3), 95-101.
- [34] Higgins, B. A., & Brittain, W. J. (2005). Polycarbonate carbon nanofibre composites. *European Polymer Journal*, 41(5), 889-893.
- [35] Pötschke, P., Fornes, T. D., & Paul, D. R. (2002). Rheological behavior of multiwalled carbon nanotube/polycarbonate composites. *Polymer*, 43(11), 3247-3255.
- [36] Ahmad, S. H., Yahya, S. Y., & Rasid, R. (2011). Reinforced thermoplastic natural rubber (TPNR) composites with different types of carbon nanotubes (MWNTS). In *Carbon Nanotubes-Synthesis, Characterization, Applications*. InTech.
- [37] Paleo, A. J., Sencadas, V., Hattum, F. W. J., Lanceros-Méndez, S., & Ares, A. (2014). Carbon nanofiber type and content dependence of the physical properties of carbon nanofiber reinforced polypropylene composites. *Polymer Engineering & Science*, 54(1), 117-128.

- [38] Deng, S. H., Zhou, X. D., Zhu, M. Q., Fan, C. J., & Lin, Q. F. (2013). Interfacial toughening and consequent improvement in fracture toughness of carbon fibre reinforced epoxy resin composites: induced by diblock copolymers. *Express Polymer Letters*, 7(11), 925-935.
- [39] Chow, W. S., Bakar, A. A., Ishak, Z. M., Karger-Kocsis, J., & Ishiaku, U. S. (2005). Effect of maleic anhydride-grafted ethylene-propylene rubber on the mechanical, rheological and morphological properties of organoclay reinforced polyamide 6/polypropylene nanocomposites. *European Polymer Journal*, 41(4), 687-696.
- [40] Al-Saleh, M. H., & Sundararaj, U. (2011). Review of the mechanical properties of carbon nanofiber/polymer composites. *Composites Part A: Applied Science and Manufacturing*, 42(12), 2126-2142.
- [41] Sharma, S., Chandra, R., Kumar, P., & Kumar, N. (2016). Mechanical Properties of Carbon Nanofiber Reinforced Polymer Composites-Molecular Dynamics Approach. *JOM*, 68(6), 1717-1727.
- [42] Thorvaldsen, T., Johnsen, B. B., Olsen, T., & Hansen, F. K. (2015). Investigation of theoretical models for the elastic stiffness of nanoparticle-modified polymer composites. *Journal of Nanomaterials*, 2015, 1.
- [43] Chafidz, A., Kaavessina, M., Al-Zahrani, S., & Ali, I. (2014). Multiwall carbon nanotubes filled polypropylene nanocomposites: Rheological and electrical properties. *Polymer Engineering & Science*, 54(5), 1134-1143.
- [44] Ceccia, S., Ferri, D., Tabuani, D., & Maffettone, P. L. (2008). Rheology of carbon nanofiber-reinforced polypropylene. *Rheologica Acta*, 47(4), 425-433.
- [45] Verma, P., Verma, M., Gupta, A., Chauhan, S. S., Malik, R. S., & Choudhary, V. (2016). Multi walled carbon nanotubes induced viscoelastic response of polypropylene copolymer nanocomposites: Effect of filler loading on rheological percolation. *Polymer Testing*, 55, 1-9.
- [46] Naderi, G., Lafleur, P. G., & Dubois, C. (2008). The influence of matrix viscosity and composition on the morphology, rheology, and mechanical properties of thermoplastic elastomer nanocomposites based on EPDM/PP. *Polymer composites*, 29(12), 1301-1309.



- [47] Mishra, J. K., Hwang, K. J., & Ha, C. S. (2005). Preparation, mechanical and rheological properties of a thermoplastic polyolefin (TPO)/organoclay nanocomposite with reference to the effect of maleic anhydride modified polypropylene as a compatibilizer. *Polymer*, 46(6), 1995-2002.
- [48] Choi, Y. K., Sugimoto, K. I., Song, S. M., Gotoh, Y., Ohkoshi, Y., & Endo, M. (2005). Mechanical and physical properties of epoxy composites reinforced by vapor grown carbon nanofibres. *Carbon*, 43(10), 2199-2208.
- [49] Parameswaranpillai, J., Dubey, V. K., Sisanth, K. S., Jose, S., Zachariah, A. K., Siengchin, S., Salim, N.V., & Hameed, N. (2016). Tailoring of interface of polypropylene/polystyrene/carbon nanofibre composites by polystyrene-block-poly (ethylene-ran-butylene)-block-polystyrene. *Polymer Testing*, 51, 131-141.
- [50] Deng, H., Bilotti, E., Zhang, R., & Peijs, T. (2010). Effective reinforcement of carbon nanotubes in polypropylene matrices. *Journal of applied polymer science*, 118(1), 30-41.
- [51] Augustine, J. M., Maiti, S. N., & Gupta, A. K. (2012). Mechanical properties and crystallization behavior of toughened polyamide-6/carbon nanotube composites. *Journal of Applied Polymer Science*, 125(S1), E478–E485
- [52] Assouline, E., Lustiger, A., Barber, A. H., Cooper, C. A., Klein, E., Wachtel, E., & Wagner, H. D. (2003). Nucleation ability of multiwall carbon nanotubes in polypropylene composites. *Journal of Polymer Science Part B: Polymer Physics*, 41(5), 520-527.
- [53] Valentini, L., Biagiotti, J., Kenny, J. M., & Santucci, S. (2003). Morphological characterization of single-walled carbon nanotubes-PP composites. *Composites Science and Technology*, 63(8), 1149-1153.
- [54] Khare, R. A., Bhattacharyya, A. R., Panwar, A. S., Bose, S., & Kulkarni, A. R. (2011). Dispersion of multiwall carbon nanotubes in blends of polypropylene and acrylonitrile butadiene styrene. *Polymer Engineering & Science*, 51(9), 1891-1905.
- [55] Razavi-Nouri, M., Ghorbanzadeh-Ahangari, M., Fereidoon, A., & Jahanshahi, M. (2009). Effect of carbon nanotubes content on crystallization kinetics and morphology of polypropylene. *Polymer Testing*, 28(1), 46-52.

- [56] Sui, G., Zhong, W. H., Fuqua, M. A., & Ulven, C. A. (2007). Crystalline structure and properties of carbon nanofibre composites prepared by melt extrusion. *Macromolecular Chemistry and Physics*, 208(17), 1928-1936.
- [57] Chipara, M., Lozano, K., Hernandez, A., & Chipara, M. (2008). TGA analysis of polypropylene-carbon nanofibres composites. *Polymer Degradation and Stability*, 93(4), 871-876.

.....✂.....

**POLYPROPYLENE/POLYBUTADIENE BLEND:  
EFFECT OF COMPATIBILIZERS AND NANOFILLERS****Contents****Part A***Polypropylene/polybutadiene blend: Effect of compatibilizers***Part B***Effect of nanofillers on PP/BR blend compatibilized with SEBS***Part A****POLYPROPYLENE/POLYBUTADIENE BLEND:  
EFFECT OF COMPATIBILIZERS**

*Compatibilizing effect of two nonpolar phase modifiers like poly-(styrene-*b*-butadiene-*b*-styrene) (SBS) and poly-(styrene-*b*-ethylene-*b*-butylene-*b*-styrene) (SEBS) on the mechanical, morphological, thermal and rheological properties of polypropylene/polybutadiene (80/20) blend were investigated. The analysis of the mechanical properties establish SEBS as a better compatibilizer compared to SBS. Investigation on the morphology of the SEBS compatibilized blends reveal homogenous morphology with reduced particle size distribution and improved interfacial adhesion. The trends in mechanical properties combined with morphological analysis suggest the localization of SEBS at the interface forming a core-shell morphology. Dynamic rheological studies also reveal improved interaction of PP and BR phases with SEBS suggesting SEBS as a better compatibilizer. Investigations on thermal properties were carried out by Differential scanning calorimetry (DSC) and Thermogravimetric analysis (TGA).*

### 5A.1 Introduction

Blending an elastomer with a thermoplastic polymer to develop thermoplastic elastomers (TPEs) is a superior alternative to crosslinked rubbers as TPEs combine the elastic property of the rubber with the processability of thermoplastic polymers<sup>1,2</sup>. Among TPE blends, thermoplastic olefins (TPOs) are the blends formed by the addition of elastomers such as ethylene-propylene diene monomer (EPDM)<sup>3</sup>, natural rubber (NR)<sup>4</sup> and acrylonitrile-butadiene rubber (NBR)<sup>5</sup> to polypropylene. Studies on PP/EPDM blends have been carried out by several researchers by changing the blend compositions and is well documented in literature<sup>6,7</sup>. Most of the plastic/rubber blends are thermodynamically immiscible with great interfacial tension and a phase separated morphology. The reduction in interfacial tension is therefore necessary to improve the mechanical properties of the blend. Generally, the judicious choice of a compatibilizer as a phase modifier can lead to a homogeneous and fine morphology of the minor phase in the polymer matrix. Distribution of appropriately chosen block copolymers at the polymer interface can alter the interfacial characteristics between two immiscible polymer phases. Compatibilizers offer interfacial modification mainly by reducing the interfacial tension between the phases. Compatibilizer reduces the coalescence of the dispersed particles there by decreasing the sizes of the dispersed phase domains in an immiscible polymer blend<sup>8</sup>. The phase modifiers act as interfacial agents to promote interfacial adhesion between the blend components which facilitates stress transfer across the interfaces and results in the compatibilization of the immiscible blends<sup>9</sup>.

Styrenic block copolymers constitute an important class of compatibilizers and have hard blocks that segregate into a glassy hard phase

and soft blocks that segregate into a rubbery soft phase. The effectiveness of poly-(styrene-*b*-butadiene-*b*-styrene) (SBS) and poly-(styrene-*b*-ethylene-butylene-*b*-styrene) (SEBS) as compatibilizers and also as toughening agents in improving the ductility and toughness of PP is well studied in literature<sup>10</sup>. Bartlett *et al.*<sup>11</sup> studied the compatibilization of PP/PS blends with SEBS triblock copolymer and found that the addition of 20 wt % of SEBS improved the impact strength and elongation at break. SEBS is found to improve the adhesion by reducing the interfacial tension between the components in PP/LLDPE blends<sup>12</sup>. A. K. Gupta *et al.*<sup>13-16</sup> have studied the tensile yield, crystallization behavior and dynamic rheological properties of blends PP/SEBS blends and postulated that the polyolefinic block EB of SEBS has better affinity with PP. Santana *et al.*<sup>17</sup> used SBS as a compatibilizing agent for PP/PS blends and found no substantial improvements in the tensile and the impact properties of the blends, but observed influence on the crystallization behavior of PP. Navratilova *et al.*<sup>18</sup> established enhanced adhesion between the phases in PP/PS blends by the interfacial activity of SBS and proved the inefficiency of SBS against particle coalescence. Studies carried out on thermoplastic elastomers based on SEBS modified EPDM/iPP blend have established improvement in mechanical properties due to phase modification<sup>19</sup>. The influence of SBS and SEBS triblock copolymers on the morphology and dynamic behavior of PP/PS immiscible blend was investigated by Macaubas and Demarquette<sup>20</sup>. Their investigations revealed the localization of SEBS at the interface and the formation of a third phase of SBS at high loading. Their studies established that SEBS is a better compatibilizer for PP/PS blends. The compatibilizing action of SBS and a random copolymer styrene butadiene rubber (SBR) on PS/BR blends have been investigated and SBS have proved to be a better compatibilizer than SBR<sup>21</sup>.

Many block copolymers are thermoplastic elastomers and are phase-separated systems that maintain the properties of the individual homopolymers<sup>22</sup>. Literature confirms that only very few studies based of polypropylene/polybutadiene blends have been carried out<sup>23,24</sup>. The structural similarity of SBS with polybutadiene rubber and compatibility of SEBS with PP, these two block copolymers are considered to be a logical choice for compatibilizing PP/BR blends. The aim of the present study is to exploit the effectiveness of SBS and SEBS in improving the mechanical properties of PP/BR blends when used as compatibilizers. This study reports the results of the effect of concentration of SBS and SEBS on the mechanical properties like tensile strength, elongation at break, Young's modulus and impact strength of thermoplastic elastomers based on PP/BR blends. The morphology of the fractured surfaces has been analyzed to understand the improvement of adhesion between PP and BR phase with the incorporation of SBS and SEBS as compatibilizers. Thermal properties have been investigated by DSC and TGA.

## **5A.2 Methodology**

### **5A.2.1 Materials**

The details of the materials used for the study are discussed in chapter 2 (section 2.1)

### **5A.2.2 Preparation of the PP/BR/SEBS and PP/BR/SBS blends**

PP/BR (80/20) blends and varying amount of compatibilizers were prepared by melt blending in a Brabender Plasticorder 170 °C and 60 rpm for 8 minutes. The hot mix from the mixing chamber was pressed in a hydraulic press and sheeted out in a two roll mill. Composition of the samples used is given in the table 5A.1

**Table 5A.1. Composition of the compatibilized blends**

Sample	PP wt%	BR wt%	X=SEBS/SBS wt%
P80	80	20	0
P80X2	80	20	2
P80X5	80	20	5
P80X8	80	20	8
P80X10	80	20	10

The test specimens were injection moulded and the mechanical, morphological, thermal and rheological properties were analyzed according to the various standards as given in chapter 2.

### 5A.3 Results and Discussion

#### 5A.3.1 Mechanical properties

##### 5A.3.1.1 Tensile properties

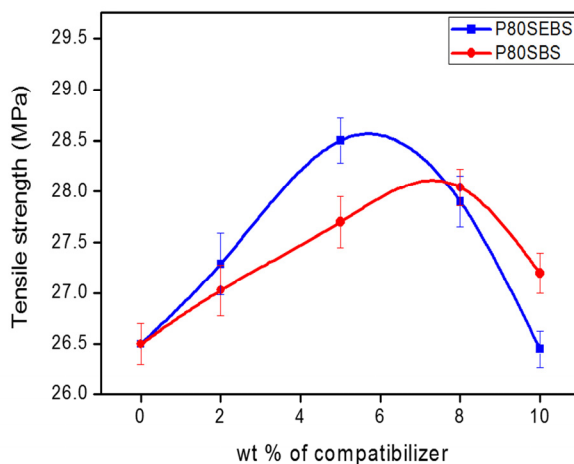


**Figure 5A.1. Variation of tensile strength with compatibilizer loading**

Variation of tensile strength of PP/BR blends with 2,5,8,10 wt % of the compatibilizers are depicted in Figure 5A.1. From the figure, it is obvious that PP/BR/SEBS blends showed improved tensile strength than PP/BR/SBS blends. For PP/BR/SEBS blends, tensile strength increased with increase in the concentration of the phase modifier up to 5 wt % and then decreased. The improved tensile strength for the SEBS modified P80 blend can be attributed to the better interaction between the EB (ethylene-butylene) midblock of SEBS with that of PP chains<sup>25</sup>. The maximum value of tensile strength of the PP/BR/SEBS blend at 5 wt % of SEBS suggest the ability of the compatibilizer to render fine distribution of the elastomer particles. This result in effective stress transfer to the matrix at this loading. The reduced tensile properties at higher loading owes to the agglomeration of SEBS at higher loading leading to poor stress transfer. George *et al.*<sup>31</sup> reported that higher loading of the compatibilizer can result in the formation of miscelles in the continuous PP phase in their studies of phenolic-modified polypropylene (Ph-PP) compatibilized PP/NBR blends<sup>26</sup>.

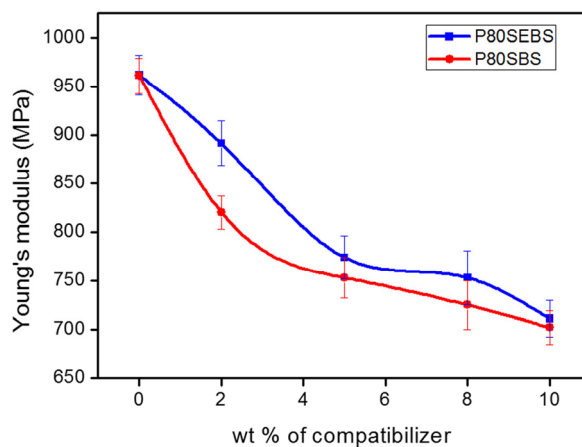
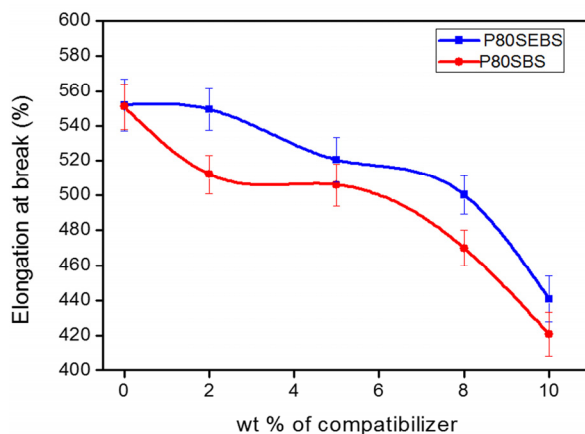


Figure 5A.2. Variation of Young's modulus with compatibilizer loading



The extent of modulus reduction with compatibilizer is shown in Figure 5A.2. It can be correlated with the lower modulus of the compatibilizers used. The decrease in modulus can be identified in terms of a core-shell morphology that consisted of a compatibilizer shell surrounding the dispersed phase at lower loading. Since good adhesion existed between the phases, the rubbery shell lowered the effective modulus<sup>27</sup>. A similar reduction in modulus was obtained when SEBS-g-MA was used as a compatibilizer in PA6/PP blend due to the elastomeric nature of SEBS-g-MA<sup>28</sup>. At higher loading, the compatibilizer may form a third elastomeric phase leading to modulus reduction.



**Figure 5A.3. Variation of elongation at break with compatibilizer loading**

The elongation at break displayed a declining trend with increase in SEBS loading as seen in Figure 5A.3. This can be explained on the basis of interaction between the compatibilizers and the PP matrix. The presence of SEBS as an interfacial compatibilizer might have restricted the mobility of PP chains hindering shear yielding of the matrix resulting in reduction of elongation at break.

### 5A.3.1.2 Impact strength

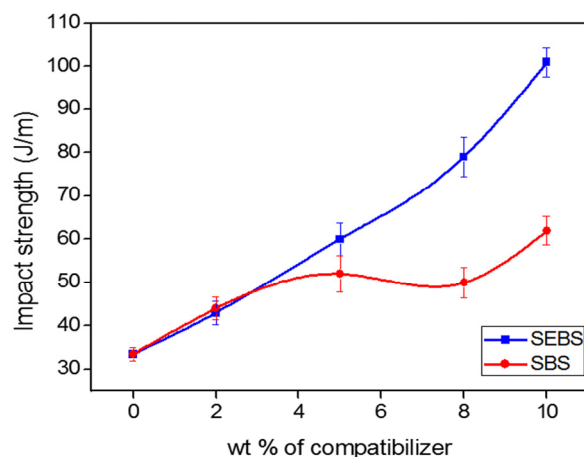


**Figure 5A.4. Variation of impact strength with compatibilizer loading**

From the Figure 5A.4, it is obvious that SEBS compatibilized PP/BR blend gave better impact strength than SBS compatibilized PP/BR blends. The improved impact strength of the PP/BR blend compatibilized with SEBS can be attributed to the better compatibility of EB midblock of the SEBS copolymer with PP than the butadiene midblock of the SBS copolymer<sup>29</sup>. Similar effect on the impact strength of PP by SEBS addition have been reported by several researchers<sup>30</sup>. When SEBS was used as a compatibilizer for PP/BR blends, only 5% of SEBS was needed for the drastic increase in the impact strength of P80 blend from 33 J/m to 60 J/m. This substantially improved impact strength for the PP/BR/SEBS blends suggested the efficiency of SEBS as a compatibilizing agent for PP/BR blends.

The trends in mechanical properties suggest the distribution of SEBS at the PP/BR interface there by improving the interfacial adhesion and reduction in particle size which is further established by the SEM studies<sup>31,32</sup>. SEBS can be considered to be a better phase modifier than SBS for the P80 blend.

### 5A.3.2 Scanning electron microscopy (SEM)

#### a) SEM photographs of tensile fractured surfaces

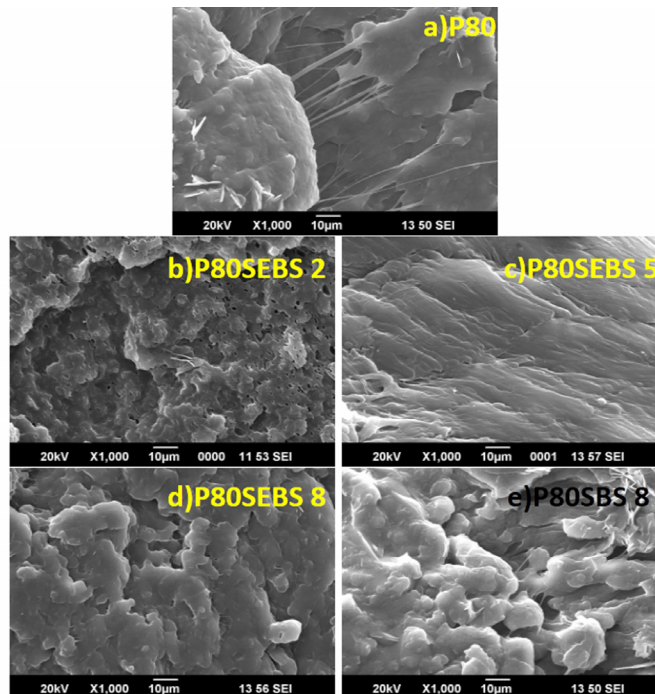


**Figure 5A.5 (a-e). SEM photographs showing the morphologies of tensile fractured surfaces**

The effect of compatibilizers on the morphological properties of P80 has been investigated by the SEM analysis. The photographs of the tensile fractured surfaces of P80 blend and PP/BR/SBS and PP/BR/SEBS blends

are shown in Figure 5A.5(a)-(e). SEM morphology of the P80 blend shown in Figure 5A.5(a) indicated extensive shear yielding of the matrix produced by repeated rubber particle cavitation. From the Figure 5A.5(c), it is evident that compatibilized blend containing 5 wt % of SEBS (P80SEBS5) displayed a morphology in which the distinction between phases was scarcely detectable and indicated lower interfacial tension. The photographs of P80SEBS5 exhibited a more homogeneous morphology due to the improved adhesion between the PP and BR phases. The reduction of domain size and interfacial tension on compatibilization have been reported by George *et al.*<sup>31</sup> in the dispersion of NBR in PP. Hence 5wt% SEBS as a compatibilizer have proved to improve the homogeneity of the system. The efficiency of SEBS as a compatibilizer can be attributed to improved interaction of EB block of SEBS with polypropylene than the interaction of butadiene segment of SEBS with PP of PP/BR blends. Studies on PP/PS blend compatibilized with SBS or SEBS as compatibilizers established a morphology in which PS droplet is encapsulated by SEBS in the PP matrix<sup>20</sup>. Based on the morphological studies and the mechanical properties, the formation of SEBS interfacial layer around the BR phase can be proposed, so that compatibilization can lead to reduction in interfacial tension and reduced dispersed domain size. Further SEM photograph P80SEBS8 blend shown in Figure 5A.5(d) and P80SBS blend shown in Figure 5A.5(e) shows a morphology with less interfacial adhesion than P80SEBS5 blends owing to the higher concentration of rubber thereby acting as a toughening agent. Interfacial saturation on the addition of compatibilizers has been reported<sup>33</sup>.

**b) SEM photographs of impact fractured surface**

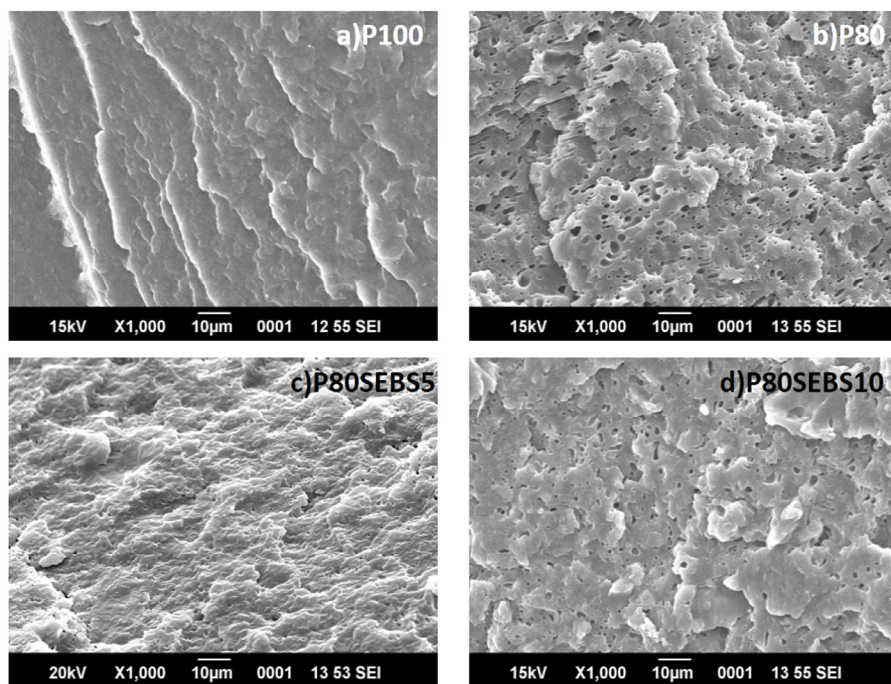


**Figure 5A.6(a-d). SEM photographs showing the morphologies of impact fractured surfaces**

SEM morphology of the impact fractured surfaces of the pure PP, P80 blend, PP/BR/SBS and PP/BR/SEBS blends are shown in Figure 5A.6(a-d). Pure PP shown in Figure 5A.6(a) clearly indicates a typical brittle fracture mode while the P80 blend shown in Figure 5A.6(b) shows the presence of elongated voids indicating a ductile mode of failure with rubber particle cavitation and plastic deformation of the matrix. P80SEBS5 blend shown in Figure 5A.6(c) exposed a homogenous morphology with reduced dispersed domain sizes with improved interfacial adhesion. All these results confirm the localization of SEBS at the interface between the

matrix and dispersed phase forming a core shell morphology<sup>34</sup>. It was reported that compatibilizer can diffuse in to the interface forming a shell around the dispersed phase reducing the interfacial tension and drop coalescence<sup>21</sup>. The reduction in size of the dispersed BR phase along with enhancement in impact strength indicated the role of 5 wt % SEBS as an efficient compatibilizer in enhancing the interfacial adhesion between PP and BR phases. The morphology of P80 blend with 10 wt % loading of SEBS (P80SEBS10) shown in Figure 5A.6(d) reflects the role of SEBS as a toughening agent rather than as a compatibilizer. Mechanical properties and morphology of P80SEBS5 blend revealed that the compatibility of the two phases was improved when 5 wt % SEBS is added a compatibilizer. Improvement in the interfacial adhesion between the dispersed and the continuous phase was achieved by the localization of SEBS at the interface. A schematic representation showing the distribution SEBS at the interface region is given in the Figure 5A.7.

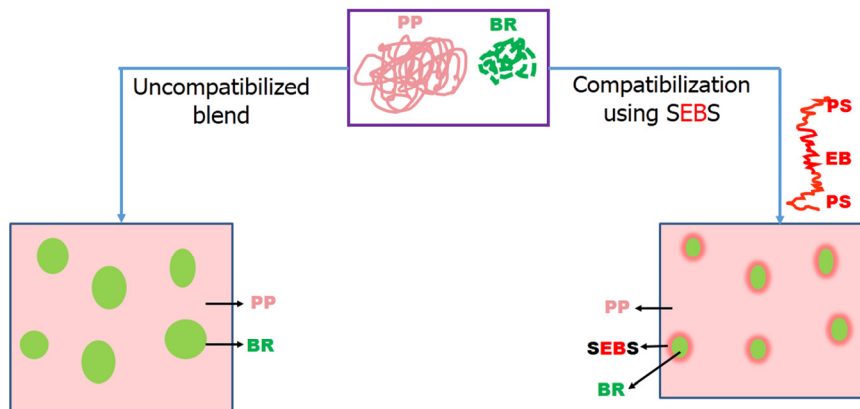


**Figure 5A.7. Schematic representation of morphology of SEBS compatibilized PP/BR blend**

### 5A.3.3 Fourier transform infrared spectroscopy (FTIR)

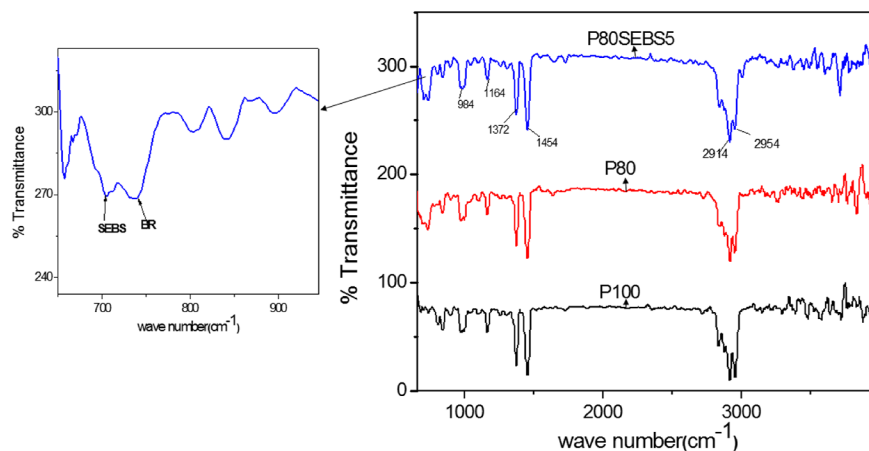


**Figure 5A.8. FTIR spectra of compatibilized PP/BR blend**

The infrared absorption spectra of pure PP, P80 blend, and SEBS compatibilized blend (P80SEBS5) is shown in Figure 5A.8. The characteristic peak of PP is observed in all the samples. In P80 blend the characteristic peak of the cis-1,4 structure of poly(cis-1,4-butadiene) is observed at  $738\text{ cm}^{-1}$ <sup>35</sup>. In compatibilized blends, the peak at  $698\text{ cm}^{-1}$  that corresponds to the  $\text{-C=C-}$  stretching in styrene moiety is clearly seen. The position of the PP and BR peaks remain unaltered in the compatibilized blend indicating that there is no chemical interaction on compatibilization with SEBS. Similar results have been reported by Chakraborty *et al.*<sup>19</sup> in their studies of EPDM/PP blends.

### 5A.3.4 Dynamic rheological analysis (DRA)

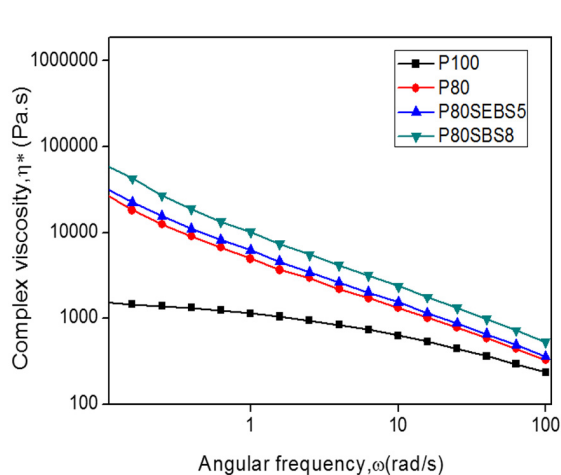


**Figure 5A.9. Complex viscosity,  $\eta^*$  as a function of angular frequency of P100, P80, P80SEBS5 and P80SBS8 samples at 190 °C**

The variation complex viscosity ( $\eta^*$ ) of pure PP, P80 blend and compatibilized blends (P80SEBS5 and P80SBS8) as a function of angular frequency ( $\omega$ ) is represented in Figure 5A.9. The P80 blend and the PP/BR/SBS and PP/BR/SEBS blends showed higher complex viscosity than the virgin PP in the studied frequency range. The figure clearly shows that pure PP shows shear thinning behavior at higher frequencies. The PP/BR blend (P80 sample) and the PP/BR/SEBS and PP/BR/SBS blends showed marked shear thinning behavior even at low frequency. The viscosity increase is more prominent at low frequency region than at the high frequency region. The viscosity of the PP/BR/SEBS blend showed only marginal improvement in viscosity, while PP/BR/SBS blend showed significant enhancement in viscosity than the P80 blend. This can be attributed to the localization of SEBS at the PP/BR interface and the reduction in the interfacial tension<sup>36</sup>. It can also be suggested that the interaction of the EB midblock of SEBS with



the PP matrix might have restricted the mobility of the PP chains. The considerable increase in the complex viscosity of SBS compatibilized blend in the entire range of frequency suggest that SBS function as elastomeric filler rather than as a compatibilizer. These observations are in line with the mechanical and morphological data.

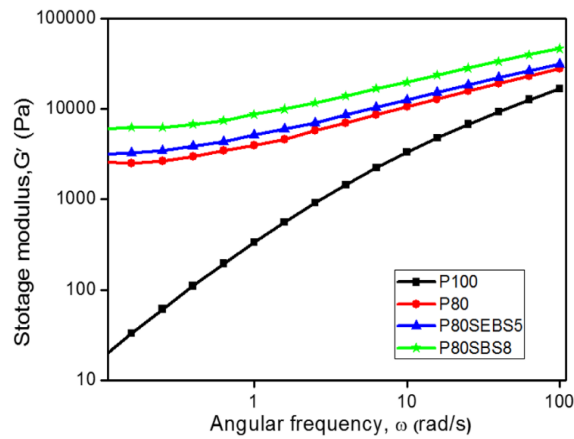


**Figure 5A.10. Storage modulus ( $G'$ ) vs. angular frequency,  $\omega$  of P100, P80, P80SEBS5 and P80SBS8 samples at 190 °C**

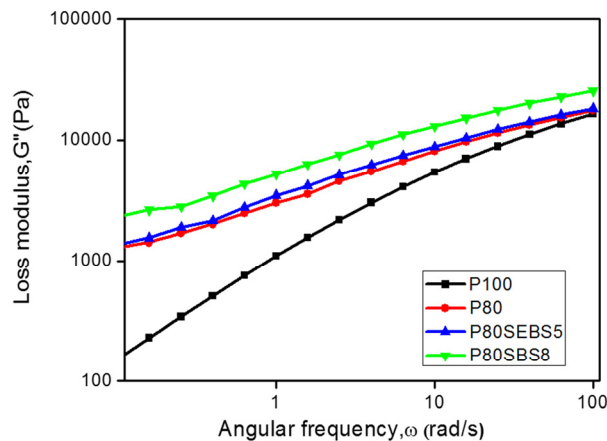


**Figure 5A.11. Loss modulus ( $G''$ ) vs. angular frequency ( $\omega$ ) of P100, P80, P80SEBS5 and P80SBS8 samples at 190°C**

Figures 5A.10 and 11 show the variation of storage modulus ( $G'$ ) and loss modulus ( $G''$ ) with angular frequency ( $\omega$ ) for pure PP, P80 blend and the PP/BR/SBS (P80SBS8) and PP/BR/SEBS (P80SEBS5) blends. The storage modulus ( $G'$ ) and loss modulus ( $G''$ ) of the PP/BR/SBS and PP/BR/SEBS blends is higher when compared to the PP/BR (P80) blend in the studied frequency range. From the Figure 5A.10, it is clear that there is only marginal improvement in the  $G'$  value of PP/BR/SEBS (P80SEBS5) blend than P80 blend. This marginal increase in the storage modulus may be due to the localization of SEBS at the PP/BR interface. The storage modulus of the PP/BR/SBS blend is significantly greater than the P80 blend. This shows the existence of SBS as an elastomeric filler rather than as a compatibilizer. At lower frequencies, there is longer relaxation time for the polymer chains and hence lower values of  $G'$  and  $G''$ <sup>37</sup>. From the graphs it is clear that the value of  $G''$  is lower than  $G'$  in the studied frequency range implying the elastic dominant nature of PP/BR, PP/BR/SBS and PP/BR/SEBS blends.

### 5A.3.5 Differential scanning calorimetry (DSC)

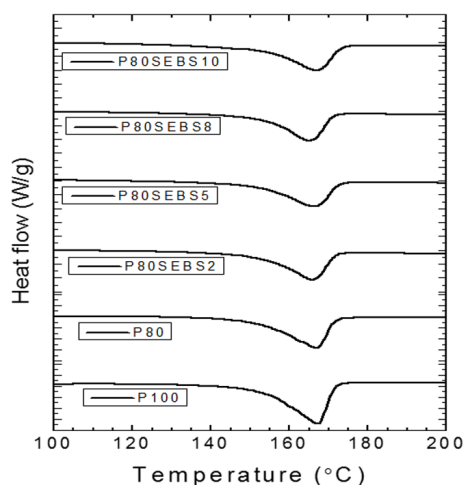
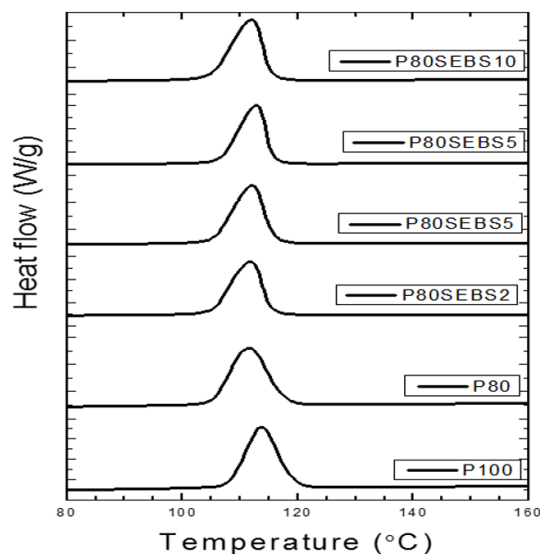


Figure 5A.12. DSC heating curves of PP/BR/SEBS samples

**Table 5A.2. Melting characteristics of PP/BR/SEBS samples**

	$T_{m,onset}$ (°C)	$T_{m,peak}$ (°C)	$T_{m,endset}$ (°C)	$\Delta H_f$ J/g	$X_c$ (%)
P100	154	167	171	93.76	45
P80	153	167	171	70.57	42
P80SEBS2	154	166	172	72.36	43
P80SEBS5	152	166	172	71.56	43
P80SEBS8	154	165	171	67.07	40
P80SEBS10	154	166	173	63.96	38

The DSC heating curves of pure PP, P80 blend and the PP/BR/SEBS blends are shown in Figure 5A.12. The onset of melting temperature ( $T_{m,onset}$ ), peak melting temperature ( $T_{m,peak}$ ), endset of melting temperature ( $T_{m,endset}$ ), enthalpy of fusion ( $\Delta H_f$ ) and percentage of crystallinity ( $X_c$ ) computed are listed in table 5A.2. It can be seen that PP/BR/SEBS blends have similar pattern of heating DSC curves.



**Figure 5A.13. DSC cooling curves of PP/BR/SEBS samples**

**Table 5A.3. Crystallization characteristics of PP/BR/SEBS samples**

Sample	$T_{c,onset}$ (°C)	$T_c$ (°C)	$T_{c,endset}$ (°C)	$\Delta H_c$ J/g
P100	119	114	108	111.68
P80	117	111	105	88.23
P80SEBS2	115	111	105	84.11
P80SEBS5	115	112	106	82.27
P80SEBS8	115	112	106	80.21
P80SEBS10	115	111	105	77.9

The crystallization characteristics obtained from cooling curves are given in Figure 5A.13 and the onset of crystallization temperature ( $T_{c,onset}$ ), peak crystallization temperature ( $T_c$ ), endset of crystallization temperature ( $T_{c,endset}$ ) and enthalpy of crystallization ( $\Delta H_c$ ) are listed in table 5A.3.

The data obtained from the DSC analysis revealed that the melting temperature ( $T_m$ ) and crystallization temperature ( $T_c$ ) of the P80 blend remains unaffected with the incorporation of SEBS. The enthalpy of fusion and percentage of crystallinity  $X_c$  of the P80 blend remained unaffected on compatibilization with SEBS. This can be attributed to the fact that the crystallization behaviour of polymers are not generally affected by compatibilizers<sup>38</sup>. At higher loading of SEBS, there is a remarkable decrease in the enthalpy of fusion and  $X_c$  values. This observation supports the agglomeration of SEBS that interrupt the capability of PP chains to undergo orientation<sup>39</sup>.

### 5A.3.6 Thermogravimetric analysis (TGA)

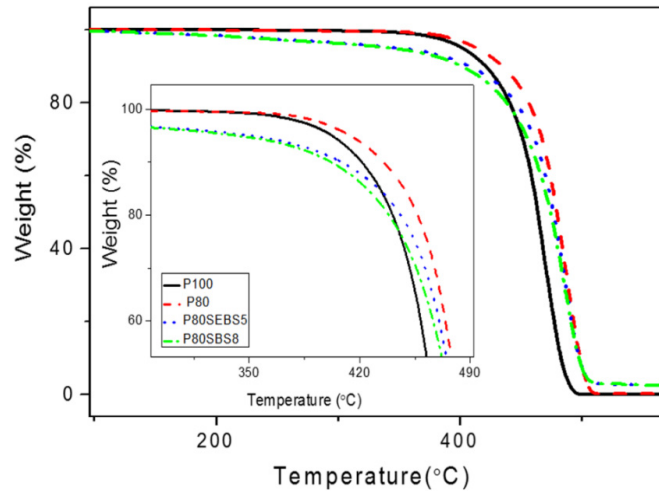


Figure 5A.14. TGA curves of P100, P80 and P80SEBS5 and P80SBS8 samples

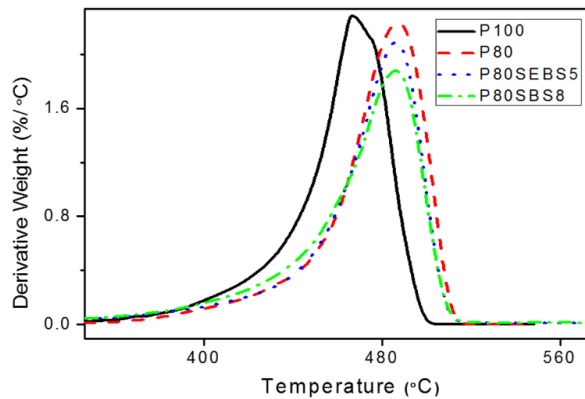


Figure 5A.15. DTG curves of P100, P80 and P80SEBS5 and P80SBS8 samples

TGA and DTG curves of PP, P80 blend and PP/BR/SEBS blends (P80SEBS5 and P80SBS8) are shown in Figure 5A.14 and 15, respectively. It can be observed that all the samples displayed single step degradation process.

**Table 5A.4. TGA parameters of P100, P80, P80SEBS5 and P80SBS8 samples**

Sample code	T <sub>onset</sub> (°C)	T <sub>10</sub> (°C)	T <sub>50</sub> (°C)	T <sub>max</sub> (°C)	T <sub>f</sub> (°C)
P100	360	421	464	467	500
P80	365	435	479	486	514
P80SEBS5	395	408	476	486	509
P80SBS8	373	402	474	486	510

The thermal degradation parameters such as onset degradation temperature ( $T_{\text{onset}}$ ), temperatures at 10% weight loss ( $T_{10}$ ) and 50% weight loss ( $T_{50}$ ), final decomposition temperature ( $T_f$ ) and maximum degradation temperature ( $T_{\text{max}}$ ) are listed in table 5A.4. The decomposition of PP/BR blend matrix started at 361 °C, whereas the onset of decomposition for P80SEBS5 was observed at 395 °C. Thus the result indicated that at the beginning stage of the decomposition stage, addition of SEBS marginally increased the thermal stability of PP/BR blend matrix. This could be ascribed to the compatibilizing action of SEBS at the PP/BR interface. Similar results were reported by Jose *et al.*<sup>40</sup> in the study of PA12/SEBS-g-MA blends. The maximum decomposition temperature and the final decomposition temperature of the P80 blend remains unaffected. For the compatibilized blends, since the compatibilizer is located at the interface between the blend components, the thermal stability was not much affected<sup>41</sup>. The thermal stability studies also established SEBS as a better compatibilizer than SBS.

## **5A.4 Conclusions**

The effect of SEBS and SBS as compatibilizers in PP/BR blend (P80 sample) was investigated. Based on the mechanical and morphological studies, 5 wt % of SEBS is found to be an efficient compatibilizer for PP/BR (P80) blend. SEBS is found to be a better compatibilizer when compared to SBS in improving the interfacial adhesion between PP and BR phase. Morphological studies show reduced dispersed domain sizes of the BR phase on compatibilization with SEBS. FTIR analysis of the SEBS compatibilized blends prove the existence of physical interaction between PP and BR phases with SEBS. The crystallization behavior and the thermal stability of the P80 blend remains unaffected on compatibilization using SEBS.

## **References**

- [1] Legge, N. R. (1987). Thermoplastic elastomers, a comprehensive review. *Hanser-Verlog*.
- [2] Holden, G. (2000). *Understanding Thermoplastic Elastomers*. Hanser. New York.
- [3] Walker, B. M., & Rader, C. P. (1979). *Handbook of thermoplastic elastomers*, Van Nostrand Reinhold. New York.
- [4] Utracki, L. A., & Wilkie, C. A. (Eds.). (2002). *Polymer blends handbook* (Vol. 1, p. 2). Dordrecht: Kluwer academic publishers.
- [5] Jose, J., Nag, A., & Nando, G. B. (2010). Processing and characterization of recycled polypropylene and acrylonitrile butadiene rubber blends. *Journal of Polymers and the Environment*, 18(3), 155-166.
- [6] Stephens, H. L., & Bhowmick, A. K. (Eds.). (2001). *Handbook of Elastomers*. Dekker.

- [7] De, S. K., & Bhowmick, A. K. (1990). *Thermoplastic elastomers from rubber-plastic blends*. Ellis Horwood.
- [8] Koning, C., Van Duin, M., Pagnouille, C., & Jerome, R. (1998). Strategies for compatibilization of polymer blends. *Progress in Polymer Science*, 23(4), 707-757.
- [9] Phinyocheep, P., Axtell, F. H., & Laosee, T. (2002). Influence of compatibilizers on mechanical properties, crystallization, and morphology of polypropylene/scrap rubber dust blends. *Journal of applied polymer science*, 86(1), 148-159.
- [10] Debolt, M. A., & Robertson, R. E. (2004). Impact strength and elongation-to-break of compatibilized ternary blends of polypropylene, nylon 66, and polystyrene. *Polymer Engineering & Science*, 44(9), 1800-1809.
- [11] Bartlett, D. W., Barlow, J. W., & Paul, D. R. (1981). SPE Tech. Pap. 27,487 (1981). *Mod. Plast*, 58, 12-60.
- [12] Flaris, V., Wasiak, A., & Wenig, W. (1993). The effect of compatibilizers on the morphology of isotactic polypropylene/linear low-density polyethylene blends. *Journal of materials science*, 28(6), 1685-1688.
- [13] Gupta, A. K., & Purwar, S. N. (1984). Melt rheological properties of polypropylene/SEBS (styrene-ethylene butylene-styrene block copolymer) blends. *Journal of applied polymer science*, 29(4), 1079-1093.
- [14] Gupta, A. K., & Purwar, S. N. (1985). Studies on binary and ternary blends of polypropylene with SEBS, PS, and HDPE. I. Melt rheological behavior. *Journal of applied polymer science*, 30(5), 1777-1798.
- [15] Gupta, A. K., & Purwar, S. N. (1984). Crystallization of PP in PP/SEBS blends and its correlation with tensile properties. *Journal of applied polymer science*, 29(5), 1595-1609.
- [16] Gupta, A. K., & Purwar, S. N. (1984). Tensile yield behavior of PP/SEBS blends. *Journal of applied polymer science*, 29(11), 3513-3531.
- [17] Santana, O. O., & Müller, A. J. (1994). Homogeneous nucleation of the dispersed crystallisable component of immiscible polymer blends. *Polymer Bulletin*, 32(4), 471-477.



- [18] Navratilova, E., & Fortelny, I. (1996). Effect of compatibilization and rheological properties of polypropylene on morphology of polypropylene/polystyrene blends. *Polymer Networks & Blends*, 6(3), 127-133.
- [19] Chakraborty, P., Ganguly, A., Mitra, S., & Bhowmick, A. K. (2008). Influence of phase modifiers on morphology and properties of thermoplastic elastomers prepared from ethylene propylene diene rubber and isotactic polypropylene. *Polymer Engineering & Science*, 48(3), 477-489.
- [20] Macaubas, P. H. P., & Demarquette, N. R. (2001). Morphologies and interfacial tensions of immiscible polypropylene/polystyrene blends modified with triblock copolymers. *Polymer*, 42(6), 2543-2554.
- [21] Joseph, Susan., (2003) Compatibilization of polystyrene/polybutadiene blends, Ph.D thesis.
- [22] Pérez, A. A., Ferrer, G. G., Ribelles, J. G., Pradas, M. M., & Sánchez, E. V. (2001). Blends of styrene-butadiene-styrene triblock copolymer and isotactic polypropylene. Reinforcing effect of polypropylene at high temperatures. *Journal of Macromolecular Science, Part B*, 40(3-4), 443-455.
- [23] Gupta, A. K., & Ratnam, B. K. (1991). Crystallization, tensile, and impact behavior of polypropylene/polybutadiene blend. *Journal of applied polymer science*, 42(2), 297-315.
- [24] Chen, Y., Chen, Y., & Yang, D. (2006). Crystallization and phase behavior of crystalline syndiotactic 1, 2-polybutadiene/isotactic polypropylene blends in solution-cast thin films. *Polymer*, 47(5), 1667-1673.
- [25] Abreu, F. O. M. S., Forte, M. M. C., & Liberman, S. A. (2005). SBS and SEBS block copolymers as impact modifiers for polypropylene compounds. *Journal of applied polymer science*, 95(2), 254-263.
- [26] George, S., Joseph, R., Thomas, S., & Varughese, K. T. (1995). Blends of isotactic polypropylene and nitrile rubber: morphology, mechanical properties and compatibilization. *Polymer*, 36(23), 4405-4416.
- [27] Jose, S., Thomas, S., Biju, P. K., & Karger-Kocsis, J. (2013). Mechanical and dynamic mechanical properties of polyolefin blends: effect of blend ratio and copolymer monomer fraction on the compatibilisation efficiency of random copolymers. *Journal of Polymer Research*, 20(12), 303.

- [28] Ishak, Z. M., Chow, W. S., & Takeichi, T. (2008). Influence of SEBS-g-MA on morphology, mechanical, and thermal properties of PA6/PP/organoclay nanocomposites. *European Polymer Journal*, 44(4), 1023-1039.
- [29] Setz, S., Stricker, F., Kressler, J., Duschek, T., & Mülhaupt, R. (1996). Morphology and mechanical properties of blends of isotactic or syndiotactic polypropylene with SEBS block copolymers. *Journal of applied polymer science*, 59(7), 1117-1128.
- [30] Vuluga, Z., Panaitescu, D. M., Radovici, C., Nicolae, C., & Iorga, M. D. (2012). Effect of SEBS on morphology, thermal, and mechanical properties of PP/organoclay nanocomposites. *Polymer bulletin*, 69(9), 1073-1091.
- [31] George, S., Ramamurthy, K., Anand, J. S., Groeninckx, G., Varughese, K. T., & Thomas, S. (1999). Rheological behaviour of thermoplastic elastomers from polypropylene/acrylonitrile-butadiene rubber blends: effect of blend ratio, reactive compatibilization and dynamic vulcanization. *Polymer*, 40(15), 4325-4344.
- [32] Rek, V., Vranješ, N., Šlouf, M., Fortelný, I., & Jelčić, Ž. (2008). Morphology and properties of SEBS block copolymer compatibilized PS/HDPE blends. *Journal of Elastomers & Plastics*, 40(3), 237-251.
- [33] Asaletha, R., Thomas, S., & Kumaran, M. G. (1995). The technological compatibilization of natural rubber/polystyrene blends by the addition of natural rubber-graft-polystyrene. *Rubber Chemistry and Technology*, 68(4), 671-687.
- [34] Radonjič, G. (1999). Compatibilization effects of styrenic/rubber block copolymers in polypropylene/polystyrene blends. *Journal of applied polymer science*, 72(2), 291-307.
- [35] Ma, G. Q., Yuan, X. B., Sheng, J., & Bian, D. C. (2002). Blends of polypropylene with poly (cis-butadiene) rubber. II. Small-angle X-ray scattering studies of the phase structure of immiscible blends of polypropylene with poly (cis-butadiene) rubber. *Journal of applied polymer science*, 83(10), 2088-2094.
- [36] Ezzati, P., Ghasemi, I., Karrabi, M., & Azizi, H. (2008). Rheological behaviour of PP/EPDM blend: the effect of compatibilization. *Iran Polym J*, 17(9), 670-679.

- [37] Lee, H. G., Sung, Y. T., Lee, Y. K., Kim, W. N., Yoon, H. G., & Lee, H. S. (2009). Effects of PP-g-MAH on the mechanical, morphological and rheological properties of polypropylene and poly (acrylonitrile-butadiene-styrene) blends. *Macromolecular research*, 17(6), 417-423.
- [38] Jose, S., Thomas, S., Biju, P. K., Koshy, P., & Karger-Kocsis, J. (2008). Thermal degradation and crystallisation studies of reactively compatibilised polymer blends. *Polymer Degradation and Stability*, 93(6), 1176-1187.
- [39] Halimatuddahlia, & Ismail, H. (2008). The effect of dynamic vulcanization on the properties of polypropylene/ethylene-propylene diene terpolymer/natural rubber (PP/EPDM/NR) ternary blend. *Polymer-Plastics Technology and Engineering*, 48(1), 34-41.
- [40] Jose, S., Thomas, P. S., Thomas, S., & Karger-Kocsis, J. (2006). Thermal and crystallisation behaviours of blends of polyamide 12 with styrene-ethylene/butylene-styrene rubbers. *Polymer*, 47(18), 6328-6336.
- [41] Parameswaranpillai, J., Joseph, G., Jose, S., & Hameed, N. (2015). Phase morphology, thermomechanical, and crystallization behavior of uncompatibilized and PP-g-MAH compatibilized polypropylene/polystyrene blends. *Journal of Applied Polymer Science*, 132(24).

## Part B

### EFFECT OF NANOFILLERS ON PP/BR BLEND COMPATIBILIZED WITH SEBS

---

*The effect of nanofillers such as nanoclay and carbon nanofibre in thermoplastic elastomer based on polypropylene/polybutadiene (PP/BR) blend compatibilized with polystyrene-block-poly(ethylene-butylene)-block-polystyrene (SEBS) was investigated. Transmission electron microscopy (TEM) of the nanocomposites reveal two different types of morphology for PP/BR/SEBS/nanoclay and PP/BR/SEBS/CNF composites. The mechanical properties of the nanocomposites are related to the selective localization of the nanofillers in the PP/BR/SEBS blends. The melt rheological properties using the Dynamic rheological analysis (DRA) show interaction of the nanofillers with the PP matrix. The effect of nanofillers in the crystallization behavior of the compatibilized blends was studied using Differential scanning calorimetry (DSC). Thermal properties reveal improved thermal properties of the nanocomposites.*

---

#### 5B.1 Introduction

Blending of polypropylene (PP) with an elastomer is an effective approach to develop thermoplastic olefin (TPOs) which combines the melt processability of PP and the elasticity of the elastomer<sup>1</sup>. The introduction of elastomers in thermoplastic matrix improves the toughness of PP, but reduce the modulus. The mechanism of toughening of PP by rubber particle depends on the rubber particle size, concentration and the interfacial adhesion between the elastomer and the PP matrix. Studies on PP/elastomer blends have established that rubber particles can act as stress concentrators

to undergo internal cavitation or debonding to relieve the triaxial stress leading to the shear deformation of the PP matrix resulting in toughness enhancement<sup>2</sup>. The toughness enhancement of the thermoplastic polymer at the cost of the reduction of the stiffness can be alleviated to a great extent by the introduction of conventional fillers in the plastic/rubber blend systems. The property enhancement is achieved only at higher loading which leads to poor processability<sup>3</sup>.

The introduction of nanofillers in the TPO matrix to develop TPO nanocomposites substantially improves the stiffness at low loading levels of the nanofiller offering better processability. This provides a cost effective approach for the development of a light weight material for automotive applications. Among the nanofillers used for preparing the nanocomposites, organoclay and CNFs has gained wide acceptance due to their exceptionally high aspect ratio<sup>4,5</sup>. Investigations on PP/rubber/nanoclay and PP/rubber/CNF composites have established that substantial improvement in the mechanical properties can be achieved at low loading levels of nanofiller<sup>6,7</sup>.

The localization of filler is crucial in the development of the morphology and the mechanical properties of polymer/rubber/nanofiller composites. When two polymers are blended with a nanofiller the final morphology of the blend, distribution of the filler inside the blend and its state of dispersion are dependent on several factors such as mixing procedure, viscosity of the phases and migration of the nanofiller between the phases<sup>8</sup>. Investigations have established three types of morphologies for polymer/elastomer/filler nanocomposites. They are (a) a phase-separated microstructure in which elastomer phase and clay layers are dispersed independently in the polymer matrix (b) an encapsulated microstructure in

which clay layers resides inside the elastomer phase (c) a mixture of both morphologies as represented in Figure 5B.1<sup>9,10</sup>.

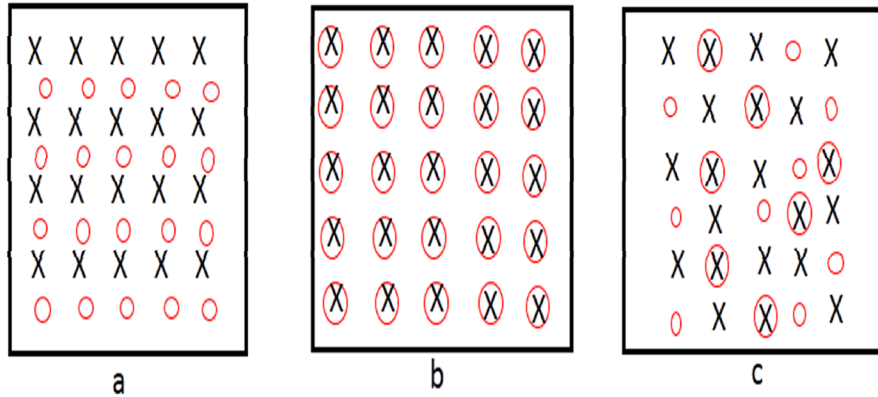


**Figure 5B.1. Schematic representation of three microstructures of fillers (X), and rubber particles (o) in PP matrix**

Enhancement in elastic modulus is reported if the filler phase and the elastomer phase are independently dispersed in the matrix. A core-shell morphology with the filler phase residing inside the elastomer phase is established to improve the impact properties of the blend<sup>10,11</sup>. This selective distribution is mainly based on the affinity of the filler with the two matrix components. Apart from this, localization of the filler is also governed by the processing conditions, the interfacial energies between the components, miscibility between the blend components, shear forces during melt mixing and the viscosity of the components. Even if all these factors are prevalent, high shear during the melt processing is an important factor responsible for the migration of the nanofillers in to the melt<sup>12</sup>. During mixing under the influence of shear, migration of nanofillers from the polymer matrix to the dispersed phase or to the interface of the blend can take place. Elias *et al.*<sup>13</sup> investigated

the migration of nanosilica particles in polypropylene/poly(ethylene-co-vinyl acetate) (PP/EVA) 80/20 blends and proposed that collisions between silica particles and the dispersed polymer drops is responsible for the migration of silica particles from the matrix toward the dispersed phase. Migration of CNF under shear from PP phase to the SEBS phase and existence of CNF at the PP/BR interface is suggested by P.J. *et al.*<sup>14</sup> in their studies on PP/SEBS/CNF blends.

Organic modification of nanoclay is not enough to attain a good level of distribution in nonpolar polymers like polypropylene (PP) and often result in hybrid structures. The compatibilizer get located at the interface between the two phases and reduce the interfacial tension. Compatibilizers like maleic anhydride grafted polypropylene (PP-g-MA) and maleated styrene-6-(ethylene-cobutylenes)-6-styrene triblock copolymer (SEBS-g-MA) are commonly used to enhance the interactions between the polymer and the inorganic filler<sup>10,15-17</sup>. The reduction of the interfacial tension with a progressive breakup of the rubber particles without coalescence and a reduction in the particle size by the preferential localization of clay layers at the rubber particle/matrix interface in presence of a compatibilizer has been reported by earlier studies<sup>18</sup>.

The effect of nonpolar polystyrene-block-poly (ethylene-butylene)-block-polystyrene (SEBS) as a compatibilizer on PP/elastomer nanocomposites by melt blending is limited<sup>19</sup> and in most studies SEBS-g-MA is used as the compatibilizer. SEBS is compatible with PP due to the butylene parts which can interact with the PP chain. Studies by Martin *et al.*<sup>20</sup> established that there existed a certain polarity between the main chain and the styrene group in SEBS so that benzyl groups can interact with the clay platelets. The compatibility of EB mid block with PP chains and the interaction of

nanoclay with SEBS, makes it a suitable choice for the preparation of polymer blend/nanoclay composites. A schematic representation possible interaction between SEBS with PP and clay platelets is as shown in the Figure 5B.2<sup>21</sup>.

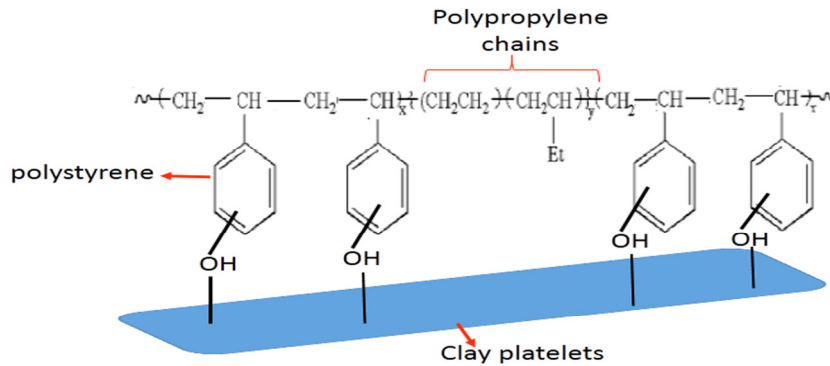


**Figure 5B.2.** Schematic representation of interaction between SEBS with PP and clay platelets

Investigations have shown that PP/PS/SEBS/CNF hybrid composites exhibited superior properties compared to those of PP/PS/ CNF composites. P.J *et al.*<sup>22</sup> had established the use of SEBS used as a potential compatibilizing agent in PP/PS systems due to the structural compatibility of the EB midblock of SEBS with PP chains and styrene phase with the polystyrene phase. It has also been reported that the addition of SEBS into PP had significant influence on the dispersion of exfoliated graphene platelets in the PP matrix<sup>23</sup>. The improved mechanical properties of the nanocomposites on compatibilization with SEBS revealed that a better distribution of CNFs in the matrix can be achieved in presence of SEBS.



The present study focuses on the compatibilizing effect of SEBS in the degree of dispersion of nanofillers to improve the properties of PP/BR nanocomposites. The analysis of the results is presented by means of mechanical, morphological, rheological and thermal properties of the resultant nanocomposites. This part reveals the efficiency of SEBS as a compatibilizing agent in the enhancement of physical properties of TPO nanocomposites based on PP/BR blend by simple melt blending technique for potential applications in polymer technology fields.

## **5B.2 Methodology**

### **5B.2.1 Materials**

The details of the polymers and nanofiller types used for the study are detailed in chapter 2 (sections 2.1).

### **5B.2.2 Preparation of PP/BR/SEBS nanocomposites**

PP/BR /nanocomposites were prepared by melt mixing process in a Brabender Plasticorder (PL 3S model) at 170 °C and 60 rpm. After softening of PP for 3 minutes, BR was introduced into the mixer and was blended for 2 minutes, followed by the addition of SEBS. The addition of 5 wt % SEBS was found to be the optimum weight percentage obtain optimum amount of compatibilizer from previous studies (chapter 5A). The mixing is further continued for 2 minutes and the nanofillers (nanoclay/ carbon nanofibre) are added. The concentration of nanofillers in composites was varied from 0.5 to 3 wt %. After 8 minutes mixing for each sample, the melt was pressed in a hydraulic press, passed through two roll mill. Compositions of the nanocomposite used are as shown in the table 5B.1. NC represents nanoclay.

Table 5B.1. Composition of PP/BR/SEBS nanocomposites

Sample	PP (wt%)	BR (wt%)	SEBS (wt%)	X=NC/ CNF (wt%)
P80	80	-	5	-
P80SEBS5	80	20	5	-
P80SEBS5X0.5	80	20	5	0.5
P80SEBS5X1	80	20	5	1
P80SEBS5X2	80	20	5	2
P80SEBS5X3	80	20	5	3
P80SEBS5X4	80	20	5	4

The test specimens were injection molded at a barrel temperature of 180 °C and then tested as discussed in chapter 2.

## 5B.3 Results and Discussion

### 5B.3.1 Mechanical properties

#### 5B.3.1.1 Tensile properties

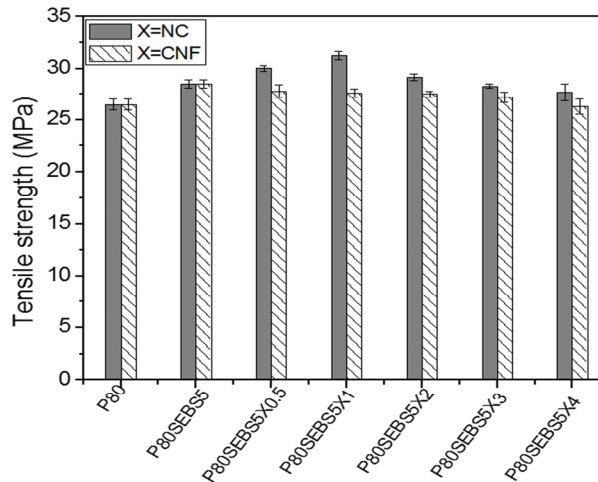
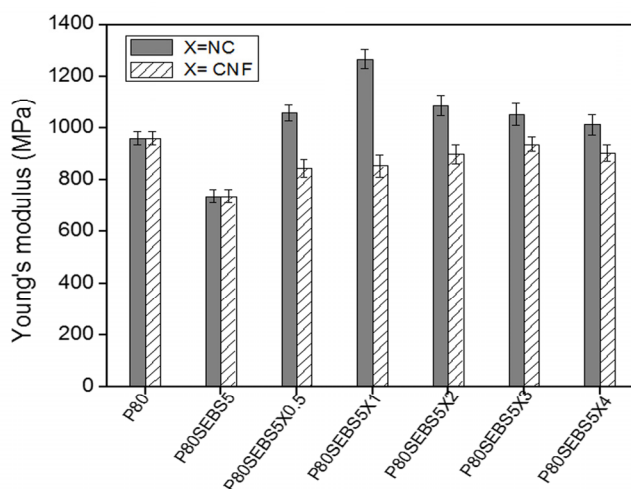


Figure 5B.3. Tensile strength of PP/BR/SEBS nanocomposites

Tensile strength of P80 blend, SEBS compatibilized blend (P80SEBS5) and PP/BRSEBS/nanoclay and PP/BR/SEBS/CNF composites are displayed

in Figure 5B.3. Both the nanocomposites showed improved tensile strength than the uncompatibilized PP/BR blend (P80). The improvement in tensile strength of PP/BRSEBS/nanoclay composites is more prominent than PP/BR/SEBS/CNF composites. From the figure it is evident that addition of nanoclay to the SEBS compatibilized blend (P80SEBS5) improved the tensile strength of the composites with a maximum at 1 wt % loading (P80SEBS5NC1). About 13 % enhancement in tensile strength was achieved with the incorporation of 1 wt % of nanoclay. The addition of CNFs reduced the tensile strength of the SEBS compatibilized blend (P80SEBS5). The improvement in tensile strength of the PP/BR/SEBS/nanoclay composites can be attributed to the reinforcing effect of nanoclay and compatibilizing effect of SEBS.



**Figure 5B.4. Young's modulus of the PP/BR/SEBS nanocomposites**

Young's modulus of P80 blend, SEBS compatibilized blend (P80SEBS5) and PP/BRSEBS/nanoclay and PP/BR/SEBS/CNF composites are displayed in Figure 5B.4. From the figure, it is clear that the Young's modulus of the compatibilized blend increased with the addition of nanofillers.

The improvement in Young's modulus of the PP/BRSEBS/nanoclay composites is more prominent than PP/BR/SEBS/CNF composites. Addition of 1 wt % of nanoclay to the compatibilized blend (P80SEBS5) showed 32% improvement in Young's modulus when compared to the P80 blend. For the PP/BR/SEBS/CNF composites, the maximum value of Young's modulus is obtained with 3 wt % addition of CNF. Thus it can be concluded that the enhancement in Young's modulus of the P80SEBS5 blend is greater with the addition of nanoclay when compared to CNF.

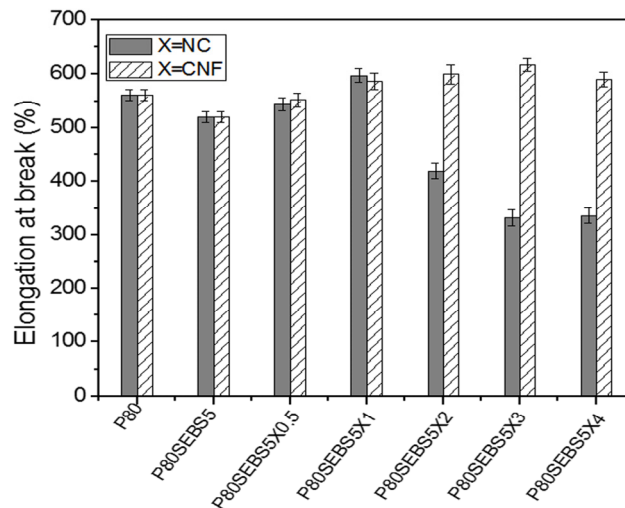


**Figure 5B.5. Elongation at break of the nanocomposites**

Elongation at break of P80 blend, SEBS compatibilized blend (P80SEBS5) and PP/BRSEBS/nanoclay and PP/BR/SEBS/CNF composites are displayed in Figure 5B.5. From the graph it is clear that PP/BR/SEBS/CNF composites showed elongation at break value similar to that of P80 blend. For the PP/BR/SEBS/nanoclay composites, maximum value of elongation at break is obtained for 1 wt % of nanoclay and with further addition of nanoclay, elongation at break got decreased. SEBS compatibilized PP/BR blend

(P80SEBS5) shows lower elongation at break than uncompatibilized PP/BR blend (P80). But in the presence of nanofillers, elongation at break improved. Therefore it can be assumed that in presence of nanofillers SEBS can improve the ductility of the blend.

### 5B.3.1.2 Impact strength

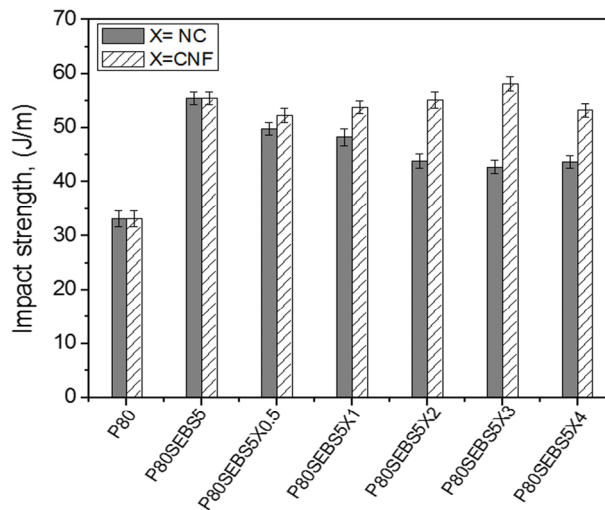


**Figure 5B.6. Impact strength of the nanocomposites**

Impact strength of the P80 blend, SEBS compatibilized blend (P80SEBS5) and PP/BRSEBS/nanoclay and PP/BR/SEBS/CNF composites are displayed in Figure 5B.6. From the graph it is obvious that SEBS compatibilized nanocomposites exhibited a remarkable increase in impact strength than P80 blend. This significant enhancement reveals the ability of SEBS to function as a compatibilizer. However when compared with the SEBS compatibilized blend (P80SEBS5), the impact strength of PP/BR/SEBS/nanoclay composites showed a reduction while PP/BR/SEBS/CNF composites retained the same. The maximum value of impact strength for the PP/BR/SEBS/CNF composites was obtained with 3 wt % of CNF.

From the analysis of the mechanical properties, it is revealed that addition of nanoclay to the SEBS compatibilized blend improved the tensile strength and Young's modulus of the P80 blend. The maximum improvement in tensile strength and Young's modulus was obtained with 1 wt % of nanoclay. Addition of CNF to the SEBS compatibilized blend improved the elongation at break and impact strength of the P80 blend. The maximum improvement in elongation at break and impact strength was obtained with 3 wt % of CNF. So further characterization of the nanocomposites is carried out with SEBS compatibilized PP/BR blend with 1 wt % nanoclay denoted as P80SEBS5NC1 and SEBS compatibilized PP/BR blend with 3 wt % CNF denoted as P80SEBS5CNF3.

### 5B.3.2 Transmission electron microscopy (TEM)

#### 5B.3.2.1 PP/BR/SEBS/nanoclay composites

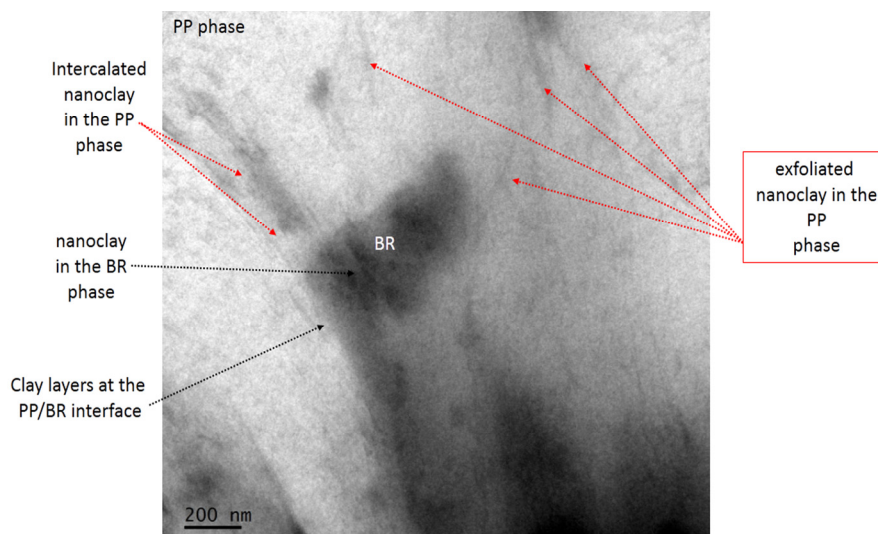
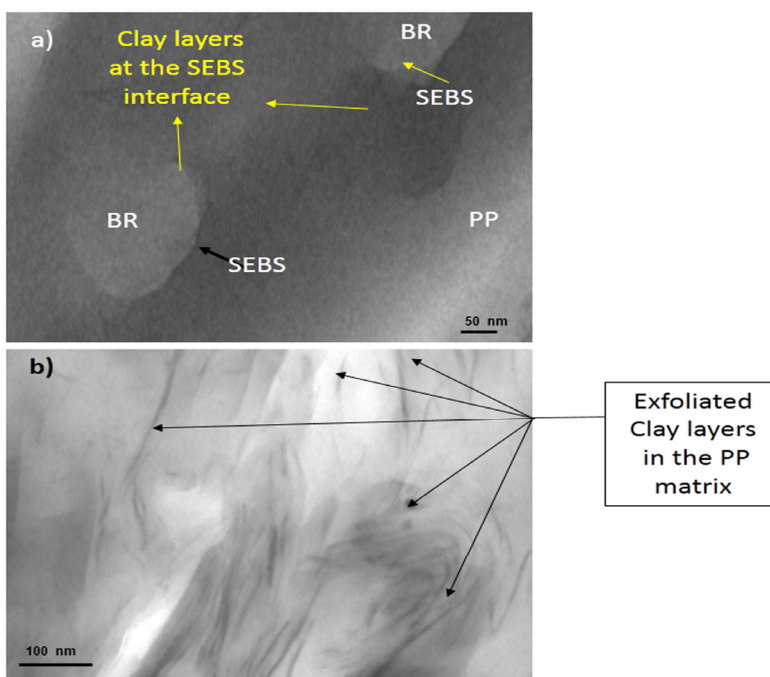


Figure 4A.2. TEM photograph of P80NC0.5 nanocomposite

A detailed analysis on the selective localization of the nanofillers in the uncompatibilized PP/BR blend (P80) and SEBS compatibilized PP/BR blend can be perceived through the analysis of the TEM images displayed in Figure 4A.2 and 5B.7.



**Figure 5B.7 (a-b). TEM photograph of P80SEBSNC1 nanocomposite**

The distribution of nanoclay in the uncompatibilized nanocomposite (P80NC0.5) is shown in Figure 4A.2 and SEBS compatibilized nanocomposite (P80SEBS5NC1) is as shown in Figure 5B.7(a) and (b). Different TEM photographs of the P80SEBS5NC1 sample is desirable to detect the distribution of nanoclay layers.

In the uncompatibilized nanocomposite (P80NC0.5) shown in Figure 4A.2 the rubber phase and clay layers are independently dispersed in

the PP phase with intercalated clay layers in the PP matrix and at the PP/BR interface. Agglomerated clay layers in the BR phase and some exfoliated clay layers in the PP matrix are also visible. In the compatibilized nanocomposite (P80SEBS5NC1) shown in Figure 5B.7, the rubber phase and clay layers are independently dispersed in the PP phase. Intercalated clay layers are seen adhered to the SEBS interfacial layer with no evidence of nanoclay in the BR phase. Clay layers are found to be effectively exfoliated in the PP matrix. These observations are consistent with the reported results<sup>24,25</sup>. The exfoliation of clay layers in the PP matrix is found to be improved in the presence of SEBS in the PP/BR blend. The presence of clay layers at the SEBS interfacial layer can be attributed to the interaction between SEBS and clay platelets as shown in Figure 5B.2. The interaction may be due to certain polarity existing in the styrene group of SEBS as established by Martin *et al.*<sup>20</sup>. The interaction between SEBS and nanoclay at the interface and might have restricted the migration of nanoclay to the dispersed BR phase. The reduced interfacial tension between the BR and PP phases due to compatibilization by SEBS also might have enabled the PP chains to enter in to the gallery spaces between the clay layers to accomplish greater extend of exfoliation of the clay layers<sup>26,27</sup>. The interaction of SEBS layer with clay platelets can be suggested to have contributed to the exfoliation of clay layers Hence it can be established that SEBS compatibilization appears to be more effective in assisting clay dispersion.

The trends shown in mechanical properties of the PP/BR/SEBS/nanoclay composite can be related to the localization of nanoclay in the blend. The enhancement in tensile strength of the P80SEBS5NC1 nanocomposite can be attributed to the selective localisation of the exfoliated nanoclay layers in the PP matrix and the formation of interfacial layer by SEBS, facilitating



better stress transfer between the matrix and the filler. An increase in the elongation at break by the incorporation of SEBS-g-MA to the PA6/PP/organoclay nanocomposite and the formation of SEBS-g-PA6 copolymer at the PP/PA6 interface has been reported<sup>28</sup>. Similarly the localization of SEBS at the PP/BR interface and improved SEBS/nanofiller interaction promotes the shear yielding of the PP matrix leading to improved elongation at break. From the TEM photographs, it is clear that the nanoclay is distributed at the SEBS interfacial layer and in the PP matrix. The distribution of rigid fillers such as nanoclay at the elastomeric SEBS layer may decrease the elasticity of this layer and leads to decreased impact strength<sup>29,30</sup>.

#### 5B.3.2.2 PP/BR/SEBS/CNF composites

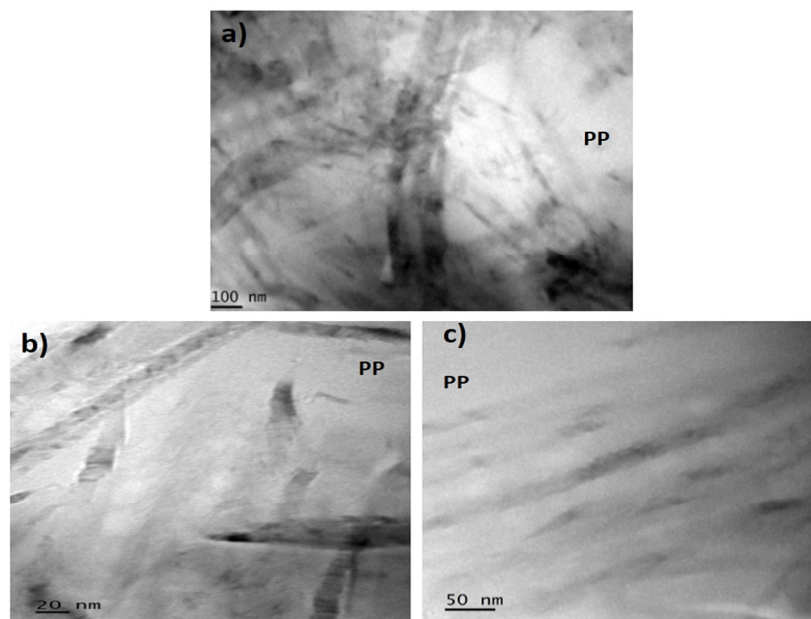


**Figure 5B.8 (a-c). TEM photograph of P80CNF3 nanocomposite at different magnifications**

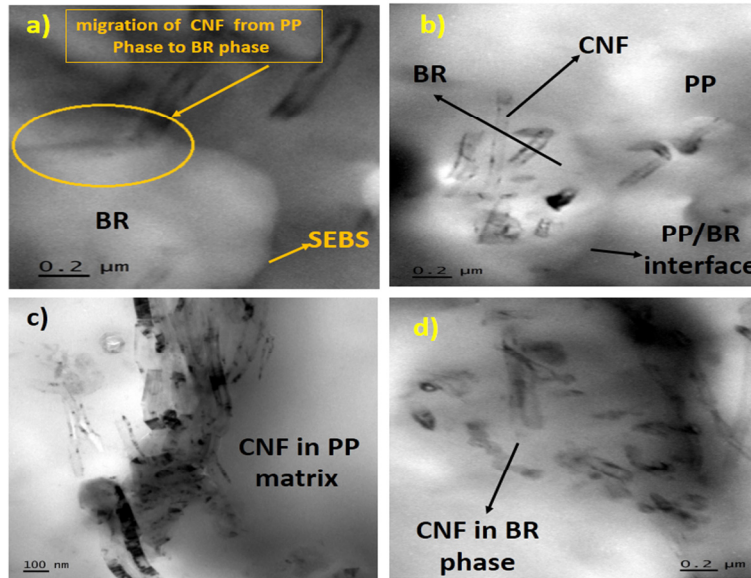


**Figure 5B.9 (a-d). TEM photograph of P80SEBSCNF3 nanocomposite**

TEM photographs of the uncompatibilized nanocomposite (P80CNF3) is shown in Figure 5B.8(a-c) and SEBS compatibilized nanocomposite (P80SEBS5CNF3) composite are shown in Figures 5B.9(a-d) .

In P80CNF3 sample shown in Figure 5B.8, CNFs were preferentially located in the PP matrix. The strong interfacial tension between the PP and the BR phases would have restricted the migration of CNF from PP in to the BR phase.

From Figure 5B.9(a), it is obvious that in P80SEBS5CNF3 nanocomposite, it can be proposed that the reduction in interfacial tension between the PP and the BR phases on compatibilization using SEBS might have enabled the migration of CNF in to the BR matrix. From the TEM images shown in Figure 5B.9(b) it is envisaged that major part of the CNFs seems to be encapsulated in the BR phase. Some CNFs can be seen in the PP matrix in

the dispersed form and also as bundles in Figure 5B.9(c). From Figure 5B.9(d), CNF seem to well dispersed in the BR phase. These observations are similar to the results reported by Bouaziz *et al.*<sup>31</sup> in their studies based on a maleated-polyethylene (MAPE) compatibilized PP/EPR/SiO<sub>2</sub> nanocomposites by melt mixing. They observed the presence of some silica nanoparticles dispersed in the matrix as the dispersed rubber phase has been saturated silica nanoparticles. Wu *et al.*<sup>32</sup> also reported the localization of CNT in the continuous phase, in the dispersed and at the interface in PLA/PCL blends prepared by two step melt blending approach.

The significantly enhanced impact strength for P80SEBSCNF3 nanocomposite can be attributed to the localization of CNF in the BR phase. It is already established the impact properties of the blend will be increased if the filler phase resides inside the toughener phase, forming a core-shell morphology in the blend<sup>11,33</sup>. Similar observation is seen in the P80SEBSCNF3 nanocomposite also. Long and Shanks<sup>9</sup> established that the filler is covered by the elastomer, it behaves partly like a rubber phase and helps in improving the elongation at break. They also suggested that the initiation of microcracks at the filler particles will be prevented and a yielded zone around the elastomer particle will be formed. This will improve the effectiveness of rubber particle in improving the impact strength of the nanocomposite. Hence the improvement in the impact strength of P80SEBS5CNF3 composite can be attributed to the core-shell morphology with CNF residing in the BR phase. But, the encapsulation of CNFs in the BR phase is found to be not so effective in improving the modulus as the reinforcing effect of the filler is decreased by the surrounding elastomer layer<sup>34,35</sup>.

Thus it can be proposed that PP/BR/SEBS/nanoclay and the PP/BR/SEBS/CNF composites exhibit two types of morphology based on the

selective localization of nanofillers in the blend matrix. The P80SEBS5NC1 composite possess the morphology in which the rubber phase and nanoclay are independently dispersed in PP matrix with the localization of the SEBS at the PP/BR interphase. While P80SEBS5CNF3 nanocomposite exhibited the morphology in which the CNFs resides inside the BR phase. Schematic representation of the morphology of PP/BR nanoclay composite and PP/BR/CNF in presence of SEBS as a compatibilizer is given in the Figures 5B.10 and 5B.11, respectively.

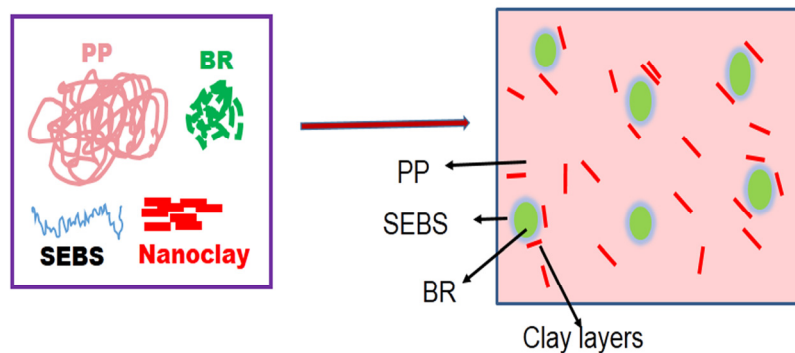


Figure 5B.10. Schematic representation of the distribution of the nanoclay layers in the P80SEBS5NC1 composite

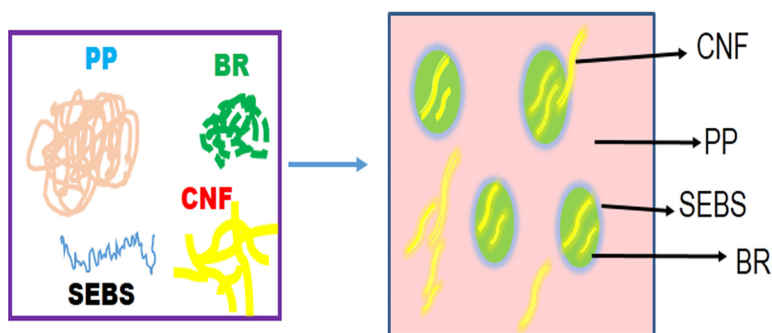
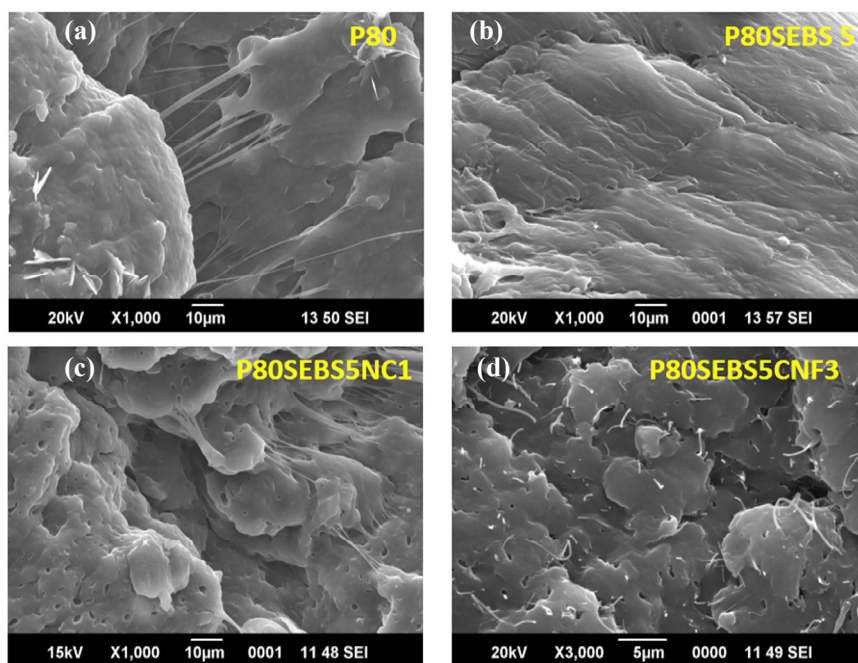


Figure 5B.11. Schematic representation of the distribution of the CNF in the P80SEBS5CNF3 composite

### 5B.3.3 Scanning electron microscopy (SEM)

#### a) SEM photograph of tensile fractured surface



**Figure 5B.12 (a-d).** SEM photographs showing the tensile fractured surface of the blends and the nanocomposites.

Figure 5B.12(a-d) shows the SEM photographs of the tensile fractured surface uncompatibilized blend (P80), compatibilized blend (P80SEBS5) and the nanocomposites. Uncompatibilized PP/BR blend (P80) shown in Figure 5B.12(a), reveals extensive shear yielding of the matrix produced by dispersed rubber particle cavitation. The photographs of SEBS compatibilized P80 blend (P80SEBS5) shown in Figure 5B.12(b) exhibited a more or less homogeneous morphology due to the improved adhesion between the PP and BR phases. Introduction of the nanofillers in the P80SEBS5 blend

altered its morphology. In the SEBS compatibilized PP/BR/nanoclay composite (P80SEBS5NC1) shown in Figure 5B.12(c), shear yielding of the matrix is visible which accounts for the improved elongation at break of the sample. Tensile fractured surfaces of the SEBS compatibilized PP/BR/CNF composite (P80SEBS5CNF3) sample shown in Figure 5B.12.(d) illustrates randomly distributed CNFs.

A closer examination of the tensile fractured surface of the P80SEBS5CNF3 sample at higher magnifications shown in Figure 5B.13 exhibited better dispersion of CNF as discrete fibres with polymer matrix adhered to the surface of CNF surface. Enhanced interfacial adhesion between the fibre and the matrix, by the addition of SEBS is clearly visible.

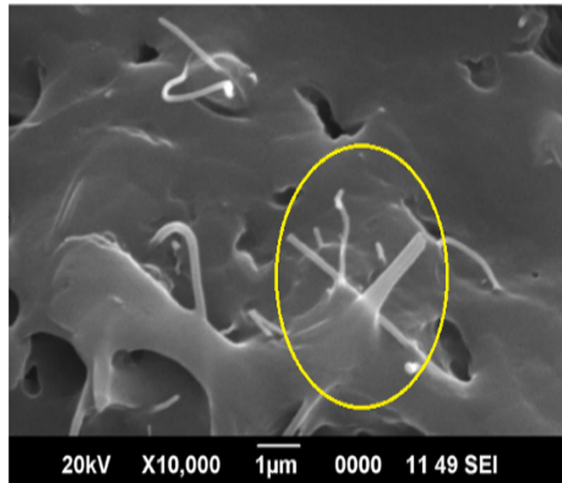


**Figure 5B.13. SEM photograph of the tensile fractured surface of the P80SEBS5CNF3 sample at high magnification**

**b) SEM photograph of impact fractured surface**

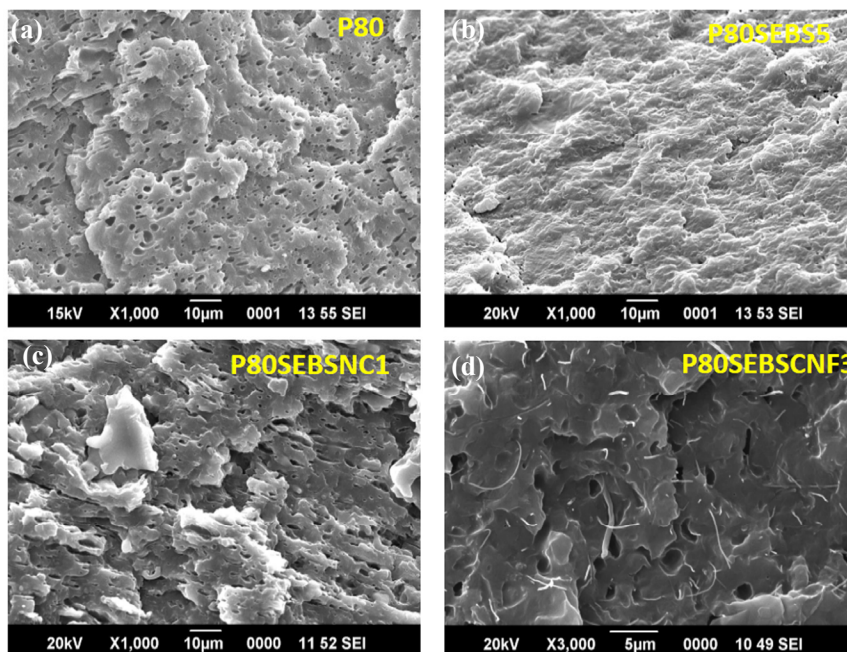


**Figure 5B.14 (a-d). SEM photographs showing the impact fractured surface of the blend and the nanocomposites**

SEM photographs showing the impact fractured surface of the uncompatibilized blend (P80), compatibilized blend (P80SEBS5) and the SEBS compatibilized nanocomposites (P80SEBSNC1 and P80SEBS5CNF3) are displayed in Figure 5B.14(a-d). SEM morphology of P80 blend shown in Figure 5B.14(a) shows the presence of elongated voids indicating rubber particle cavitation and plastic deformation of the matrix. The morphology of compatibilized P80SEBS5 blend shown in Figure 5B.14(b) shows a homogenous morphology with reduced particle size and improved interfacial adhesion. From Figure 5B.14(c), the presence of SEBS and clay layers at the PP/BR interface promotes the suppression of void coalescence

as seen in the impact fracture morphology of P80SEBSNC1nanocomposite leading to improved impact strength. Moreover, the presence of elongated voids in the P80SEBSNC1 sample suggests that the interaction between the clay layers and the SEBS compatibilizer promotes a ductile mode of impact fracture. SEM morphology of the impact fractured P80SEBSCNF3 sample shown in Figure 5B.14(d) displays random orientation of fibres in the blend matrix. It is obvious that the bundles of CNFs were significantly disentangled and distributed into the polymer due to the effects of shear forces during melt processing. It can be easily recognized that the single nanofibres are embedded into the polymer matrix. The impact fracture morphology is in quite agreement with the distribution of CNFs as envisaged by the TEM images. A closer examination of the impact fractured surface of the P80SEBS5NC3 sample at higher magnifications showed better dispersion of CNF as shown in Figure 5B.15.

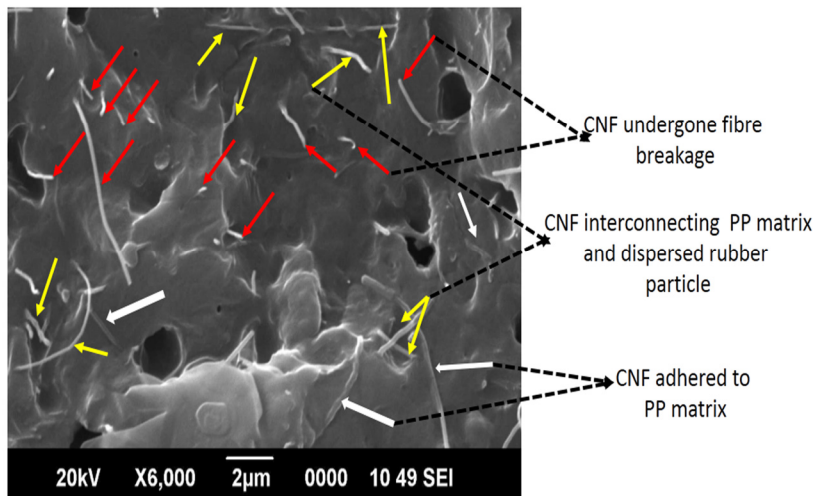


**Figure 5B.15. SEM photograph of the impact fractured surface of P80 SEBS5CNF3 at high magnification**



The reduction in interfacial tension on compatibilization with SEBS have enabled CNFs to get distributed between the PP and BR phase. The significant enhancement in impact strength of the P80SSEBSCNF3 nanocomposite is associated with the encapsulation of CNFs in the BR phase. Investigation on the morphology and toughening mechanisms in PP/SBS/organoclay system by Li *et al.*<sup>36</sup> established that the encapsulation of clay layers in the SBS phase can improve the toughness significantly. They established that debonding between the clay inclusion and the SBS rubber phase is equivalent to rubber particle cavitation leading to effective stress relief promoting large scale shear yielding in the PP matrix. Similar observation can be seen in the SEM morphologies of the P80SEBS5CNF3 sample. In the SEM morphology, cavitated rubber particle can be clearly observed. Hence the significant enhancement in the impact strength can be attributed to the debonding between the CNFs fibres and the rubber phase which is equivalent to the cavitation of BR particle. The CNFs encapsulated in the BR phase that were debonded are presented by yellow arrows. Even though the CNFs are encapsulated in the BR phase, the fibre ends seem to be embedded in the PP phase as shown in the TEM and the SEM morphologies. CNFs shown by white arrows represent the fibres that are aligned with in the crack embedded in the PP matrix. CNFs that have undergone fibre breakage is represented by red arrows. All these observation accounts for the improved impact strength of P80SEBSCNF3 sample.

### 5B.3.4 Dynamic rheological analysis (DRA)

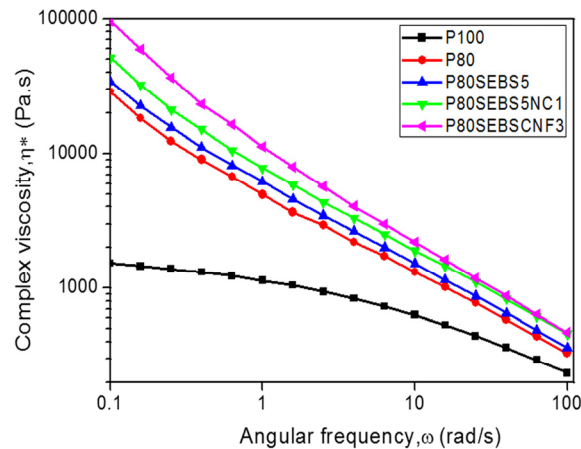


**Figure 5B.16.** Complex viscosity,  $\eta^*$  as a function of angular frequency ( $\omega$ ) of P100, P80, P80SEBS5, P80SEBS5NC1 and P80SEBS5CNF3 samples at 190 °C

The complex viscosity,  $\eta^*$  as a function of angular frequency ( $\omega$ ) linear viscoelastic behavior of P100, P80 blend, P80SEBS5, P80SEBS5NC1 and P80SEBS5CNF3 are shown in in the Figure 5B.16. Pure PP shows shear thinning behavior only at higher frequencies. But the uncompatibilized and compatibilized blends and the nanocomposites showed remarkable shear thinning behavior at lower frequencies. The introduction of nanofillers to the SEBS compatibilized P80 blend leads to a remarkable change in the complex viscosity behavior. The complex viscosity of the nanocomposites are higher than the P80 blend in the studied frequency range. The results are in accordance with earlier results where an increase in the melt viscosity on the addition of the clay platelets and the compatibilizer acting as interfacial agents were reported<sup>25</sup>. The increase in complex viscosity of the nanocomposites is due to the restriction of mobility of PP chains by the nanofillers in the matrix<sup>37</sup>.

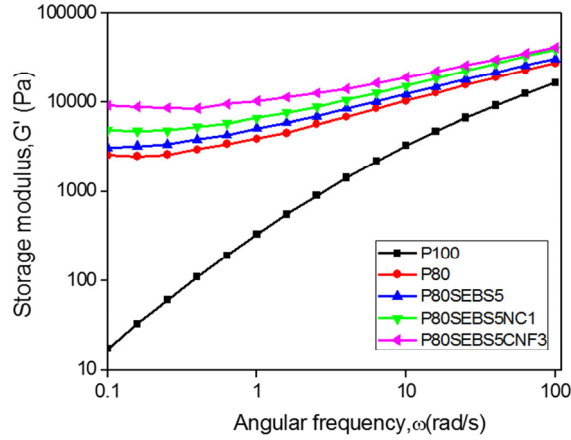


Figure 5B.17. Storage modulus,  $G'$  vs. angular frequency,  $\omega$  of P100, P80, P80SEBS5, P80SEBS5NC1 and P80SEBS5CNF3 samples at 190 °C

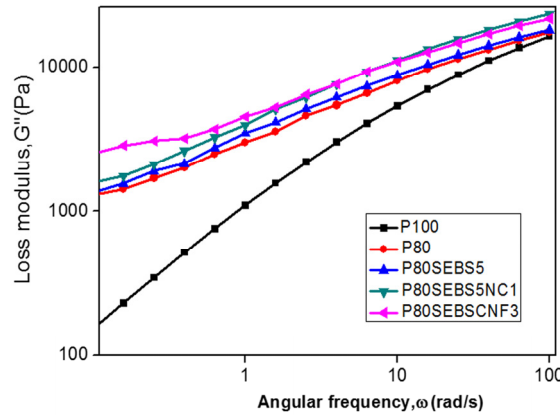
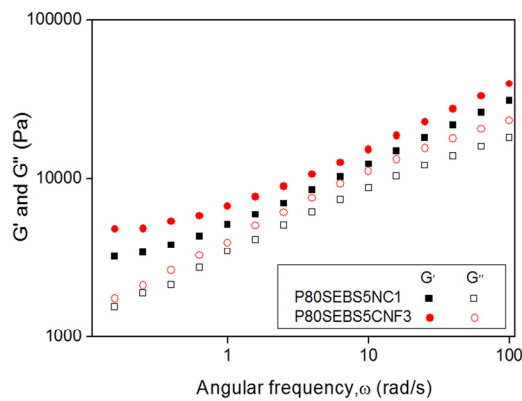


Figure 5B.18. Loss modulus,  $G''$  vs. angular frequency,  $\omega$  of P100, P80, P80SEBS5, P80SEBS5NC1 and P80SEBS5CNF3 samples at 190 °C

The variation of storage modulus ( $G'$ ) and loss modulus ( $G''$ ) of P100, P80, P80SEBS5, P80SEBS5NC1 and P80SEBS5CNF3 samples at 190°C as a function of angular frequency are shown in Figure 5B.17 and 5B.18, respectively. Storage modulus and loss modulus of the nanocomposites

increased with increase in frequencies. At lower frequencies, there is enough time for molecular relaxation and hence lower values of storage and loss modulus. At high frequencies, there is decrease in time available for relaxation of the molecules, hence high values of storage and loss modulus. The linear viscoelastic properties at high frequencies are usually governed by the matrix phase of the blend, hence the increase in storage modulus at high frequencies with the introduction of nanofillers can be attributed to the localization of nanofillers within the PP matrix phase that restricts the mobility of PP chains<sup>38</sup>. This is in agreement with the TEM findings.



**Figure 5B.19. Storage ( $G'$ ) and Loss ( $G''$ ) moduli as a function of angular frequency of P80SEBS5NC1 and P80SEBS5CNF3 samples at 190°C**

As seen from the Figure 5B.19, storage modulus ( $G'$ ) is larger than loss modulus ( $G''$ ) for the P80SEBS5NC1 and P80SEBS5CNF3 samples over the entire range of experimental frequency, hence no  $\omega_c$  (crossover frequency) is observed. As  $G'$  is dominant over  $G''$  ( $G' > G''$ ) for the nanocomposites in the complete frequency range measured, solid like elastic response at low frequencies can be recognized due to the restricted molecular mobility of the PP chains<sup>39,40</sup>. These results can be attributed to

the stronger network caused by homogenous dispersion of nanofillers in the presence of compatibilizer.

### 5B.3.5 Differential scanning calorimetry (DSC)

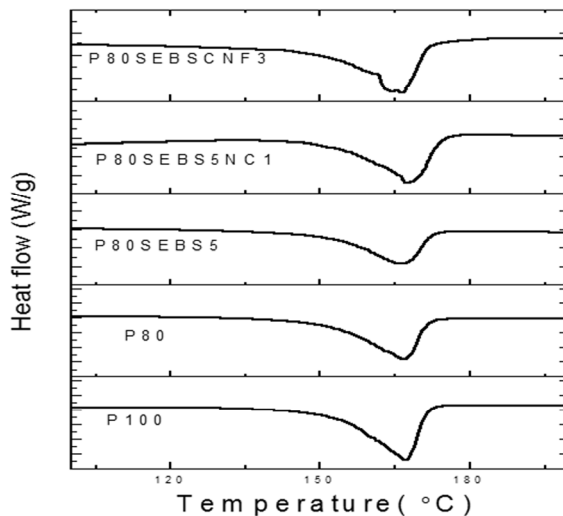


**Figure 5B.20.** DSC heating curves of PP/BR/SEBS nanocomposites

**Table 5B.2.** Melting characteristics of the PP/BR/SEBS nanocomposites

Sample	$T_{m,onset}$ (°C)	$T_m$ (°C)	$T_{m,endset}$ (°C)	$\Delta H_f$ J/g	$X_c$ (%)
P100	153	167.32	171.42	93.76	45
P80	153	166.86	171.38	70.57	42
P80SEBS5	152	166.27	172.36	71.56	42
P80SEBS5NC1	160	167.45	173.97	51.62	30
P80SEBS5CNF3	146	166.26	171.36	64.13	38

The melting characteristics of pure PP (P100), P80 blend and the SEBS compatibilized blend P80SEBS5 and the nanocomposites derived from heating curves are shown in Figure 5B.20. The onset of melting

temperature ( $T_{m,onset}$ ), peak melting temperature ( $T_m$ ), endset of melting temperature ( $T_{m,endset}$ ), enthalpy of fusion ( $\Delta H_f$ ) and percentage of crystallinity ( $X_c$ ) computed are listed in table 5B.2.

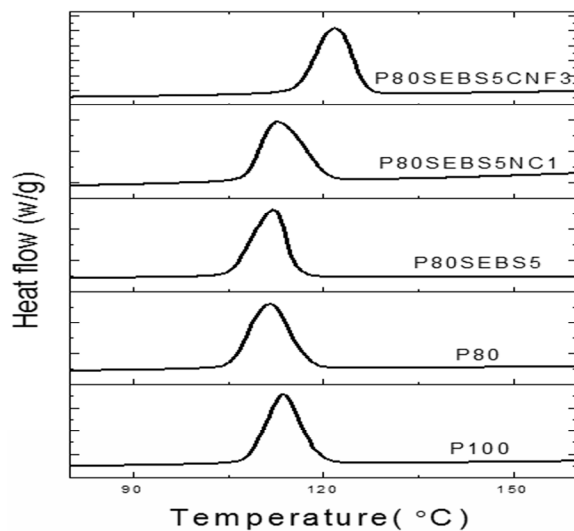


Figure 5B.21. DSC cooling curves of PP/BR/SEBS nanocomposites

Table 5B.3. Crystallization characteristics of PP/BR/SEBS nanocomposites

Sample	$T_{c,onset}$ (°C)	$T_c$ (°C)	$T_{c,endset}$ (°C)	$\Delta H_c$ J/g
P100	119	114	108	111.68
P80	117	111	105	88.23
P80SEBS5	115	112	106	82.27
P80SEBS5NC1	120	112	108	56.26
P80SEBS5CNF3	126	121	116	67.43

The crystallization characteristics obtained from cooling curves are given in Figure 5B.21. The onset of crystallization temperature ( $T_{c,onset}$ ), peak crystallization temperature ( $T_c$ ), endset of crystallization temperature ( $T_{c,endset}$ ) and enthalpy of crystallization ( $\Delta H_c$ ) are listed in table 5B.3.

The incorporation of SEBS does not show any influence on melting temperature ( $T_m$ ) and crystallization temperature ( $T_c$ ) of PP. The addition of SEBS affected the phase morphology of the PP/BR blend, but the crystallization behavior of PP remains unaffected. This is consistent with the earlier results which established that the compatibilizer does not usually interfere with the crystallization properties of polymers<sup>23</sup>. The values of  $T_m$  and  $T_c$  of the nanocomposites remain unaltered with the addition of nanoclay which indicates the weak nucleating effect of nanoclay in the PP matrix in the presence of SEBS as a compatibilizer. An increase in the value of  $T_c$  of the P80SEBS5CNF3 sample was detected which proves that the CNFs dispersed in PP matrix can promote heterogeneous nucleation. The decrease in the degree of crystallinity with the nanofillers can be attributed to the hindrance offered by the nanoclay layers and CNFs present in the PP matrix that restricts the mobility of the PP macromolecular chains and prevents crystallization of PP chains<sup>41</sup>.

### 5B.3.6 Thermogravimetric analysis (TGA)

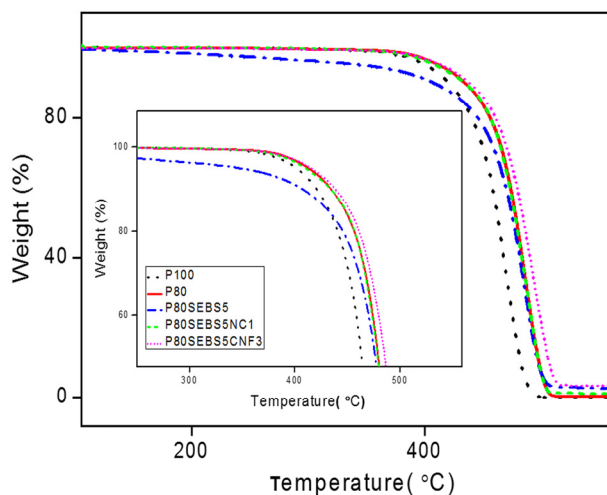


**Figure 5B.22.** TGA curves of PP/BR/SEBS nanocomposites

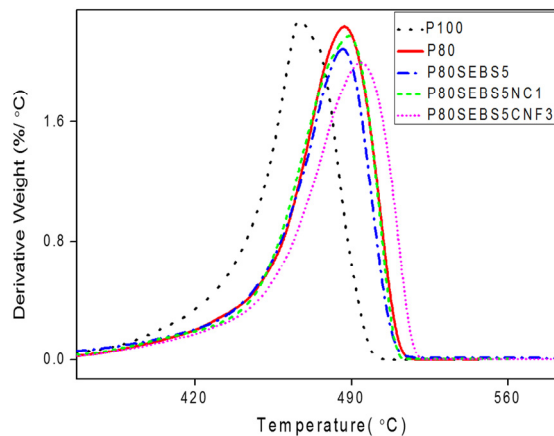


**Figure 5B.23. DTG curves of PP/BR/SEBS nanocomposites**

Figure 5B.22 and 5B.23 shows the TGA and DTG curves of curves of PP, uncompatibilized P80 blend P80SEBS5 and the PP/BR/SEBS nanocomposites. It can be observed that all the samples displayed single step degradation process. The thermal degradation parameters such as onset degradation temperature  $T_{\text{onset}}$ , temperatures at 10% weight loss ( $T_{10}$ ) and 50% weight loss ( $T_{50}$ ), final decomposition temperature ( $T_f$ ), maximum degradation temperature ( $T_{\text{max}}$ ) are listed in table 5B.4.

**Table 5B.4. TGA parameters of PP/BR/SEBS nanocomposites**

SAMPLE	$T_{\text{onset}}$ (°C)	$T_{10}$ (°C)	$T_{50}$ (°C)	$T_{\text{max}}$ (°C)	$T_f$ (°C)
P100	360	421	464	467	500
P80	365	435	479	486	514
P80SEBS5	395	408	476	486	509
P80SEBSNC1	379	434	479	488	510
P80SEBS5CNF3	367	439	485	494	516



The enhancement of the final decomposition temperature ( $T_f$ ) and the temperature at maximum rate of weight loss ( $T_{max}$ ) reflects thermal stability of both the nanocomposites. The enhancement of thermal stability suggest the efficient dispersion of nanoparticles that hampered the diffusion of volatile decomposition products in the nanocomposites. P80SEBS5CNF3 sample shows better thermal stability than P80SEBS5NC1 nanocomposite. The presence of CNFs dispersed in the PP matrix and in the BR phase helps in the uniform conduction of heat and avoid heat concentration thereby enhancing the thermal stability. The enhancement in TGA parameters with CNF loading suggests interaction between carbon nanofibre and polymeric matrix<sup>42</sup>.

#### **5B.4 Conclusions**

Compatibilization of PP/BR blend containing 20 wt % BR (P80) using 5 wt % SEBS improve the dispersion of BR phase and nanofillers in the matrix. TEM analysis of the nanocomposites reveal two different types of morphology for the PP/BR/SEBS/nanoclay and PP/BR/SEBS/CNF composites. Nanoclay and carbon nanofibre show different distributions in the blend and the mechanical properties of the nanocomposites are related to these distribution. P80SEBS5NC1 sample show enhancement in tensile strength, Young's modulus and elongation at break. In P80SEBS5NC1 sample, BR phase and clay layers are independently dispersed in the PP phase with intercalated clay layers adhered to the SEBS interfacial layer and no evidence of nanoclay in the BR phase. Clay layers are found to be effectively exfoliated in the PP matrix. The stiffness enhancement rather than toughness improvement of the composite is related to the localisation of nanofillers in the PP/BR/SEBS blend. P80SEBS5CNF3 sample show remarkable improvement in elongation at break and impact strength. In

P80SEBS5CNF3 samples, BR phase and CNFs are independently dispersed in the PP phase and CNFs were seen encapsulated in the BR phase. The reduction in interfacial adhesion by compatibilization with SEBS may have enabled the migration of CNFs to the BR phase resulting in a core-shell morphology. The enhancement in elongation at break and impact strength of P80SEBS5CNF3 sample is associated with the localization of CNFs in the matrix. The increase in the complex viscosity, storage modulus and loss modulus of the nanocomposites in melt rheological analysis indicated interaction between the nanofillers and the PP matrix. The increase in peak crystallization temperature ( $T_c$ ) of P80SEBS5CNF3 nanocomposite indicates the nucleating effect of CNF. In P80SEBS5NC1 nanocomposite  $T_c$  remains unaffected which shows the weak nucleating effect of nanoclay. For both the nanocomposites the percentage of crystallinity decreases. TGA studies reveal that the incorporation of nanofillers improved the thermal stability of PP/BR/SEBS blend.

## References

- [1] Drobny, J. G. (2007). *Handbook of Thermoplastic Elastomer*, William Andrew Publishing
- [2] Panda, B. P., Mohanty, S., & Nayak, S. K. (2015). Mechanism of toughening in rubber toughened polyolefin—a review. *Polymer-Plastics Technology and Engineering*, 54(5), 462-473.
- [3] Lee, H. S., Fasulo, P. D., Rodgers, W. R., & Paul, D. R. (2005). TPO based nanocomposites. Part 1. Morphology and mechanical properties. *Polymer*, 46(25), 11673-11689.
- [4] Paul, D. R., & Robeson, L. M. (2008). Polymer nanotechnology: nanocomposites. *Polymer*, 49(15), 3187-3204.

- [5] Feng, L., Xie, N., & Zhong, J. (2014). Carbon nanofibers and their composites: a review of synthesizing, properties and applications. *Materials*, 7(5), 3919-3945.
- [6] Martins, C. G., Larocca, N. M., Paul, D. R., & Pessan, L. A. (2009). Nanocomposites formed from polypropylene/EVA blends. *Polymer*, 50(7), 1743-1754.
- [7] Liao, C. Z., & Tjong, S. C. (2011). Effects of carbon nanofibers on the fracture, mechanical, and thermal properties of PP/SEBS-g-MA blends. *Polymer Engineering & Science*, 51(5), 948-958.
- [8] Fenouillot, F., Cassagnau, P., & Majesté, J. C. (2009). Uneven distribution of nanoparticles in immiscible fluids: morphology development in polymer blends. *Polymer*, 50(6), 1333-1350.
- [9] Long, Y., & Shanks, R. A. (1996). PP–elastomer–filler hybrids. I. Processing, microstructure, and mechanical properties. *Journal of Applied Polymer Science*, 61(11), 1877-1885.
- [10] Bagheri-Kazemabad, S., Khavandi, A., & Chen, B. (2013). Evaluation of toughening mechanisms of polypropylene/ethylene–octene copolymer/maleic anhydride-grafted poly (ethylene-co-octene)/clay nanocomposite. *Polymer International*, 62(4), 566-572.
- [11] Matonis, V. A., & Small, N. C. (1969). A macroscopic analysis of composites containing layered spherical inclusions. *Polymer Engineering & Science*, 9(2), 90-99.
- [12] Laoutid, F., François, D., Bonnaud, L., & Dubois, P. (2013). Using Nanosilica to Fine-Tune Morphology and Properties of Polyamide 6/Poly (propylene) Blends. *Macromolecular Materials and Engineering*, 298(3), 328-338.
- [13] Elias, L., Fenouillot, F., Majesté, J. C., Martin, G., & Cassagnau, P. (2008). Migration of nanosilica particles in polymer blends. *Journal of Polymer Science Part B: Polymer Physics*, 46(18), 1976-1983.
- [14] Parameswaranpillai, J., Joseph, G., Shinu, K. P., Salim, N. V., Hameed, N., & Jose, S. (2015). High performance PP/SEBS/CNF composites: Evaluation of mechanical, thermal degradation, and crystallization properties. *Polymer Composites*.

- [15] Tjong, S. C., & Meng, Y. Z. (2003). Impact-modified polypropylene/vermiculite nanocomposites. *Journal of Polymer Science Part B: Polymer Physics*, 41(19), 2332-2341.
- [16] Balkan, O., Demirer, H., Ezdeşir, A., Yildirim, H., & Yilmazer, Ü. (2007). Effects of SEBS and SEBS-g-MA Modifications on the Fracture Behavior of i-Pp/Glass Bead and i-Pp/Wollastonite Composites. *Proceedings of 8th International Fracture Conference, Turkey*.
- [17] Filippi, S., Dintcheva, N. T., Scaffaro, R., La Mantia, F. P., Polacco, G., & Magagnini, P. (2009). Effects of organoclay on morphology and properties of nanocomposites based on LDPE/PA-6 blends without and with SEBS-g-MA compatibilizer. *Polymer Engineering & Science*, 49(6), 1187-1197.
- [18] Macaubas, P. H. P., & Demarquette, N. R. (2001). Morphologies and interfacial tensions of immiscible polypropylene/polystyrene blends modified with triblock copolymers. *Polymer*, 42(6), 2543-2554.
- [19] El-Midany, A. A., & Ibrahim, S. S. (2011). Interfacial role of compatibilizers to improve mechanical properties of silica–polypropylene composites. *Physicochemical Problems of Mineral Processing*, 46, 295-305.
- [20] Martín, Z., Jimenez, I., Gomez, M. A., Ade, H., & Kilcoyne, D. A. (2009). Interfacial interactions in PP/MMT/SEBS nanocomposites. *Macromolecules*, 43(1), 448-453.
- [21] Sanporean, C. G., Vuluga, Z., Radovici, C., Panaitescu, D. M., Iorga, M., deClaville Christiansen, J., & Mosca, A. (2014). Polypropylene/organoclay/SEBS nanocomposites with toughness–stiffness properties. *RSC Advances*, 4(13), 6573-6579.
- [22] Parameswaranpillai, J., Dubey, V. K., Sisanth, K. S., Jose, S., Zachariah, A. K., Siengchin, S.,...& Hameed, N. (2016). Tailoring of interface of polypropylene/polystyrene/carbon nanofibre composites by polystyrene-block-poly (ethylene-ran-butylene)-block-polystyrene. *Polymer Testing*, 51, 131-141.

- [23] Parameswaranpillai, J., Joseph, G., Shinu, K. P., Jose, S., Salim, N. V., & Hameed, N. (2015). Development of hybrid composites for automotive applications: effect of addition of SEBS on the morphology, mechanical, viscoelastic, crystallization and thermal degradation properties of PP/PS-x GnP composites. *RSC advances*, 5(33), 25634-25641.
- [24] Liu, Y., & Kontopoulou, M. (2006). The structure and physical properties of polypropylene and thermoplastic olefin nanocomposites containing nanosilica. *Polymer*, 47(22), 7731-7739.
- [25] Mehta, S., Mirabella, F. M., Rufener, K., & Bafna, A. (2004). Thermoplastic olefin/clay nanocomposites: morphology and mechanical properties. *Journal of Applied Polymer Science*, 92(2), 928-936.
- [26] Ganguly, A., Bhowmick, A. K., & Li, Y. (2008). Insights into montmorillonite nanoclay based ex situ nanocomposites from SEBS and modified SEBS by small-angle X-ray scattering and modulated DSC studies. *Macromolecules*, 41(16), 6246-6253.
- [27] Carastan, D. J., & Demarquette, N. R. (2006, February). Microstructure of nanocomposites of styrenic polymers. In *Macromolecular symposia* (Vol. 233, No. 1, pp. 152-160).
- [28] Ishak, Z. M., Chow, W. S., & Takeichi, T. (2008). Influence of SEBS-g-MA on morphology, mechanical, and thermal properties of PA6/PP/organoclay nanocomposites. *European Polymer Journal*, 44(4), 1023-1039.
- [29] Treasa Sunitha George, (2016), Ph.D thesis, Cochin University of Science and Technology.
- [30] El-Midany, A. A., & Ibrahim, S. S. (2011). Interfacial role of compatibilizers to improve mechanical properties of silica-polypropylene composites. *Physicochemical Problems of Mineral Processing*, 46, 295-305.
- [31] Bouaziz, A., Massardier, V., Louizi, M., & Jaziri, M. (2015). Reinforcement of polyolefins-based nanocomposites: combination of compatibilizer with high shear extrusion process. *Polymer Engineering & Science*, 55(10), 2328-2338.

- [32] Wu, D., Lin, D., Zhang, J., Zhou, W., Zhang, M., Zhang, Y., ... & Lin, B. (2011). Selective localization of nanofillers: effect on morphology and crystallization of PLA/PCL blends. *Macromolecular Chemistry and Physics*, 212(6), 613-626.
- [33] Ou, Y. C., Guo, T. T., Fang, X. P., & Yu, Z. Z. (1999). Toughening and reinforcing polypropylene with core-shell structured fillers. *Journal of applied polymer science*, 74(10), 2397-2403.
- [34] Matonis, V. A., & Small, N. C. (1969). A macroscopic analysis of composites containing layered spherical inclusions. *Polymer Engineering & Science*, 9(2), 90-99.
- [35] Chiang, W. Y., Yang, W. D., & Pukanszky, B. (1992). Polypropylene composites. II: Structure-property relationships in two-and three-component polypropylene composites. *Polymer Engineering & Science*, 32(10), 641-648.
- [36] Li, Y., Wei, G. X., & Sue, H. J. (2002). Morphology and toughening mechanisms in clay-modified styrene-butadiene-styrene rubber-toughened polypropylene. *Journal of materials science*, 37(12), 2447-2459.
- [37] Mishra, J. K., Hwang, K. J., & Ha, C. S. (2005). Preparation, mechanical and rheological properties of a thermoplastic polyolefin (TPO)/organoclay nanocomposite with reference to the effect of maleic anhydride modified polypropylene as a compatibilizer. *Polymer*, 46(6), 1995-2002.
- [38] Ceccia, S., Ferri, D., Tabuani, D., & Maffettone, P. L. (2008). Rheology of carbon nanofiber-reinforced polypropylene. *Rheologica Acta*, 47(4), 425-433.
- [39] Chafidz, A., Kaavessina, M., Al-Zahrani, S., & Ali, I. (2014). Multiwall carbon nanotubes filled polypropylene nanocomposites: Rheological and electrical properties. *Polymer Engineering & Science*, 54(5), 1134-1143.
- [40] Verma, P., Verma, M., Gupta, A., Chauhan, S. S., Malik, R. S., & Choudhary, V. (2016). Multi walled carbon nanotubes induced viscoelastic response of polypropylene copolymer nanocomposites: Effect of filler loading on rheological percolation. *Polymer Testing*, 55, 1-9.

- [41] Lozano, K., & Barrera, E. V. (2001). Nanofiber-reinforced thermoplastic composites. I. Thermoanalytical and mechanical analyses. *Journal of Applied Polymer Science*, 79(1), 125-133.
- [42] Chatterjee, A., & Deopura, B. L. (2006). Thermal stability of polypropylene/carbon nanofiber composite. *Journal of applied polymer science*, 100(5), 3574-3578.

.....✂.....

**SUMMARY AND CONCLUSIONS**

A brief summary of the study, major conclusions and scope of future work are given in this chapter.

Thermoplastic elastomers (TPEs) were introduced commercially in 1960 and a variety of TPEs have evolved since then. Among the TPE blends, thermoplastic olefins (TPOs) based on plastic/rubber blends have tremendous commercial importance as they combine the processability of thermoplastics and elasticity of the elastomer. Blending of polypropylene (PP) with elastomers is a promising approach to develop TPEs with diverse applications depending on the PP/elastomer ratio. The dispersed elastomer phase improves the impact strength of PP, but has a detrimental effect on the stiffness and strength of the material. Though addition of inorganic fillers can improve the strength and stiffness, higher loading of the filler is required which leads to poor processability. The introduction of nanofillers in TPOs to develop TPO nanocomposites can revolutionize the TPE field.

TPEs based on polypropylene/polybutadiene (PP/BR) blends are prepared by melt blending and the mechanical, morphological, rheological and thermal properties of the blends were studied with reference to blend ratio. The mechanical properties of the blends were strongly influenced by blend ratio. The tensile strength and Young's modulus of PP decrease with



increase in BR content, whereas the elongation at break and impact strength increase significantly. The experimental tensile strength data of PP/BR blends were compared with predictive models such as Nielsen's first power law model, Nielsen's two-third power law model and Nicolais-Narkis model. It is found that the experimental values are in good agreement with Nielsen's two-third power law model confirming a matrix droplet morphology with BR as spherical inclusions. The impact strength increases with increase in the BR content. A maximum value of elongation at break is obtained for the blend with 20 wt % BR (P80 blend). About 280 % enhancement in elongation at break and 80 % improvement in impact strength are achieved. Therefore the optimum blend ratio for maximum toughness of PP was optimized to be 80/20 PP/BR (P80). SEM studies reveal a two phase morphology for the blends. The dominant mechanism of deformation during tensile testing of the P80 sample was analyzed and the enhanced elongation at break for the P80 sample (PP/BR;80/20 blend) was found to be due to massive shear yielding caused by repeated cavitation of rubber particles. The melt rheological studies reveal that thermoplastic elastomers based on PP/BR blend is melt processable. DMA studies confirm the decrease in stiffness of the PP matrix with the introduction of the BR phase. The nucleating effect of BR on PP matrix is not very strong as revealed by DSC studies. Thermogravimetric studies confirm the improved thermal stability of the blend.

Blending of 20 wt % BR with PP resulted in an increase in elongation at break and impact strength of PP, but the strength and stiffness got decreased. Hence the enhancement of stiffness of the PP/BR blend by the introduction of nanofillers was attempted. The two nanofillers selected for the reinforcement of the matrix were nanoclay and carbon nanofibre.

Thermoplastic polyolefin (TPO)/nanoclay composite based on PP/BR/cloisite 93 A was prepared. XRD results suggest a complete exfoliation of the nanoclay layers in the matrix without any structural change in PP from  $\alpha$  phase to  $\beta$  phase. TEM studies reveal the distribution of partially exfoliated and intercalated clay layers in the PP matrix. Nanoclay layers are also found in the BR phase and at the PP/BR interface. The introduction of 0.5 wt % of nanoclay results in the enhancement of tensile strength and Young's modulus and marginal improvement in impact strength. The mechanical properties after attaining a maximum at 0.5 wt % gradually decrease and then remain almost constant up to 4 wt %. There is a drastic reduction after 4 wt % of nanoclay addition due to agglomeration. The presence of clay layers in the PP matrix reduces the ability of the matrix to undergo plastic deformation and results in the reduction of elongation at break. Halpin-Tsai micro mechanical model was used to determine the aspect ratio of the filler which was estimated to be 45. The melt rheological properties and DMA studies show evidence for interaction of nanoclay with the polymer chains indicating better processing characteristics of the nanocomposites. Thermal stability improves at lower loading levels of nanoclay due to the barrier effect of delaminated clay layers.

The TPO nanocomposites based on PP/BR blends have been prepared without a compatibilizer and surface modification of CNF. XRD results show that CNFs do not induce a structural change of PP from  $\alpha$  phase to  $\beta$  phase. TEM and SEM photographs reveal homogeneous distribution of CNF in the form of individual nanofibers in the PP matrix. The tensile strength and modulus of the PP/BR matrix are significantly improved with the addition of CNFs and attain maximum at 3 wt % loading. Modified Halpin-Tsai equation that considers the effect of random orientation and

agglomeration of CNFs fitted well with the experimental values of Young's modulus. The SEM of the tensile and impact fractured samples reveal fibre breakage rather than fibre pull out indicating improved adhesion of CNF with PP matrix. The melt rheological studies reveal that the PP/BR/nanoclay composites are melt processable. DSC studies show the nucleating effect of CNFs. TGA studies reveal improved thermal stability of PPBR/CNF composites.

Incorporation of nanoclay and CNF in PP/BR blend promotes TPO nanocomposites with enhanced tensile strength and Young's modulus. But the impact strength is improved only marginally and elongation at break is affected adversely. In order to improve the impact strength and elongation at break of the nanocomposites, an effort was made to compatibilize the PP/BR (80/20) blend using block copolymers followed by the reinforcement using the nanofillers.

Compatibilization of the P80 blend using block copolymers has been carried out. The influence of poly(styrene-*b*-butadiene-*b*-styrene) (SBS) and poly(styrene-*b*-ethylene-*co*-butylene-*b*-styrene) (SEBS) as compatibilizers on the P80 blend were evaluated and the efficiency of the compatibilizers was established. The mechanical, morphological and rheological analysis reveal that 5 wt % of SEBS (P80SEBS5) is a better choice of compatibilizer compared to SBS for PP/BR blend. Improved efficiency of SEBS compared to SBS on compatibilization is ascribed to better interaction of SEBS at the interface due to the compatibility between the EB (ethylene-butylene) mid block and PP. The compatibilizing action is apparent from the better homogeneity associated with compatibilizer incorporation. Addition of 5 wt % of SEBS show reduction in dispersed domain sizes leading to a better dispersion of minor phase as observed in SEM photographs. Thus it is

expected that effective stress transfer can occur at this particular loading of SEBS and 5 wt % of SEBS was optimized for compatibilizing PP/BR (P80) blend. The reduction in tensile strength and modulus upon the addition of the compatibilizer at higher concentration can be due to the agglomeration of the compatibilizer. FTIR analysis of the SEBS compatibilized blends show evidence for physical interaction between the two phases and SEBS. As expected, the crystallization behaviour of blend is not affected by the presence of compatibilizers

In order to attain a desirable combination of improvements in the stiffness and the retention of the impact strength, nanocomposites were developed by the introduction of nanoclay and carbon nanofibre in the SEBS compatibilized PP/BR blend.

SEBS compatibilized PP/BR/nanoclay composite with 1 wt % nanoclay (P80SEBS5NC1) and PP/BR/carbon nanofibre composites with 3 wt % CNF (P80SEBS5CNF3) were optimized based on the mechanical properties. The morphological, rheological and thermal properties of these nanocomposites were investigated. Both the nanocomposites show improved mechanical properties than the P80 blend. TEM analysis of the nanocomposites reveal two different types of morphology for the two SEBS compatibilized PP/BR/nanocomposites. Two different types of distribution of nanofillers in the blend were observed. SEBS forms an interfacial layer around the BR phase in both the nanocomposites. In P80SEBS5NC1 sample, the rubber phase and clay layers were independently dispersed in the PP phase. The clay layers were also found adhered to the SEBS layer at the PP/BR interface. In P80SEBS5CNF3 sample, the CNFs were dispersed in the PP matrix and also seen to be encapsulated in the BR phase. SEBS compatibilized PP/BR/nanoclay composite (P80SEBS5NC1) show significant improvement in

Young's modulus while PP/BR/CNF composite (P80SEBS5CNF3) show significant improvement in impact strength when compared to the P80. The enhancement in Young's modulus shown by the P80SEBS5NC1 sample can be attributed to the phase separated morphology of the nanoclay and BR phase. More over, the clay layers adhered at the elastomeric SEBS layer decrease the elasticity and lead to decreased impact strength of P80SEBSNC1 when compared to P80SEBS5. The enhancement in the impact strength of the compatibilized PP/BR/CNF composite than P80SEBS5 can be attributed to the formation of a core-shell morphology with CNF encapsulated in the dispersed BR phase. The trends in mechanical properties of the nanocomposites are also strongly supported by the SEM morphologies of the tensile and impact fractured specimens. The increase in the peak crystallization temperature  $T_c$  of P80SEBS5CNF3 nanocomposite as observed in the DSC studies confirms the nucleating effect of CNF and unaltered  $T_c$  of the P80SEBS5NC1 nanocomposite indicate the weak nucleating effect of nanoclay. TGA studies show CNF to be a better nanofiller in improving the thermal stability of the SEBS compatibilized PP/BR blend.

SEBS compatibilized PP/BR nanocomposites can be a valuable class of cost effective and light weight engineering materials which will be useful in automotive applications requiring stiffness and toughness.

### **Future scope of the work**

- 1) The possibility of restricting and localizing nanofillers in the desired matrix by adopting different melt mixing protocols.
- 2) Synergistic effect of nanoclay and CNF in the uncompatibilized and compatibilized PP/BR blends could be explored.

- 3) The effect of most widely used compatibilizers like MA-g-PP and SEBS-g-MA can be investigated.
- 4) The use of PP/BR nanocomposite for the fabrication of useful products.

.....✂.....

## ||| List of Publications |||

### Research Publications

- [1] **P.G Sreedevi**, M.A.Shadiya, Joseph Rani, Carbon nanofiber reinforced thermoplastic elastomer based on polypropylene/polybutadiene blend: theoretical modeling of Young's modulus of the nanocomposites with respect to the orientation and agglomeration of carbon nanofiber Journal of Polymer Engineering,(2018) doi.10.1515/polyeng-2017-0408
- [2] **Sreedevi P G**, Rani Joseph and Philip Kurian, Morphology and tensile failure in injection molded polypropylene/polybutadiene blends, Proceedings, Swadeshi Science movement, Kerala (2015).
- [3] **Sreedevi P G**, Rani Joseph and Philip Kurian, Morphology and mechanical properties of Thermoplastic elastomers prepared from SEBS compatibilized polypropylene and polybutadiene blends, Proceedings, Swadeshi Science Movement, Kerala (2014) :ISBN: 978-81-928129-2-2
- [4] Rani Joseph, **Sreedevi P G**, Effect of polybutadiene content on the Morphology, Mechanical, Thermal and Viscoelastic Properties of Polypropylene, Plastics and Rubber Srilanka 14 (2014): 8-13.
- [5] **Sreedevi P G**, Shadiya M A, Rani Joseph, Philip Kurian, polypropylene/ polybutadiene blends: Investigation on the phase morphology, Mechanical, thermal and crystallization properties, Polymers and Polymer composites (communicated)
- [6] **Sreedevi P G**, Shadiya M A, Rani Joseph, Philip Kurian, Thermoplastic elastomer based on polypropylene/polybutadiene blend: Effect of nanoclay on the mechanical, morphological, rheological and thermal properties, Journal of elastomers and plastics (communicated)
- [7] **Sreedevi P G**, Shadiya M A, Rani Joseph and Philip Kurian, Effect of carbon nanofibre loading on the mechanical and morphological properties of polypropylene / polybutadiene blends, Polymer Composites (Communicated)

### **Papers Presented in National/International Conferences**

- [1] **Sreedevi P G**, Rani Joseph and Philip Kurian, Morphology and mechanical properties of Thermoplastic elastomers prepared from SEBS compatibilized polypropylene and polybutadiene blends, 24<sup>th</sup> Swedeshi Science Congress at Thunchath Ezhuthachan Malayalam University, Tirur, Malappuram, Kerala from 6-8 November 2014, (302-306).
- [2] **Sreedevi P G**, Rani Joseph and Philip Kurian ,Morphology and tensile failure in injection molded polypropylene/polybutadiene blends, 25th Swadeshi Science Congress at Sree Sankaracharya University of Sanskrit, Kalady from 5 - 8 of November 2015.
- [3] **Sreedevi P G**, Rani Joseph and Philip Kurian, Tensile behavior and morphology relationship in injection molded polypropylene /polybutadiene blends, UGC sponsored National seminar on Modern trends in Chemistry by Sree Kerala Varma College , from 12-13 November 2015, Thrissur, 2015 (won Second Best paper award).
- [4] **Sreedevi P G**, Rani Joseph and Philip Kurian, Thermoplastic elastomer nanocomposites from polypropylene/polybutadiene/nanoclay Cloisite 93A: Investigation on mechanical properties and morphology, 28<sup>th</sup> Kerala Science Congress, from 28–30 January 2016 , Calicut University Campus, Thenhippalam, Malappuram.
- [5] **Sreedevi P G**, Rani Joseph and Philip Kurian, Role of nanoclay on the morphology and mechanical properties of polypropylene /polybutadiene blends, in International conference-Advances in Polymer Technology (APT 2016) conducted by the Dept. of Polymer Science and Rubber Technogy, CUSAT from 25/02/2016 to 26/02/2016.
- [6] **Sreedevi P G**, Rani Joseph and Philip Kurian, Effect of carbon nanofibre loading on the mechanical and morphological properties of polypropylene / polybutadiene blends, International Symposium on New Trends in Applied Chemistry (NTAC -2017) 9-11 February 2017, Department of Chemistry, Sacred Heart College (Autonomous), Thevara, Kochi, Ernakulam.

.....✪.....



## Curriculum Vitae



### Sreedevi P. G.

Nandanam  
Pattenchery Lane  
Petta  
Poonithura P.O, Pin-682038  
Ernakulam

Mob: + 9847039933

E mail: sreedevipramod@gmail.com

### Educational Qualification

- MSc Chemistry, Sacred Heart College, Thevara, Kochi.
- B Ed. (Physical Science) St. Joseph's Training College for women, Ernakulam.
- Qualified UGC CSIR JRF NET –JUNE 2008, SET (2005).

### Teaching and Training Experience

- 9 years of Teaching experience as Higher Secondary School Teacher.
- 8 years of research experience in Polymer Science & Rubber Technology, CUSAT.

### Awards

National Award- Rashtrapathi Guide Award (1996).

### Personal Details

Date of Birth : 13-10-1980  
Sex : Female  
Nationality : Indian  
Marital Status : Married  
Father's Name : B Gopalakrishna Panicker  
Husband's Name : E.G Pramod Kumar  
Language Proficiency : English, Hindi, Malayalam.  
Official Address : HSST Chemistry  
GHSS Cheriyamundam  
Tirur, Malappuram

.....✍.....

## Supplementary information based on reviewers' comments

Reviewer 1

From TEM image in Figure 4A.2, it is not very clear about exfoliation and intercalation phenomena? Provide EDX of the same figure.

EDX spectrum of the P80NC0.5 sample is shown in the Figure 4A.22. EDX spectra permit the quantitative estimation of the elements present in the sample in terms of atomic and weight percentages. The peaks corresponding to O, Al, Si and Mg atoms in the EDX spectrum confirm the presence of nanoclay in the PP/BR blend matrix.

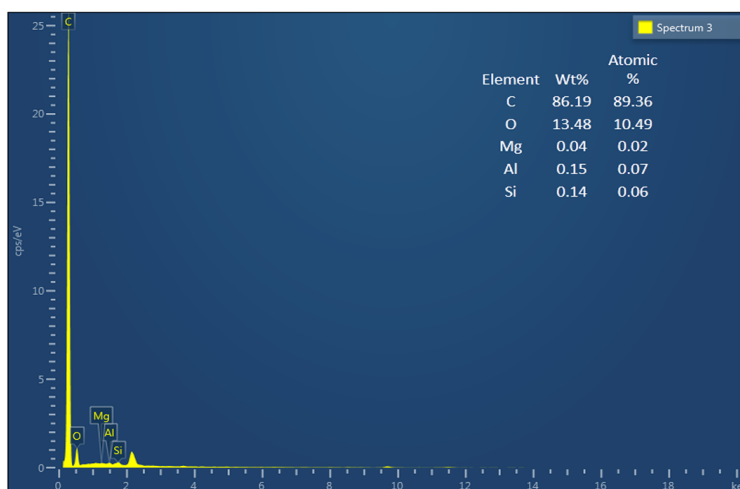
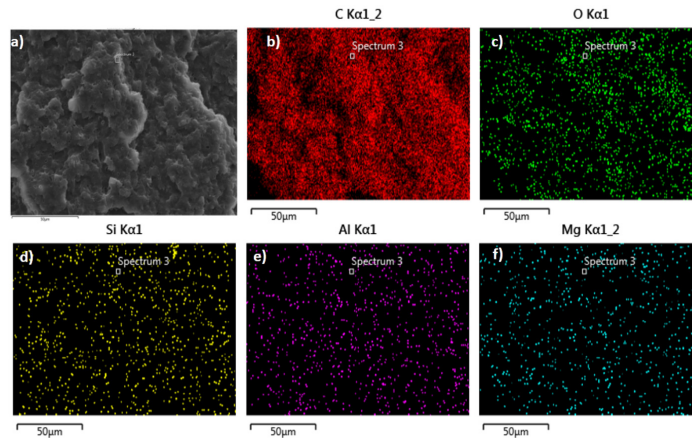


Figure 4A.22 EDX spectra of P80NC0.5 sample

The distribution of the elements could be determined in such a way that the software maps the elements present on the SEM image by X-ray analysis. The distributions of C, O, Si, Al and Mg atoms in the P80NC0.5 sample is shown in figures 4A.23(b-f). These observations further support the better dispersion of nanoclay in the PP/BR blend matrix as suggested by the TEM studies<sup>1</sup>.

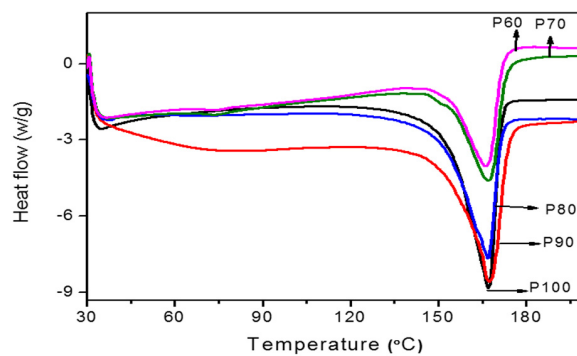


**Figure 4A.23 (a) Electronic image. (b)–(f) Mapping of elements found on the image of P80NC0.5 sample**

Reviewer 2

In page 99, it is mentioned that DSC is shown from 30 °C to 200 °C. But a much narrower range is actually shown.

DSC thermogram from 30 °C to 200 °C is shown as in figure below.



## References

- [1] Yuhana, N. Y., Ahmad, S., Kamal, M. R., Jana, S. C., & Bahri, A. R. (2012). Morphological study on room-temperature-cured PMMAgrafted natural rubber-toughened epoxy/layered silicatenanocomposite. *Journal of Nanomaterials*, 82.